Institut für Geowissenschaften
Mathematisch-Naturwissenschaftliche Fakultät
Universität Potsdam

Wissenschaftsdisziplin:
Geologie

Organic geochemical characterization of the Yacoraite Formation (NW-Argentina)-paleoenvironment and petroleum potential

Dissertation
Von
Ricardo Ruiz-Monroy
zur Erlangung des akademischen Grades
Doctor rerum naturalium
Dr. rer. nat.
in der Wissenschaftsdisziplin "Geochemie"

eingereicht an der
Mathematisch-Naturwissenschaftlichen Fakultät
der Universität Potsdam

Ort und Tag der Disputation: Potsdam, den 06.09.2021

"Dedicada a esa vocecita sutil y persuasiva que me anima
a confiar, persistir en la en la vida e ir más allá"

Hauptbetreuer:	Prof. Dr. Manfred Strecker
Betreuer:	Prof. Dr. Brian Horsfield
Mentor:	Dr. Robert Ondrak
Gutachter:	Prof. Dr. Christian Hallmann
	Dr. habil. Jan-Claudius Schwarzbauer

Published online on the
Publication Server of the University of Potsdam:
https://doi.org/10.25932/publishup-51869
https://nbn-resolving.org/urn:nbn:de:kobv:517-opus4-518697

Abstract

This dissertation was carried out within the framework of the international and interdisciplinary research training group StRATEGy whose aim is to study geological processes occurring at different time and spatial scales that have shaped the southern Central Andes. The study focusses on the shales and carbonates of the Yacoraite Fm. deposited in the Salta rift basin (NW Argentina) during the Maastrichtian to Danian, and is divided into the Tres Cruces, Metán-Alemanía, and Lomas de Olmedo sub-basins. The Yacoraite Fm. is considered the potential source rock for most oil fields in NW Argentina.

The overall motivation for this research was to provide new insights into the occurrence of marine and lacustrine settings during the deposition of the Yacoraite Fm. in the Tres Cruces and Metán-Alemanía sub-basins. Other important aspects assessed in this research are the likely transformation of organic matter of the Yacoraite Fm. into oil as well as its genetic relation to selected produced oils and natural oil seep samples. Fifty-two outcropping samples from the Yacoraite Fm. collected in the Tres Cruces and Metán-Alemanía sub-basins, seven oil seep samples from the Tres Cruces and Lomas de Olmedo sub-basins and eight produced oils from the latter sub-basin were evaluated.

Characterization of the depositional environment and kerogen types of the Yacoraite Fm. was performed using various geochemical analyses encompassing pyrolysis, chromatography, spectrometry and petrography. Minerals were analyzed by X-ray diffraction. The elemental composition of rock samples was determined by X-ray fluorescence and more precise quantification was done by ICP-MS analysis. The study of the hydrocarbon potential of the Yacoraite Fm. was addressed by the following analyses of its organic matter and modeling procedures:

- The assessment of the amount, quality, and thermal maturity of the organic matter;
- Measurement of the rate of thermal cracking (bulk kinetics) of the organic matter into oil;
- The extrapolation of high heating rate kinetics to low heating rates at geological conditions using the first-order kinetic approach provided by the Arrhenius equation;
- The prediction of the composition (compositional kinetics) and the phase behavior of its first-formed petroleum;
- The specific activation energy distribution of the bulk kinetics of representative samples collected in the Tres Cruces sub-basin were used in the 1D-basin modeling, enabling a comparison between the timing of oil generation and the timing of the formation of structural traps. Subsequently, the implications of these variables on the accumulation of oil in the Tres Cruces sub-basin was assessed.

The characterization of produced oils and oil seep samples was carried out by chromatographic and spectrometric techniques. Genetic relationships (source rock-oil correlation) of the oil seep samples in the Tres Cruces sub-basin was studied by comparing their compositional affinities to rock extracts

from outcropping samples of the Yacoraite Fm. in the same sub-basin. Since no rock samples were available from the Lomas de Olmedo sub-basin, the source-rock correlation for the oil seep samples and the produced oils assume that the Yacoraite Fm. in this sub-basin has similar organofacies as in the Tres Cruces and Metán-Alemanía sub-basins.

The results of this research indicate that the deposition of the Yacoraite Fm. began in marine environments. Lacustrine settings developed during the middle part and predominated towards the end of the deposition in the Tres Cruces and Metán-Alemanía sub-basins. In general, the kerogen of the Yacoraite Fm. is predominantly composed of Type II, II/III, and Type III kerogens. The latter is largely found in samples from the Yacoraite Fm. whose TOC values were low. In these samples, the content of Type III kerogen could be overestimated with Rock-Eval pyrolysis due to hydrocarbon adsorption on mineral surfaces (mineral-matrix effect). Organic petrography showed that the organic particles of the Yacoraite Fm. correspond mainly to alginites and some vitrinite-like particles. Pyrolysis-GC of whole-rock samples indicated that the Yacoraite Fm. generates low sulphur oils with a mainly Paraffinic-Naphthenic-Aromatic Low Wax composition and Paraffinic High Wax oils. Minor contributions of Paraffinic Low Wax Oil and Gas condensate-generating facies are also predicted. Mineral-matrix effects can lead to an overestimation of the gas-prone character and were considered.

Extrapolation of bulk kinetics experiments to a geological heating rate of 3 K/Myr reveals that the oil generation from the Yacoraite Fm. in the Tres Cruces sub-basin occurs in a range of approximately 60 °C. The onset (10%TR) of oil generation occurs at geological temperatures from 108 °C to 132 °C. The complete transformation of the organic matter into oil (90%TR) is reached at temperatures between 142 °C and 169 °C. The gas exsolution from the oil occurs at pressures below 200 bar as predicted from PVT-compatible compositional kinetics with subsequent separation of two phases and the increase in liquid viscosity at depths <1.8 km. The analysis of outcrop samples of the Yacoraite Fm. collected in the Metán-Alemanía and Tres Cruces sub-basins document that their maturity is at least at the onset of oil generation. The formation is more mature in the deeper buried centers of the basins being in the main oil window, as indicated by the presence of genetically related oil seep samples and supported by predictions of thermal modeling.

The results of 1D-basin modeling indicate that the onset (10%TR) of oil generation occurred between ≈10 Ma and ≈4 Ma. Most of the oil (from ≈50% to 65%) was generated before the structural traps associated with the Diaguita tectonic phase (c.a. 2.5 Ma) formed. The amount of oil generated after the formation of structural traps and potentially accumulated in them accounts for ≈10%. The petroleum system risk assessment identifies the generally low TOC content and variable thickness of Yacoraite Fm. as important factors that may determine the low volumes of generated and migrated oil. Additional risks are associated with the lack of information regarding the existence of reservoirs and the quality of the seals.

Oil-source rock correlations based on depositional-, age- and maturity-related biomarkers show that the oil samples of the Caimancito oil field and from Well-10 of the Martinez del Tineo oil field

were generated from the Yacoraite Fm., while partial correlations are determined between this formation and the oil samples from Well-18 and Chirete x100-1. According to the project partners, it is most likely the Devonian Los Monos Fm. Oil-oil correlations reflect the source oil-source rock correlations mentioned above and were supported by the ratios of light hydrocarbons using the classical approach of Halpern (1995).

An anomalously high uranium content was measured in one sample at the base of the Yacoraite Fm. in the west sector of the Metán-Alemanía sub-basin. High radiation doses appear to be the cause for the very low hydrocarbon generation during Rock-Eval pyrolysis. The sample is composed mainly of alginites with minor amounts of terrigenous material and plots in the field of Type IV kerogen in a pseudo-Van Krevelen diagram. Since radiation induces aromatization in the kerogen structure, it potentially mimics higher thermal maturity as determined by vitrinite reflectance. The higher T_{max} is caused by the high adsorption of hydrocarbons on the highly-aromatized kerogen and the contribution of hydrocarbons adsorption on mineral surfaces.

The lack of biomarkers in the solvent-extracted portion (bitumen) of the same highly-irradiated sample prevents the characterization of kerogen type and the depositional environment. However, unlike Py-GC results for kerogen, GC-FID analysis on extracted bitumen still shows *n*-alkanes, pristane, and phytane. This may not only indicate a different response of bitumen and kerogen to radiation, at least in the magnitude, but also offers an alternative for kerogen typing in samples where the kerogen is highly affected by radiation which makes its classification unreliable. In this example, the ratios of pristane/*n*-C_{17} and phytane/*n*-C_{18} in bitumen indicate that a Type II/III kerogen composes this sample, which is consistent with the presence of alginite as the main organic component and some vitrinite-like particles.

In conclusion, molecular geochemical analyses have documented the presence of gammacerane in extracts of the Yacoraite Fm. which indicate the development of hypersaline conditions as well as the changing depositional environment of the Yacoraite Fm. from marine towards lacustrine settings. The variability of organofacies of this formation in the Tres Cruces and Metán-Alemanía sub-basins is a consequence of the changes in the depositional environment. Future work may provide insights into the evolution of paleosalinity during Yacoraite Fm. deposition by using specific proxies e.g., methyltrimethyltridecylchromans. Future research may include characterizing the NSO fraction of these oils as well as elucidating possible fractionation during expulsion, migration, and accumulation. A regional study is needed to clarify the uncertainties associated with the existence of the reservoir, the quality of the seals and to improve the data-input for thermal modeling for the Tres Cruces sub-basin.

Studies that aim to increase the database of the concentration of methyldiamantanes (3- + 4-) and methyladamantanes (1- + 2-) in produced oils will provide a threshold for the assessment of oil cracking. Further research is aimed at helping to understand how the distribution of uranium can affect the different responses of bitumen and kerogen to radiation.

Zusammenfassung

Diese Dissertation wurde im Rahmen des internationalen und interdisziplinären Graduiertenkollegs StRATEGy durchgeführt. Diese Gruppe hat sich zum Ziel gesetzt, geologische Prozesse zu untersuchen, die auf unterschiedlichen zeitlichen und räumlichen Skalen ablaufen und die südlichen Zentralanden geprägt haben. Diese Studie konzentriert sich auf die Tonsteine und Karbonate der Yacoraite Fm., die zwischen Maastricht und Dan im kreidezeitlichen Salta-Grabenbecken abgelagert wurden. Das ehemalige Riftbecken liegt im Nordwesten Argentiniens und gliedert sich in die Teilbecken Tres Cruces, Metán-Alemanía und Lomas de Olmedo. Die Yacoraite Fm. wird als potentielles Ausgangsgestein für die meisten Ölfelder in NW-Argentinien angesehen.

Die übergreifende Motivation für diese Studie war es, neue Erkenntnisse über die Entwicklung der marinen und lakustrinen Bedingungen während der Ablagerung der Yacoraite Fm. in den Tres Cruces und Metán-Alemanía Sub-Becken zu gewinnen. Weitere wichtige Aspekte, die im Rahmen dieser Dissertation untersucht wurden, sind die Umwandlung von organischer Materie der Yacoraite Fm. in Öl sowie deren genetische Beziehung zu ausgewählten produzierten Ölen und natürlichen Ölaustritten. Das verwendete Probenset bestand aus zweiundfünfzig Proben von Aufschlüssen der Yacoraite Fm., die in den Unterbecken Tres Cruces und Metán-Alemanía gesammelt wurden, sieben Ölaustritt-Proben aus den Unterbecken von Tres Cruces und den Lomas de Olmedo und acht produzierte Öle aus dem Unterbecken von Olmedo.

Die Charakterisierung der Ablagerungsbedingungen und der Kerogentypen der Yacoraite Fm. wurde mit verschiedenen geochemischen Analysen durchgeführt, welche die Methoden der Pyrolyse, der Chromatographie, der Spektrometrie und der Petrographie umfassen. Die Mineralkomponenten wurden mittels Röntgendiffraktometrie analysiert. Weiterhin wurde die Elementzusammensetzung der Gesteinsproben mittels Röntgenfluoreszenz bestimmt und eine genauere Quantifizierung erfolgte mit Hilfe der ICP-MS-Analyse. Diese Studie wendet das Organofazies-Konzept an, das neben der Charakterisierung des Kerogens auch die Bestimmung der Zusammensetzung des erstgebildeten Erdöls in der Yacoraite Fm. ermöglicht. Wichtig war bei diesem Ansatz, dass die Laborergebnisse auf die geologischen Verhältnisse extrapoliert wurden. Dies wurde durch die folgenden Analysen der organischen Substanz und Modellierungsverfahren angegangen:

- Die Abschätzung der Menge, Qualität und thermischen Reife der organischen Materie;
- Die Messung der thermischen Umwandlungsrate organischer Materie in Öl (Gesamtkinetik);
- Die Extrapolation der Kinetik hoher Heizraten im Labor zu niedrigen Heizraten geologischer Bedingungen unter Verwendung der Arrhenius-Gleichung, die kinetische Modelle erster Ordnung erzeugt;
- Die Vorhersage der Zusammensetzung (Kompositionskinetik) und des Phasenverhaltens des initial gebildeten Erdöls;
- Spezifische Aktivierungsenergieverteilungen der Gesamtkinetik von repräsentativen Proben aus dem Tres Cruces Sub-Basin wurden in einer 1D-Beckenmodellierung verwendet. Dies ermöglicht einen zeitlichen Vergleich zwischen Ölgenese und der Bildung struktureller Fallen, und erlaubt eine Bewertung dieser Variablen auf die Öl-Akkumulation im Teilbecken von Tres Cruces.

Die Charakterisierung der produzierten Öle und Ölaustritte wurde mittels gas-chromatographischen und spektrometrischen Techniken durchgeführt. Genetische Zusammenhänge bzw. Erdöl-Muttergesteinskorrelationen der Ölaustritte und der Gesteinsextrakte der Yacoraite Fm. wurden im Tres Cruces-Teilbecken untersucht. Da aus dem Lomas de Olmedo-Teilbecken keine

Gesteinsproben zur Verfügung standen, wird bei der Muttergesteinskorrelation für die Ölaustritte und produzierten Öle von einer ähnlichen Organofazies der Yacoraite Fm. wie in den Tres Cruces- und Metán-Alemanía-Teilbecken ausgegangen.

Die Ergebnisse meiner Studie zeigen, dass die Ablagerung der Yacoraite Fm. unter marinen Bedingungen begann und sich bis zum Ende der Ablagerung in den Tres Cruces- und Metán-Alemanía-Becken ein lakustrines Milieu entwickelte. Im Allgemeinen besteht das Kerogen der Yacoraite Fm. überwiegend aus den Kerogentypen II, III und II/III-Mischungen. Der Kerogentyp III findet sich vor allem in Proben aus der Yacoraite Fm., deren TOC-Werte niedrig sind. Aufgrund der Adsorption von Kohlenwasserstoffen an den Mineraloberflächen (Mineralmatrixeffekt) könnte der Gehalt an Typ-III-Kerogen mit der Rock-Eval-Pyrolyse in diesen Proben überschätzt werden. Untersuchungen mittels organischer Petrographie zeigen, dass die organischen Partikel der Yacoraite Fm. hauptsächlich aus Alginiten und einigen Vitrinit-artigen Partikeln bestehen. Die Pyrolyse-GC der Gesteinsproben zeigte, dass die Yacoraite Fm. schwefelarme Öle mit einer überwiegend Wachs-armen paraffinisch-naphthenisch-aromatischen Zusammensetzung und paraffinische Wachs-reiche Öle generiert. Geringe Anteile paraffinischer, Wachs-armer Öle und einer Gaskondensat-generierenden Fazies werden ebenfalls vorausgesagt. Auch hier wurden Mineralmatrixeffekte berücksichtigt, die zu einer quantitativen Überschätzung des gasbildenden Charakters führen können.

Die Extrapolation der gesamtkinetischen Experimente auf eine geologische Heizrate von 3 K/Myr. Jahren zeigt, dass die Ölbildung der Yacoraite Fm. im Tres Cruces Sub-Basin in einem Bereich von etwa 60 °C stattfindet. Die initiale Ölbildung (10 %TR) erfolgt bei geologischen Temperaturen von 108 °C bis 132 °C. Die vollständige Umwandlung der organischen Materie in Erdöl (90 %TR) wird bei Temperaturen zwischen 142 °C und 169 °C erreicht. Wie in der PVT-Analyse (PhaseKinetics, di Primio & Horsfield, 2006) vorhersagt, tritt das Entgasen des Öls mit der daraus folgenden Trennung zwei Phasen und dem Anstieg der Viskosität bei Drucken unter 200 bar und in Tiefen von <1,8 km auf. Die Aufschlussproben der Yacoraite Fm. aus den Teilbecken Metán-Alemanía und Tres Cruces zeigen, dass ihre thermische Reife mindestens dem Beginn der Ölerzeugung entsprechen und die Formation sich in tieferen, zentralen Teilen des Beckens am Ölfenster befindet. Dies wird durch das Auftreten von genetisch verwandten Ölaustritten und durch die Vorhersagen der thermischen Modellierung unterstützt.

Die Ergebnisse der 1D-Beckenmodellierung zeigen, dass der Beginn (10 %TR) der Ölgenese zwischen ≈10 Ma und ≈4 Ma stattfand. Der größte Teil des Öls (von ≈50 % bis 65 %) wurde vor der Entwicklung struktureller Fallen gebildet, die während der plio-pleistozänen Diaguita Deformatiosphase gebildet wurden. Nur ≈10 % des insgesamt generierten Öls wurde nach der Entstehung struktureller Fallen gebildet und potentiell darin gefangen. Wichtige Faktoren in der Risikobewertung dieses Erdölsystems, welche die geringen Mengen an generiertem und migriertem Öl bestimmen können, stellen die allgemein niedrigen TOC-Gehalte und die variable Mächtigkeit der Yacoraite Fm. dar. Weitere Risiken sind mit einer niedrigen Informationsdichte über potentiell vorhandene Reservoirstrukturen und die Qualität der Deckgesteine verbunden.

Erdöl-Muttergesteinskorrelationen mittels Ablagerungs-, Alters- und Reife-bezogener Biomarker zeigen, dass die Ölproben des Caimancito Ölfeldes und der Bohrung-10 des Martinez del Tineo Ölfeldes aus der Yacoraite Fm. generiert wurden, während schwache Korrelationen zwischen dieser Formation und den Ölproben aus Bohrung-18 und Chirete x100-1 festgestellt wurden. Die Ölproben aus Bohrung-11 und Río Pescado zeigen keine Korrelation und wurden aus einem anderen Muttergestein gespeist. Nach Angaben der Projektpartner handelt es sich höchstwahrscheinlich um die devonische Los Monos Fm. Die Öl-Öl-Korrelationen spiegeln die Erdöl-Muttergesteinskorrelationen wider und wurden durch die Verhältnisse leichter Kohlenwasserstoffe nach dem klassischen Ansatz von Halpern (1995) unterstützt. In den Ölproben von Río Pescado und Bohrung-11 fehlen die meisten der Biomarker, wodurch sie sich von den übrigen Ölen unterscheiden. Die Probe aus der Bohrung-11 erwies sich als eine Mischung von Ölen unterschiedlicher thermischer Reife. Das am wenigsten reife Öl in dieser Mischung enthält Stigmastan und korreliert mit der Ölprobe aus der Bohrung Caimancito-

21. Die reifste Probe ist durch höhere Konzentrationen von Diamantanen und Adamantanen gekennzeichnet.

Ein ungewöhnlich hoher Urangehalt in einer Probe an der Basis der Yacoraite Fm. im westlichen Sektor des Metán-Alemanía-Teilbeckens wurde mit einem Geigerzähler identifiziert und mittels XRF und ICP-MS quantifiziert. Sie bietet die Möglichkeit, die Auswirkungen der Strahlung auf den Kerogentyp, seine thermische Reife und die Art der gebildeten Kohlenwasserstoffe zu untersuchen. Dieses radioaktive Element stammt aus den präkambrischen/paläozoischen Graniten der Region. Hohe Strahlungsdosen scheinen die Ursache für die sehr geringe Kohlenwasserstoffbildung während der Rock-Eval-Pyrolyse zu sein. Die Probe besteht hauptsächlich aus Alginiten mit geringen Mengen an terrigenem Material und ist in einem Pseudo-Van Krevelen-Diagramm im Typ IV-Kerogenfeld eingezeichnet. Die thermische Reife ist höher als die von Proben in der näheren Umgebung, wie Vitrinitreflexionsgrade und der gemessenen Rock-Eval T_{max} zeigen. Die Auswirkungen von Intrusionen wurden als zusätzliche Wärmequelle, die nur diese Probe betrifft, ausgeschlossen. Da die Strahlung eine Aromatisierung in der Kerogenstruktur induziert, zeigt die Vitrinitreflexionsmessung möglicherweise eine höhere thermische Reife. Die höheren T_{max}-Werte werden durch die hohe Adsorption von Kohlenwasserstoffen auf dem hocharomatisierten Kerogen und den Mineraloberflächen verursacht.

Das Fehlen von Biomarkern im lösungsmittelextrahierten Anteil (Bitumen) dieser hoch-radioaktiven Probe verhindert die Charakterisierung des Kerogentyps und der Ablagerungsmilieus. Im Gegensatz zu den Py-GC-Ergebnissen für Kerogen zeigt die GC-FID-Analyse von extrahiertem Bitumen jedoch weiterhin *n*-Alkane, Pristan und Phytan. Dies kann nicht nur auf eine unterschiedliche Reaktion von Bitumen und Kerogen auf Strahlung hinweisen, zumindest in dieser Größenordnung, sondern bietet auch eine Alternative für die Kerogen-Typisierung dieser Proben, in denen eine Kerogenklassifizierung durch die Strahlung unzuverlässig ist. In diesem Beispiel deuten die Verhältnisse von Pristan/*n*-C_{17} und Phytan/*n*-C_{18} im Bitumen darauf hin, dass diese Probe aus einem Typ II/III-Kerogen besteht, was das Vorhandensein von Alginiten als organischer Hauptkomponente und einigen Vitrinit-artigen Partikeln bestätigt.

Zusammenfassend lässt sich sagen, dass geochemische Analysen auf molekularer Ebene das Vorhandensein von Gammaceran in Extrakten der Yacoraite Fm. dokumentiert haben, was auf die Entwicklung hypersalinarer Bedingungen sowie auf den Wechsel des Ablagerungsmilieus dieser Formation von marinen zu lakustrinen Bedingungen hinweist. Die Variabilität der Organofazies dieser Formation in den Teilbecken Tres Cruces und Metán-Alemanía ist eine Folge der Veränderungen in des Ablagerungsmilieus. Zukünftige Arbeiten könnten Aufschluss über die Entwicklung der Paläosalinität während der Ablagerung der Yacoraite Fm. geben, indem sie spezifische Proxies wie z.B. Methyltrimethyltridecylchromane verwenden. Zukünftige Untersuchungen könnten die Charakterisierung der NSO-Fraktion dieser Öle sowie die Klärung einer möglichen Fraktionierung während der Ablagerung, Migration und Akkumulation zum Ziel haben. Eine regionale tektonische Studie kann die Unsicherheiten im Zusammenhang mit der Existenz von Erdölreservoiren und der Qualität der Deckgesteine klären und den Datendichte für eine thermische Modellierung des Tres Cruces-Teilbeckens verbessern. Bessere Datensätze für die Konzentration von Methyldiamantanen (3- + 4-) und Methyladamantanen (1- + 2-) in den produzierten Ölen helfen einen Schwellenwert für die Bewertung der sekundären thermischen Ölumwandlung festzulegen. Zum besseren Verständnis wie der Urangehalt die unterschiedlichen Reaktionen von Bitumen und Kerogen auf Strahlung beeinflusst, muss weitere Forschung angestrebt werden.

Kurze Version der Ergebnisse

Diese Dissertation wurde im Rahmen des internationalen und interdisziplinären Graduiertenkollegs StRATEGy durchgeführt. Diese Gruppe hat sich zum Ziel gesetzt, geologische Prozesse zu untersuchen, die auf unterschiedlichen zeitlichen und räumlichen Skalen ablaufen und die südlichen Zentralanden geprägt haben. Diese Studie konzentriert sich auf die Tonsteine und Karbonate der Yacoraite Fm., die zwischen Maastricht und Dan im kreidezeitlichen Salta-Grabenbecken abgelagert wurden. Das ehemalige Riftbecken liegt im Nordwesten Argentiniens und gliedert sich in die Teilbecken Tres Cruces, Metán-Alemanía und Lomas de Olmedo. Die übergreifende Motivation für diese Studie war es, neue Erkenntnisse über die Entwicklung der marinen und lakustrinen Bedingungen während der Ablagerung der Yacoraite Fm. in den Tres Cruces und Metán-Alemanía Sub-Becken zu gewinnen. Weitere wichtige Aspekte, die im Rahmen dieser Dissertation untersucht wurden, sind die Umwandlung von organischer Materie der Yacoraite Fm. in Öl sowie deren genetische Beziehung zu ausgewählten produzierten Ölen und natürlichen Ölaustritten. Die Ergebnisse meiner Studie zeigen, dass die Ablagerung der Yacoraite Fm. unter marinen Bedingungen begann und sich bis zum Ende der Ablagerung in den Tres Cruces- und Metán-Alemanía-Becken ein lakustrines Milieu entwickelte. Im Allgemeinen besteht das Kerogen der Yacoraite Fm. überwiegend aus den Kerogentypen II, III und II/III-Mischungen. Der Kerogentyp III findet sich vor allem in Proben aus der Yacoraite Fm., deren TOC-Werte niedrig sind. Aufgrund der Adsorption von Kohlenwasserstoffen an den Mineraloberflächen (Mineralmatrixeffekt) könnte der Gehalt an Typ-III-Kerogen mit der Rock-Eval-Pyrolyse in diesen Proben überschätzt werden. Untersuchungen mittels organischer Petrographie zeigen, dass die organischen Partikel der Yacoraite Fm. hauptsächlich aus Alginiten und einigen Vitrinit-artigen Partikeln bestehen. Die Pyrolyse-GC der Gesteinsproben zeigte, dass die Yacoraite Fm. schwefelarme Öle mit einer überwiegend Wachs-armen paraffinisch-naphthenisch-aromatischen Zusammensetzung und paraffinische Wachs-reiche Öle generiert. Geringe Anteile paraffinischer, Wachs-armer Öle und einer Gaskondensat-generierenden Fazies werden ebenfalls vorausgesagt. Auch hier wurden Mineralmatrixeffekte berücksichtigt, die zu einer quantitativen Überschätzung des gasbildenden Charakters führen können.

Die Ergebnisse einer zusätzlich durchgeführten 1D-Beckenmodellierung zeigen, dass der Beginn (10 %TR) der Ölgenese zwischen ≈10 Ma und ≈4 Ma stattfand. Der größte Teil des Öls (von ≈50 % bis 65 %) wurde vor der Entwicklung struktureller Fallen gebildet, die während der plio-pleistozänen Diaguita Deformatiosphase gebildet wurden. Nur ≈10 % des insgesamt generierten Öls wurde nach der Entstehung struktureller Fallen gebildet und potentiell darin gefangen. Wichtige Faktoren in der Risikobewertung dieses Erdölsystems, welche die geringen Mengen an generiertem und migriertem Öl bestimmen können, stellen die allgemein niedrigen TOC-Gehalte und die variable Mächtigkeit der Yacoraite Fm. dar. Weitere Risiken sind mit einer niedrigen Informationsdichte über potentiell vorhandene Reservoirstrukturen und die Qualität der Deckgesteine verbunden.

Acknowledgments

While writing this section I have become aware of the many people involved that have accompanied me during this journey, helping me to overcome personal and professional challenges. I want to express my sincere gratitude to them in the following lines. First a bit of history... I became interested in getting deeper into organic geochemistry when I read the paper titled “From petroleum-type organofacies to hydrocarbon phase prediction”. In that paper, the way in which results of laboratory experiments can be extrapolated to natural conditions captured my attention. I knew I wanted to understand more and get involved in this kind of research. I would like to express my gratitude to Prof. Dr. Rolando di Primio and Prof. Dr. Brian Horsfield, authors of the mentioned paper, who in 2013 kindly welcomed me for an internship in the organic Geochemistry section at GFZ… and this journey started.

I am grateful to Dr. Hans-Martin Schulz and to Dr. Robert Ondrak who trusted me as a Ph.D. candidate. In 2016 I started my studies in the framework of the wonderful interdisciplinary and international initiative consolidated as the training group (StRATEGy), funded by the German Research Foundation (DFG) and the federal state of Brandenburg. I acknowledge the leadership, courage and endeavor of Prof. Manfred Strecker, my supervisor at the University of Potsdam who was supportive during all this time. During this journey I was also accompanied by my co-supervisor Prof. Dr. Eduardo Rossello from Universidad de Buenos Aires, who besides was with me during the sampling campaign and provided me with some produced oil samples. My experience in this project was facilitated by a group of research coordinators, Dr. Andreas Bergner, Dr. Henry Wichura, and Dr. Veronica Torres, who were receptive and helpful.

The German Research Centre for Geosciences and the organic geochemistry section hosted me providing me with a comfortable office and an academic atmosphere in which I had the chance to interact with colleagues from which I learned. At an institutional level I am grateful to Geomark Research for providing five of the produced oils samples and the respective data. I went through the core of my work with the academic support from Dr. Robert Ondrak as my mentor from whom I acknowledge his patience and who helped me out with my Spanglish. His empathic aptitude was reflected in his gesture of welcoming me into his home and in this way, make my arrival in Germany easier. Great contributions to my work came from my supervisor Prof. Dr. Brian Horsfield, whose contagious joy, positively encouraged my progress. Additional contributions to my work came from Argentinian counterparts Dr. Gilda Collo, with whom I worked at Córdoba University, and Prof. Dr. Ricardo Alonso, from Salta University.

This dissertation also benefited from the opportune and fruitful comments from Dr. Dr. Kai Mangelsdorf, acting head of the organic geochemistry section and my colleagues Dr. Nicolaj Mahlstedt, Dr. Mareike Noah, Dr. Stefanie Pötz, Dr. Volker Ziegs, Dr. Shengyu Yang, Dr. Christian Meeßen, Dr. Sibiao Liu, M.Sc. Wera Schmidt. I would not have been successful without the high-quality process

and results provided by the technical staff at GFZ. From the organic geochemistry section: Ferdinand Perssen, Cornelia Karger, Anke Kaminsky, Kristin Günther, and Dipl.-Inf. Mirco Rahn. I am grateful to Heike Rothe from the inorganic and isotopic geochemistry to provide ICP-MS analysis for this study. This research also benefited from international network cooperation. I am grateful to Lic. Ileana Perassi at Laboratorio de Minerales de Arcillas, CICTERRA – CONICET and well as German Bonilla from iNCLAY S.A.S (Colombia) for their cooperation with X-ray diffraction and X-ray fluorescence data, respectively.

Fortunately for my nerves, I had the support of Claudia Engelhardt, Tanja Klaka-Tausche, Melanie Olschimke, Claudia Rößling, and Frauke Stobbe to surf administrative and bureaucracy tasks of living and studying in a new country. During these years I have built good memories thanks to Karsten Adler, Valentina Cortassa, Michele Vallati with whom I shared different seasons, coffees, walks, laughs, and drinks. Fortunately for me and the people who can read German, Volker Ziegs and Karsten Adler help me out with the translation of the abstract of this Dissertation into German language. Figures were largely improved by the graphic design advice from Corinna Kalich from whom I also received a good mood and positivism.

To the essential group of people from which I have received love and who have encouraged me to go further through their unconditional support. This is an additional opportunity to write my gratitude to all of them. My father, German Ruiz, mother Blanca Monroy, brother Giovanni and sister Marvick. To my daughter Antonella, whose presence draws a smile on my face. Diana Köblös has become a VIP member of this clan and also helped shape the first English-versions of this dissertation. No one could warn her that it was not going to be easy at all.

Table of Contents

Abstract III
Zusammenfassung VI
Acknowledgments IX
1. Introduction 1
1.1 Principal research goals 1
1.2 Brief geological summary of the Cretaceous Salta Rift 3
1.3 Brief geological summary 5
1.4 Characteristics of the Salta Rift basin 6
1.5 Geological background and tectonic evolution of the Salta Rift basin 7
1.6 Cretaceous to Cenozoic basin fill of the Salta Rift 9
1.7 Facies and depositional environments of the Yacoraite Formation 12
1.8 Aspects of the petroleum system in NW Argentina 14
1.9 The Carbon cycle in the Earth system and petroleum generation 16
1.9.1 The Carbon cycle 17
1.9.2 Biomass generation, preservation and accumulation 17
1.9.3 Organic matter classification-kerogen type 18
1.9.4 Petroleum and its relation to former forms of life 20
1.9.5 Organic matter transformation and petroleum generation 20
2. Samples and methods 23
2.1 Sampling procedure 23
2.2 Sample preparation 23
2.2.1 Rock samples 23
2.2.2 Extraction and analysis of bitumen 24
2.3 Chemical characterization of organic matter 24
2.3.1 Bulk elemental composition and bulk-flow pyrolysis 24
2.3.2 Thermovaporisation (T-vap) and Pyrolysis-gas chromatography (Py-GC) 25
2.3.3 Bulk hydrocarbon generation - bulk kinetics 26
2.3.4 PhaseKinetics 26
2.3.5 Organic petrography and vitrinite reflectance 27
2.4 Mineral composition - inorganic characterization 27
2.4.1 X-ray diffraction 27
2.4.2 Elemental chemical composition of the rock samples, X-ray fluorescence 29
2.4.3 Uranium content 29
2.5 Characterization of rock extracts, oil seep samples and produced oils 30
2.5.1 Gas chromatography-flame ionization detection (GC-FID) 30
2.5.2 Gas chromatography-mass spectrometry (GC-MS) 30
2.5.3 Compound-specific stable carbon isotopes 31
3. Depositional environment and kerogen type of the Yacoraite Fm. 32
3.1 Mineral assemblages and chemical composition 32
3.1.1 Mineral archives of the depositional environment of the Yacoraite Formation 32
3.1.2 Paleoclimate conditions inferred from clay mineralogy 34
3.1.3 Chemical elements as archives of the depositional environment of the Yacoraite Fm. 36
3.2 Kerogen type of the Yacoraite Formation 39
3.2.1 Element-based classification 39
3.2.2 Molecular typing of kerogen (pyrolysis-GC) 43
3.2.3 Organic matter typing - insights from organic petrology 45
3.2.4 Organic matter typing- insights from biomarkers 46
3.2.5 Redox conditions developed during the deposition of the Yacoraite Formation 46
3.2.6 Marine vs. lacustrine conditions during the deposition of the Yacoraite Fm. 48
3.3 Conclusions 51
3.3.1 General conclusions 51
3.3.2 Specific conclusions 52
4. Effects of maturation, radiolysis and mineral matrix 54
4.1 Thermal maturity of the Yacoraite Fm. 54
4.1.1 Maximum temperature (T_{max}) - Rock-Eval pyrolysis 54
4.1.2 Vitrinite reflectance 58
4.2 Mineral diagenesis 60

4.3 Inorganic controls of organic chemical composition 62
4.3.1 The role of minerals on kerogen properties 62
4.3.2 The effect of radiation on kerogen properties 65
4.3.3 The overlapping effects of mineral matrix and radiation 69
4.4 Conclusions 70
5. Characteristics and origin of produced oils and oil seep samples 71
5.1 Inferences regarding source characteristics from produced oils and oil seep samples 71
5.1.1 Evolution of redox conditions 71
5.1.2 Source lithofacies 72
5.1.3 Water-column stratification 73
5.1.4 Marine versus lacustrine depositional setting 75
5.1.5 Terrigenous versus aquatic organic-matter types 78
5.2 Age-related biomarkers in produced oils and oil seep samples 82
5.2.1 General considerations 82
5.2.2 Age assignment based on steranes ratios 82
5.3 Maturity of produced oils and oil seep samples 85
5.3.1 Maturity assessment based on hopanes and sterane isomerization 85
5.3.2 Maturity assessment based on aromatic hydrocarbons 88
5.3.3 Maturity assessment based on diamondoids 90
5.4 Biodegradation of produced oils and oil seep samples 93
5.4.1 Biodegradation in produced oils 94
5.4.2 Biodegradation in oil seep samples 96
5.5 Source rock - oil correlations 98
5.5.1 Correlations based on depositional environment and kerogen type 98
5.5.2 Correlations based on diamantanes 101
5.5.3 Oil-source correlations in the context of source-rock age 103
5.6 Oil-oil correlations 104
5.6.1 Correlations based on diamondoids 104
5.6.2 Correlations bases on light hydrocarbons 106
5.7 Conclusions 107
5.7.1 Characteristics of the source rock for produced oil and oil seep samples as inferred from source-rock correlations. 107
5.7.2 Biodegradation of produced oils and oil seep samples 109
5.7.3 Oil - oil correlations 109
6. Petroleum generating properties of the Yacoraite Fm. 110
6.1 Organofacies and primary oil composition 110
6.2 Bulk kinetics of kerogen to hydrocarbon conversion of the Yacoraite Fm. 115
6.3 Physical properties-PVT of the primary petroleum 120
6.4 Conclusions 125
7. Petroleum generation in space and time – basin modeling 125
7.1 Input parameters for the 1D model 126
7.2 Boundary conditions 129
7.3 Calibration data 130
7.4 The conceptual model 131
7.5 Results 131
7.5.1 The effects of burial and heat-flow evolution on the Yacoraite Fm. 131
7.5.2 Modeling hydrocarbon generation using source rock-specific kinetics 132
7.5.3 The petroleum system elements and exploration risks 134
7.6 Conclusions 134
8. Summary and perspectives 135
9. References 138
10. Appendix 154

List of figures

Fig. 1.1. Map of the southern central Andes showing the major geological provinces (after Jordan et al., 1983) and the study area in NW Argentina. 3
Fig. 1.2. Map of the Salta Rift basin in NW Argentina and sampling locations. 7
Fig. 3.1. Variation in carbonates (red line) and detrital minerals (blue line) in samples of the Yacoraite Fm. 33
Fig. 3.2. X-ray diffractograms of the grain size fraction <2 μm in samples of the Yacoraite Fm. 35
Fig. 3.3. (a) Variations in illite/mica and smectite content in the fraction <2 μm of the Yacoraite Fm. in the southern sector of the Tres Cruces sub-basin. (b) Interpreted climate variations based on illite/mica and smectite variations. 36
Fig. 3.4. Chemical elemental ratios used to characterize the depositional environment of the Yacoraite Fm. in the Tres Cruces sub-basin. 37
Fig. 3.5. Total sulphur (TS) vs. TOC in whole-rock samples of the Yacoraite Formation. 39
Fig. 3.6. Fe_2O_3/TiO_2 ratios vs. $Al_2O_3/(Al_2O_3+Fe_2O_3)$ ratios determined for the Yacoraite Formation. 39
Fig. 3.7. Histograms of parameters used to assess the organic richness and kerogen type in samples of the Yacoraite Fm. 40
Fig. 3.8. Modified Van Krevelen diagram of HI vs. OI based on Rock-Eval pyrolysis of whole-rock samples of the Yacoraite Fm. 41
Fig. 3.9. S2 vs. TOC plots for samples of the Yacoraite Fm. (a) Tres Cruces sub-basin, (b) Metán-Alemanía sub-basin. 43
Fig. 3.10. Hydrocarbon chain-length distribution (Py-GC) of total C_1-C_5 resolved pyrolysates, C_6-C_{14} n-alk-1-enes plus n-alkanes, and C_{15}+ n-alk-l-enes plus n-alkanes of the Yacoraite Fm. samples. 44
Fig. 3.11. Photomicrographs under incident light and oil immersion of polished whole-rock samples of the Yacoraite Fm. 45
Fig. 3.12. Pristane/n-C_{17} ratios vs. phytane/n-C_{18} ratios of extracts of the Yacoraite Fm. 46
Fig. 3.13. Variation in Pristane vs. phytane in the aliphatic fraction of extracts of the Yacoraite Formation. 47
Fig. 3.14. $C_{34}S/C_{35}S$ hopanes ratios vs. pristane/phytane ratios of extracts of the Yacoraite Fm. 48
Fig. 3.15. Dibenzothiophene (DBT)/phenanthrene (P) ratios vs. pristane (Pr)/phytane (Ph) ratios of extracts of the Yacoraite Fm. 49
Fig. 3.16. ($C_{31}R/C_{30}$) hopane ratios vs. (C_{26}/C_{25}) tricyclic terpane ratios of extracts from the Yacoraite Formation. 50
Fig. 4.1. Hydrogen Index (HI) vs. T_{max} plot to classify kerogen types and to provide thermal maturity assessment in whole-rock samples of the Yacoraite Fm. 55
Fig. 4.2. The difference in Rock-Eval pyrolysis curves for sample #37, revealing that S2 is composed of hydrocarbons from thermal degradation of kerogen and bitumen. 56
Fig. 4.3. Histograms of the vitrinite reflectance (%Ro) measurements on whole-rock samples of the Yacoraite Fm. 59
Fig. 4.4. Mineral diagenesis-metamorphism for samples of the Yacoraite Fm. collected in the Valle del Tonco 61
Fig. 4.5. Comparison of Rock-Eval parameters between whole-rock and kerogen concentrates. 63
Fig. 4.6. Reconstructed Rock-Eval pyrograms of whole-rock samples (black lines) and kerogen concentrates (red lines) of the Yacoraite Fm. 64
Fig. 4.7. Uranium / total organic carbon ratio (TOC) vs. age of the Yacoraite Fm. 65
Fig. 4.8. Py-GC chromatograms of whole-rock samples of the Yacoraite Fm. 66
Fig. 4.9. Aromaticity (% o-xylene compared to nonane and 2,3-dimethylthiophene) vs. uranium concentration (ppm) in whole-rock samples. 67
Fig. 4.10. Ternary plot of hydrocarbon chain-length distribution of pyrolysates (Py-GC) in samples of the Yacoraite Fm. 68
Fig. 5.1. Variation in Pristane vs. phytane in the aliphatic fraction in produced oil samples and one oil seep sample from the Lomas de Olmedo sub-basin. 72
Fig. 5.2. Cross plot of pristane/ (pristane + phytane) ratios vs. C_{27} diasteranes/(diasteranes + regular steranes) for produced oil samples from the Lomas de Olmedo sub-basin. 73
Fig. 5.3. GC-MS mass chromatograms of hopane distribution m/z=191 in the saturated fraction of produced oil samples from the Lomas de Olmedo sub-basin and representative oil seep samples collected in the Tres Cruces and the Lomas de Olmedo sub-basins. 74
Fig. 5.4. Gammacerane Index vs. Pristane (Pr)/phytane (Ph) of produced oil samples from the Lomas de Olmedo sub-basin (circles) and oil seep samples collected in the Tres Cruces and the Lomas de Olmedo sub-basins (triangles). 75

Fig. 5.5. Pristane (Pr)/Phytane (Ph) ratio vs. Dibenzothiophene (DBT)/Phenanthrene (P) ratio in produced oils (circles) from the Lomas de Olmedo sub-basin and oil seep samples collected in the Tres Cruces and the Lomas de Olmedo sub-basins (triangles). 76
Fig. 5.6. GC-MS chromatograms of tricyclic terpane distribution m/z=191 in the saturate fraction of produced oil from the Lomas de Olmedo sub-basin and representative oil seep samples collected in the Tres Cruces and the Lomas de Olmedo sub-basins. 77
Fig. 5.7. Cross plot of $C_{31}R/C_{30}$ hopane vs. C_{26}/C_{25} tricyclic terpanes in produced oils samples from the Lomas de Olmedo sub-basin and oil seep samples collected in the Tres Cruces and the Lomas de Olmedo sub-basins. 78
Fig. 5.8. Ternary plot of $\alpha\alpha\alpha C_{27}R$, $\alpha\alpha\alpha C_{28}R$ and $\alpha\alpha\alpha C_{29}R$ steranes in produced oil samples from the Lomas de Olmedo sub-basin and oil seep samples collected in the Tres Cruces and the Lomas de Olmedo sub-basins. 79
Fig. 5.9. C_{29}/C_{27} regular steranes ratio vs. Pristane (Pr)/ phytane (Ph) ratio of produced oil samples from the Lomas de Olmedo sub-basin and oil seep samples collected in the Tres Cruces and the Lomas de Olmedo sub-basins. 80
Fig. 5.10. Pristane/n-C_{17} vs. Phytane/n-C_{18} ratios in produced oil samples from the Lomas de Olmedo sub-basin. 81
Fig. 5.11. Dimethyldiamantane index-1 (DMDI-1) vs. Ethyladamantane index (EAI) of produced oil samples from the Lomas de Olmedo sub-basin. 82
Fig. 5.12. Evolution of C_{28}/C_{29} steranes ratio used to the assessment of the age of produced oil samples from the Lomas de Olmedo sub-basin and oil seep samples collected in the Tres Cruces and the Lomas de Olmedo sub-basins. 84
Fig. 5.13. Hopane isomerization based on (S)/(S+R) isomer ratio in produced oil samples from the Lomas de Olmedo sub-basin and oil seep samples collected in the Tres Cruces and the Lomas de Olmedo sub-basins. 86
Fig. 5.14. Sterane isomerization based on ratios of ($\beta\beta$) to ($\alpha\alpha$) steranes and (S) to (R) C_{29} steranes in produced oil samples from the Lomas de Olmedo sub-basin and oil seeps samples collected in the Tres Cruces and Lomas de Olmedo sub-basins. 87
Fig. 5.15. GC-MS chromatograms of phenanthrenes m/z=178+192 in the aromatic fraction of produced oil from the Lomas de Olmedo sub-basin and oil seep samples collected in the Tres Cruces and the Lomas de Olmedo sub-basins. 89
Fig. 5.16. Concentrations of C_{29} stigmastane vs. concentration of 3- + 4-methyldiamantanes in produced oil samples from the Lomas de Olmedo sub-basin. 92
Fig. 5.17. Concentrations of methyladamantanes (1- + 2-) vs. methyldiamantanes (3- + 4-) in produced oil samples from the Lomas de Olmedo sub-basin. 93
Fig. 5.18. GC-FID chromatograms of produced oils from the Lomas de Olmedo sub-basin and representative oil seep samples collected in the Tres Cruces and the Lomas de Olmedo sub-basins... 95
Fig. 5.19. GC-MS chromatograms of naphthalenes m/z = 128, 142, 156, 170 for produced oils from the Lomas de Olmedo sub-basin and representative oil seep samples collected in the Tres Cruces and the Lomas de Olmedo sub-basins. 97
Fig. 5.20. Relative amount of C_{31} to C_{35} homohopane (%) in rock extracts of the Yacoraite Fm. from the Tres Cruces and Metán-Alemanía sub-basins, produced oils from the Lomas de Olmedo sub-basin and oil seep samples collected in the Tres Cruces and the Lomas de Olmedo sub-basins. 100
Fig. 5.21. GC-MS chromatograms of diamantanes in the saturate fraction of produced oils from the Lomas de Olmedo sub-basin and one representative rock extract of the Yacoraite Fm. from the Tres Cruces sub-basin. 101
Fig. 5.22. Distributions of the relative concentrations of diamantanes (referred to 5-α-androstan, 5 mg/ml) in the aliphatic fraction of (a) produced oils from the Lomas de Olmedo sub-basin, oil seep samples collected in the Tres Cruces and the Lomas de Olmedo sub-basins and (b) source-rock extracts from the Yacoraite Fm. 102
Fig. 5.23. GC-MS chromatograms of hopanes distribution m/z=191 in the saturate fraction of rock extracts of representative samples of the Yacoraite Fm. in the Tres Cruces sub-basin. 104
Fig. 5.24. GC-MS chromatograms of adamantanes in the saturate fraction of produced oils from the Lomas de Olmedo sub-basin. 105
Fig. 5.25. Distribution of relative concentrations of adamantanes (referred to 5-α-androstan, 5 mg/ml) in the aliphatic fraction of produced oil samples from the Lomas de Olmedo sub-basin. 106
Fig. 5.26. Light hydrocarbon star diagrams for produced oil samples from the Lomas de Olmedo sub-basin. 107

Fig. 6.1. Ternary plot of hydrocarbon chain-length distribution (Py-GC) of total C_1-C_5 resolved pyrolysates, C_6-C_{14} n-alk-1-enes plus n-alkanes, and C_{15+} n-alk-l-enes plus n-alkanes in samples of the Yacoraite Fm. 111
Fig. 6.2. Kerogen classification of samples from the Yacoraite Fm. using specific compounds (after di Primio and Horsfield, 1996) 113
Fig. 6.3. Ternary plot of hydrocarbon chain-length distribution of mobile hydrocarbons fraction by Thermo vaporization (T-vap) in samples of the Yacoraite Fm. 114
Fig. 6.4. The ratio of C_{15+}/C_6-C_{14} n-alkanes as calculated from Py-GC (X-axes) and T-vap (Y-axes) for samples of the Yacoraite Fm. 115
Fig. 6.5. Activation energy distribution (kcal/mol) and the frequency factor (A, 1/s) calculated for selected whole-rock samples from the Yacoraite Fm. see text for discussion 117
Fig. 6.6. Calculated geological temperatures (X-axes) at which different transformation ratios (Y-axes) are reached for kerogen to petroleum transformation in samples of the Yacoraite Fm. for a heating rate of 3 K/Myr. 119
Fig. 6.7. PhaseKinetics 14-compounds models for selected samples of the Yacoraite Fm. Generated fluids are mainly composed of liquid hydrocarbons. 122
Fig. 6.8. Calculated Gas/Oil ratio (GOR) as a function of kerogen transformation (TR) in samples of the Yacoraite Fm. 123
Fig. 7.1. Sketch of the interpreted cross-section based on seismic line 1225 showing the present-day configuration of the sediments at depth. 126
Fig. 7.2. Paleo heat-flow histories used in thermal modeling for the stratigraphic succession in the Tres Cruces sub-basin. 130
Fig. 7.3. Burial histories of the stratigraphic succession in the Tres Cruces sub-basin and their impact on the thermal maturity of the Yacoraite Fm. 132
Fig. 7.4. Transformation ratios (TR) of the kerogen in hydrocarbons under different scenarios considered in the thermal modeling for the stratigraphic succession in the Tres Cruces sub-basin. .. 133

List of tables

Table 4.1. Vitrinite reflectance (Ro) and fluorescence in whole-rock samples of the Yacoraite Formation. 58
Table 4.2. Kerogen type and thermal maturity parameters in whole-rock samples and kerogen concentrates of the Yacoraite Formation and their relation to clay mineral composition. 63
Table 5.1. The methylphenanthrene Index (MPI-1) and the calculated maturity expressed as vitrinite reflectance (Ro, %) for the produced oils and one oil seep in this study. 90
Table 5.2. Some parameters used to determine the extent of biodegradation in produced oils and oil seep samples 94
Table 7.1. Customized lithological composition for the stratigraphic succession in the Tres Cruces sub-basin. 127
Table 7.2. Thickness, age, and paleo-water depth of the deposition in the Tres Cruces sub-basin used as input data for 1-D modeling. This model assumes no erosion but thickness correction due to the dip of the stratigraphic layers caused by tectonics. 128

1. Introduction

1.1 Principal research goals

The organic geochemical characterization of organic matter in sedimentary rocks can provide essential data to understand the processes and conditions during its deposition and transformation into hydrocarbons (Carrol and Bohacs, 2001; Peters et al., 2005a). Consequently, the interpretation of such data can contribute to the exploration and production of hydrocarbons by improving our knowledge regarding the quality and quantity of organic matter from which the petroleum is ultimately formed because the quality of a source rock depends very much on the type and amount deposited (Radke et al., 1997; Dembicki, 2009). In addition, not only the primary production of organic matter and its geochemical transformation is important, but also the conditions for preservation must be favorable (Littke et al., 1997).

The characterization of organic matter deposition provides important insights into its bulk petroleum potential. This is achieved by pyrolyzing rock samples and it helps to quantify the yield of hydrocarbons, but it does not offer insights into petroleum composition (Espitalié et al., 1977). For this, molecular typing (Horsfield, 1997) establishes a link between organic matter and its precursors, and it allows predicting the composition of the first-formed petroleum. The other important parameter controlling petroleum potential is the thermal maturity of the organic matter, which is mainly controlled by burial and determines the timing of petroleum generation (Tissot and Welte, 1984). Not only sediment deposition increases burial, but also tectonic loading during orogenic processes is key to reach the necessary burial depth and temperatures for petroleum generation (McCarthy et al., 2011).

The rate of hydrocarbon generation is temperature-controlled (Poelchau et al., 1997) and influenced by intrinsic properties of the organic matter, and therefore, studies of the kinetics of this transformation are essential to understand hydrocarbon generation (Pepper and Corvi, 1995; Schenk et al., 1997). Importantly, chemical and structural variations in the organic matter imply that even under the same thermal stress similar types of organic matter generate petroleum at different rates (di Primio and Horsfield, 2006). Kinetic studies have shown that the generalized kinetics consider neither the heterogeneous kinetic nature of the kerogen classes nor the organofacies variability in a source rock (Tegelaar and Noble, 1994; Peters et al., 2005b; di Primio and Horsfield, 2006). Therefore, default kinetic parameters increase uncertainties of petroleum generation modeling, which can be reduced by carrying out kinetic analyses of the organic matter from specific geological formations under study (di Primio and Horsfield, 2006).

The accurate assessment of the petroleum system requires a profound knowledge of its components i.e., the source rock, the carrier rock, and the reservoir (Magoon and Schmoker, 2000). Burial and basin modeling integrates those elements into the basin evolution and provides insights into the process of hydrocarbon generation, migration, and accumulation (Rodrigues Duran et al., 2013)

with the predictive scope of hydrocarbon generation in space and time, and with the direct consequence for hydrocarbon exploration (di Primio and Horsfield, 2006).

Secondary processes affecting rocks prone to petroleum formation, such as biodegradation, fractionation, and secondary cracking change the composition of the first-formed petroleum, obscuring its original characteristics, which constitutes a major challenge for organic matter characterization and source-oil and oil-oil correlations (Thompson, 1988; Dieckmann et al., 1998; Wenger et al., 2002). The assessment of secondary processes in oil well and oil seep samples may improve our understanding of their habitat at the source rock, the reservoir, or surface conditions (Dieckmann et al., 1998; Moldowan et al., 2015).

Furthermore, the study of the sedimentary organic matter contributes to reconstruct depositional environments (di Pasquo et al., 2015); it can help to resolve questions if organic matter was deposited in marine, lacustrine or fluvial systems or it may provide important clues for an assessment of paleogeographic conditions during deposition (Narváez and Volkheimer, 2011). This includes tectonic settings (Bohacs et al., 2000), questions regarding ocean connectivity (Marengo, 2006), as well as local climatic conditions (Quattrocchio et al., 2005). By establishing a direct link between specific precursors and the sedimentary organic matter, the concept of molecular typing and organofacies (Horsfield, 1997) by analyzing whole-rock samples thus provides valuable insights into the evaluation of depositional environments. Due to the genetic link between former organisms and petroleum (Radke et al., 1997), organic compounds (biomarkers) separated from rock extracts and oils offer pivotal information for depositional environment reconstruction (Fang et al., 2019; Peters et al., 2005a).

The first goal of this study was to reconstruct depositional environments and conditions for organic matter preservation and accumulation based on the characterization of the organic matter as geological archive. To reach this goal rock samples, oil seeps and produced oils were analyzed by geochemical, mineralogical and petrographic techniques. The second goal was to evaluate the factors that determine the petroleum potential, i.e., quantity, quality, and thermal maturity of source rocks at basin or sub-basin scale. An integral part of this goal was to predict the composition and physical properties of the first-formed petroleum of different organofacies of a regionally important petroleum-bearing unit in the morphotectonic provinces of NW Argentina (Fig. 1.1). The rocks analyzed in this thesis were collected from the Cretaceous Yacoraite Formation, which is associated with post-rift subsidence in a region that now is an integral part of the Cenozoic Andean orogen. This region is commonly referred to as the Salta Rift, an extensional province that was compressionally inverted during Andean mountain building, providing numerous outcrops of the Yacoraite Formation. Access to naturally generated oil on the surface (oil seeps) or from the subsurface (produced oil) is fundamental to such an undertaking, because their study allows the contribution of different source rocks to be defined and oil mixtures to be identified. An important challenge here is the assessment of secondary processes to unravel the original composition.

1.2 *Brief geological summary of the Cretaceous Salta Rift*

The geological evolution of NW Argentina is tightly associated with the formation of the Salta Rift basin and its subsequent sedimentary infill in the Cretaceous to the Early Cenozoic, followed by its later incorporation into the Andean orogenic belt in the Cenozoic (Mon and Salfity, 1995; Salfity and Marquillas, 1994; Montero-López et al., 2020). In the study area the rift basin is further sub-divided into the Olmedo, Tres Cruces, and Metán-Alemanía basins (Fig. 1.2a). The Cretaceous to Eocene Salta Group deposited in the sub-basins of the Salta Rift comprises the syn-rift Pirgua subgroup and the Balbuena and Santa Barbara post-rift subgroups (Salfity and Marquillas, 1994; Marquillas et al., 2005). Of particular interest is the organic-rich Yacoraite Fm. deposited during the Maastrichtian to Danian (Marquillas and Salfity, 1988; Stinco and Barredo, 2014), because in parts of the basin the Yacoraite Fm. is a prolific source rock for petroleum (Disalvo et al., 2002; Stinco and Barredo, 2014). The economic potential of the Yacoraite Fm. has been one of the driving forces to study its geological evolution because a good understanding of the processes and conditions during its deposition may contribute to improving exploration and production efforts.

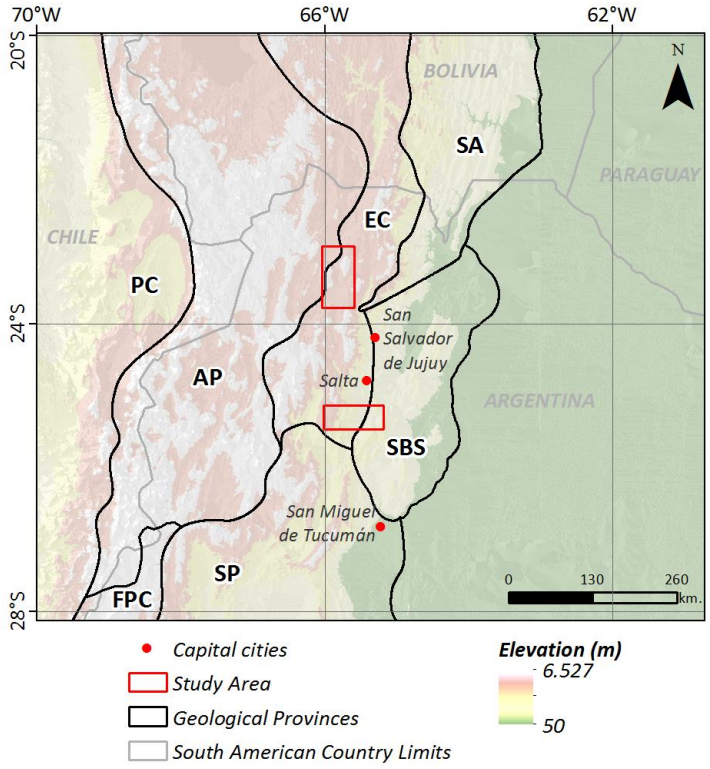

Fig. 1.1. Map of the southern central Andes showing the major geological provinces (after Jordan et al., 1983) and the study area in NW Argentina. PC: Principal Cordillera; FPC: Frontal-and Precordillera; AP: Atiplano- Puna plateau; EC: Eastern Cordillera; SP: Sierras Pampeanas; SBS: Santa Bárbara Systems; SA: Subandean

As a result of the different deformation styles, the NW Argentine foreland evolved as a broken foreland during the Cenozoic, deforming the Cretaceous strata (Jordan and Alonso, 1987; Strecker et al., 1989; Moretti et al., 1996; Monaldi et al., 2008), with far-reaching implications for hydrocarbon generation (McGroder et al., 2015; D'Ambrosio et al., 2021). As a consequence of this different geological evolution of the sub-basins that form the Salta Rift basin, the petroleum production mainly comes from the comparatively weakly deformed and deeper buried Lomas de Olmedo sub-basin

(Disalvo et al., 2002; Hernández et al., 2008; Grosso et al., 2013). The oil discoveries in the Tres Cruces, and Metán-Alemanía sub-basins are apparently not of commercial importance (Disalvo et al., 2002; Hernández et al., 2008). This factor has discouraged further exploration in this vast region of high tectonostratigraphic complexity and basin inversion (Jordan and Alonso, 1987; Kley et al., 2005; Iaffa et al., 2011; 2013; Arnous et al., 2020).

The hydrocarbon generation remains poorly understood in the broken and highly compartmentalized foreland incorporating the Tres Cruces and Metán-Alemanía sub-basins (Becker et al., 2015; Summa et al., 2015). Potential renewed oil exploration in the highly deformed Tres Cruces and Metán-Alemanía sub-basins, however, might benefit from the characterization of representative organofacies of the Yacoraite Fm. In addition, insights into the kinetics of the transformation of the organic matter in hydrocarbons, the prediction of the composition of the first-formed petroleum, and its physical properties may contribute to understand the habitat of hydrocarbons in this environment. In addition, this data may help to improve conceptual models on the thermal maturity of the Yacoraite Fm. that may integrate the effects of the uplift and formation of the orogenic Puna Plateau in the Andean interior (Summa et al., 2015).

Recent discoveries of the accumulation of petroleum in the Cretaceous lacustrine carbonates in the South Atlantic have triggered increased interest in their study in other regions of South America (Sallet et al., 2016; Herlinger et al., 2017). The efforts to understand the architecture and distribution of such facies are challenged by the limited access of subsurface samples (Muniz and Bosence, 2018). Stromatolites and bioclastic carbonates facies of the well-exposed Yacoraite Fm. are analogs of such oil-bearing carbonate facies of the South Atlantic (Deschamps et al., 2020) and, therefore represent a very important subject to be studied.

The characterization of the depositional environment of the Yacoraite Fm. has remained controversial as suggested by the different interpretations covering shallow marine and lacustrine settings (Marquillas et al., 2005; Sánchez and Marquillas, 2010; Narváez and Volkheimer, 2011; Roemers-Oliveira et al., 2015; Deschamps et al., 2020; Gomez et al., 2020). The decrease in extensional tectonic subsidence caused by superseding Andean uplift beginning during the Late Cretaceous (Urien et al., 1995; McQuarrie et al., 2005) might have affected the connectivity to the marine realm and may have severed potential connections with the Caribbean realm, which in turn influenced the depositional environment that may have transitioned from shallow marine and even lacustrine condition during the time when the Yacoraite Fm. was deposited (Sempere et al., 1997; Marquillas et al., 2005). However, the main pulses of the Andean orogeny occurred much later during the Late Eocene to Early Oligocene, Late Miocene, and Plio-Pleistocene and led to the structural inversion of the Tres Cruces and Metán-Alemanía sub-basins and other areas (Jordan and Alonso, 1987; Mon and Salfity, 1995; Salfity and Marquillas, 1999; Starck, 2011). Different interpretations of the depositional environment of the Yacoraite Fm. may reflect differences in the sub-basin history, or alternatively reflect the high

susceptibility of shallow-water depositional environments to tectonic and climatic changes (Kelts, 1988).

The depositional environments of the Yacoraite Fm. may also record global events including the rise of sea level during the Late Cretaceous, the K/T transition, as well as local climate changes and tectonics. Combined, these characteristics make NW Argentina an outstanding natural laboratory to study and characterize organic matter and to reconstruct depositional environments that led to important accumulations of organic-rich layers of the Yacoraite Fm. interesting as hydrocarbon georesources. The occurrence of oils seeps that denote the presence of active source rock in the Tres Cruces sub-basin, and the successful oil production in Lomas de Olmedo sub-basin make NW Argentina an outstanding natural laboratory to study the differences in burial histories and the organic matter from its deposition to its transformation in hydrocarbons. This effort is facilitated by easily recognizable and extraordinary outcrops of the Yacoraite Fm. in the Tres Cruces and Metán-Alemanía sub-basins and the amount of previous studies that have accumulated a rich sedimentary, structural, and geochronological database (for a review see Viramonte et al., 1984; Galliski and Viramonte, 1988; Salfity and Marquillas, 1999; Sánchez and Marquillas, 2010).

1.3 Brief geological summary

This dissertation aims to study the organic matter of the Yacoraite Fm. spanning from depositional environments to the transformation to petroleum. The research focuses on outcrop samples retrieved from the Tres Cruces and Metán-Alemanía sub-basins, oil seeps collected in the Tres Cruces and Lomas de Olmedo sub-basins, and produced oils from the latter sub-basin. The study integrates source rock analyses, field observations, and the geological evolution into a thermal model to unravel the burial history and thermal evolution of Yacoraite Fm. in the Tres Cruces sub-basin. The applied approach uses specific kinetic parameters of different organofacies of the Yacoraite Fm. to elucidate hydrocarbon generation, migration, and possible accumulation. For the first time, this dissertation also presents the prediction of the composition of first-formed petroleum from the Yacoraite Fm. and its physical properties. This analytical information is of high value to choose the targets for oil and gas resources and to allocate drilling logistics in the underexplored Tres Cruces sub-basin. Finally, the analysis of the organic geochemistry of the petroleum source rock also offers constraints on conceptual exploration models.

To cover the study of organic matter of the Yacoraite Fm. I organized this dissertation into the following structure: After introducing the Salta Rift basin in greater detail in Chapter 1, I describe the geological framework and the evolution of this basin from its Mesozoic origin to the Cenozoic when it became integrated into Andean mountain-building processes. Subsequently, I present in more detail the state-the-art of interpretations regarding the depositional environment of the Yacoraite Fm., with particular attention to similarities and differences between the different sub-basins. This enables me to place this research in the context of the carbon cycle, because source rocks and petroleum are important

sinks for carbon and our intense use of fossil fuels changes the dynamics of this cycle with far-reaching consequences. Chapter 2 describes in detail aspects from the sampling campaign to the analytical techniques used to analyze rock samples, rock extracts, oil seeps, and produced oils. In Chapter 3, I use organic compounds and minerals to characterize the depositional environment of Yacoraite Fm. in the Tres Cruces and the Metán-Alemanía sub-basins. I use proxies to constrain the maximum depth, salinity and evaluate the conditions for organic preservation. Here, I establish the foundations for source-oil correlations.

In Chapter 4, I present the maturity assessment of samples of the Yacoraite Fm. and compare it to mineral assemblages. This chapter presents the organofacies variability of the Yacoraite Fm., which influences the composition of the first-formed petroleum and its physical properties. This chapter also analyzes the effects of minerals and radiation on the organic parameters to assess the thermal maturity and petroleum potential of the Yacoraite Fm. In Chapter 5, I analyze organic compounds isolated from oil seeps collected in the Tres Cruces and Lomas de Olmedo sub-basins and from produced oils. I interpret the depositional environmental characteristics of the source rocks of these oils. In the absence of rock samples from Lomas de Olmedo, I establish genetic relations of those oils to the Yacoraite Formation based on the characterization of this formation that I presented in Chapter 3. In Chapter 6, based on the chain-length distribution of the pyrolysates of Yacoraite Fm. I characterize the composition of its first-formed petroleum. In addition, I use the PhaseKinetics approach (di Primio and Horsfield, 2006) that integrates the evolution of the composition of hydrocarbons at different laboratory-transformation rates into bulk kinetics to predict the physical properties i.e., the gas to oil ratio (GOR), the saturation pressure (Psat) and volumetric factor (Bo) of the hydrocarbons that the Yacoraite Fm. can generate. In Chapter 7, I evaluate the petroleum generation of the Yacoraite Fm. using a basin modeling approach that integrates kinetic analyses on selected organofacies. I use regional studies to define lithology and thickness of the stratigraphic succession and constrain the evolution of heat flow. Finally, in Chapter 8, I summarize the most important achievements regarding the depositional environment of the Yacoraite Fm., its petroleum potential, and suggest areas for future research.

1.4 Characteristics of the Salta Rift basin

Today, the Cretaceous Salta Rift basin is primarily located in the Andes and their foreland of NW Argentina, close to the international borders with Bolivia and Chile (Fig. 1.2a). It extends over 53.000 km^2 in NW Argentina (Stinco and Barredo, 2014), and is part of an extensional basin which developed in the Cretaceous as an intracratonic rift controlled by regional zones of crustal weakness (Hongn et al., 2011; Rossello and López de Luchi, 2005) parallel to the Pacific border of the South American continent (Starck, 2011). The Cenozoic sub-Andean basins in Bolivia, Argentina, and Perú were superposed on these extensional sub-basins and record the transition from thermal subsidence during the final stages of extensional tectonic processes to subsidence associated with thrust loading

during Andean mountain building (Mon and Salfity, 1995; Starck and Vergani, 1996; Cristallini et al., 1997; Rubiolo, 1999; Becker et al., 2015).

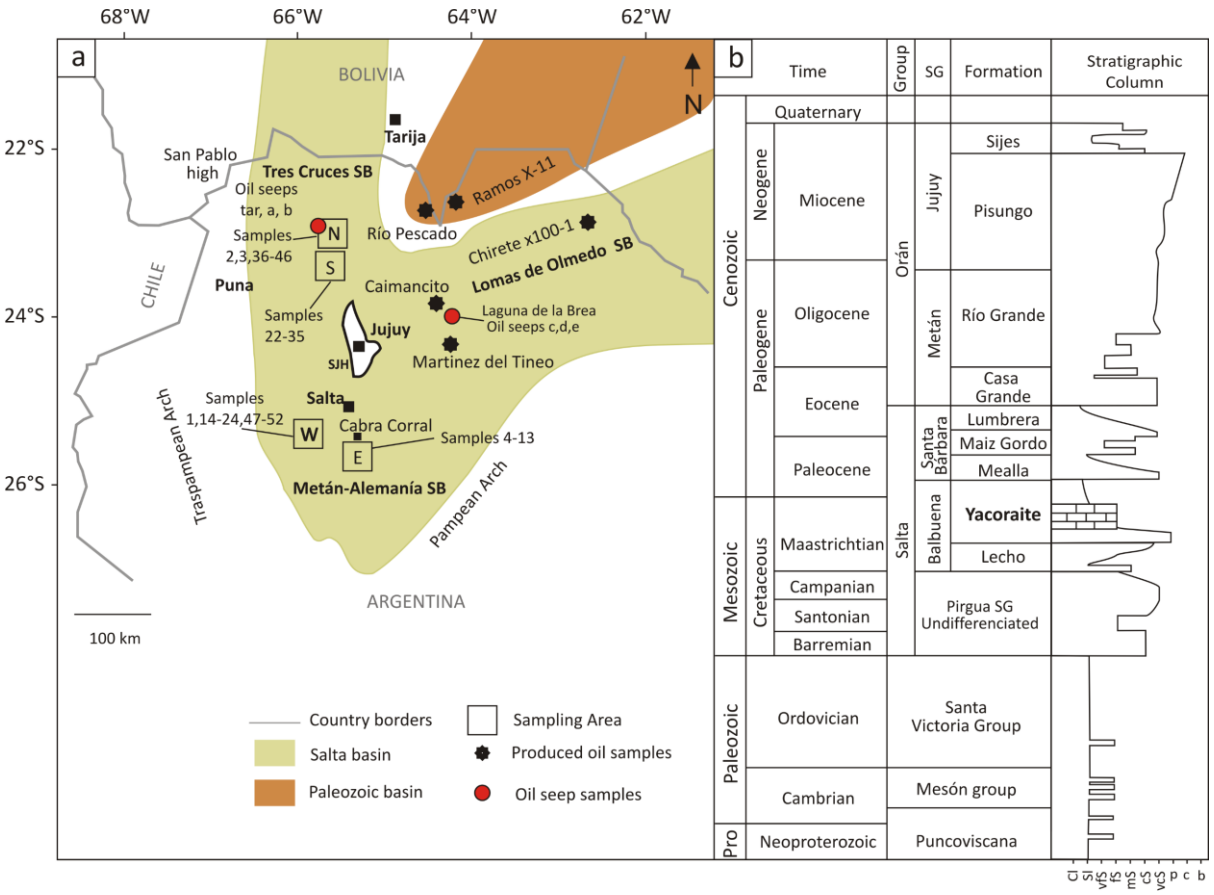

Fig. 1.2. Map of the Salta Rift basin in NW Argentina and sampling locations. (a) Distribution of the Salta Rift basin and the Paleozoic basin, after Disalvo (2002); Marquillas et al. (2005) and Legarreta and Villar (2011). SJH: Salta-Jujuy High. Red squares indicate sampling locations where rocks and oil seep samples were collected. (TC) Tres Cruces, (MA) Metán-Alemanía sub-basins. The sectors where samples were collected are north, south (N, S) and east and west (E, W). The location of the oil fields and wells is indicated by black dots. (b) The stratigraphic nomenclature and the stratigraphic column in the Tres Cruces sub-basin are based on Boll and Hernández (1986), Marquillas et al. (2005) and Sánchez and Marquillas (2010).

1.5 Geological background and tectonic evolution of the Salta Rift basin

The Salta Rift basin is divided into three main depocenters (Fig. 1.2a). The Tres Cruces sub-basin with northwest-southeast orientation, the combined Metán-Alemanía sub-basin with southeast-northwest direction, and the Lomas de Olmedo sub-basin with east-west orientation (Disalvo et al., 2002; Marquillas et al., 2005; Hernández et al., 2008). These halfgrabens are arranged in a "Y" shape in map view (Starck, 2011), radiating from an inferred triple junction (Burke and Dewey, 1973) marked by the Salta-Jujuy High (Marquillas et al., 2005). Although initially isolated, those sub-basins finally coalesced during the late-stage of basin evolution (Mon and Salfity, 1995).

Because of its structure, coeval magmatism, and sedimentary facies distribution, the Salta basin is classified as a rift basin (Grier et al., 1991; Salfity and Marquillas, 1994), whose erosional and sedimentary processes, as well as magmatism were controlled by extensional tectonics and the associated changes of topography and relief over time (Viramonte et al., 1984; Galliski and Viramonte,

1988; Mon and Salfity, 1995; Marquillas et al., 2005). The Salta Rift basin evolved during the Early Cretaceous due to the extensional forces acting on the South American continental plate associated with the combined effects of the opening of the South Atlantic and coeval Pacific subduction, which ultimately resulted in the formation of normal-fault bounded basins, high topography associated with horst blocks, volcanic flows and magmatic intrusions (Alvarez, 1999 and references therein; Starck, 2011).

The extensional processes started in the south and propagated northward, thus forming a basin which extends into Bolivia and possibly into northern Chile, while the Lomas de Olmedo sub-basin extends into Paraguay (Salfity and Marquillas, 1994; Kley et al., 2005). Synchronous to extensional faulting, which caused thinning and heating of the lithosphere, there is evidence for regional uplift of pre-rift sediments during that time (Becker et al., 2015). In the north and west sector of the Lomas de Olmedo sub-basin, this uplift caused pronounced erosion of footwall areas of the extensional blocks, estimated to have been between 3.5 and 5 km. The eroded sediments filled the accommodation space created by the coeval hanging-wall subsidence, forming a sedimentary fill intercalated with or cross-cut by mafic volcanics (Galliski and Viramonte, 1988; Salfity and Marquillas, 1994). Subsequently, cooling and subsidence of the extended and heated crust generated additional accommodation space for the deposition of sediments during the subsequent Paleogene post-rift phase (Starck, 2011).

During the Cenozoic Andean orogeny, which has been active until the present-day, the basin and the basin-bounding faults have been affected by shortening, especially during the Late Eocene to Early Oligocene, Late Miocene and Plio-Pleistocene. These episodes have been informally grouped into the Inca, Quechua, and Diaguita deformation, respectively (Jordan and Alonso, 1987; Mon and Salfity, 1995; Salfity and Marquillas, 1999). The Inca phase represents the onset of the Andean deformation that started west of the current Central Andes at 46 Ma (Oncken et al., 2006) and which produced little structural deformation (Salfity and Marquillas, 1999). The deformation propagated into the Tres Cruces region immediately south of the Bolivia-Argentina border (Coutand et al., 2001), successively creating a broken-foreland basin (Rubiolo, 1999; Montero-López et al., 2020), which was subsequently involved in a regional, thermally driven uplift event that generated the Altiplano-Puna Plateau (Garzione et al., 2017). After Tibet, the Puna Plateau in the center of the orogen is the Earth's second largest orogenic plateau; to the west it is bounded by the volcanic arc of the western Cordillera, to the east it is bounded by the thick-skinned thrust belt of the Eastern Cordillera (Jordan et al., 1983; Allmendinger et al., 1983).

During the Quechua phase (15-10 Ma), the Puna region was shortened and thickened (Coutand et al., 2001) due to convergence between the oceanic Nazca and the continental South American plates (Martinod et al., 2010), which have continued to influence the tectonics of South America until the present day. The overall deformation style was characterized by isolated range uplifts that generated a broken foreland and due to the increased aridity in the lee of the developing orographic barriers, the intermontane basins became structurally and hydrologically isolated (Coutand et al., 2001), often associated with the structural inversion of the normal faults bounding the different sub-basins of the

Salta Rift (Salfity and Marquillas, 1999; Kley et al., 2005). During the Diaguita phase (ca. 2.5 Ma), the Andean orogeny folded the sequences of Cretaceous-Cenozoic deposits and continued breaking these units during uplift aided by reverse faults that were inverted former normal faults bounding the sub-basins of the Salta Rift (Salfity and Marquillas, 1999; Salazar et al., 2009). The Tres Cruces and the Metán-Alemanía sub-basins were strongly affected by these processes. The Lomas de Olmedo sub-basin farther northeast, however, was affected to a lesser degree (Starck, 2011), which is documented in its western sector by minor occurrences of eroded clasts from the Yacoraite Fm. that are found in the Late Miocene to Early Pliocene Piquete Fm. (Salfity and Marquillas, 1999).

1.6 Cretaceous to Cenozoic basin fill of the Salta Rift

Sedimentation in the Salta Rift basin started during the Early Cretaceous and continued until the Paleogene (Marquillas et al., 2005) in sub-basins with different degrees of subsidence (Starck, 2011). During sedimentation magmatic events occurred during the Early Cretaceous, Late Cretaceous, and finally at the end of sedimentation in the Paleogene (Galliski and Viramonte, 1988). The sedimentary rocks associated with the Salta Rift are known as the Cretaceous to Eocene Salta Group (Fig. 1.2b). The Salta Group is divided into the Pirgua, Balbuena, and Santa Bárbara subgroups. The Pirgua subgroup represents the deposits of the syn-rift stage (Marquillas et al., 2005), while the other two subgroups were deposited during the post-rift thermal subsidence (Salfity and Marquillas, 1994; Marquillas et al., 2005). In the Metán-Alemanía sub-basin the basement rocks consist of Neoproterozoic phyllites of the Puncoviscana Formation, while in the Tres Cruces and the Lomas de Olmedo sub-basins the exposed basement units comprise pelites and sandstones of the Lower and Upper Paleozoic (Marquillas et al., 2005) Mesón and Santa Victoria groups (Turner, 1964).

The Pirgua subgroup was deposited between the Early Cretaceous and the Early Maastrichtian (Sabino, 2004; Marquillas et al., 2005) and covers the Neoproterozoic basement rocks. The Pirgua subgroup is divided into La Yesera, Las Curtiembres, and Los Blanquitos formations. The La Yesera Fm. is characterized by basal conglomerates and at the top by sandstones and pelites that were deposited in fluvial fans and braided rivers. Except in the Tres Cruces sub-basin, the Las Curtiembres Formation consists of red/green/gray pelites and thin sandstone bodies deposited in a widespread freshwater-to-brackish, shallow lacustrine depositional environment (Marquillas et al., 2005). The final syn-rift Los Blanquitos Fm. is characterized by a succession of medium- to coarse-grained sandstones in the middle and conglomerates in the upper section, deposited by rivers on whose banks carbonate-bearing paleosoils formed due to semi-arid climate conditions (op.cit.).

During the Maastrichtian and the Early Paleocene post-rift phase, sediments of the Balbuena subgroup filled the accommodation space formed in the post-rift phase by thermal subsidence (Iaffa et al., 2011). The Balbuena subgroup consists of the Lecho Fm., the Yacoraite Fm., and the Olmedo/Tunal Fm. The onset of deposition of the Late Cretaceous Lecho Fm. occurred in a lacustrine environment that transitioned into a distal braided-river environment. In the Tres Cruces and the Metán-Alemanía

sub-basins, the Lecho Formation is composed of fine-grained sandstones, limestones, shales, and claystones (Marquillas et al., 2005; Sánchez and Marquillas, 2010). In the Tres Cruces sub-basin, the Yacoraite Fm. starts with a fining-upward succession grading from conglomerates to sandstones and siltstones deposited during flooding, followed by oolitic limestones, grainstone, packstone, wackestone, mudstone, and stromatolite layers. Minor occurrences of sandstone and calcareous concretions are also reported (Hernández et al., 2008; Sánchez and Marquillas, 2010).

Marquillas et al. (2007) distinguished four members for the Yacoraite Fm. in the Metán-Alemanía sub-basin. From the bottom to the top these are: The Amblayo Member at the base, which is composed of dolomitic limestones, followed by sandstones and limestones of the Güemes Member. These strata are superseded by the Alemanía Member, which is characterized by dolomitic limestone and siltstones. These units are overlain by the stromatolitic Juramento Member at the top. In the Lomas de Olmedo sub-basin, a transgressive surface identified by electric well-log data characterizes the onset of the deposition of the Yacoraite Fm. over the underlying Lecho Fm. This contact is also characterized by an increase in radiogenic elements as indicated in the gamma-ray logs (Starck, 2011). High uranium contents have been reported at the base of the Yacoraite Fm. in the Metán-Alemanía sub-basin. The uranium is thought to be sourced from the granitic basement rocks of the Pampean and Traspampean Arches (Salfity and Marquillas, 1999; Ferreira et al., 2013).

In the Lomas de Olmedo sub-basin, the Yacoraite Fm. has been divided into two members based on well-log data: the Puesto Guardian and the Las Avispas members separated by a siltstone/claystone section. Petrographic analyses in a core from the Caimancito xp-4 well (Fig. 2) show that the Puesto Guardian Member consists of packstones and wackestones. The Las Avispas Member is composed of medium- to coarse-grained oolitic grainstones, thin layers of bioclastic grainstone, and mudstone. Extensive dolomitization of carbonates was also observed in this member (Grosso et al., 2013). The Late Danian Olmedo Fm., which is well expressed in the Lomas de Olmedo sub-basin, is composed of evaporitic sediments containing gypsum and micrite and grey/black shales deposited under anoxic conditions in a hypersaline lake indicating arid conditions (Marquillas et al., 2005; Starck, 2011). The Olmedo Fm. is the lateral equivalent of the Tunal Fm. in the Metán sub-basin, which was deposited in a perennial lake with restricted circulation under less evaporitic conditions compared to the conditions that prevailed in the northern basins (Marquillas et al., 2005).

The post-rift stage in the Middle Paleocene is represented by the strata of the Santa Bárbara subgroup (Alvarez, 1999), which is divided into the Mealla, Maíz Gordo and Lumbrera formations. Towards the center of the Salta Rift basin, the Santa Bárbara subgroup was deposited in lacustrine environments, while coeval fluvial depositional environments had developed towards the margins of the basin (Marquillas et al., 2005). In the Tres Cruces sub-basin, the lower section of the Mealla Fm. consists of a fining-upward succession from conglomerates to siltstones with paleosoils. Its upper part above the hiatus is a coarsening-upward sequence evolving from siltstones to fine-grained sandstones.

These units are associated with deposition in a fluvial system with sinuous channels developed on a low-slope alluvial plain (Sánchez and Marquillas, 2010). At the eastern margin of the Metán-Alemanía sub-basin, the exposed Mealla Fm. is composed of a fining-upward succession from fine- to medium-grained sandstones deposited in an environment with meandering rivers (Marquillas et al., 2005; Starck, 2011 and references therein). The Mealla Fm. in the Lomas de Olmedo sub-basin is composed of stromatolitic limestones, shales, and marls that dominate towards the top and that were deposited in a shallow brackish, closed lacustrine environment (Ramos et al., 2006 and references therein; Starck, 2011).

The Maíz Gordo Fm. in the Tres Cruces sub-basin is composed of coarse- to fine-grained sandstones, including dispersed Cambrian quartzite clasts deposited in fluvial channels with intercalations of fine-grained sandstones and the presence of paleosoils with carbonate concretions (Sánchez and Marquillas, 2010). In the western sector of the Metán-Alemanía sub-basin, the Maíz Gordo Fm. consists of coarse- to fine-grained sandstones that are interpreted to have been deposited in a braided-river environment. In the eastern sector of the Metán-Alemanía and the Lomas de Olmedo sub-basins, three sections of the Maíz Gordo Fm. can be distinguished. Siltstones and fine-grained sandstones form the base, carbonates the middle section, while an erosive base indicates the beginning of the upper section. The upper section consists of green shale, mudstones, grainstones, and oolitic packstones deposited in a lacustrine setting (Marquillas et al., 2005).

Another erosive contact separates the Maíz Gordo Fm. from the Lumbrera Fm. in the Tres Cruces sub-basin. There, the Lumbrera Fm. is composed of conglomerates at the base, which gradually change to sand- and siltstones towards the top deposited in a muddy-sandy plain environment under semi-arid conditions (Sánchez and Marquillas, 2010). In the Lomas de Olmedo sub-basin, the Lumbrera Fm. is mainly composed of marls (Ramos et al., 2006). In the Metán-Alemanía sub-basin, red siltstones, sandstones, and conglomerates characterize this unit (Starck, 2011). To the east in this sub-basin, an erosive episode must have removed the Lumbrera Fm. as Neogene units directly cover the Maíz Gordo Formation (Starck, 2011). The Maíz Gordo formation was deposited during the transition from the active extensional tectonic conditions (i.e., Salta subgroup) and thermal basin subsidence to the beginning of compressional tectonics related to the Andean orogeny (Starck, 2011).

The processes that led to the sedimentary fill of the Salta Rift basin ended in the Late Eocene to Early Oligocene with the onset of the Incaic phase of deformation, which caused a diachronous and spatially disparate basin inversion (Marquillas et al., 2005; Carrera et al., 2006; Monaldi et al., 2008 and references therein). The time and magnitude of inversion varied throughout the Salta rift sub-basins, being rather limited in the Lomas de Olmedo sub-basin and more extensive in the Metán-Alemanía and the Tres Cruces sub-basins (Starck, 2011; Grier et al., 1991).

In the Tres Cruces sub-basin, the Cretaceous sequence is covered by 5000 m of Cenozoic sediments, namely the Casa Grande, the Río Grande, the Pisungo and the Sijes formations (Boll and Hernández, 1986). The oldest two units were deposited in a foreland basin from the Middle Eocene to

the Middle Miocene (Bond and López, 1995; Herrera et al., 2012). The Casa Grande Fm. was conformably deposited on the Lumbrera Fm. The Casa Grande Fm. is composed of up to 800 m of sandstones, calcareous siltstones, lenses of fine-grained conglomerate and conglomeratic sandstones, deposited in alluvial fans and ephemeral streams (Boll and Hernández, 1986). The Río Grande Fm. consists of 1800 m of conglomerates and sandstones deposited in meandering and anastomosing rivers (Boll and Hernandez, 1986). Between 750 m to 2500 m of fluvial conglomerates and sandstones the Pisungo Fm. (Late Miocene?) overlies the Río Grande Fm. unconformably (Boll and Hernandez, 1986). An angular unconformity separates the Sijes Fm. (Pliocene?) from the Pisungo Fm. The Sijes Fm. consists of 120 m of sandstones, conglomerates, and calcareous siltstones deposited in anastomosing rivers intercalated with volcanic tuffs.

1.7 Facies and depositional environments of the Yacoraite Formation

The marine strata of the Yacoraite Fm. record the last Mesozoic marine transgression at the end of the Cretaceous (Marquillas et al., 2007) that was associated with long-wavelength, regional thermal subsidence during the post-rift stage (Sempere et al., 1997; Becker et al., 2015) and global sea-level rise (Alvarez, 1999; Salfity and Marquillas, 1999). The transgressive and regressive episodes recorded in this unit were probably linked to Milankovitch cycles (Uliana et al., 2014 and references therein). Humid conditions generally prevailed during the deposition of the Yacoraite Fm. (Marquillas et al., 2005).

The marine transgression into the region of NW Argentina and Bolivia has been discussed in a Pacific and Atlantic context (França et al., 1995; Rossello and Mozetic, 1999; Marquillas et al., 2005; Marquillas et al., 2011). A Pacific transgression from the west is considered unlikely because the Cordillera de la Costa of Chile was already an area of high topography by Cretaceous time (Marquillas et al., 2011), making a marine connection unlikely. In addition, the Late Cretaceous sedimentary deposits in northern Chile correspond to a depositional environment that was dominated by alluvial fans (e.g., Hartley, 1993), which therefore points to the absence of such a corridor and connectivity with the Pacific (Marquillas et al., 2005; Marquillas et al., 2011). However, an alternative connection with the Pacific could have existed through Perú and Bolivia (França et al., 1995; Rossello and Mozetic, 1999), as suggested by similar facies of sedimentary units there that show some affinity with the Yacoraite Fm. These are the upper Vilquechico Fm. in Perú and the El Molino Fm. in Bolivia (Marquillas and Salfity, 1988; Marquillas et al., 2011). Additional correlations between the Yacoraite Fm. and the El Molino Fm. of Bolivia are supported by the presence of fish fossils (Leanza, 1969).

An Atlantic transgression from the south through the Chaco-Paraná basin has also been deemed unlikely due to micropaleontological studies (Marengo, 2006). Yet, similar facies were encountered in the Mariano Boedo Fm., but this unit was deposited during the Late Oligocene to Miocene (op. cit.). This age is much younger than the depositional age of the Yacoraite Fm. (Marquillas et al., 2011 and references therein). The most likely connectivity of an epicontinental sea with the world's oceans during

the deposition of the Yacoraite Fm. existed between this part of South America and the Caribbean (e.g., Sempere et al., 1997; Marquillas et al., 2005). During the marine transgression, the Salta-Jujuy high was almost completely covered by sediments generated in this shallow sea (Marquillas and Salfity, 1988). The existence of such a marine corridor is not only supported by similar lithofacies at a regional scale, but also by marine faunas found in Colombia, Ecuador, Perú, and Bolivia (Marquillas et al., 2005; Marquillas et al., 2011). Dinosaur tracks suggest transient low water-level and transient terrestrial conditions (Meyer et al., 2001).

In the Tres Cruces sub-basin, the depositional environments were continental to marine littoral (Sánchez and Marquillas, 2010). Stable carbon and oxygen isotopic compositions of carbonates from the Yacoraite Fm. (Marquillas et al., 2007), strontium isotope data (Terra et al., 2012), the fossil assemblage represented by gastropods and fishes (Cónsole-Gonella et al., 2012), and palynoflora support a marine environment (Narváez and Volkheimer, 2011). This marine environment was influenced by brackish and freshwater conditions (Sánchez and Marquillas, 2010., Narváez and Volkheimer, 2011) developed in a protected lagoonal and supratidal zone, respectively (Sánchez and Marquillas, 2010). Based on lithofacies analysis, a lacustrine depositional environment was interpreted for the strata of the upper section of the Yacoraite Fm. (pers. Comm. M. Vallati, 2019).

In the Lomas de Olmedo sub-basin strontium-isotope data also suggest a marine depositional environment during the deposition of the Yacoraite Fm. (Terra et al., 2012). The occurrence of charophytes, indicative of the development of local brackish conditions in this sub-basin (Marquillas et al., 2005 and references therein), however, suggests recurring changes between freshwater and saline depositional environments. In the Metán-Alemanía sub-basin, the marine character of the depositional environment with the development of brackish environments was interpreted based on palynoflora and sedimentology analyses (Narváez and Volkheimer, 2011). In this sub-basin, Marquillas et al. (2007) divided the Yacoraite Fm. in four members: the Amblayo, Güemes, Alemanía and Juramento members. The basal Amblayo and the Alemanía members were deposited in a marine environment. The Güemes Member was deposited under the influence of continental conditions and the Juramento Member documents the gradual transition into a freshwater depositional environment (op. cit.). Deposition in lacustrine environments is not explicitly mentioned in these earlier studies.

Lacustrine environments were interpreted for this sub-basin based on strontium-isotope analyses carried out on the limestone facies (Terra et al., 2012), lithofacies analyses (Deschamps et al., 2020), and microbial filaments in stromatolites in the Cabra Corral dam area southeast of Salta (Roemers-Oliveira et al., 2015), where lacustrine environments were specifically interpreted for the upper part of the Yacoraite Fm. based on sedimentological information focused on clay mineralogy (Gomez et al., 2020). From the middle through the youngest deposits of the Yacoraite Fm. marine conditions again prevailed (Marquillas et al., 2007).

The marine ingression during the onset of the deposition of the Yacoraite Fm. was coeval with stratal evidence for the effects of a local regression in the eastern and western sectors of the Metán-

Alemanía sub-basin. These changes were most likely associated with the structural evolution of the Pampean and Traspampean arches, respectively, and the ensuing erosion affecting the strata of the Pirgua subgroup (Salfity and Marquillas, 1999). The change in lithology from green and black shales at the base of the Yacoraite Fm. to oolitic sandstones and stromatolites towards the top tracks the marine regression in the Yacoraite Fm. Particularly in the Metán-Alemanía sub-basin, desiccation cracks and dinosaur tracks are unambiguous evidence of a sedimentary cycle with diminishing water depths that finally ended in the Late Cretaceous to Early Paleocene (Alonso, 1980., Marquillas et al., 2005).

Besides sea-level changes, the shallow marine environment was affected by the effects of a dry climate (Marquillas et al., 2005) that led to the development of hypersaline conditions and the deposition of thin levels of gypsum, as well as the formation of halite pseudomorphs (Uliana et al., 2014 and references therein). Importantly, and relevant for the topic of this thesis, the organic-rich black shales of the Yacoraite Fm. are petroleum-source rocks (Disalvo et al., 2002; Stinco and Barredo, 2014; Uliana et al., 2014). For the formation of organic-rich sediments not only high productivity is needed, but the existence of anoxic conditions is an additional key factor as it allows the preservation of sediments rich in organic material (Tissot and Welte, 1984; Littke et al., 1997).

1.8 Aspects of the petroleum system in NW Argentina

Naturally occurring heavy oils were already reported in the north of the Salta Rift basin in the 18th century and the prospection and production began in the 19th century (Yrigoyen, 2007). The presence of oil seep samples was detected in the Quebrada Galarza, Lomitas, Barro Negro, Mina Aguilar, Laguna de la Brea and Arroyo Garrapatal. In addition to open-pit exploitation at the latter two sites, there were successful efforts to extract petroleum from the shales of the Yacoraite Fm. nearby Rosario de la Frontera (Starck, 2011). This was known as the “El emprendimiento de Lola Mora” operated by the sculptor Lola Mora who sought to raise money to supplement her income from artwork (Alonso, 2018).

The Yacoraite Fm. is one of the main source rocks in the Salta Rift basin. Its organic matter content varies considerably with total organic carbon (TOC) ranging from 0.1-12% (Disalvo et al., 2002), and with S2 (hydrocarbon compounds released by thermal degradation of kerogen) ranging from 6-60 mg HC/g rock, a Hydrogen Index (HI) between 300-750 mg HC/g TOC (Stinco and Barredo, 2014), and kerogen type II-III as the main organic constituents (Stinco and Barredo, 2014; Uliana et al., 2014).

The maturity of the Yacoraite Fm. varies considerably between the different sub-basins. In the Lomas de Olmedo sub-basin, which is the main oil-producing area, the Yacoraite Fm. is currently located in the wet-gas window (Disalvo et al., 2002). The Yacoraite Fm. is immature to early mature in the Metán-Alemanía and Tres Cruces sub-basins (Disalvo et al., 2002; Stinco and Barredo, 2014), where only small amounts of hydrocarbons were found in a limited number of wells (Alvarez, 1999). The higher thermal maturity in the Lomas de Olmedo sub-basin is the result of more pronounced subsidence

and burial by Cenozoic rocks, such as the Orán Group (Ramos et al., 2006) as well as its less pronounced tectonic inversion compared to the other sub-basins (Grier et al., 1991).

The Lomas de Olmedo sub-basin is the most oil-productive sub-basin, followed by the Metán-Alemanía sub-basin in the south, while in the Tres Cruces sub-basin no accumulations of commercial interest were found (Disalvo et al., 2002; Hernández et al., 2008). Oils produced from the Lomas de Olmedo sub-basin were sourced from shales and proximal carbonates (Hernández et al., 2008). Oil and gas have mainly been retrieved from structural traps and stratigraphic reservoirs with primary or secondary porosity in which the Yacoraite Fm. is the main reservoir (Mon and Salfity, 1995., Salfity and Marquillas, 1999; Disalvo et al., 2002; Grosso et al., 2013).

Structural traps mainly consist of anticlines created during the compressive Cenozoic Andean deformation which fractured carbonates and sandstones (Disalvo et al., 2002; Grosso et al., 2013). These fractures host significant amounts of petroleum; this is the case at Caimancito, located in the western sector of the Lomas de Olmedo sub-basin, which is the most productive block in the Salta Rift basin (Salfity and Marquillas, 1999; Disalvo et al., 2002; Hernández et al., 2008). This single block contains half of the accumulated oil in the region and has produced nearly 10 Mio m^3 oil (Grosso et al., 2013). In this block the estimated amount of oil within the Yacoraite Fm. is 24.4 Mio m^3, with 42°API and a volume factor (Bo, defined as oil volume ratio at reservoir conditions to that at the surface) of 2.23 m^3/Sm^3 (Grosso et al., 2013). Fractured reservoirs are also found in the Cuchuma oil field in the Metán-Alemanía sub-basin, the Valle Morado gas field, and the Lumbrera oil field (Disalvo et al., 2002).

The reservoirs with primary porosity mainly consist of sandstones of the Yacoraite Fm. in the Yacarecito, El Vinalar del Norte, Climaco, Pozo Escondido, Cañada Grande, La Bolsa, dos Puntitas (Disalvo et al., 2002), Puesto Guardián and El Divisadero Sur oil fields (Alvarez, 1999). Other reservoirs of this type are the sandstones of the Paleocene Maíz Gordo, the Eocene Lumbrera Fm. of the Santa Bárbara subgroup (Hernández et al., 2008; Grosso et al., 2013), and andesites (Cesaretti et al., 2000) with porosity up to 25% at the oil fields of Palmar Largo in the eastern sector of the Lomas de Olmedo sub-basin (Alvarez, 1999). Diagenesis has produced secondary porosity by dissolving carbonates in oil fields of which Puesto Guardián is the most important (Disalvo et al., 2002). The Olmedo Fm. provides the seal for the accumulated oil in the fractured reservoirs of the Yacoraite Fm., while this formation itself provides the seal for the accumulated oil in its sandstones (Mon and Salfity, 1995., Disalvo et al., 2002). Claystones of the Maíz Gordo and Lumbrera formations are suitable as stratigraphic reservoirs (Marquillas et al., 2005; Hernández et al., 2008) as documented in the Caimancito block (Grosso et al., 2013).

In the Lomas de Olmedo sub-basin, hydrocarbons have variable compositions ranging from gas condensates at the Pozo Escondido to heavy oils in the Martinez del Tineo area (Disalvo et al., 2002). Fluid inclusions in different levels of the Yacoraite Fm. have also variable oil compositions. In samples from the Pozo Escondido well, heavy and asphaltic oils were trapped in the lower section of the

Yacoraite Fm. (Cesaretti et al., 2000). Lighter paraffinic and gaseous hydrocarbons, i.e., methane, ethane, and propane, were trapped in the upper section of this formation. These pronounced compositional differences were attributed to the effects of fractionation during primary migration; in such a scenario the oil may have migrated into sandstone reservoirs, where it was further degraded thermally, causing the bitumen to fill spaces (Cesaretti et al., 2000).

Besides the Yacoraite Fm., the Silurian Kirusillas and the Devonian Los Monos formations are additional source rocks in NW Argentina (Cruz et al., 2002; Cruz et al., 2008; Hernández et al., 2008; Legarreta and Villar, 2011; Stinco and Barredo, 2014; Uliana et al., 2014) that are relevant for the topics addressed in this dissertation. Those formations were deposited in the Paleozoic sedimentary basin that underlies the Cenozoic sub-Andean fold-and -thrust belt in the south of Bolivia and in the extreme north of Argentina (op. cit.). In Bolivia, the Kirusillas Fm. has a TOC content of about 0.5%, and in some exceptional cases, over 1%, and has a gas-prone character (Cruz et al., 2002). In the Lomas de Olmedo sub-basin, this formation has not been reached by wells (Uliana et al., 2014), which prevents its geochemical characterization. Additionally, due to adverse timing between generation/migration and trap formation, it is unlikely that oils sourced from the Kirusillas Fm. have been accumulated and contribute to the current production of conventional hydrocarbons in the sub-Andean basins of NW Argentina (Uliana et al., 2014).

The organic-matter content of the Los Monos Fm. varies from 0.5 % to 1 % TOC, and rarely exceeds values of >1.5 % (Stinco and Barredo, 2014). The organic matter is composed of Type II (algal-amorphous kerogen), Type III, and Type IV kerogens (Legarreta and Villar, 2011). Type II/III mixtures have also been reported (Cruz et al., 2008; Legarreta and Villar, 2011). The source-rock quality has been reported as being poor to fair, and mainly gas-prone (op. cit.). The relatively low organic-matter content is associated with strata of significant thickness between 500-1000 m and wide areal extent (Uliana et al., 2014). In the Lomas de Olmedo sub-basin, the unit is in the oil window with increasing thermal maturity westward and reaching the wet gas-condensate window (Legarreta and Villar, 2011).

Due to low organic-matter content and kerogen type, the expulsion of hydrocarbons from the Los Monos Fm. likely starts at a vitrinite-reflectance equivalent in the range from 0.9 % Ro to 1.0 % Ro (Cruz et al., 2008; Uliana et al., 2014). Rock samples equivalent to the Los Monos Fm. taken from wells drilled in NW Argentina display a higher degree of maturity at shallower depths compared to adjacent regions of Bolivia (Cruz et al., 2002). Although values were not provided, Cruz et al. (op. cit.) postulated a southward-increasing heat flow for the Paleozoic Basin, because these areas appear to have had the same tectonic evolution (Cruz et al., 2002; Monaldi et al., 2008; DeCelles et al., 2011).

1.9 The Carbon cycle in the Earth system and petroleum generation

Petroleum is a mixture of hydrocarbons, i.e., compounds that exclusively consist of carbon and hydrogen, such as saturated and aromatic hydrocarbons. Other chemical elements, such as nitrogen, sulphur or oxygen can be also present such as in the case of resins and asphaltenes (Tissot and Welte,

1984). As the Yacoraite Fm. was an important carbon sink during the Cretaceous I will briefly review the characteristics of the carbon cycle. More specifically, I briefly summarize the processes governing the composition and occurrence of organic matter in sedimentary environments, as well as its role as a source of petroleum. In the context of the carbon cycle, petroleum and its precursors are a major sink for carbon (Zhu et al., 2016), and due to the intensive use of fossil it has a major impact on society today and in the future (Abas et al., 2015).

1.9.1 The Carbon cycle

The carbon cycle refers to the connectivity between different processes in which this element adopts a variety of forms in chemical compounds while changing its molecular pairing with other compounds with the different compartments in the Earth system. These include the hydrosphere, the atmosphere, the biosphere, and the lithosphere - and the exchange across spheres through cycling and recycling over different timescales (e.g., Canuel and Hardison, 2018). The carbon atom constitutes the major element in organic compounds, but it is also ubiquitous in inorganic compounds. Chemical bonds in organic compounds are typically covalent, while ionic bonds dominate inorganic compounds. As a highly distinctive feature, organic carbon concatenates to each other, creating polymers (Tissot and Welte, 1984), including essential molecules such as proteins in living organisms.

Based on the different timescales of the processes involved, the carbon cycle can be divided into two sub-cycles with linked processes at the Earth's surface and in the subsurface. With a carbon budget of $\approx 3 \times 10^{12}$ t, the shorter timescale involves processes that operate within a range of days to hundreds of years (Tissot and Welte, 1984); this part of the carbon cycle operates on geological timescales (i.e., several 10^6 yrs) and it is best characterized by biomass generation via photosynthesis of autotrophic organisms. The second sub-cycle has a carbon budget four orders in magnitude higher and involves the incorporation of carbon into sediments as well as the eventual transformation of organic materials to petroleum (Tissot and Welte, 1984). Approximately 0.01% to 0.1% of the organic carbon in sediments is oxidized to CO_2 creating the link between the two sub-cycles when the CO_2 is released into the atmosphere (Tissot and Welte, 1984). The CO_2 is released at the surface by direct oxidation of the organic matter due to the presence of free oxygen. In the subsurface CO_2 is produced via bacterial activity at shallow depth during diagenesis and decarboxylation reactions associated with the thermal degradation of kerogen during the diagenesis/catagenesis stage (Tissot and Welte, 1984).

1.9.2 Biomass generation, preservation and accumulation

Part of the carbon dioxide from the atmosphere will dissolve in the water of lakes and oceans, where biota uses it in photosynthesis or to form shells, bones and skeletons (Simkiss and Wilbur, 1989; Zehr and Kudela, 2009; Myrbo, 2012). After those organisms die, carbon associated with biogenic carbonates can be deposited. In land ecosystems carbon dioxide in the atmosphere is also captured by plants as autotrophic organisms and used in biomass generation (Canuel and Hardison, 2018). Non-biogenic carbonates precipitate when water becomes supersaturated in carbon dioxide (De Groot, 1965).

Once the autotrophic organisms die, they can be subsequently transformed again. Under oxic conditions, their organic molecules will be oxidized to release CO_2 as the final product and provide it to the atmosphere, where it will feed into the shorter carbon cycle (Tissot and Welte, 1984; Canuel and Hardison, 2018). Conversely, the preservation of organic matter in marine and lacustrine environments will occur when anoxic conditions prevail, and sediment will ultimately bury this material. The following oxygen depletion mechanisms, and thus potential preservation of organic matter, play an important role in sedimentary environments and are relevant with respect to the different environments that gave rise to the Yacoraite Fm.:

- The accumulation of fine-grained, low permeable sediments in depositional environments with restricted water movement and decreased oxygenation (Poelchau et al., 1997). The Black and Baltic seas are excellent contemporary examples of these silled basins with reduced connectivity with other water bodies and the global ocean (Demaison and More, 1980).

- The increase in salinity causes a decrease in oxygen solubility (Lange et al., 1972). Water stratification can be developed due to hypersalinity and a turnover of lake waters is not possible. The Lane Shale member of the Eocene Green River Shale was likely deposited in such an environment (Horsfield et al., 1994).

- High sedimentation rates remove the organic matter from the depositional interface. In this way, organic matter is protected not only from oxygen, but also from degradation caused by living organisms (Littke et al., 1997, and references therein). However, high sedimentation rates may also produce low TOC contents by dilution (Tyson, 2001).

- Oxygen depletion may result from consumption during the oxidation of organic matter (Littke et al., 1997). The decreasing availability of oxygen ultimately slows down and stops microbial oxidation of organic matter. However, organic matter is not only altered by aerobic microorganisms. Under anoxic conditions anaerobic microbes degrade organic matter via fermentation as well (Tissot and Welte, 1984). Both processes, respiration under aerobic conditions and fermentation, are oxidation-reduction reactions. One compound or element acts as an electron donor, others react as electron acceptors and the released energy is used by the microbes. Under anoxic conditions, different microbe communities use different electron acceptors than molecular oxygen, such as nitrates, manganese oxides, iron oxides, sulphates or carbon dioxide (Tissot and Welte, 1984; Schink, 2006).

1.9.3 Organic matter classification-kerogen type

Carbohydrates, lipids, and proteins are the main types of organic components common to living organisms in which these compounds have structural functions or serve as a source of energy. Those components have a different resistance to microbial degradation and, therefore can be selectively preserved during early diagenesis (de Leeuw and Largeau, 1993). Kerogen is formed either by repolymerization of previously microbially degraded compounds such as polysaccharides and proteins or by selective preservation of resistant macromolecules, such as cutins and suberans (de Leeuw and

Largeau, 1993). In light of this, kerogen can be considered as a mixture of complex macromolecules (Béhar and Vandenbroucke, 1987).

Kerogen has been classified according to different chemical and physical criteria. A traditional method involves direct observation under the microscope (petrography). Based on its relief, shape, structure, and relative reflectance (Tissot and Welte, 1984), kerogen may be classified into three categories: liptinite, vitrinite, and inertinite. Other methods for kerogen typing use either its bulk or molecular composition. Van Krevelen plots (in honor to the chemist Dirk Willem van Krevelen) use the atomic H/C and O/C ratios to distinguish kerogen types. This method requires kerogen isolation prior to analysis.

With Rock-Eval™ pyrolysis, it is possible to measure the bulk hydrocarbon and CO_2 amounts evolving during the heating of an organic-matter bearing rock sample. Two indexes are derived from Rock-Eval analysis that were proposed to substitute elemental H/C and O/C determinations in kerogen typing (Espitalié et al., 1977). These are the Hydrogen Index (HI) defined as 100*(mg of hydrocarbons/total organic carbon) and the Oxygen Index (OI) defined as 100*(mg of CO_2/total organic carbon). In these methods, the calculated parameters are pooled from the different organic constituents in the sample instead of being related to individual specific precursors. Four kerogen types were described, each with decreasing hydrogen content: Type I, Type II, and Type III. Tissot and Welte, (1984) recognized an additional kerogen type, which they referred to as “dead carbon”, because this organic matter cannot generate hydrocarbons due to its low H/C ratio.

Organic matter from different origins has different compositions, elemental proportions, which results in different indexes and they plot in different regions of the HI vs. OI diagrams, which are often used to differentiate between different kerogen types. Kerogen typing offers important data for the assessment of depositional environments as living organisms are adapted to live in certain depositional environments. For example, higher-plant tissues deposited in environments with terrestrial input, such as in deltas, are primarily composed of cellulose and lignin with lower HI and higher OI. On the other hand, in lacustrine and marine settings far from terrigenous sediment contributions, algae, which are mostly composed of lipids, cellulose and aliphatic biopolymers, may constitute the most important biogenic material deposited (Tissot and Welte, 1984). However, inferring the depositional environment only with Rock-Eval kerogen typing can be misleading (Carrol and Bohacs, 2001).

When pyrolysis is coupled with gas chromatography (Py-GC) in the analysis of kerogens, it is possible to identify variability in structure and composition at the molecular level. Thus, molecular kerogen typing (Horsfield, 1997) uses the distribution of total range C_1-C_5, and n-alkanes and n-alkenes in the range C_6-C_{14} and C_{15+}. This way kerogen typing not only reflects the composition of the organic precursors and depositional environments, but it is also useful to predict the composition of the first-formed petroleum, which is the petroleum as originally generated within the source rock. Subsequent processes involved fractionation of the originally generated oil (di Primio and Horsfield, 1996; Horsfield, 1997).

1.9.4 Petroleum and its relation to former forms of life

Former living organisms are precursors for oil and most of the natural gas occurrences. Evidence of such a direct genetic relationship includes similarities in chemical composition and optical properties, such as the interaction with polarized light (Radke et al., 1997 and references therein). Both of these aspects constitute the foundation for the use of specific organic compounds (biomarkers) to trace back their precursors (living organisms). Biomarkers thus can be considered as molecular fossils and they have been extensively used in deciphering source rocks and to characterize and to categorize oils. Combined, this is therefore relevant with respect to the following aspects of petroleum geology:

the definition of depositional environments; discussed here in sections 3.2 and 5.1;
the development of relative chronostratigraphies; presented here in section 5.2;
the assessment of thermal maturation; applied here in section 5.3; and
the evaluation biodegradation; this aspect is applied here in section 5.4.

For example, the presence of gammacerane which is a compound derived from bacterivorous ciliates (Sinninghe Damsté et al., 1995) suggests water-column stratification, and it is therefore useful in the identification and characterization of depositional environments. The thermal maturity assessments using biomarkers relies on the isomerization and, therefore, on the increase of one specific isomeric form over the other with increasing thermal maturity (Peters et al., 2005a).

1.9.5 Organic matter transformation and petroleum generation

Three main stages involve organic matter transformation under natural thermal stress conditions: diagenesis, catagenesis, and metagenesis. These three stages are characterized by the progressive decrease in hydrogen and carbon enrichment, which consequently decreases H/C and O/C ratios. During diagenesis, organic matter is transformed at lower temperatures than approximately 50 °C. Microbial activity plays an important role in the biopolymer (protein and carbohydrates) transformation. Carboxylic acids, ketones, and esters start being removed during this process. These compounds are entirely removed during the subsequent catagenesis; here, a decrease of aliphatic carbon and an increase of aromatic carbon is observed. It is under these conditions where oil and wet gas are generated.

During metagenesis the carbon enrichment may reach up to 91% during and carbon is present only as part of aromatic compounds and condensed structures. Limited amounts of methane are expected to be generated from the cracking of kerogen and from previously generated hydrocarbons (Tissot and Welte, 1984). However, recent studies revealed a considerable amount of gas generation in this zone (Mahlstedt and Horsfield, 2012). Overall, the composition of the first-formed petroleum depends on the organic constituents in the source rock. Hydrogen-rich organic matter is prone to generate oil, whereas gas is expected to be mainly, but not exclusively, generated from terrigenous organic matter material with a low hydrogen content (Littke et al., 1997).

Methods and techniques for thermal maturity assessment

Organic-matter properties, e.g., composition, structure, optical characteristics, change under thermal stress, and therefore, can be used as indices of thermal maturation. Changes occurring in the visible spectra allow using color scales to assess thermal transformation in organic tissues, i.e., thermal alteration indexes in pollen and spores. A review of optical thermal maturity parameters can be found in Hartkopf-Fröder et al. (2015). The reflected light from vitrinite (woody tissues) has been measured in polished samples relative to a standard under a light-source of 546 nm. Additional technical details can be found in (Stach et al., 1982; Mukhopadhyay, 1994). Vitrinite-reflectance values increase with thermal maturity due to compositional and structural rearrangements. Due to these changes, the aromaticity and condensation of aromatic moieties increase (Hartkopf-Fröder et al., 2015). Vitrinite-reflectance values lower than 0.5% characterize the changes that have taken place in the diagenetic zone. Catagenesis is constrained by 0.5% Ro to 2% Ro. Higher Ro values than 2% characterize the metagenesis zone.

As mentioned above, the thermal conditions at which hydrocarbons are generated depend on the chemical composition and therefore on kerogen type. The onset of hydrocarbon generation in Type I kerogen is at about 0.7% Ro, being the highest compared to Type II and III kerogens. Oil generation from Type II kerogen starts at comparatively lower vitrinite-reflectance values of 0.5% Ro. The onset of oil generation for Type III kerogen is at about 0.6% Ro (Tissot and Welte, 1984; Espitalié, 1986). Mainly liquid hydrocarbons with minor amounts of gas are generated from these kerogen types with values of ≈1.3% Ro. From this point up to ≈2% Ro is the wet gas and condensate window, where gases are mainly generated with an increasing amount of methane. Between 2% Ro and 4% Ro is the domain of metagenesis, where dry gas (mainly methane) is generated (Tissot and Welte, 1984). On the same samples used for vitrinite reflectance, it is also possible to carry out a qualitative and quantitative assessment regarding the fluorescence of liptinitic components. Fluorescence changes from vivid green/yellow color at low maturity towards dark brown, and finally becomes extinct at the end of the oil window at ≈1.3% Ro.

Another maturity parameter frequently used is T_{max}, which is the temperature of the maximum hydrocarbon-generation rate during Rock-Eval pyrolysis. With increasing thermal maturity under natural conditions, the weaker bonds are broken first. Chemical bonds that persist under progressive heating in natural environments are more stable, requiring more energy to be broken (Espitalié et al., 1977). The same principles govern pyrolysis in the laboratory. Thermally labile compounds in low-maturity samples require less energy (temperature) than the more stable, mature samples. T_{max} values then accordingly increase with the thermal maturity of the samples. At the molecular level, the assessment of the thermal maturity relies on different thermal stabilities of the specific compounds. Biomarkers can be used for the assessment of different stages of oil generation up to the level of a late mature stage, when they are no longer effective as maturity indicators. Hopane and sterane isomerization can be mentioned as examples in this context. For example, hopane isomerization can be

applied to define immature to early stage of oil generation (Seifert and Moldowan, 1980). More energy is required in the sterane isomerization, and therefore it is suitable in the thermal maturity assessment from immature to mature stages of oil generation (Mackenzie et al., 1981; Seifert and Moldowan, 1986).

Minerals in sedimentary rocks can also be used as thermal maturity indicators, although their transformation follows different mechanisms and rates. For example, with increasing burial it is observed that changes in clay mineral assemblages and their crystallinities occur such as the increasing crystallinity of illite (Kübler and Jaboyedoff, 2000), as well as the progressive conversion of smectite to illite (Velde, 1992). Mineral proxies for an assessment of mineral diagenesis and organic proxies as thermal maturity parameters have been correlated with hydrocarbon generation and compiled in different correlation charts (Kübler and Jaboyedoff, 2000; Hartkopf-Fröder et al., 2015), which need specific calibration for a particular geothermal regime (Radke et al., 1997).

Methods and techniques to anticipate the composition of first-formed petroleum

It is possible to anticipate if a rock is more oil- or gas-prone using the estimation of the amount of different organic constituents by organic petrography or the bulk characterization by Rock-Eval pyrolysis. If pyrolysis is coupled with gas chromatography (Py-GC), it is possible to identify specific compounds that may evolve during heating. Molecular kerogen typing (Horsfield, 1997) uses the distribution of the compound according to the number of carbon atoms in their molecules. This is the total spectrum from C_1-C_5, n-alkanes/-enes in the ranges between C_6-C_{14} and C_{15+}. The distributions of those three ranges are used for detailed prediction of petroleum composition into five classes: paraffinic oil low wax, paraffinic-naphthenic-aromatic low wax, paraffinic oil high wax, paraffinic-naphthenic-aromatic high wax, gas, and condensates.

Petroleum migration and accumulation

Once generated, petroleum can move from its organic precursors driven by pore saturation and/or generation pressure mechanisms (Mann et al., 1997; Cornford et al, 1998). The generation rate and concentration of hydrocarbons control the hydrocarbons expulsion from source rocks (Eseme et al., 2007). Further movement places the petroleum in a carrier rock where petroleum moves by buoyancy forces (Mann et al., 1997) through a network of connected pores until it reaches possible reservoirs. The petroleum movement is additionally affected by its composition and the external physical conditions of pressure and temperature that influence the sedimentary basin. The amount and the gas composition control the phase behavior. Exsolution of free gas from the petroleum mixture generates an increase in resistance to movement when the fluid is exposed to lower pressures than the so-called bubble point. The liquid composition of petroleum controls the miscibility of the individual compounds or compound groups in the petroleum admixture. In this way, liquid composition affects the saturation pressure, which is the pressure at which gases separate from the liquid phase (Danesh, 1998). The phase behavior of the first-formed petroleum can be predicted by using the PhaseKinetics approach (op. cit.) as shown in section 6.3.

2. Samples and methods

This chapter describes the methodological approach regarding sampling, screening, and detailed analyses carried out on rock samples, oil seep samples, and produced oils.

2.1 Sampling procedure

Geological maps from the Argentinean Geological Survey (SEGEMAR) at a scale of 1:250.000 combined with published data were used to identify suitable locations of outcrops of the Yacoraite Fm. with the aim to collect samples in the Salta and Jujuy provinces. The sampling campaign took place in October 2016 with the participation of Dr. R. Ondrak from the German Research Centre for Geosciences (GFZ), Prof. E. Rossello, from the University of Buenos Aires and PhD student V. Cortassa from the same university. Fifty-two outcrop samples, mainly comprising shales, marls, and stromatolites were collected from the Tres Cruces and Metán-Alemanía sub-basins (Fig. 1.2a). Samples were collected after removing the altered surface until reaching fresh rock without apparent signs of weathering. These samples were wrapped in aluminum foil to preserve their physical integrity and to prevent contamination. Samples were assigned to the lower, middle, and upper sections of the Yacoraite Fm. The section collected at Valle del Tonco in the western sector of the Metán-Alemanía sub-basin is inverted, as documented in the geological maps (SEGEMAR, 2006).

In addition, eight produced oils were provided for this project from different wells in the Lomas de Olmedo sub-basin. Five of them were provided by GeoMark Research as part of an ongoing cooperation with Prof. B. Horsfield, GFZ Potsdam. These oils are from the Caimancito oil field (Caimancito-23 and Caimancito-30), the Martinez del Tineo oil field (Wells-10 & Well-18), and the Ramos X-11 oil field (Well-11). Prof. Rossello provided the other three oil samples (Caimancito-21, Río Pescado and Chirete x100-1).

Oil seep samples were retrieved from the Tres Cruces sub-basin and in the Laguna de la Brea location in the western sector of the Lomas de Olmedo sub-basin (Fig. 1.2a) as listed below:

- Two samples from the Laguna de la Brea mud-oil mixture (LB_M-O),
- One sample from the Laguna de la Brea water-oil mixture (LB_W-O),
- Two samples from the Barro Negro mud-oil mixture (Tres Cruces sub-basin) (BN_M-O)
- One tar sample collected in the north sector of the Tres Cruces sub-basin and,
- One fresh oil seep sample from the Tres Cruces sub-basin.

Fig. 1.2a shows the location of sampled rocks, oil seep samples, and produced oils. Table 1 of the appendix lists the details concerning the exact location and the description of the material.

2.2 Sample preparation

2.2.1 Rock samples

The rock samples were broken into pieces with a hammer. Some pieces were prepared for organic petrology. Other pieces were crushed and ground into powder to provide whole-rock samples.

Part of these whole-rock samples was extracted to carry out chemical analysis of their bitumen. Another part of the whole-rock samples was used without extraction for mineralogical and chemical analysis e.g., X-ray diffraction, X-ray fluorescence, Rock-Eval pyrolysis.

2.2.2 Extraction and analysis of bitumen

Powdered rock samples, including the tar sample were extracted with a mixture of dichloromethane-methanol (v/v 9:1) for 24 hours at 50°C using a Soxhlet apparatus. The samples mixed with water were first vacuum-filtered before extraction while the fresh oil sample required no extra preparation step.

The bitumen extracts were dissolved in 250µl of dichloromethane/methanol (v/v 99:1) and treated with a 40-fold excess of *n*-hexane to precipitate the asphaltenes. Then, 5α-androstan (5mg/ml) and ethylpyrene (1mg/ml) were added as internal standards for the aliphatic and aromatic fractions, respectively. The volume of each standard (ml) was added equally to the mass (mg) of bitumen extract. Subsequently, the bitumen was separated into an aliphatic, aromatic and the NSO fraction using a medium-pressure liquid chromatography (MPLC) instrument as described by Radke et al. (1980) in preparation for gas chromatography with flame ionization detection (GC-FID) and gas chromatography-mass spectrometry.

2.3 Chemical characterization of organic matter

2.3.1 Bulk elemental composition and bulk-flow pyrolysis

The total organic carbon (TOC) was measured on an aliquot of approximately 200mg of powdered rock with a Leco SC-632 instrument after the removal of inorganic carbon (carbonates) with hydrochloric acid (HCl, 10%) at 60°C ± 5°C. After this treatment, samples were washed with distilled water to remove all traces of HCl and water-soluble chlorides. The total sulphur content (TS) was measured on 100mg of powdered sample with a Leco S-200 total evaporation analyzer. Further details on the measurement procedure can be found in Prinz et al. (2017).

Bulk-flow pyrolysis of powdered rocks was carried out to assess the hydrocarbon potential, thermal maturity, and kerogen type. These analyses were conducted on a Hawk instrument by APT laboratories (Norway). This instrument resembles the Rock-Eval by design. Two aliquots (≈80mg) of each sample were analyzed. One aliquot consists of a whole-rock powder sample. The other one was pre-extracted whole-rock powder sample with a mixture of dichloromethane and methanol (v/v 9:1) using an Accelerated Solvent Extraction (ASE 3000) system at 75°C and 50 bars.

The sample measurement of the Rock-Eval and Hawk instrument is, in principle, very similar. Samples are heated to 300°C for a duration of 3 minutes to vaporize the free (unbound) hydrocarbons, which form the S1 peak. Then the temperature in the oven is increased by 25°C/min to 650°C. Hydrocarbons generated during this heating range from the kerogen matrix and heavy polar bitumen are measured and result in the S2 peak. The released CO_2 is continuously measured up to a temperature of 390 °C by an infrared detector and registered as the S3 peak. At higher temperatures, the CO_2 is

thought to derive from the decomposition of thermally labile carbonates. The temperature at which the S2 peak reaches its maximum is measured and reported as T_{max}, which is a thermal maturity parameter for a given organic-matter type.

Parameters for the source-rock assessment were calculated from the pyrolysis results of whole-rock samples as follows: The Hydrogen Index (HI) = (S2/TOC) *100 is reported as mg HC/g TOC, the Oxygen Index (OI) = S3/TOC)*100 is reported as mg CO_2/g TOC, the Petroleum Potential (PP) = S1+S2, and the Production Index (PI) = S1/(S1+S2). When S2 and TOC values are close to zero, they are at the same magnitude as the uncertainty of the measurement, and the calculated HI can be biased. Thus, these parameters were not calculated for samples with TOC or S2 values lower than 0.05 in their respective units. The contribution of bitumen carryover and pyrolysis to the S2 peak was calculated by subtracting the S2 measured for the pre-extracted aliquot ($S2_X$) from the S2 measured for the whole-rock aliquot. The combination of parameters before and after extraction allowed determining the following characteristics:

The total bitumen content = $S1+(S2-S2_X)$

The proportion of kerogen derived hydrocarbons in the S2 peak = $S2_X/S2$

The proportion of bitumen in the S2 peak = $1-(S2_X/S2)$

Total oil (bitumen)/ kerogen ratio = $[S1+ (S2-S2_X)]/S2$

Based on low HI suggesting important terrestrial input that contrast with the predominant presence of alginites, mineral interference during the pyrolysis experiments was suspected in samples collected in the western sector of the Metán-Alemanía sub-basin (samples #47, #48, #50, and #51). To further validate this inference, their kerogen was concentrated. Initially, pieces of rocks approximately 1mm in diameter were treated with hydrochloric acid (≈3.7%) at 60-70°C for approximately 12 hours to remove carbonates. The acid was then decanted, and the samples were washed with distilled water until a pH of 6-6.5 was reached. Subsequently, silicates were dissolved using hydrofluoric acid (40%) at 60-70°C for at least 24 hours. The acid was decanted, and the samples were washed until they reached a pH of 7. Finally, the samples were again treated with HCl to remove remaining carbonates and fluorides, and washed until a neutral pH was reached (Weiss et al., 2000).

2.3.2 Thermovaporisation (T-vap) and Pyrolysis-gas chromatography (Py-GC)

Although the total amount of free hydrocarbons in the source rock is quantified as the S1 peak in pyrolysis, it inherently does not provide information regarding the specific hydrocarbon composition. Thermovaporisation (T-vap) overcomes this problem, because the furnace is coupled with a gas chromatograph. Similarly, the identification of individual compounds generated during thermal degradation is possible when using Pyrolysis-GC (Py-GC) at equivalent temperatures at which the S2 peak (Rock-Eval) is recorded. For both Thermovaporisation and Pyrolysis-GC, peak identification was done by comparison of the retention times of n-alkenes, n-alkanes, aromatic hydrocarbons,

alkylthiophenes and alkylphenols to the in-house reference sample BH-005. Integration of the peaks was done using Chemstation® software. Quantification was made using n-C_4 standard reference gas.

T-vap and Pyrolysis-GC analyses were carried out in a Quantum MSSV-2 Thermal Analyzer. Between 5-50mg of the powder sample were placed in the middle of an MSSV glass capillary tube. Subsequently, pre-cleaned powder quartz (pre-heated at 600°C in air for one minute) and glass wool (pre-heated at 600°C in air for approx. 45 mins.) were added from both sides of the tubes. Finally, tubes were sealed with a hydrogen flame. For thermovaporisation, a MSSV-tube was placed in the furnace and heated isothermally at 300°C for five minutes. After this, the tube was broken with a piston, and the helium carrier gas transported the free hydrocarbon fraction onto the gas chromatographic column (HP ultra-1, dimethylpolysiloxanphase, 50 mm long and a film thickness 0.52µm).

Finally, the free hydrocarbon fraction was measured with a Flame Ionization Detector (FID). Furthermore, the remaining bound hydrocarbons were pyrolyzed by increasing the temperature of the heating block from 300-600°C with a heating rate of 50°C/min (Horsfield, 1989; Horsfield et al., 2015). Once this temperature was reached, it was kept constant for one minute. The pyrolysis products were collected in a cryogenic trap (liquid nitrogen) from which they were later liberated by ballistic heating (held at 320°C for 10mins.) and analyzed with the same chromatographic column as described above.

2.3.3 Bulk hydrocarbon generation - bulk kinetics

Hydrocarbons are generated from organic matter under increasing thermal stress through a large number of parallel pseudo-reactions (e.g., Schenk et al., 1997). The transformation rate at which this process takes place depends on the organic-matter composition (kerogen type). Generally, the organic matter in rock samples is a mixture of different constituents. Bulk kinetics allow to determine the suite of activation energies that are required to generate hydrocarbons from macromolecules, and the frequency factor representing the frequency of possible collisions between molecules for the reaction to take place. The kinetic data set can then be extrapolated to geological timescales to simulate the degree of thermal transformation under geological burial conditions.

For the bulk kinetics assessment, samples were analyzed using a Source Rock Analyzer (SRA) with different heating rates (0.7; 2; 5; 15 °C/min). Released products were measured by a flame ionization detector (FID) at a constant helium gas flow of 50 ml/min. Kinetics 2000 ® and KMOD ® programs were used for data processing. Optimization of discrete activation energy (Ea) was done with a single, variable frequency factor (A). Extrapolation to geological conditions was performed using the KMOD ® program. The temperatures over which petroleum generation takes place were calculated using the kinetic parameters assuming a linear geological heating rate of 3 K/Myr, this being typical for many sedimentary basins (Schenk et al., 1997).

2.3.4 PhaseKinetics

PhaseKinetics is a compositional kinetics approach developed by di Primio and Horsfield (2006). It was used in this dissertation to understand the compositional changes of the oil generated during artificial non-

isothermal maturation of samples of the Yacoraite Fm. and to predict their physical properties. This approach characterizes the composition of the first-formed petroleum using pyrolysis-GC (Horsfield, 1989). Different aliquots of the samples are heated in closed-system using microscale sealed vessel (MSSV) tubes to study the changes in the petroleum composition under thermal stress. For this purpose, powder samples are placed in MSSV tubes, whose ends are subsequently sealed. The tubes are heated with a heating rate of 0.7 °C/min to final temperatures corresponding to those at which 10%, 30%, 50%, 70%, and 90% transformation ratio are reached in bulk kinetic experiments. Subsequently, the tubes are broken using a piston, and the generated products are released and analyzed by GC-FID. Quantification is carried out by adding *n*-butane as an external standard.

The hydrocarbons generated during MSSV experiments are grouped into 14 pseudo compositions that describe the evolution of the liquid- and gas-phase composition over the thermal transformation. To define the gas fraction, seven hydrocarbons are used (C_1, C_2, C_3, i-C_4, n-C_4, i-C_5, n-C_5), while the liquid fraction is represented by seven pseudo boiling ranges (C_{7-15}, C_{16-25}, C_{26-35}, C_{36-45}, C_{46-55}, C_{56-80}). This compositional description was populated into the activation energy distribution from bulk kinetics. Physical properties, e.g., saturation pressure (Psat), the gas-to-oil ratio (GOR), and volume factor (βo), were calculated using PVT-Sim®.

2.3.5 Organic petrography and vitrinite reflectance

Organic petrography allows the detailed visual inspection of organic particles to determine maceral composition and thus corroborating the kerogen classification obtained by the pyrolysis. In addition, the reflectance of the vitrinite particles can be determined, representing a widely used thermal maturity parameter (Hartkopf-Fröder et al., 2015).

Based on the pyrolysis results, 16 samples containing Type III or II/III kerogen were chosen since they are expected to have more terrigenous organic matter and therefore more vitrinite particles. Samples with TOC lower than 0.2 % were not considered, even if identified as Type III kerogen, because of the low prospects of finding vitrinite particles in whole-rock samples. Sample #30 containing kerogen Type I (HI= 1015 mgHC/g TOC) and sample #51 were also prepared to corroborate their kerogen type by direct inspection of their organic macerals. Vitrinite reflectance (%Ro) was measured on randomly oriented particles in pieces of rocks cut perpendicular to bedding and embedded in resin. Measurements were performed under immersion oil (n_e =1.518 at 23 °C) using a Zeiss Axio Scope microscope equipped with a 50×/1.0 Epiplan- NEOFLUAR oil immersion objective. Before each sample was analyzed, the microscope was calibrated with a leuco-saphire standard (0.592 % reflectance). For a more detailed description of sample preparation and microscopic equipment, see Sachse et al. (2011).

2.4 Mineral composition - inorganic characterization

2.4.1 X-ray diffraction

The clay size mineral fraction of is too small for optical microscopy and is therefore studied by X-ray diffraction. The interplanar distances at which diffraction occurs are seen as peaks in a

diffractogram and are used to identify minerals in whole powder preparations. As clay minerals are not fully recognized in whole-rock powder preparations, additional treatments were applied to facilitate clay mineral identification. They involve the use of ethylene-glycol and heating inside an oven. Measurements of the Full Width at Half Maximum (FWHM) of the illite were carried out to define mineral diagenesis and can be used together with other thermal maturity parameters to estimate the intensity of erosion linked to climate conditions (Chamley, 1989).

The determination of mineral composition was carried out on 2 grams of whole-rock powder samples, which were placed in the holder sample as non-oriented powder. Analyses were performed using CuKα radiation at 40 kV. Randomly oriented whole-rock powders were run from 4º2θ to 70º2θ with a step size of 0.05º 2θ and a counting time of 3s/step. Mineral identification in whole-rock samples was done with the PDF2 XRD database and quantification with High Score plus® from Panalytical.

For specific analysis of clay-mineral fractions smaller than 2 μm pieces of rock were first tested for the presence of carbonate by checking effervescence after adding hydrochloric acid (10 %). When present, carbonates were removed with Morgan solution (buffered acetic acid/acetate, pH=5) for 24 hours. Organic matter was destroyed by using hydrogen peroxide. After these treatments, samples were washed with deionized water, and particles larger than 2 μm were separated by centrifugation. The fraction < 2 μm was dispersed in deionized water using a solution of sodium hexametaphosphate (0.001M). The fraction < 2 μm was deposited in a glass-sample holder and allowed to dry. Particle size was controlled by a laser analyzer HORIBA LA-950. Dispex 40 based on organic polymer was used to enhance the dispersion of the particles for illite-crystallinity measurements.

Fractions smaller than 2μm were analyzed three times in the same subsample, air-dried, ethylene-glycol solvated (12h inside a desiccator containing ethylene glycol at 50ºC), and heated (4h, 500ºC). In the air-dried preparation, diffraction peaks indicate the interplanar distances of the minerals. Ethylene glycol is introduced into the interlaminar space of the expandable clay minerals. This expansion is observed as an increase in interlaminar distance. Later with the heated preparation the resistance of the laminar structure to temperature is evaluated. The comparison of the behavior of the peaks in these three different preparations allows identifying groups of clay minerals. Every subsample was scanned from 4°2θ to 35°2θ with a step size of 0.02°2θ and a count time of 17s per step. The identification of clay minerals was done by comparison of the diffractograms of three different types of preparation for each sample, i.e., air dried, ethylene glycol solvated, and heated (Thorez, 1976; Moore and Reynolds, 1997). Relative abundances of clay minerals were calculated by using the mineral intensity factors (MIF) of Moore and Reynolds (1997).

The Full Width at Half Maximum (FWHM) was measured for illite in the ethylene glycol solvated aliquot to avoid the influence of expandable minerals. FWHM values were expressed as Kübler values (CIS scale) and Kübler values (Basel lab) following the recommendations of the last standardization exercise (Warr and Ferreiro-Mählmann, 2015). First, the FWHM of the international calibration samples (Warr and Rice, 1994; Warr and Ferreiro-Mählmann, 2015), i.e., SWI, SW2, SW3.

SW4 and MF1C were measured. These values were plotted against their published Kübler values (CIS scale) of Warr and Ferreiro-Mählmann (2015). Both of these two groups of measurements had direct proportionality whose linear fit (R^2=0.967) had the following equation:

Kübler index (CIS scale) = 0.9895 *(FWHM) + 0.1034

To make these results comparable with the most recent work in this regard, Kübler values (CIS scale) values were converted to Kübler values (Basel lab) by rearranging the published equation (Warr and Ferreiro-Mählmann, 2015) which turns into:

Kübler values (Basel lab) = Kübler values (CIS scale) – 0.036/ 1.1523 (R^2 = 0.986)

Samples of the Yacoraite Fm. were analyzed in the same diffractometer and under the same conditions as the calibration samples. The FHWM values of the Yacoraite Formation samples were first converted to Kübler values (CIS scale) and subsequently converted to Kübler values (Basel lab) using the respective equations. In this way, they were available in the appropriate format to be used in the interpretation of diagenetic zones (Warr and Ferreiro-Mählmann, 2015).

2.4.2 Elemental chemical composition of the rock samples, X-ray fluorescence

There incorporation of some chemical elements, e.g., copper, nickel, zinc in the sediments is strongly controlled by the redox conditions of the depositional environment (Acharya and Chakrabarti, 2019). These elements were used as proxies for redox condition assessment. X-ray fluorescence was chosen because it provides a quick mineral quantification of chemical elements. Powder samples were homogenized and placed in capsules with thin-film (4 μm) of polypropylene at the bottom. Analyses were carried out with a BRUKER Tracer GeoQuant IV equipped with a tube of Rhodium, at a maximum voltage of 40 kV. A detector with 10 mm 2 XFlash SDD, with a typical resolution of 145 eV at 100.000 cps, was used. To increase the detection of light chemical elements, a portable vacuum was used. Results are expressed as oxides (%) and minor elements in parts per million (ppm).

2.4.3 Uranium content

Uranium is also redox-sensitive, and enrichments of this element have been reported in the Metán-Alemanía sub-basin (Salfity and Marquillas, 1999; Ferreira et al., 2013). A Geiger counter was used in this study for a rapid, qualitative evaluation of the radioactivity in the collected samples. Sample #51 and its neighbors were chosen to carry out analytical uranium quantification by ICP-MS. Uranium was quantified twice in different aliquots in each sample. A minimum of 200 mg of powdered and dried sample material was acid-digested in hydrofluoric acid (HF), perchloric acid ($HClO_4$), and Aqua Regia (HCl + HNO_3, 3:1); the concentrations of these acids were 37 % and 63 %, respectively. Data were acquired in A Galileo 4870 equipment under pulse-jumping mode. For details, see Romer and Hahne (2010).

2.5 Characterization of rock extracts, oil seep samples and produced oils

Analyses on the extracted bitumen allowed inferring the depositional environment, the kerogen type, and thermal maturity of the rock from which it was generated. This information was compared with analyses carried out on rocks samples, e.g., pyrolysis, organic petrography, further strengthening the deduced interpretations.

2.5.1 Gas chromatography-flame ionization detection (GC-FID)

Whole oil samples were measured in a GC-FID (HP 6890, Agilent Technology, USA) equipped with an HP PONA-column (Agilent Technology, Germany) of 50 m length, 0.2 mm ID, 0.5 µm film thickness, using 2,2,4 trimethyl isopentane as standard. The oven was programmed to start at 30 °C, hold for 10 min. Afterward, the temperature increased with a rate of 2 °C/min up to 60 °C and held for 10 min. Using a second ramp of 4 °C/min, the temperature increased up to 320 °C and held for 35 min. The aliphatic fraction was analyzed for the produced oils, oil seep samples, and source rock extracts using a similar GC-FID system as described before but equipped with an Ultra 1 Methyl Siloxane column with a film thickness of 0.33 µm. The heating program of the oven temperature ran from 40-325°C with a heating rate of 5°C/min.

2.5.2 Gas chromatography-mass spectrometry (GC-MS)

Biomarkers such as tricyclic terpanes, hopanes, steranes, naphthalenes, phenanthrenes were detected in the aliphatic and aromatic fractions of the rock extracts, oil seep samples, and produced oils. Non-biomarker, i.e., diamantanes and adamantanes, were detected in the aliphatic fraction. Relative concentrations were calculated using peak areas related to standard concentrations. The occurrence, ratios, and concentrations of different biomarkers were used to characterize the depositional environment, assess the thermal maturity, propose genetic relations, i.e., source rock-oil correlations, and suggest oil-oil correlations.

Analyses were carried out using a Trace GC Ultra gas chromatograph coupled to a DSQ mass spectrometer (Thermo Electron Corp.). The GC was equipped with Thermo PTV injection system and an SGE BPX5 fused silica capillary column (50 m x 0.22 mm ID and 0.25 m film thickness). Helium was used as a carrier gas. Samples were heated in the GC oven from 50-310 °C at a rate of 3 °C/min, followed by an isothermal phase of 30 min. The injector temperature was programmed from 50-300°C. The MS was operated in electron-impact ionization mode (EI) at 70 electron volts (eV). Full scan mass spectra for compound identification were recorded for mass-to-charge ratios (*m/z)* 50 to 600 at a scan rate of 1.5 scans/s.

To improve the resolution in the analyses of specific compounds such as steranes and hopanes, samples were measured in the multiple reaction monitoring (MRM) MS-mode. In this scan-mode, degradation fragments in relation to selected specific target molecular ions are monitored. Due to the ion selection, the sensitivity for the detection of the target compounds is significantly increased. These MS experiments were carried out with an HP 6890A gas chromatograph (Agilent Technology, USA)

coupled to a Finnigan MAT 95XL mass spectrometer. The column and the temperature program were similar to the one used for full scan GC-MS. The MS was operated in electron impact ionization mode (EI) at 70 eV. Molecular ion-fragment transitions of the selected compounds (compound list) were monitored with a scan rate of 1 scan/s.

2.5.3 Compound-specific stable carbon isotopes

Stable carbon-isotope signatures of pristane and phytane were used to validate their use as proxies for the assessment of the redox conditions during the time of source-rock deposition. The carbon isotopic compositions of these and other saturated hydrocarbons were measured by GC-IRMS that consisted of a GC unit (7890N, Agilent Technology, USA) connected to a GC-Isolink coupled via open split to a Delta V Plus mass spectrometer (ThermoFisher Scientific, Germany). For carbon-isotope analysis, the organic substances of the GC effluent stream were oxidized to CO_2 in the combustion furnace held at 940 °C on a CuO/Ni/Pt catalyst. Up to 3 µl of saturated fraction were injected into the programmable temperature vaporization inlet (PTV, Agilent Technology, USA) with a septumless head, working in split/splitless mode. The injector had a constant temperature of 280 °C. The saturated fractions were separated on a fused silica capillary column (HP Ultra 1.50 m x 0.2 mm ID, 0.33 µm FT, Agilent Technology, Germany).

The temperature program started at 40 °C, held for 2 minutes, and was then increased at a rate of 4 °C/min to 300 °C, held for 45 min. Helium, set to a flow rate of 1.0 ml/min, was used as the carrier gas. All saturated hydrocarbon fractions were measured in triplicate mode. The standard deviation was ≤0.3 ‰ for all compounds and samples. The quality of the isotope measurements was checked regularly by measuring different *n*-alkane standards with a known isotopic composition, provided by Campro Scientific, Germany and Arndt Schimmelmann, Indiana University, USA. The values were expressed in the δ-notation relative to the Vienna PeeDee Belemnite (VPDB) standard.

3. Depositional environment and kerogen type of the Yacoraite Fm.

In this chapter, the results of the inorganic and organic analyses of the samples from the Yacoraite Fm. are presented. The inorganic part includes the bulk mineral and clay-mineral analyses. The amounts of carbonates and detrital minerals were used to infer changes in sea level during the marine Cretaceous transgression. In this context, clay-mineral assemblages were used as paleoclimate proxies. In addition, chemical elemental ratios were used to assess the redox conditions and to get insight into the water depth during the deposition of the Yacoraite Fm. The analyses of the organic material allowed determining the amounts of organic matter and type (i.e., kerogen type), as well as the characterization of the depositional environment and its changes during the deposition of the Yacoraite Fm. With this information, this chapter provides the foundation for source-oil correlations that will be discussed in section 5.5.

3.1 Mineral assemblages and chemical composition

The Yacoraite Fm. was deposited during a global marine transgression (Cónsole-Gonella and Marquillas, 2014). As in other studies, lithological and mineral compositions are expected to reflect changes in sea level (e.g., Pomar and Ward, 1995; Zhao et al., 2006). For example, detrital compositions with low carbonate content predominate at low sea levels. As the sea level rises, the contribution of detrital minerals decreases due to the greater distance to the source of the sediments, while the carbonate content (mainly calcite) increases due to better developed marine conditions (op. cit.).

3.1.1 Mineral archives of the depositional environment of the Yacoraite Formation

Mineral analyses by X-ray diffraction (XRD) (Table 2, appendix) show that the Yacoraite Fm. is predominantly composed of variable amounts of quartz, calcite, feldspars, and muscovite in the Tres Cruces and the Metán-Alemanía sub-basins. Albite and microcline feldspars are present as well, although not in all samples. Gypsum and dolomite are minor constituents mainly found in the Metán-Alemanía sub-basin what agrees with recent studies (Gomes et al., 2020). Ankerite, on the other hand, is present where dolomite is absent. The predominance of diagenetic dolomite was observed in 70 % of a total of 623 samples retrieved from the Lomas de Olmedo sub-basin (Grosso et al., 2013). In this sub-basin, dolomite was precipitated as cement in the pore spaces after carbonate dissolution caused due to the presence of CO_2 and carboxyl ions that had been released during thermal maturation of organic matter (Cesaretti et al., 2000).

Carbonates (calcite, dolomite, ankerite) and detrital minerals (quartz, feldspars, muscovite) inversely co-vary with an R^2 of 0.81 (n=8) in the southern sector of the Tres Cruces sub-basin (Fig. 3.1a) and R^2=0.91 (n=4) in the western sector of the Metán-Alemanía sub-basin (Fig. 3.1b). These are the only localities shown because, there a more complete stratigraphic succession of the Yacoraite Fm. was sampled. Based on carbonate vs. detrital content in the Tres Cruces sub-basin (Fig. 3.1a) and the Metán-Alemanía sub-basin (Fig. 3.1b), sea-level changes were interpreted (Fig. 3.1c). The significant

increase in carbonates during the deposition of the middle and upper sections of the Yacoraite Fm. suggests a rising sea level at that time. The upper part records the maximum flooding conditions with the maximum carbonate production followed by a shallowing-upward sequence in both sub-basins. This sequence is likely related to decreasing tectonic subsidence in NW Argentina during the Yacoraite Fm. deposition (Sempere et al., 1997; Marquillas et al., 2005) probably from the Maastrichtian onwards (del Papa and Salfity, 1999). A rising sea level followed by a shallowing-upward sequence is also documented in the western sector of the Metán-Alemanía sub-basin based on carbon and oxygen isotopes (Marquillas et al., 2007).

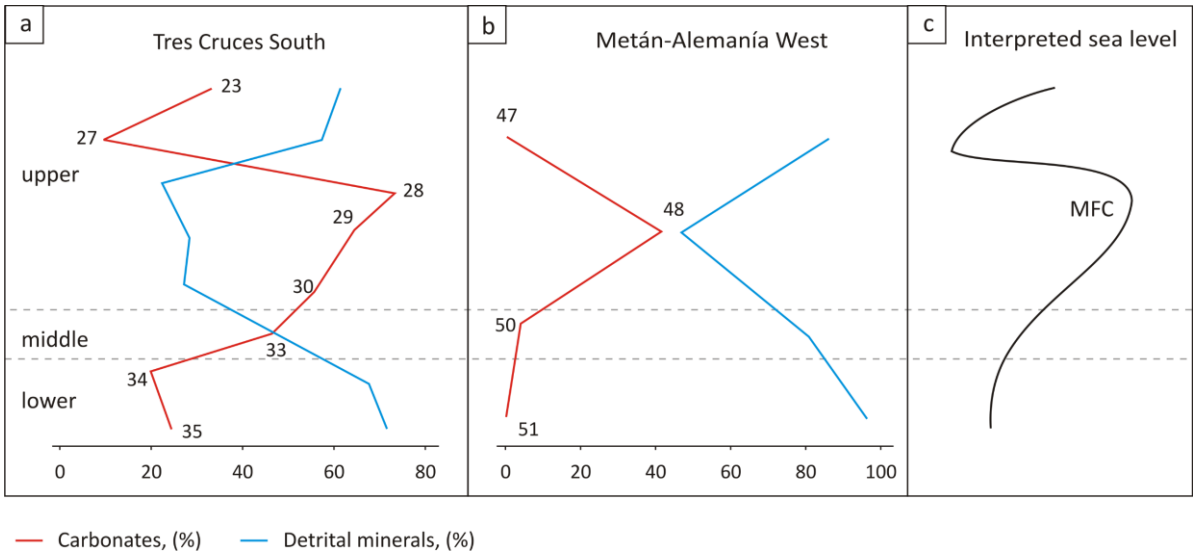

Fig. 3.1. Variation in carbonates (red line) and detrital minerals (blue line) in samples of the Yacoraite Fm. (a) The southern sector of the Tres Cruces sub-basin. (b) The western sector of the Metán-Alemanía sub-basin. (c) Interpreted sea-level changes based on carbonate and detrital mineral variations. MFC: Maximum flooding conditions. Sea level increased during the deposition of the middle to early upper sections of the Yacoraite Fm. in the southern sector of the Tres Cruces sub-basin; the upper part of the formation also registered a marine regression, and finally a renewed sea-level rise documented in the strata at the top.

At the top of the Yacoraite Fm. in the Tres Cruces sub-basin, a marine transgression caused a renewed increase in carbonate content. The slight increase in detrital minerals at this stage may have been associated with significant freshwater influence in the context of evolving lacustrine settings (Sánchez and Marquillas, 2010). The Yacoraite Fm. was deposited during a marine north-south-advancing transgression on the South American continent (Sempere et al., 1997; Marquillas et al., 2005; Marquillas et al., 2011). The Metán-Alemanía sub-basin is located farther south of the Tres Cruces sub-basin. This might be the reason why the carbonate content is high in the Tres Cruces sub-basin and why the last stages of the marine ingression were not recorded in Metán-Alemanía sub-basin. Alternatively, a marine stage may not have been recognized due to the limited number of samples analyzed.

Regionally widespread tuff intercalations mainly at the base of the Yacoraite Fm. have been documented (Marquillas et al., 2011). Authigenic zeolites are generally formed from the chemical alteration of such volcanic material (e.g., Chamley, 1989). Zeolitization explains the presence of

analcime in several samples of the Yacoraite Fm. Analcime contents are lower than 9 % at the base (sample #20) and middle Yacoraite Fm. (sample #50) in the western sector of the Metán-Alemanía sub-basin and the southern sector of the Tres Cruces sub-basin (samples #33 & #34). Analcime contents reach up to 21 % in the upper section in the western sector of the Metán-Alemanía sub-basin (sample #16) and the southern sector of the Tres Cruces sub-basin (samples # 25 & #27).

3.1.2 Paleoclimate conditions inferred from clay mineralogy

The formation of detrital clay minerals depends largely on weathering (Chamley, 1989). Climate is the main force controlling the efficiency and speed of weathering, which make clay minerals suitable as paleoclimate proxies (Chamley, 1989; Righi and Meunier, 1995; Do Campo et al., 2018). The potential use of clay mineralogy for paleoclimate interpretations is discussed for the southern sector of the Tres Cruces sub-basin, where a complete stratigraphic sequence was analyzed for the clay-mineral composition.

The clay mineralogy (<2 μm) of the Yacoraite Fm. in the Tres Cruces and the Metán-Alemanía sub-basins is dominated by variable amounts of smectite and illite/mica (Fig. 3.2 and Table 3, appendix). Significant amounts of kaolinite of up to 26 % are found in the northern sector of the Tres Cruces sub-basin in the middle section of the Yacoraite Fm. Minor amounts of chlorite are found in all sectors except in the north of the Tres Cruces sub-basin. Illite is the only mineral in the smallest fraction (<2μm) in sample #51 collected in the western sector of the Metán-Alemanía sub-basin. The absence of detrital minerals, e.g., quartz and feldspars, point to the authigenic origin of this clay mineral in this sample.

The formation of smectite in this set of samples is probably linked to the diagenetic alteration of volcanic material as indicated by its good positive correlation with analcime (R2=0.7, n=7). Smectite is formed under alternating humid and dry periods in a warm climate (e.g., Singer, 1984; Chamley, 1989). Clay mineral associations dominated by illite/mica are formed under dry and cold climates where physical weathering prevails (Do Campo et al., 2018). The alternation between warm and cold climate with humid and dry episodes explains why in the set of samples of the Yacoraite Fm. the increase of smectite inversely correlates with illite/mica (Fig. 3.3a, R2=0.99, n=7). Warm and humid conditions were established from the lower section of the Yacoraite Fm. through its middle section (Fig. 3.3b). Additionally, small amounts of kaolinite (sample #35) indicate a more important role of hydrolysis suggesting a tropical to subtropical humid climate (Chamley, 1989; Righi and Meunier, 1995). The development of a dry and cold climate from the upper middle through the lower upper section facilitated weathering under low hydrolyzing conditions, consequently enhancing the illite/mica content (sample #30). A warm climate followed with alternation of humid and dry periods, as indicated by the increase in smectite content.

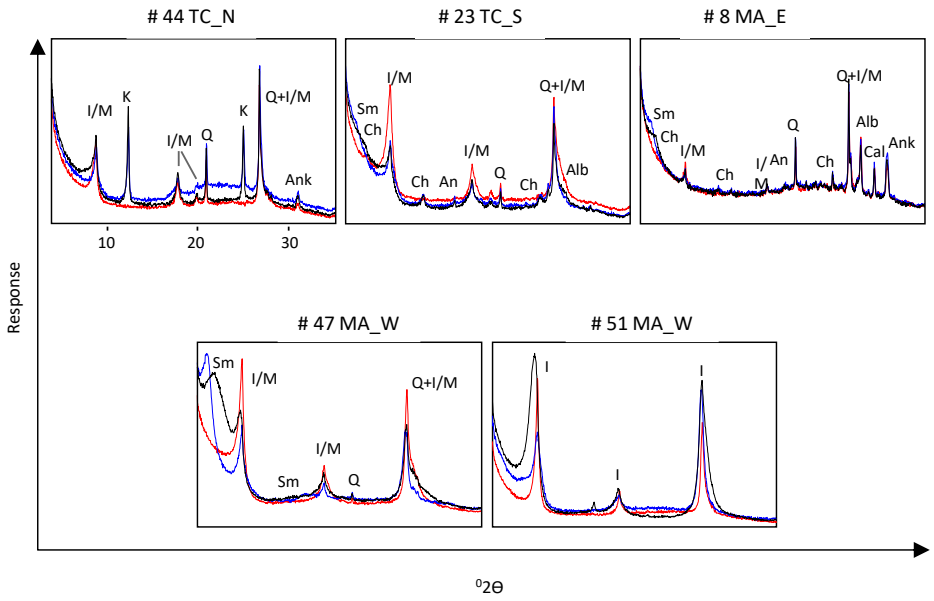

Fig. 3.2. X-ray diffractograms of the grain size fraction <2 μm in samples of the Yacoraite Fm. Note the difference in mineral composition between samples # 47 and #51. Sample #47 (upper section) is composed of detrital minerals, e.g., quartz and albite suggesting that illite in this sample is also detrital. Lack of detrital minerals in sample #51 (lower section) suggests that illite in this sample is authigenic. Q: Quartz, Alb: albite, Cal: calcite, Ank: ankerite, An: analcime, I: illite/mica, Sm: smectite, Ch: chlorite. **Black diffractogram**: air-dried rock powder; **blue diffractogram**: ethylene-glycol solvated material; **red diffractogram**: samples heated up to 500 °C. Smectite expandability when solvated with ethylene glycol and its subsequent collapse at 500 °C is seen in sample #47 from the western sector of the Metán-Alemanía sub-basin. X-axis: position 2°θ. Y-axis counts per second (CPS). (TC) Tres Cruces and (MA) the Metán-Alemanía sub-basins. Sectors where samples were collected: north, south (N, S); east and west (E, W).

The increase of the illite/mica content of sample #23 is interpreted to be an indicator of cooling climate conditions at the end of the time when the Yacoraite Fm. was deposited (Fig. 3.3a). This succession of climatic changes matches the warming/cooling/warming/cooling succession that occurred during Maastrichtian times (Li and Keller, 1998; Keller and Abramovich, 2009). Those interpretations were based on planktic and benthic foraminifera-stable isotope data from two DSDP 525 sites drilled in the South Atlantic at a similar latitude to the Salta Rift basin in sediments temporally equivalent to the middle through upper sections of the Yacoraite Formation.

The cold periods occurred between 68-69.5 Ma and between 66.25-66 Ma (Keller et al., 2016). Similar climate variations during the Late Cretaceous were observed in sediments at northern latitudes and indicate that climate variations occurred at a global scale, probably triggered by changes in ocean circulation (Linnert et al., 2011). The increase of smectite content in the upper section of the Yacoraite Fm. (samples #28 & #29) is likely to have been caused by predominant chemical weathering that coincided with the maximum flooding conditions (compare Fig. 3.1c and Fig. 3.3a) when the climate was tropically to subtropically humid, as suggested by the kaolinite content (Chamley, 1989; Righi and Meunier, 1995) in sample #39 (Table 3, appendix).

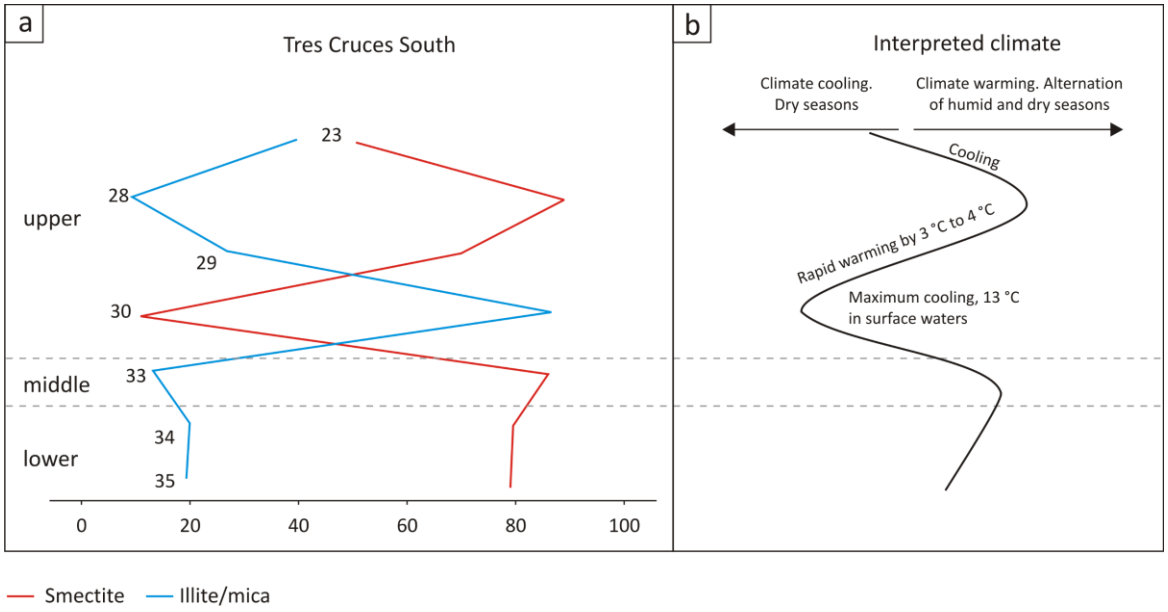

Fig. 3.3. (a) Variations in illite/mica and smectite content in the fraction <2 μm of the Yacoraite Fm. in the southern sector of the Tres Cruces sub-basin. (b) Interpreted climate variations based on illite/mica and smectite variations. These climate variations successions temporally coincide with the maximum cooling and rapid warming interpreted from planktic and benthic foraminifera-stable isotopes for the Maastrichtian (After Li and Keller, 1998). Physical weathering predominates in dry and cold conditions, enhancing the illite/mica content in sediments. Chemical weathering prevails in a warm climate where humid and dry periods alternate.

3.1.3 Chemical elements as archives of the depositional environment of the Yacoraite Fm.

Different parameters derived from elemental ratios have been used to evaluate the depositional environment. Nesbitt and Young (1982) used variations in oxides of aluminum, calcium, sodium, and potassium to assess different types of weathering. The Ca/(Ca+Fe) ratio was found to be sensitive to salinity and, therefore, is often used to characterize different conditions of depositional settings (Nelson, 1967; He et al., 2019). Ratios below 0.6 indicate lacustrine depositional environments, while ratios >0.8 indicate marine settings. Transitional settings are characterized by intermediate ratios. Variations in the Ca/(Ca+Fe) ratios in Fig. 3.4a resemble changes in carbonates content (mainly calcite) in Fig. 3.1a. This suggests that calcite is the main calcite-bearing mineral.

According to the Ca/(Ca+Fe) ratio, the lower Yacoraite Fm. (samples #34 & #35) was deposited in a transitional setting during the marine transgression (Fig. 3.4a). Marine environments dominated at the beginning of the deposition of the middle section (sample #33) with the subsequent development of lacustrine settings during the end of the deposition of the middle section (samples #31 & #32) (Fig. 3.4a). The deposition of the lower strata of the upper section (sample #30) occurred during a rise in sea level (Fig. 3.4a and elemental composition in Table 4 and Table 5, appendix). The sea level continued to rise during the deposition of samples #29 & #28. Subsequently, lacustrine settings predominated (samples #27, #26 & #24). At the end of the deposition of the upper section, transitional settings between lacustrine and marine environments evolved (Fig. 3.4a).

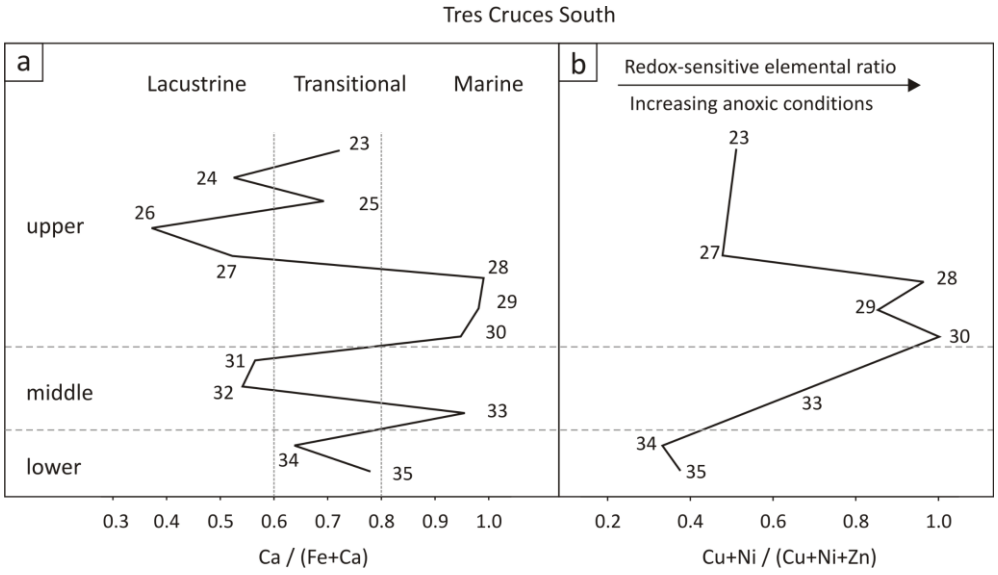

Fig. 3.4. Chemical elemental ratios used to characterize the depositional environment of the Yacoraite Fm. in the Tres Cruces sub-basin. (a) Ca/(Ca+Fe) ratio to differentiate lacustrine, marine, and transitional depositional settings. Transitional environments developed during the onset of the deposition of the Yacoraite Fm. Lacustrine settings evolved during the sedimentation of the middle section of the Yacoraite Fm. with predominant marine conditions towards the end of the deposition that generated the middle section and the beginning of the sedimentation of the upper section. Towards the top, lacustrine deposits dominate and record the subsequent development of a transitional environment. (b) Redox-sensitive chemical elements ratio. (Cu+Ni/Cu+Ni+Zn) suggest that anoxic conditions mainly existed during the deposition of the middle, and at the beginning of the upper sections.

Variations in the amount of redox-sensitive chemical elements, e.g., Ni, Cu, and Zn make them suitable as paleoenvironmental proxies to evaluate redox conditions at the time of deposition (e.g., Acharya and Chakrabarti, 2019). Ni and Cu are associated with reducing conditions, and Zn is associated with more oxic environments. Due to an opposite redox behavior, the (Cu+Ni)/ (Cu+Ni+Zn) ratio is used as a proxy for redox conditions (Fig. 3.4b). With a good inverse correlation (R2=0.96, n=8), the variation of these elements closely resembles the variation of detrital minerals (Fig. 3.1a), which in turn is inversely correlated with sea level (Fig. 3.1c). Consequently, the most anoxic conditions were established during times of high sea-levels and inundation.

Uranium is another redox-sensitive chemical element that may provide information on environmental conditions (Tribovillard et al., 2006). The Yacoraite Fm. documents uranium-enrichment at the base of its lower section. In the southern sector of the Tres Cruces sub-basin, sample #35 has a uranium content of 300 ppm while in the western sector of the Metán-Alemanía sub-basin, sample #51 has a concentration of 4400 ppm. The uranium content of sample #51 is two orders of magnitude greater than samples from the middle and upper sections (samples # 47 & #50). The uranium content of sample #35 is two orders of magnitude higher compared to sample #34 and one order of magnitude greater than that of samples from the upper section (sample #30; see elemental composition of tables 4 and 5, appendix).

The uranium enrichment at the base of the Yacoraite Formation was coeval with deposition (Ferreira et al., 2013 and references therein). This enrichment was the result of weathering of the

Precambrian and Paleozoic basement rocks (Salfity and Marquillas, 1999) once it was uplifted, forming the Pampean and Traspampean arches. In addition, regional differences are probably related to proximity to the source i.e., the granites. The deposition of uranium would have been possible in anoxic conditions where uranium (VI) in solution precipitates as U (IV) (Klinkhammer and Palmer, 1991). The heterogeneous distribution of uranium in the granitic bodies of the basement may explain why other samples in the stratigraphic succession do not have similar uranium contents. Additionally, sea-level rise would have prevented exposition and erosion of those granitic bodies, which precluded uranium to be incorporated into other samples.

The occurrence of organic sulphur indicates reducing conditions during the time of deposition (e.g., Berner and Raiswell, 1984). TOC vs. total sulphur (TS) plots have been used to assess the incorporation of sulphur in sediments and to characterize the depositional environment (Berner and Raiswell, 1984; Littke et al., 1997; Song et al., 2014). For marine environments, the observed TOC/TS ratios are typically between 0.5 and 5. For freshwater environments, where sulphur supply and sulphate reduction are limited, these ratios are generally greater than 10. Brackish environments are characterized by TOC/TS ratios in between those of freshwater and marine environments (Berner and Raiswell, 1984). The normal marine line (NML) is characterized by TOC/TS=2.8 and the euxinic Black Sea has a TS=0.6*TOC+1.14 (Song et al., 2015). Fig. 3.5 is a TOC vs. TS plot for samples of the Yacoraite Fm. The percentage of sulphur in sulphur-bearing minerals (Table 2, appendix) was subtracted from the total sulphur content. This was the case for example of samples #10, #39, and #47 in which gypsum was quantified by XRD.

According to organic petrography analyses, samples #11 and #48 have disseminated pyrite, the existence of this mineral was not detected by XRD. In these samples, gypsum was the only sulphur-bearing mineral detected, but it does not seem to affect the overall interpretation of the depositional characteristics as they consistently plot within the same region as the bulk of the other samples from the upper section of the Yacoraite Fm. Pyrite and gypsum were not detected in samples #18 and #51 (Table 2, appendix) in which total sulphur amounts to 0.37 % and 0.09 %, respectively. With those amounts, if all sulphur is pyritic, the stoichiometric content of this mineral should be 0.7 % and 0.1 % being below of the detection limit of XRD.

Taken together, the majority of the analyzed samples from the Yacoraite Fm. must have been deposited under anoxic and sulfate-reducing conditions; this assessment is supported by the TOC/TS ratio because samples generally plot above the NML (Fig. 3.5). Two samples (#35 & #47) were deposited in brackish environments. In contrast, sample #51 was deposited in a freshwater environment. Anoxic conditions were not established by the time of the deposition of sample #51 according to its position in the TOC vs. TS plot. However, when inspected under the microscope, ubiquitous pyrite is observed in this sample. As no mineralized veins caused by hydrothermal fluids were observed, pyrite in this sample is interpreted as primary sedimentary mineral. Its presence indicates deposition under reducing conditions and no further appreciable alteration after deposition.

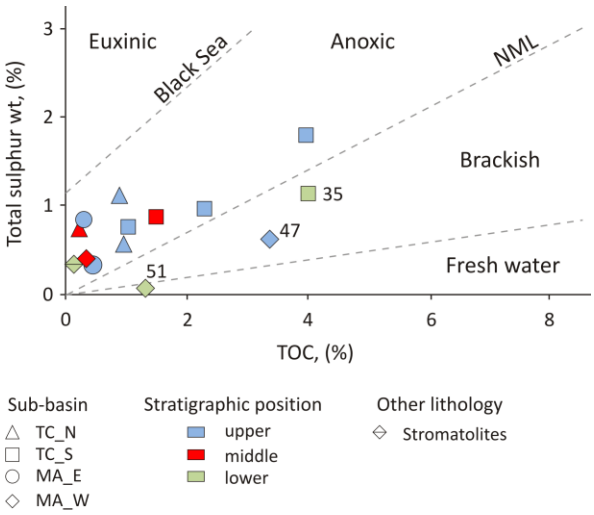

Fig. 3.5. Total sulphur (TS) vs. TOC in whole-rock samples of the Yacoraite Formation. Most samples plot in the field of marine anoxic environments. A brackish environment is represented by two samples from the southern sector of the Tres Cruces sub-basin (sample #35) and the eastern sector of the Metán-Alemanía sub-basin (sample #47). Sample #51 represents deposition in a freshwater environment. NML: Normal marine line. (TC) Tres Cruces, (MA) Metán-Alemanía sub-basins. The sectors where samples were collected are north, south (N, S) and east and west (E, W).

The Yacoraite Fm. was deposited in a shallow marine environment within the Salta Rift basin (Marquillas et al., 2005). Elemental ratios, such as $Al_2O_3/Al_2O_3+Fe_2O_3$ and Fe_2O_3/TiO_2 have previously been used for water depth assessments (Zong et al., 2016; He et al., 2019). According to these parameters, the Yacoraite Fm. was deposited at water depths of less than 200m, which is compatible with an environment characterized by a shallow epicontinental sea (Fig. 3.6). The presence of present-day stromatolites in East African Rift lakes and Holocene shorelines (Casanova, 1986; Hillaire-Marcel et al., 1986; Cohen et al., 1997) helps to constrain the maximum depth to only a few tens of meters. Based on additional lithofacies analysis Deschamps et al. (2020) interpreted that in the Alemanía sub-basin the Yacoraite Fm. deposited in lacustrine environments at maximum depths around 40m.

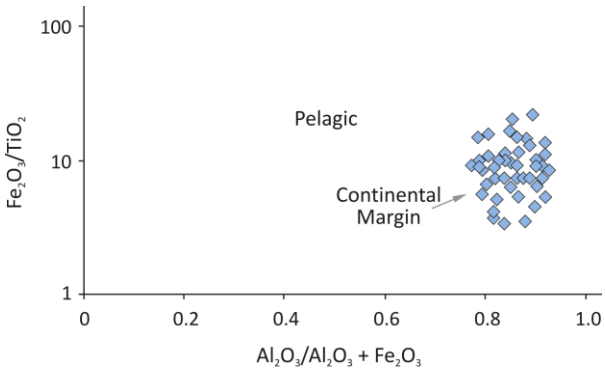

Fig. 3.6. Fe_2O_3/TiO_2 ratios vs. $Al_2O_3/(Al_2O_3+Fe_2O_3)$ ratios determined for the Yacoraite Formation. These parameters suggest that the Yacoraite Fm. was deposited at water depths of <200 m regardless of the sub-basin where they were retrieved. After Zong et al. (2016).

3.2 Kerogen type of the Yacoraite Formation

3.2.1 Element-based classification

The organic parameters for kerogen typing discussed below can be affected by thermal maturity and oxidation of the organic matter. For example, the HI decreases with thermal stress (Cornford et al.,

1998). The samples from the Yacoraite Fm. are at the onset of petroleum generation (Section 4.1); therefore, the effects of thermal maturity on these samples are safely ruled out. Parameters derived from Rock-Eval pyrolysis, such as HI and OI, represent an "average" of the properties of the organic matter in each sample. They are related to the type of organic matter (kerogen) influenced in turn by the depositional environment. In thermally immature rocks, HI values >600 mg HC/g TOC characterize Type I kerogen, usually formed in lacustrine settings. Marine Type II kerogen associated with marine environments has a HI between 300-600 mg HC/g TOC. In Type II/III mixtures, the HI values are between 200-300 mg HC/g TOC. Terrigenous Type III kerogen is characterized by a HI between 50-200 mg HC/g TOC. HI values below 50 mg HC/g TOC are characteristic of Type IV kerogen (Peters and Cassa, 1994).

The Yacoraite Fm. exhibits a wide spectrum of TOC and S2 values (Fig. 3.7a, b and Table 6, appendix). In general, samples collected in the Tres Cruces sub-basin have higher S2 and TOC values than those from the Metán-Alemanía sub-basin. Most of the samples from the Tres Cruces sub-basin have TOC values below 1 % and S2 values below 5 mg HC/g rock. Higher TOC and S2 values were measured in the southern sector of the Metán-Alemanía sub-basin with TOC values between 1-4% and S2 between 5- 40 mg HC/g rock. Only one sample (#3) from the northern sector exhibits relatively high TOC values of 6.9 % and S2 of 41 mg HC/g rock. In general, samples retrieved from the Metán-Alemanía sub-basin have TOC values below 0.5 % and S2 values below 2.5 mg HC/g rock, with one sample (#47) from the western sector reaching values of 3.36 % TOC and 8.95 mg HC/g rock S2 (Fig. 3.7a, b).

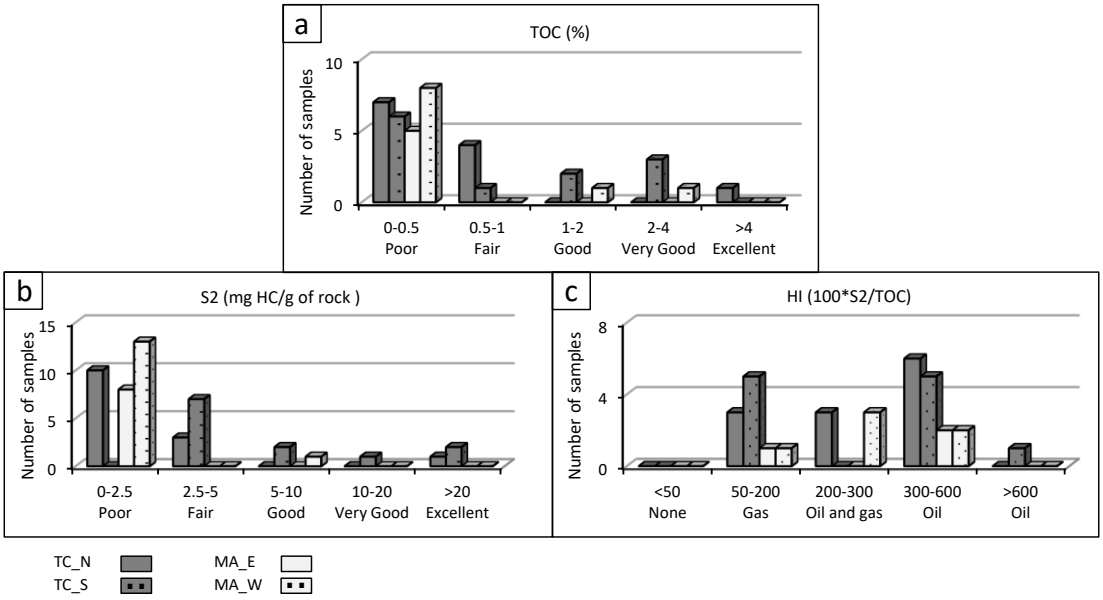

Fig. 3.7. Histograms of parameters used to assess the organic richness and kerogen type in samples of the Yacoraite Fm. (a) TOC. (b) S2, measured in pyrolysis Rock-Eval. (c) Hydrogen Index. Most of the samples from the Yacoraite Fm. have a TOC below 1 %, S2 values below 5 mg HC/g rock, and HI values between 300 mg HC/g TOC and 600 mg HC/g TOC, indicative of Type II kerogen. (TC) Tres Cruces, (MA) Metán-Alemanía sub-basins. The sectors where samples were collected are north, south (N, S) and east and west (E, W).

The pronounced variation of TOC and S2 values results in a significant variability of HI values for the Yacoraite Fm. In general, HI values are in the range from 60-600 mg HC/g TOC (Fig. 3.7c), suggesting that Type II-III kerogens and admixtures are the main components. These values are not specifically associated with any particular sub-basin or position in the stratigraphic succession (Fig. 3.8). There are two samples with the highest and the lowest HI, respectively. Sample #30 has a Type I kerogen (HI = 1015 mg HC/g TOC), which is typically associated with lacustrine environments (Espitalié, 1986). With a very low HI (11 mg HC/g TOC), sample #51 contains Type III or even Type IV kerogen. The tar sample collected in the northern sector of the Tres Cruces sub-basin has a HI value of 538 mg HC/g TOC that is similar to the nearby shale sample #40 of the upper section of the Yacoraite Fm., which is characterized by a HI value of 547 mg HC/g TOC.

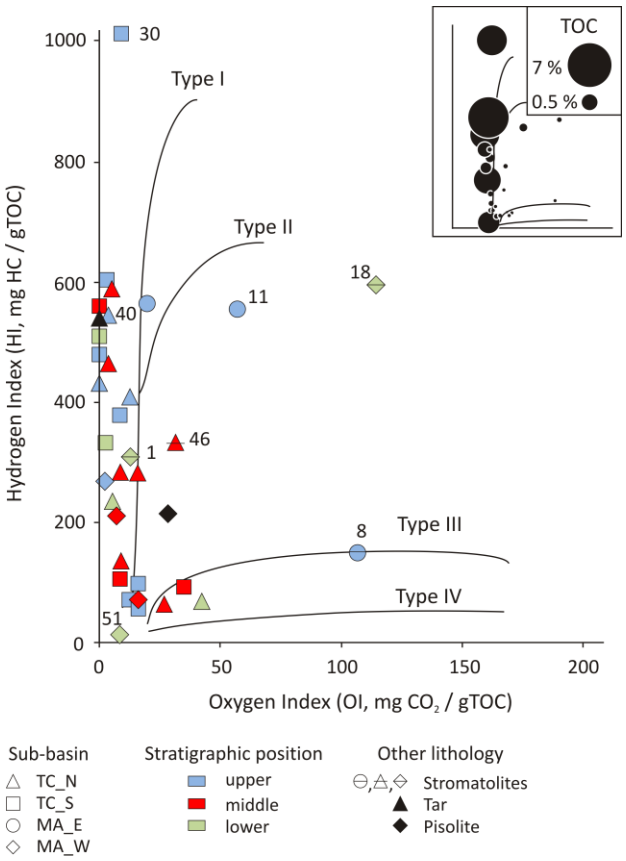

Fig. 3.8. Modified Van Krevelen diagram of HI vs. OI based on Rock-Eval pyrolysis of whole-rock samples of the Yacoraite Fm. The Yacoraite Fm. is predominantly composed of Type II, II/III kerogen mixtures that suggest marine organic-matter input, as well as some Type III kerogen indicative of terrestrial organic-matter input. Inset: TOC bubble diagram in the HI vs. OI plot. Samples with TOC <0.5% consistently plot as Type III kerogen, suggesting mineral-matrix effect (MME) interferences. (TC) Tres Cruces, (MA) Metán-Alemanía sub-basins. The sectors where samples were collected are north, south (N, S) and east and west (E, W).

Regardless of the location in the sub-basins or the stratigraphic succession, the OI values are lower than 60 mg CO_2/g TOC (Fig. 3.8 and Table 6, appendix). One exception is sample #11 from the upper section of the Yacoraite Fm., which was collected in the eastern sector of the Metán-Alemanía sub-basin with an OI of 58 mg CO_2/g TOC and the two stromatolite samples. One of the stromatolite samples (sample #8) was collected in the upper section of the Yacoraite Fm. in the eastern sector of the Metán-Alemanía sub-basin. This sample has an OI of 108 mg CO_2/g TOC. The other (sample #18) was collected in the lower section of the Yacoraite Fm. in the western sector of the same sub-basin. This sample has an OI of 115 mg CO_2/g TOC.

During pyrolysis experiments, some of the generated hydrocarbons can be adsorbed on mineral surfaces (mineral-matrix effect, MME), which prevents the correct quantification of the S2 peak, resulting in low HI values, thereby overestimating the contribution of terrestrial input. Although samples with different organic richness can be affected, e.g., HI from 14 to 997 mg HC/g TOC (Mukhopadhyay, 1989; Horsfield et al., 1994), samples with low TOC content (i.e., <2 %, according to Dembicki, 2009; <0.5 %, according to Peters, 1986) are especially susceptible. The MME magnitude depends on the nature of the association between the minerals and the organic matter (Rahman et al., 2017). Samples of the Yacoraite Fm. that plot as Type III kerogen also have low TOC values (<0.3 %, see inset in Fig. 3.8), whereby kerogen typing in these samples is likely biased by MME. In consequence the input of Type III kerogen in those samples is likely overestimated due to artefacts during pyrolysis Rock-Eval. Sample #51, with a TOC=1.3 % is likely not to be affected by MME. Like the other samples, the organic matter in sample #51 predominantly consists of alginites and oxidation of the organic matter was not observed during inspection by organic petrography. Therefore, maceral composition and oxidation are ruled out as the cause of its low HI which is presumably due to radiolysis as addressed in section 4.3.2.

Stromatolites in the Yacoraite Fm. are associated with different kerogen types based on pyrolysis, i.e., Type III kerogen (sample #8), II/III kerogen (samples #1 & #46), and Type II kerogen (sample #18). The higher OI of 108 mg CO_2/g TOC in stromatolite #8 (Fig. 3.8 and Table 6, appendix) and 115 mg CO_2/g TOC for sample #18 might be due to the presence of certain carbonates that decomposed thermally, thus increasing S3 peaks (Peters, 1986). However, carbonates in those samples correspond to non-thermal labile calcite and dolomite, as analyzed by XRD (Table 2, appendix). The content of carbonates in sample #8 is 88 % and only corresponds to calcite. In sample #18, the calcite content is 66 %, and dolomite content is 17 %. Variability in the organic composition of stromatolites reflects the diversity of their microbial communities. Some Paleozoic stromatolites with Type I kerogen consist of *G. prisca.* The Type II kerogen in Devonian stromatolites consists of *Nostocaceae-like* filamentous alginite (Stasiuk, 1994). Mesozoic stromatolites containing prasinophytes have been reported to be composed of Type II, II/III kerogen (McKirdy et al., 1980; McKirdy and Hahn, 1982). Type II kerogen can form from a large variety of marine biota mixed with subsidiary amounts of humic organic matter. Humic kerogen is derived either from land-plant residues or bacterial cell-wall lipids.

The Type III and IV kerogen identified in stromatolites might be formed from mucopolysaccharides of cyanobacteria that show elemental compositions similar to those of vitrinite or fusinite (McKirdy et al., 1980; McKirdy and Hahn, 1982). Pyrolytic organic acids can enhance OI values in samples with a TOC lower than 0.5 % (Peters, 1986). This can be the case for stromatolites (samples #8 & #18) with comparatively higher OI and a relatively low TOC of 0.03 % and 0.15 % TOC, respectively. No measurements of pyrolytic organic acids were carried out to support this interpretation. Organic matter can be affected by oxidation during transport, deposition or diagenesis, consequently increasing OI (e.g., Durand and Monin, 1980). Additional oxidation is caused by weathering or grinding

during sample preparation (Peters, 1986). Apart from the stromatolites mentioned, the rest of the samples from the Yacoraite Fm. have an OI lower than 60 mg CO_2/g TOC. These values indicate no or negligible oxidation of organic matter during deposition and no subsequent oxidation in the geological environment or during sampling/handling. The low OI are therefore indicative of good organic-matter preservation.

S2/TOC plots are used for combined kerogen typing of an entire set of samples (Langford and Blanc-Valleron, 1990; Dahl et al., 2004). The Yacoraite Fm. is mainly composed of Type II kerogen as indicated by S2/TOC trends in the samples collected in the Tres Cruces sub-basin (Fig. 3.9a) and the Metán-Alemanía sub-basin (Fig. 3.9b). The slightly higher terrestrial input in the western sector of the Metán-Alemanía sub-basin is reflected in Type II-III kerogen admixtures (green dashed line in Fig. 3.9b). Linear trends in TOC vs. S2 have correlation coefficients (R^2) of 0.81 and 0.99 (black lines in Fig. 3.9a, b) for the set of samples collected in the Metán-Alemanía and the Tres Cruces sub-basins, respectively. This positive correlation is related to a uniform kerogen type (Dahl et al., 2004) and/or no pronounced oxygen-content changes in bottom water during deposition (Langford and Blanc-Valleron, 1990). This type of analysis is more robust in the Tres Cruces sub-basin due to the greater amount of data (23 data points) compared to the Metán-Alemanía sub-basin (11 data points).

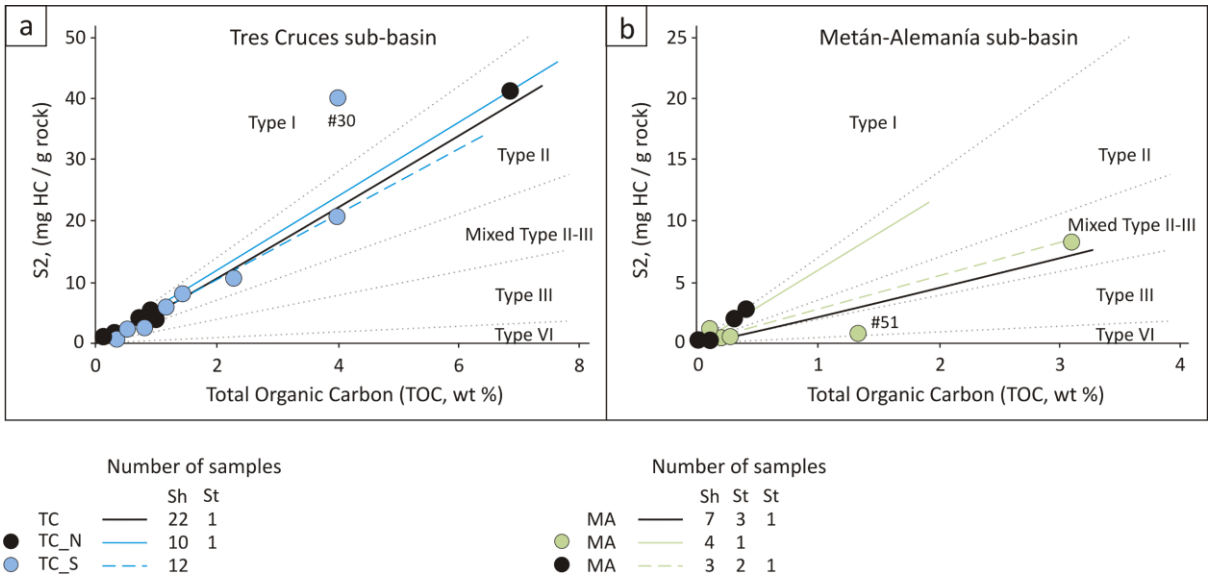

Fig. 3.9. S2 vs. TOC plots for samples of the Yacoraite Fm. (a) Tres Cruces sub-basin, (b) Metán-Alemanía sub-basin. The Type II kerogen is the main kerogen type of these samples. Mixed type II/III kerogen indicates some contribution of Type III kerogen in the western sector of the Metán-Alemanía sub-basin. Black lines mark the kerogen-type trend for the sub-basin. Sample #30 with the highest HI (1015 mg HC/g TOC) and sample #51 with the lowest HI (11 mg HC/g TOC) were not included to determine the trend line and to calculate R^2. Continuous lines mark the trends for sectors in the north (N) and east (E), dashed lines for south (S) and west (W). Samples are shales/marls (Sh), stromatolites (St), and pisolite (Pis), with the number of samples indicated by n.

3.2.2 Molecular typing of kerogen (pyrolysis-GC)

Organic geochemical signatures of marine, lacustrine, and brackish environments exist in the Tres Cruces and Metán-Alemanía sub-basins on different stratigraphic levels of the Yacoraite Fm.,

indicating changes in depositional environment during deposition. Hydrocarbon chain-length distribution (HCLD) can be used to describe changes in the depositional environment of the Yacoraite Fm., as discussed below. According to their HCLD the lower units of the Yacoraite Fm. were deposited under marine conditions in the southern sector of the Tres Cruces sub-basin (samples #34, #35 & #37) and the western sector of the Metán-Alemanía sub-basin (stromatolites #1 & #18; Fig. 3.10a). In the latter, sample #51 was deposited in an environment with predominant terrestrial input as indicated by its position in the left corner of the ternary plot that corresponds with the gas hydrocarbon range (C_1-C_5). However according this sample is highly mature according to T_{max} and vitrinite reflectance (cf. section 4.1) which can explain its gas generation potential. This potential is presumably caused by radiolysis (cf. section 4.3.2).

The middle section of the Yacoraite Fm. in the Tres Cruces sub-basin still shows a marine influence, as suggested by HCLD (sample #45 in Fig. 3.10b). Lacustrine environments evolved during this time (samples #33, #42 & #44). Samples #2 and #46 (stromatolite) from the northern sector of the Tres Cruces sub-basin and sample #50 from the west sector of the Metán-Alemanía sub-basin were deposited with higher terrigenous input, as indicated by its HCLD in (Fig. 3.10b). The upper section of the Yacoraite Fm. in the Tres Cruces sub-basin was deposited in a lacustrine setting (Fig. 3.10c). In the Metán-Alemanía sub-basin the signature of marine environments becomes stronger towards the top of the stratigraphic succession in the western sector (sample #47), while in the eastern sector (sample #11) marine, and finally lacustrine conditions superseded. Sample #48 was deposited with high terrestrial input.

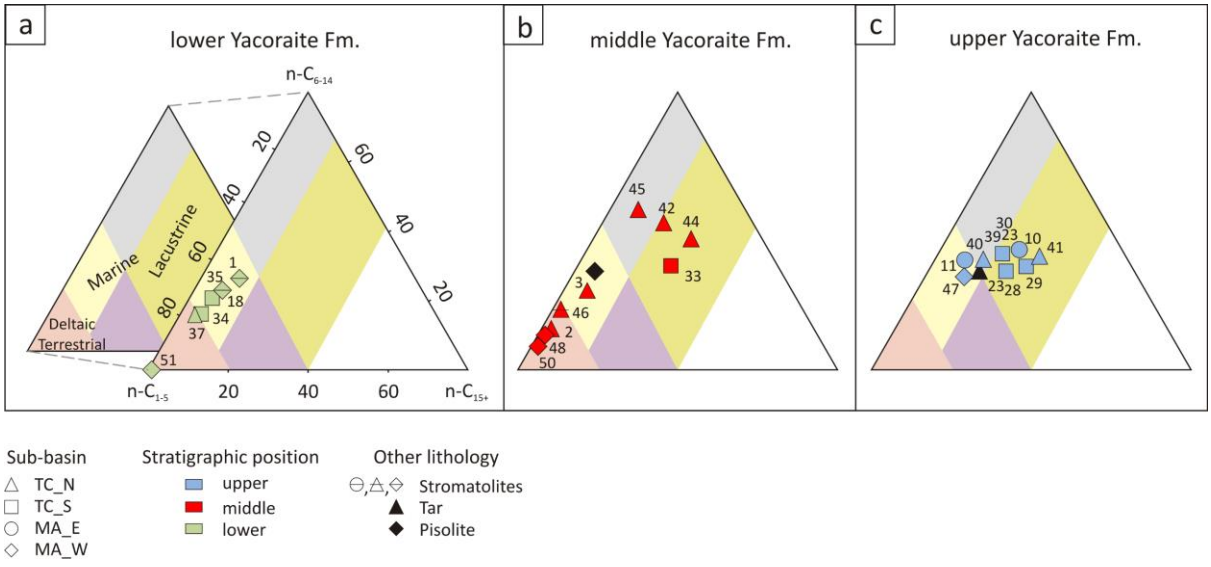

Fig. 3.10. Hydrocarbon chain-length distribution (Py-GC) of total C_1-C_5 resolved pyrolysates, C_6-C_{14} n-alk-1-enes plus n-alkanes, and C_{15}+ n-alk-l-enes plus n-alkanes of the Yacoraite Fm. samples. Interpretation of depositional environment interpretations after Horsfield (1997). (a) Marine environments predominated during the onset of the deposition of the Yacoraite Fm. (b) The middle section of the Yacoraite Fm. was predominately deposited in a marine setting with occasional transitions to lacustrine environments. (c) Lacustrine environments became predominant during the deposition of the upper section of the Yacoraite Fm. in the Tres Cruces sub-basin and the eastern sector of the Metán-Alemanía sub-basin. (TC) Tres Cruces, (MA) Metán-Alemanía sub-basins. Sectors where samples were collected are north, south (N, S) east and west (E, W).

3.2.3 Organic matter typing - insights from organic petrology

Organic petrography allows to directly identify kerogen particles, supporting kerogen interpretations based on other indirect methods such as Rock-Eval pyrolysis. Organic petrography has demonstrated that the Yacoraite Fm. in both the Tres Cruces and the Metán-Alemanía sub-basins mainly consists of alginite (Fig. 3.11), which makes up 80-90 % of the total amount of organic matter. This supports the Type II kerogen interpreted from Rock-Eval pyrolysis (Fig. 3.8) and S2-TOC trends (Fig. 3.9). Sample #51 is also predominantly composed by alginites (Fig. 3.11f) and has a slightly higher terrigenous input reflected by more vitrinite-like particles. The increase of terrigenous input in this sample is probably due to proximal conditions that existed to the south of the Valle del Tonco (Hernández et al., 2008), suggesting the Traspampean arc (Salfity and Marquillas, 1999) as a source of sediments. It is unlikely that this small amount of terrestrial input causes the low S2 and HI values as has been argued in other studies (e.g., Eglinton et al, 1990). The position of this sample in the HI vs. OI plot (Fig. 3.8) and TOC vs. S2 plot (Fig. 3.9b) can be due to the predominant presence of Type III or IV kerogen or alternatively be the consequence of its spent generation potential. High inertinite content could result in a low HI (Wilkins, 1999). However, no inertinites were observed in organic petrography. The good preservation of organic matter and the presence of ubiquitous pyrite suggest that oxidation can be ruled out as cause of kerogen alteration. Kerogen properties in sample #51 are presumably affected by radiolysis as addressed in section 4.3.2.

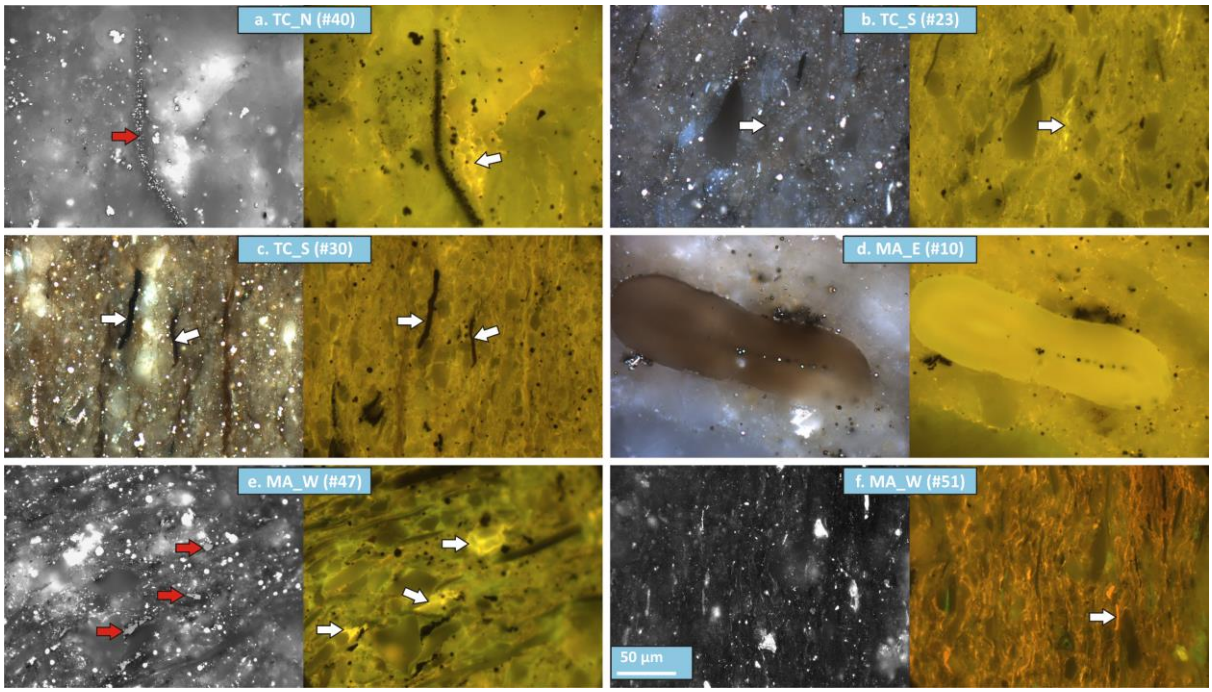

Fig. 3.11. Photomicrographs under incident light and oil immersion of polished whole-rock samples of the Yacoraite Fm. Photos are paired as white light, followed by the corresponding UV fluorescence picture. Alginites are the main organic constituent of the Yacoraite Fm. regardless of the sub-basin. (a) Bitumen associated with abundant pyrite. (b) Discrete lamalginite. (c) Bitumen in sample 30 (HI= 1015 mg HC/g TOC). (d) Telalginite (Tasmanite). (e) Indigenous small vitrinite and lamalginite, right. (f) Elongated alginite. The scale is identical for all photos. (TC) Tres Cruces, (MA) Metán-Alemanía sub-basins. The sectors where samples were collected are north, south (N, S) and east and west (E, W).

3.2.4 Organic matter typing- insights from biomarkers

In the Yacoraite Fm. the Pr/n-C_{17} ratios are between 0.4 and 5. Ph/n-C_{18} ratios are between 0.3 and 4 (Fig. 3.12 and Table 7, appendix). These values support the interpretation that Type II kerogen is the main organic constituent of the Yacoraite Fm., although with some terrigenous contributions, which is shown by the existence of Type II/III kerogen mixtures in Fig. 3.12. This interpretation is compatible with the alginite predominance of organic petrography. This also applies to sample #51, but is not in agreement with the Type III/IV kerogen interpreted for this sample from OI vs. HI plot (Fig. 3.8) and from the TOC vs. S2 plot (Fig. 3.9). As the TOC, the S2 and consequently the HI are reduced due to increasing thermal stresses; the kerogen type III or IV interpreted for sample #51 based on those parameters, can be caused by higher thermal maturity compared to the other samples and therefore, does not reflect the kerogen type. Thermal maturity is addressed in section 4.1 and inorganic influences affecting the thermal assessment of sample #51 are presented in section 4.3. The lower section of the Yacoraite Fm. (green in Fig. 3.12) in the Tres Cruces sub-basin and the eastern sector of the Metán-Alemanía sub-basin seem to have had a slightly higher terrestrial input.

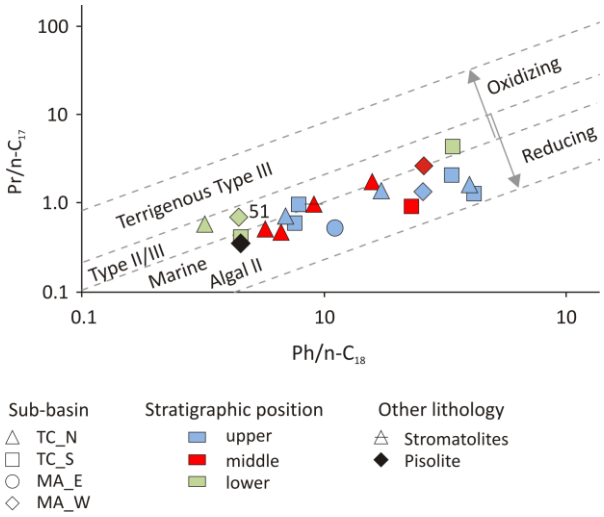

Fig. 3.12. Pristane/n-C_{17} ratios vs. phytane/n-C_{18} ratios of extracts of the Yacoraite Fm. The Yacoraite Fm. was deposited under predominant reducing conditions. The Type II kerogen was the main organic constituent with some terrigenous input, as suggested by II/III kerogen mixtures. (TC) Tres Cruces, (MA) Metán-Alemanía sub-basins. The sectors where samples were collected are north, south (N, S) and east and west (E, W).

3.2.5 Redox conditions developed during the deposition of the Yacoraite Formation

In geological depositional environments, the transformation from phytol to either pristane or phytane depends on the redox conditions. Pristane is formed under oxic conditions after oxidation of phytol to phytenic acid and subsequent loss of its carboxyl group (Peters et al., 2005a). Under reducing conditions, phytane is predominantly formed from its immediate dihydrophytol precursor after phytol reduction (op. cit.). Redox conditions during the Yacoraite Fm. deposition were evaluated using the pristane/phytane (Pr/Ph) ratio in addition to Pr/n-C_{17} and Pr/n-C_{18} ratios shown in Fig. 3.12. In samples from the Yacoraite Fm. the Pr/Ph ratios are between 0.3 and 1.3 The slightly higher phytane concentrations (Fig. 3.13a), especially in samples collected in the upper section of the Yacoraite Fm. in the Tres Cruces sub-basin (samples #30 & #39) indicates prevailing anoxic conditions during deposition. The isoprenoids pristane and phytane are only suitable as redox proxy, if they share a

common precursor (Peters et al., 2005a). If one of them is enriched due to additional input from a different source, the use of the Pr/Ph ratio is biased (Risatti et al., 1984). The Pr/Ph ratio increases with thermal maturity until the later stage of diagenesis (Brooks et al., 1969). Similarly, $\delta^{13}C$ values for pristane and phytane in the Yacoraite Fm. (Fig. 3.13b) indicate that they originated from a similar precursor and, therefore, are suitable as parameters to determine paleo redox conditions. The exception is sample #30 with a $\delta^{13}C$ difference of 2.5 ‰ between pristane (28.7 ‰ ± 0.16 ‰) and phytane (31.5 ‰ ± 0.11 ‰), which suggests a slight variation in the precursors.

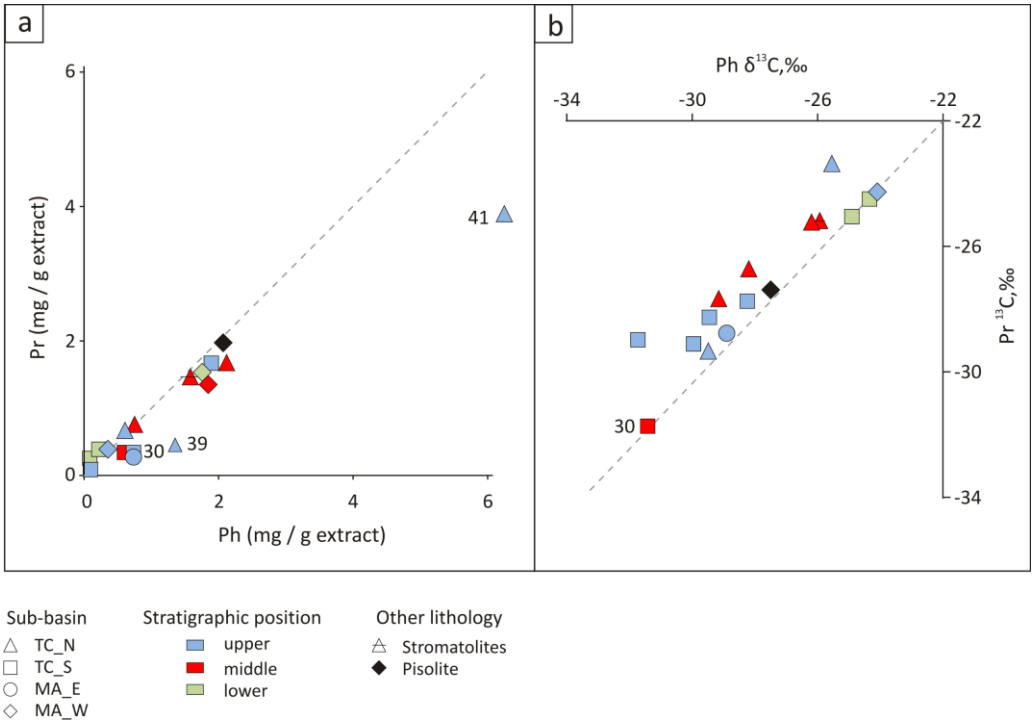

Fig. 3.13. Variation in Pristane vs. phytane in the aliphatic fraction of extracts of the Yacoraite Formation. (a) Higher phytane concentration compared to pristane indicates anoxic conditions during the deposition of the Yacoraite Fm. (b) Pristane vs. phytane $\delta^{13}C$ concentrations. Similar $\delta^{13}C$ concentrations in pristane and phytane indicate a common precursor; therefore, their use as a proxy to assess redox conditions in this set of rock samples is reliable. (TC) Tres Cruces, (MA) Metán-Alemanía sub-basins. The sectors where samples were collected are north, south (N, S) and east and west (E, W).

Higher concentrations of phytane compared to pristane suggest the development of anoxic conditions during the deposition of the Yacoraite Fm. This is supported by Pr/Ph vs. $C_{34}S/C_{35}S$ hopane biomarkers (Fig. 3.14) and agrees with the presence of pyrite. These conditions favored the good organic-matter preservation. A slight predominance of $C_{34}S$ compared to $C_{35}S$ in the bottom samples resulted in ratios of $C_{34}S$ to $C_{35}S$ close to, but below 1.5 (Table 7, appendix). No $C_{34}S$ nor $C_{35}S$ hopanes were detected in samples from the lower section of the Yacoraite Fm. collected in the southern sector of the Tres Cruces sub-basin (samples #34 & #35) and the western sector of the Metán-Alemanía sub-basin (sample #51). Therefore, no $C_{34}S/C_{35}S$ ratios were calculated for those samples. In samples of the middle section of the Yacoraite Fm., the predominance of $C_{34}S$ over $C_{35}S$ becomes a little more pronounced, and consequently, their ratios are close, but higher than 1.5. Similar amounts of $C_{34}S$ and $C_{35}S$ hopanes were measured in most of the samples at the top of the Yacoraite Fm., regardless of the

sub-basin they came from. Consequently, these samples have a $C_{34}S$ to $C_{35}S$ ratio close to one. Neither $C_{34}S$ nor $C_{35}S$ hopanes were detected in samples from the upper section of the Yacoraite Fm. (samples #47 & #48) in the western sector of the Metán-Alemanía sub-basin (Table 7, appendix).

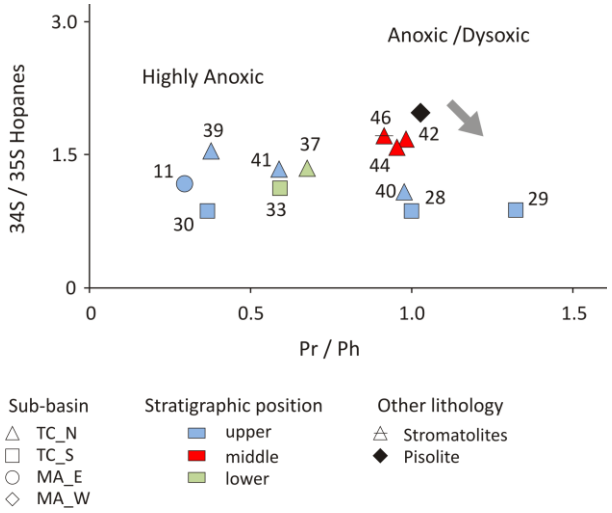

Fig. 3.14. $C_{34}S/C_{35}S$ hopanes ratios vs. pristane/phytane ratios of extracts of the Yacoraite Fm. The prevalence of reducing/anoxic depositional environments is interpreted during the Yacoraite Fm. deposition. (TC) Tres Cruces, (MA) Metán-Alemanía sub-basins. The sectors where samples were collected are north, south (N, S) and east and west (E, W).

3.2.6 Marine vs. lacustrine conditions during the deposition of the Yacoraite Fm.

Under sulphate-reducing conditions, the reactive sulphur can be incorporated into organic matter (Tissot and Welte, 1984). The dibenzothiophene to phenanthrene ratio (DBT/P) is indicative of such a process and provides insights into the conditions that prevailed in the depositional environment (Hughes et al., 1995). Phenanthrene exists in all analyzed samples of the Yacoraite Fm. Some samples lack DBT irrespectively of their location in the sub-basins or the stratigraphic succession (Table 7, appendix). In all samples of the Yacoraite Fm. analyzed in this study, a predominance of phenanthrene over dibenzothiophene is observable, with a DBT/P ratio below 0.6 regardless of sample location within the sub-basins or within the stratigraphic succession. The upper section of the Yacoraite Fm. exhibits a higher DBT/P ratio compared to its lower and middle sections (Table 7, appendix).

According to Hughes et al. (1995), a DBT/P>1 is indicative of carbonate rocks. However, in this study, shales/marls with a high carbonate content, e.g., samples #28 (72 %), #29 (64 %), #40 (78 %), #41 (71 %), #42 (95 %) and stromatolite #46 (82 %), have a DBT/P ratio of <1. Therefore, inferences about the lithology of a rock type cannot rely only on interpretations based on DBT/P ratio obtained from extracts. On the one hand, in this set of samples, DBT/P shows marginal variations that are possibly due to an unsteady sulphur supply during incorporation into the organic matter. On the other hand, iron competes for sulphur forming pyrite within the same depositional environment, therefore, the incorporation of sulphur into organic matter decreases. In samples reflecting such a process, the pyrite content is generally <<10%, indicating low iron availability. Therefore, this was not a factor precluding sulphur incorporation into organic matter. The low DBT/P ratios are likely due to low supply of DBT precursors in the depositional environment.

Samples #30 and #34 have the highest pyrite content of 8 % and 9 %, respectively (Table 2, appendix). This indicates higher sulphur and iron availability compared to other samples. However, there is a difference in the incorporation of sulphur into organic matter, as documented by the DBT content. Sample #30 has nearly half the DBT content compared to phenanthrene. In sample #34 DBT was not detected. As mentioned above, this difference may result from reactive iron competing for sulphur. Once a part of the available sulphur has reacted with iron, the remainder could be incorporated into the organic matter as might have been the case with sample #30. In sample #34 all, or at least a large amount of the available sulphur had reacted with iron, thus prohibiting sulphur incorporation into DBT. Most of the samples of the Yacoraite Fm. have Pr/Ph and DBT/P ratios <1 (Fig. 3.15), which suggests they were deposited in a low-sulphur lacustrine environment. Samples #29, #34 & #35 have a Pr/Ph ratio >1 and were deposited in either lacustrine or marine environments, both characterized by a low availability of sulphur.

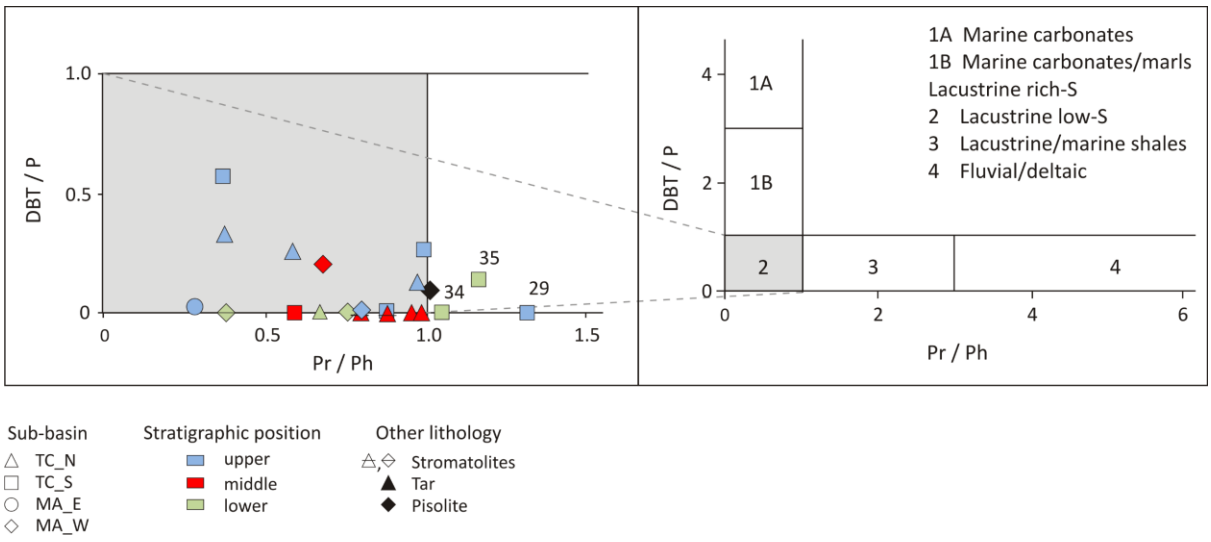

Fig. 3.15. Dibenzothiophene (DBT)/phenanthrene (P) ratios vs. pristane (Pr)/phytane (Ph) ratios of extracts of the Yacoraite Fm. Low DBT/P ratios <1 indicate low sulphur incorporation into the organic matter. (TC) Tres Cruces, (MA) Metán-Alemanía sub-basins. The sectors where samples were collected are north, south (N, S) and east and west (E, W).

Since sulphur incorporation into organic matter is controlled by Eh and pH and because these factors are not specifically restricted to lacustrine or marine environments, the DBT/P ratio is of limited value to infer depositional environments, yet it is a useful parameter to evaluate sulphur incorporation into organic matter (Hughes et al., 1995). Radke et al. (2001) found that extracts of mature (0.68 %Ro to 0.88 %Ro) and overmature (1.44 %Ro) samples of the marine Toarcian Posidonia Shale in NW Germany plot in the region of low-sulphur lacustrine depositional environments. These authors attributed the low DBT/P ratio to phenanthrene generation and pointed out the thermal-maturity effect on this ratio. The set of samples analyzed in this thesis is slightly mature (section 4.1). Therefore, the effect of thermal stress on DBT/P ratios can be ruled out. Low sulphur incorporation into organic matter is expected in freshwater or brackish lakes, where fermentation prevails on sulphate reduction (Hughes

et al., 1995). Following the criteria defined by these authors, i.e., Pr/Ph<1, DBT/P<1 and Fe>S, fermentation, rather than sulphate reduction must have been the dominant process during the deposition of the Yacoraite Fm. However, the presence of pyrite in these samples is proof that sulphate reduction took place.

Well-documented evidence of changes in ratios of C_{26}/C_{25} tricyclic terpanes vs. $C_{31}R/C_{30}$ hopanes supports the assessment of the depositional environment (Peters et al., 2005a). C_{26}/C_{25} tricyclic terpane ratios of <1 and $C_{31}R/C_{30}$ hopanes ratios >0.25 indicate deposition in marine environments. Typically, lacustrine settings have C_{26}/C_{25} tricyclic terpane ratios >1 (Zumberge, 1987). Marine and lacustrine environments cannot be distinguished with C_{26}/C_{25} tricyclic terpanes ratios between ≈1 and ≈1.35. In samples of the Yacoraite Fm. the C_{26}/C_{25} tricyclic terpane ratios vary between approximately 1 and 2 in most of the samples collected in the Tres Cruces sub-basin. Tricyclic terpanes were not detected in samples #34 & #40 from the upper section of the Yacoraite Fm. In this sub-basin, $C_{31}R/C_{30}$ hopane ratios vary between 0.2 and 0.4 (Fig. 3.16 and Table 7, appendix).

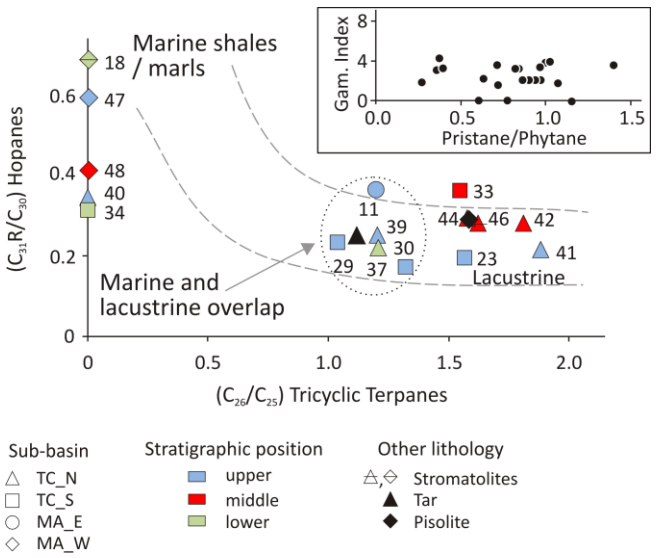

Fig. 3.16. ($C_{31}R/C_{30}$) hopane ratios vs. (C_{26}/C_{25}) tricyclic terpane ratios of extracts from the Yacoraite Formation. The Yacoraite Fm. exhibits signatures characteristic of marine and lacustrine environments. Some samples plot in a region where marine or lacustrine environments cannot be unambiguously defined (overlapping zone). Inset: Pristane/phytane vs. Gammacerane Index (see description in text). Stratification of the water column is indicated by gammacerane presence and was likely developed due to hypersalinity. This biomarker was not detected in samples #35, #41, and #51. Modified from Peters et al. (2005a). (TC) Tres Cruces, (MA) Metán-Alemanía sub-basins. The sectors where samples were collected are north, south (N, S), east and west (E, W).

In the Metán-Alemanía sub-basin, tricyclic terpanes were only detected in sample #11 from the upper section of the Yacoraite Fm. collected in the eastern sector. The analyzed samples from the western sector of the Metán-Alemanía sub-basin lack C_{25} and C_{26} tricyclic terpanes, regardless if they are from the lower (sample #51) or upper (samples #47 & #48) sections of the Yacoraite Fm. In this sub-basin, $C_{31}R/C_{30}$ hopane ratios of up to 0.7 were calculated for the lower section of the Yacoraite Fm. (sample #18). In contrast, the upper section shows $C_{31}R/C_{30}$ hopane ratios of 0.4 (sample # 48) and 0.6 (sample #47).

Based on the absence of tricyclic terpane and hopane ratios, the lower section of the Yacoraite Fm. was likely deposited under marine conditions (sample #34) in the southern sector of the Tres Cruces sub-basin. The ratio of tricyclic terpanes and hopanes plotted in Fig. 3.16, does not allow to unambiguously distinguish between lacustrine and marine environments in the northern sector of this

sub-basin (sample #37). This is also the case for some samples from the middle and the upper sections of the Yacoraite Fm. C_{26}/C_{25} tricyclic terpane and $C_{31}R/C_{30}$ hopane ratios indicate the existence of lacustrine environments during the deposition of the middle and upper Yacoraite Fm. in the Tres Cruces sub-basin (Fig. 3.16). In addition to their proximity in the field, the similar tricyclic terpane and hopane ratios of tar (black triangle in Fig. 3.16) and sample #39, suggest similar precursors/environments and a possible genetic relationship between them. In the western sector of the Metán-Alemanía sub-basin, the lower (sample #18) and the upper (sample #47) sections of the Yacoraite Fm. were likely deposited under marine conditions (Fig. 3.16). In the eastern sector of this sub-basin, C_{26}/C_{25} and $C_{31}R/C_{30}$ hopane ratios do not allow a clear distinction between marine and lacustrine environments during the deposition of the upper section of the Yacoraite Fm. (sample #11).

The presence of gammacerane is an indicator for water-column stratification developed in marine and lacustrine settings due to hypersalinity or temperature gradients (Sinninghe Damsté et al., 1995; Peters et al., 2005a). The Yacoraite Fm. was deposited in an environment characterized by shallow water depths (Marquillas et al., 2005), a setting where the development of temperature gradients is unlikely. Therefore, the presence of gammacerane in samples of the Yacoraite Fm. is probably indicative of hypersalinity. Most of the Yacoraite Fm. samples have Gammacerane Indexes (10*gammacerane /(gammacerane + $C_{30}\alpha\beta$-hopane) between 2 and 6 (inset in Fig. 3.16 and Table 7, appendix). In hypersaline environments the solubility of oxygen in water is limited (Lange et al., 1972), which favors the development of anoxic conditions and improves the preservation of organic matter (Tissot and Welte, 1984; Littke et al., 1997) as it could have happened in samples of the Yacoraite Fm.

Gammacerane was not detected in samples #35 & #41 from the upper section of the Yacoraite Fm., both collected in the Tres Cruces sub-basin, and sample #51 from the lower section in the western sector of the Metán-Alemanía sub-basin. The C_{26}/C_{25} tricyclic terpane ratio of 1.9 and $C_{31}R/C_{30}$ hopane ratio of 0.2 in sample #41 support a deposition in a lacustrine environment with predominant freshwater input, as inferred from the absence of gammacerane. No C_{26}/C_{25} tricyclic terpanes and $C_{31}R/C_{30}$ hopanes were detected in samples #35 and #51, which prevents the interpretation of depositional environments using these biomarkers.

3.3 Conclusions

3.3.1 General conclusions

The strata constituting the Yacoraite Fm. were initially deposited in a marine environment within the Metán-Alemanía and the Tres Cruces sub-basins. This depositional system evolved toward a lacustrine setting during the deposition of the middle part of the sequence and dominated depositional processes toward the end of deposition in the Tres Cruces sub-basin. The presence of gammacerane in extracts of the Yacoraite Fm. from both sub-basins and different stratigraphic positions, suggest the existence of water-column stratification during the deposition of the Yacoraite Fm. This water-stratification was unlikely favored by the development of temperature gradients because the Yacoraite

Fm. was deposited in shallow water depths. Therefore, water-column stratification was more likely caused by hypersalinity. Under these conditions, oxygen solubility decreased, and reducing conditions prevailed, thus favoring organic matter preservation.

Similar variations in mineral content (carbonate vs. detrital) in the southern sector of the Tres Cruces sub-basin and the western sector of the Metán-Alemanía sub-basin reflect changes in water depth during the marine transgression. This suggests that such variations can be followed on a basin scale and may prove to be useful as a stratigraphic tool. Ratios between specific chemical elements indicate that the Yacoraite Fm. was deposited in the Tres Cruces and the Metán-Alemanía sub-basins at water depths of less than 200 m. The presence of stromatolites, however, indicates deposition at shallower depths of possibly 60 m or less. Based on variations of the smectite and illite/mica contents it is inferred that climate was variable during deposition. The greatest variability must have occurred associated with repeated warming and cooling cycles as inferred from the deposits that constitute the upper section.

3.3.2 Specific conclusions

The lower section of the Yacoraite Formation - the onset of a transgression

According to the hydrocarbon-chain length distribution (HCLD), marine conditions were established in the southern and northern sectors of the Tres Cruces sub-basin and the western sector of the Metán-Alemanía sub-basin. This agrees with the dominance of alginites, Type II kerogen (HI values between 300 mg HC/g TOC to 600 mg HC/g TOC), the data represented in the TOC vs. S2 plots and the Pr/n-C_{17} and Ph/n-C_{18} plots. In the northern sector of the Tres Cruces sub-basin, a C_{26}/C_{25} tricyclic terpane ratio of 1.21 and a $C_{31}R/C_{30}$ hopane ratio of 0.24 do not allow further discrimination of marine and lacustrine environments.

The slightly higher terrigenous input as inferred from Pr/n-C_{17} vs. Ph/n-C_{18} and lower HI values (235 mg HC/g TOC) in sample #37 compared to samples #34 and #35 (HI=334 mg HC/g TOC and 509 mg HC/g TOC, respectively) is likely due to the greater proximity of the northern sector of the basin to the San Pablo high compared to the southern sector. In the western sector of the Metán-Alemanía sub-basin, sample #51 mainly contains alginites and some terrestrial vitrinite-like particles, which agrees with the observed Pr/n-C_{17} vs. Ph/n-C_{18} ratios. The predominant generation of hydrocarbons in the gas range and low HI values (11 mg HC/g TOC) point toward a dominant terrestrial input reflected by this sample. The low HI does not reflect the kerogen type in this sample and is likely affected by other factors e.g., thermal maturity and/or radiolysis. (cf. sections 4.1 and 4.3.2).

The middle section of the Yacoraite Formation - evolution of lacustrine environments

The deposition of the Yacoraite Fm. in the Tres Cruces sub-basin took place in hypersaline marine and later lacustrine environments. The marine influence is interpreted by the HLCD of sample #45 and HI of sample #3 (597 mg HC/g TOC). Lacustrine sedimentary environments continued to prevail during the deposition of samples #33, #42, and #44, as suggested by HLCD, the C_{26}/C_{25} tricyclic

terpane ratio between 1.55 and 1.79, and a $C_{31}R/C_{30}$ hopane ratio between 0.28 and 0.41. Although the Tricyclic terpane ratio of 1.29 and a hopane ratio of 0.28 of sample #45 do not allow a clear distinction between marine and lacustrine depositional environments, its gammacerane content suggest it was deposited in a hypersaline environment. Sample #45 is classified by the Pr/n-C_{17} and Ph/n-C_{18} ratios as Type II kerogen. This kerogen type agrees with the dominance of alginites in this sample. Because of the low TOC content (0.23 %), sample #45 may have been affected by artefacts during pyrolysis, which would explain its low HI (279 mg HC/g TOC). Therefore, it is concluded that this HI does not reflect the corresponding kerogen type.

In the southern sector of the Tres Cruces sub-basin, the organic matter of stromatolite sample #46 consists of Type II kerogen according to Pr/n-C_{17} vs. Ph/n-C_{18} values. The notable higher terrestrial input as suggested by HCLD and HI (336 mg HC/g TOC) is rather the consequence of stromatolite composition. Because of its low TOC (0.28 %), the sample from the western sector of the Metán-Alemanía sub-basin (#50) is susceptible to artefacts during pyrolysis experiments, and therefore, the values of HLCD and HI (68 mg HC/g TOC) indicating high amounts of terrigenous input are not representative of the depositional environment. No samples of this interval were available from the Metán-Alemanía sub-basin.

The upper section of the Yacoraite Formation - protracted lacustrine environments

Lacustrine environments dominated during the deposition of the Yacoraite Fm. in the Tres Cruces sub-basin, as suggested by HCLD (samples #23, #28, #29, #30, #39 & #41), with alginites being the principal organic constituents. Sample #30 has a high HI of 1015 mg HC/g TOC, which typically indicates lacustrine sedimentary environments. Samples #23 and #41 have C_{26}/C_{25} tricyclic terpane ratios between 1.5 and 1.9, respectively, and a $C_{31}R/C_{30}$ hopane ratio of 0.2 for both samples, thus supporting their lacustrine origin. The C_{26}/C_{25} tricyclic terpane ratio between 1.02 and 1.35, the $C_{31}R/C_{30}$ hopane ratio between 0.18 and 0.24 in samples #28, #29, #30, #37 and #39 are neither indicative of marine nor lacustrine environments. These samples were deposited under hypersaline conditions and are predominantly composed of alginites, as documented by organic petrography (except sample #37, which was not selected for this analysis). Except for sample #30, the other samples have HI values between 384-600 mg HC/g TOC indicative of Type II kerogen. The tar sample is likely genetically related to the upper section of the Yacoraite Fm. This sample has HCLD, C_{26}/C_{25} tricyclic terpanes, and $C_{31}R/C_{30}$ hopane ratios similar to sample #39.

A Pr/Ph ratio of 0.98 and $C_{31}R/C_{30}$ hopanes ratio of 0.33 (sample #40), a C_{26}/C_{25} tricyclic terpane ratio of 1.89, a $C_{31}R/C_{30}$ hopane ratio of 0.22, and phytane concentrations of > 2 mg/g in sample #41 indicate a lacustrine depositional environment in the northern sector of the Tres Cruces sub-basin. Sample #40 was deposited in hypersaline environments. The absence of gammacerane in sample #41 indicates the influence of freshwater conditions, excluding the possibility of hypersaline conditions. Under these depositional conditions, mainly Type II kerogen was deposited with HI values between

547-415 mg HC/g TOC. In the eastern sector of the Metán-Alemanía sub-basin, sample #11 was deposited under marine and sample #10 under lacustrine conditions, as indicated by their HLCD distribution. The C_{26}/C_{25} tricyclic terpane ratio of 1.21 and a $C_{31}R/C_{30}$ hopane ratio of 0.4 do not allow to distinguish marine from lacustrine settings for sample #11, although its deposition occurred under hypersaline conditions.

The predominance of lacustrine settings in the Tres Cruces sub-basin towards the end of the deposition of the Yacoraite Fm. coincides with reaching maximum flooding conditions. This interpretation agrees with the existence of coastal-lagoon carbonate depositional environments at Maimará in the present-day Eastern Cordillera and in the southern sector of this former sub-basin (Cónsole-Gonella et al., 2017). In the western sector of the Metán-Alemanía sub-basin, the absence of tricyclic terpanes in addition to a $C_{31}R/C_{30}$ hopane ratio of 0.42 and 0.59 for samples #48 and #47, respectively, suggests deposition in a marine environment. The presence of gammacerane indicates deposition under hypersaline conditions. Alginites are the predominant maceral in these samples. Sample #48 records a higher terrigenous input compared to sample #47 based on its HI (206 mg HC/g TOC), Pr/n-C_{17} vs. Ph/n-$C_{18,}$ and its chain-length distribution. The limited number of samples in this sector of the Metán-Alemanía sub-basin may be an additional reason, why evidence for the existence of a lacustrine setting was not detected during this period in this sub-basin.

4. Effects of maturation, radiolysis and mineral matrix

4.1 Thermal maturity of the Yacoraite Fm.

4.1.1 Maximum temperature (T_{max}) - Rock-Eval pyrolysis

T_{max} is the temperature at which the maximum amount (weight) of hydrocarbons is generated from thermal degradation of kerogen during Rock-Eval experiments (S2 peak). By applying a constant heating rate of 25°C/min from 300–550°C, kerogen cracking not only depends on temperature, but also on the speed at which chemical reactions take place which in turn relates to the chemical structure of the kerogen (Espitalié, 1986). Therefore, Tmax not only reflects the thermal maturity of the kerogen but also depends on the cracking kinetics of kerogen types (Espitalié, 1986; Peters, 1986). The Tmax roughly defining the onset of oil generation from Types II and III kerogen is 435°C though in reality this is variable. Type I kerogen has a higher Tmax for the onset of oil generation of 440°C, again with some variability. A Tmax of 455-465°C marks the end of oil generation for Types II and III, respectively.

The HI values of the samples of the Yacoraite Fm. range between 60 mg HC/g TOC and 600 mg HC/g TOC (Fig. 4.1), indicating that Type II-III kerogens and admixtures are the main components. T_{max} values for the Yacoraite Fm. vary from 423-446°C (Fig. 4.1 and Table 6, appendix) indicating a thermal maturity of this formation in the range from immature to peak-oil window conditions. Lower HI and higher T_{max} values correspond to samples with low TOC content (see inset Fig. 4.1). These low TOC

values are likely the consequence of low productivity regarding organic matter, rather than low preservation. In general, the organic matter in these samples is not or only slightly oxidized as suggested by relative lower OI than 50 mg CO_2/g TOC and no evidence of oxidation as observed in organic petrography (Fig. 3.11). Samples with low TOC values are especially susceptible to the mineral-matrix effect (Peters, 1986), suggesting that neither their low HI are reliable for kerogen typing, nor their relatively higher T_{max} values can be used a maturity parameter.

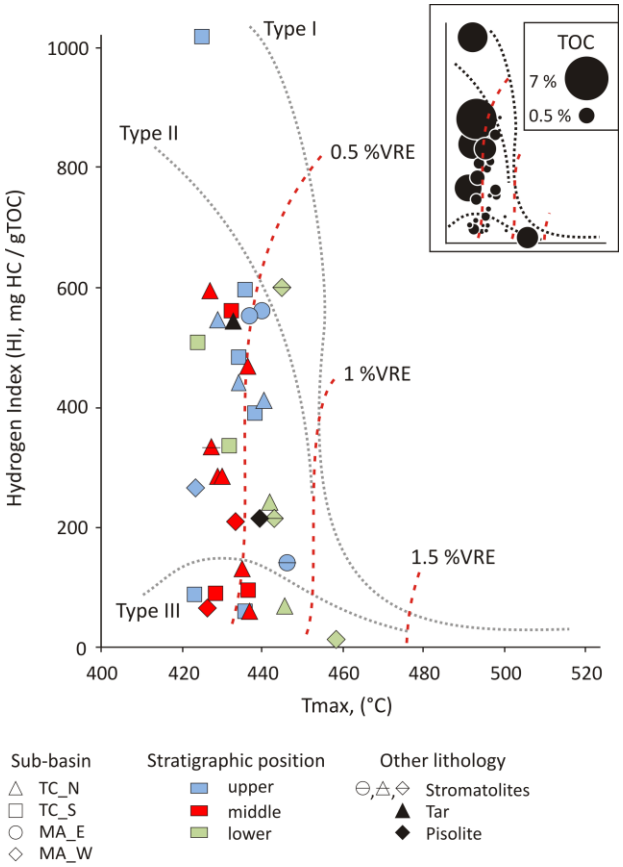

Fig. 4.1. Hydrogen Index (HI) vs. T_{max} plot to classify kerogen types and to provide thermal maturity assessment in whole-rock samples of the Yacoraite Fm. Red dashed lines mark maturity isolines, and black dotted lines separate kerogen types. Inset: TOC bubble diagram in the HI vs. T_{max} plot. Samples with TOC <0.5 % have higher T_{max} values suggesting mineral-matrix effect (MME) interference. When only T_{max} values of samples with TOC > 0.6 % are considered, the Yacoraite Fm. is at the onset of petroleum generation. (TC) Tres Cruces, (MA) Metán-Alemanía sub-basins. The sectors where samples were collected are north, south (N, S) and east and west (E, W).

The MME may cause the partial adsorption of hydrocarbons and NSO compounds generated during pyrolysis on the mineral surfaces of the sample instead of immediately releasing them to the detector. While they are adsorbed, the oven temperature continues to rise causing their thermal cracking. The cracking products are released at higher temperatures than the pyrolyzed hydrocarbons, and therefore, higher T_{max} values are measured (Espitalié, 1986; Peters, 1986). The magnitude of the MME and the biases it causes on T_{max} measurements depends on the type and amount of sorptive minerals, and the amount of organic matter that can be cracked by pyrolysis.

When only samples of the Yacoraite Fm. with TOC higher than 0.6 % are considered, the T_{max} values vary from 429 °C to 437 °C and from 425 °C to 436 °C for the northern and southern sectors of the Tres Cruces sub-basin, respectively. For the Metán-Alemanía sub-basin, only one sample from the western sector has a TOC value greater than 0.6 %, and its T_{max} is 424 °C. These results indicate that T_{max} values lower than 440 °C are most realistic to determine the thermal maturity in this set of samples

of the Yacoraite Fm. Since T_{max} increases as a consequence of the MME, samples with the lower T_{max} can be considered to be less affected or not affected by this artefact. With this criterion, the T_{max} values vary from 426 °C to 439 °C in samples from the western sector of the Metán-Alemanía sub-basin, while only one measurement with 437 °C represents the eastern sector. Based on the T_{max} values, the samples of the Yacoraite Fm. composed of Type II and II/III kerogen are at the onset of petroleum generation in the Tres Cruces and the Metán-Alemanía sub-basins.

The S1 peak during Rock-Eval experiments represents retained/adsorbed organic compounds in the samples with the carbon number mostly in the range from C_1 to ≈C_{32} (Peters, 1986). The S2 peak is composed of high-boiling hydrocarbons and NSO compounds generated from the thermal degradation of kerogen and bitumen (Clementz, 1979; Katz, 1983; Espitalié et al., 1985; Delvaux et al., 1989). Nevertheless, some of the C_{16+} hydrocarbons are not completely volatilized during the initial heat to 300 °C where the S1 peak is recorded and may be carried into the S2 peak (Tarafa et al., 1983). A significant amount of thermally degraded compounds from bitumen may mislead the thermal maturity assessment by shifting T_{max} to lower values (Clementz, 1979). To evaluate this effect, extracted and unextracted samples where pyrolyzed. A comparison of the pyrolysis curves before and after solvent extraction shows the amount of adsorbed hydrocarbons and bitumen in addition to the amount of hydrocarbons generated by thermal cracking of kerogen from samples of the Yacoraite Fm. as exemplified by the results of sample #37 (Fig. 4.2) (See Rock-Eval data for all samples in Table 6, appendix).

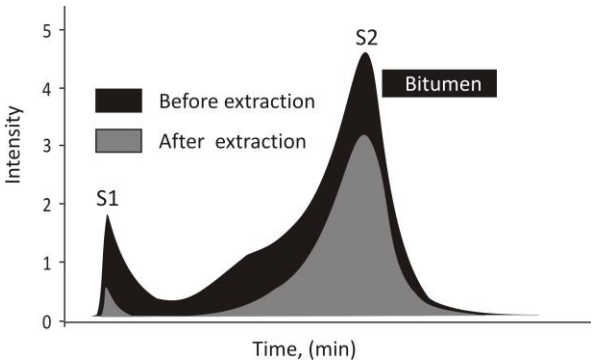

Fig. 4.2. The difference in Rock-Eval pyrolysis curves for sample #37, revealing that S2 is composed of hydrocarbons from thermal degradation of kerogen and bitumen. The black-shaded curve represents the pyrolysis-yield before solvent extraction. The gray shaded curve represents the pyrolysis-yield after solvent extraction. The difference in area corresponds to bitumen content, which indicates the S2 peak is not only comprised of kerogen, but also bitumen. The remaining S1 peak after extraction is likely due to the presence of residual solvent.

Both S1 and S2 values are lower after extraction compared to unextracted samples, except in samples with a hydrocarbon content of ≈0.1 mg HC/g of rock and less being probably below the limit measurement error of the analysis. While the remaining S1 peak after extraction is attributable to trapped residual solvent (Han et al., 2015), the decrease of the S2 peak height and area after solvent extraction in the set of samples of the Yacoraite Fm. indicates that this peak does not only represent kerogen conversion, but also generated bitumen, which agrees with the onset of oil generation. Migrated oil is an unlikely explanation because of the fine-grained lithology and the absence of cracks or fractures in the samples that could have served as migration paths for oils generated from other rocks.

The question arises if those bitumen components could have suppressed T_{max} values (Espitalié, 1986; Peters, 1986; Mukhopadhyay, 1994; Snowdon, 1995). This is not the case here, because T_{max} values are similar before and after extraction, varying not more than 6°C (Table 6, appendix). It has been suggested that T_{max} suppression takes place at high bitumen (oil) to kerogen proportions (Peters, 1986). Here, however, even when the total bitumen/kerogen ratio [(S1+(S2-$S2_X$)]/(S2 in kerogen) in shales is as high as 5 (sample #42) or 21 for tar samples, similar T_{max} values were measured for non-extracted and extracted samples. The T_{max} of the tar sample (#53) is similar to that measured in the surrounding shales (samples #39, #40 in Fig. 4.1 and Table 6, appendix). This suggests its similar behavior under thermal stress and furnishes reliable information regarding its thermal maturity. The conversion of bitumen into volatile hydrocarbons under thermal stress was found to resemble the thermal evolution of Type II kerogen (Hosseini et al., 2017).

The similar T_{max} values before and after extraction indicate that T_{max} is not suppressed in this set of samples. For the tar sample with the higher bitumen/kerogen ratio, similar T_{max} before and after extraction also suggests that the bitumen composition and not only high bitumen/kerogen ratios are the responsible for T_{max} suppression. There are two samples with exceptional T_{max} values. One is sample #30 from the Tres Cruces sub-basin, which has Type I, as indicated by its HI of 1015 mg HC/g TOC. This sample has a T_{max} of 425°C, which is much lower than the T_{max} of approximately 440 °C typically expected for this kerogen type. Lamalginite is the main organic constituent of this sample (Fig. 3.11c) while *Botryococcus* is normally associated with lacustrine environments.

The presence of other heteroatoms like nitrogen and oxygen makes the adjacent bonds weak (Claxton et al., 1993), therefore lowering T_{max}. Tegelaar and Noble (1994) noted that the amount of organic sulphur was high in thermally labile alginitic kerogen, which could explain the lower T_{max} compared to the "stereotyped" T_{max} for Type I kerogen. However, the low sulphur incorporation into organic matter in sample #30, as indicated by a dibenzothiophene/phenanthrene ratio of 0.58 (Fig. 3.15 and Table 2, appendix), refutes this idea to explain the characteristics of the sequences analyzed here. Thermal lability was shown to be linked to kerogen structure, in particular the presence of alicyclic and oxygen-containing moieties for a low-maturity sequence of lacustrine sediments from the Washakie Basin (Horsfield et al., 1994). This also does not seem to be applicable to the samples analyzed here, because the Oxygen Index is uniformly low.

On the other hand, sample #51 (lower Yacoraite Fm.) has a higher T_{max} (458 °C) than sample #50 (T_{max} = 426°C) from the middle section and samples #47 (T_{max} = 424 °C) & #48 (T_{max} = 433 °C) from the upper Yacoraite Fm. in the west sector of the Metán-Alemanía sub-basin. The measured distance between the lower and the upper sections of the Yacoraite Fm. is less than 80 m (vertical distance in the stratigraphic succession <80 m). Therefore, the difference in T_{max} between the lower and upper sections of the Yacoraite Fm. cannot be caused by differences in burial; instead, it might suggest the effect of localized heat sources only affecting sample #51. No intrusive bodies or hydrothermal mineralization caused by hot fluid flow were detected in the study area and their existence is highly

unlikely at this location (Geological map of Metán, 2566 IV). A significantly lower T_{max} of 406°C was measured in the kerogen concentrate of sample #51, indicating a mineral-matrix effect on this parameter. Inorganic influences on kerogen properties of this sample will be addressed in section 4.3.

4.1.2 Vitrinite reflectance

Vitrinite originates from the woody tissues of terrigenous vascular plants. Because its reflectance increases with thermal stress, the measurement of vitrinite reflectance is well established for determining thermal maturity (Stach et al., 1982; Dow, 1977; Taylor et al., 1998). Regardless of the biases associated with sample preparation and measurement, some processes other than maturation have been found to alter vitrinite reflectance with the potential misinterpret maturity. Processes that can suppress vitrinite reflectance are impregnation by bitumen (Suarez-Ruiz et al., 1994), lipid incorporation into kerogen from which vitrinite-like particles are formed (Mukhopadhyay, 1994), and the incorporation of hydrogen into kerogen through its reaction with H_2S generated from sulphate-reducing bacteria (e.g., Quick, 1994).

Vitrinite-reflectance values are between 0.47-0.66 %Ro for samples collected from the Yacoraite Fm. in the southern sector of the Tres Cruces sub-basin (seven samples, Table 4.1). In the northern sector of the same sub-basin, values are between 0.50-0.65 %Ro (three samples). In the eastern sector of the Metán-Alemanía sub-basin, two vitrinite-reflectance values of 0.41 %Ro and 0.55 %Ro were measured. In the western sector of this sub-basin, two of the samples have a vitrinite reflectance of 0.52 %Ro and 0.54 %Ro, respectively. Histograms of the vitrinite-reflectance measurements of selected samples are shown in Fig. 4.3

Table 4.1. Vitrinite reflectance (%Ro) and fluorescence in whole-rock samples of the Yacoraite Formation.

Sample	Sub-basin	Organic Petrography			
		Ro, %	N	St.Dev	UV Fluorescence
10	MA_E	NF	NC	NC	Yellowish
11	MA_E	0.55	3	0.081	Yellowish
18	MA_W	NF	NF	NF	Yellowish
23	TC_S	0.64	9	0.12	Yellowish
28	TC_S	NF	NF	NF	Yellowish
29	TC_S	0.48	13	0.06	Yellowish
30	TC_S	0.66	19	0.112	Yellowish
33	TC_S	NF	NF	NC	Yellowish
34	TC_S	0.67	3	0.166	Yellowish
35	TC_S	0.55	3	0.104	Yellowish
39	TC_N	0.5	8	0.03	Yellowish
40	TC_N	0.55	8	0.04	Yellowish
45	TC_N	0.65	4	0.065	Yellowish
47	MA_W	0.54	8	0.124	Yellowish
48	MA_W	0.52	2	0.057	Yellowish
51	MA_W	1.07	15	0.077	Brownish

TC: Tres Cruces sub-basin, north (N) and south (S). MA: Metán-Alemanía sub-basin, east (E) and west (W). N: Number of measurements (%Ro) on indigenous vitrinites. St. Dev: Standard deviation. NF: no vitrinite found. NC: Not calculated.

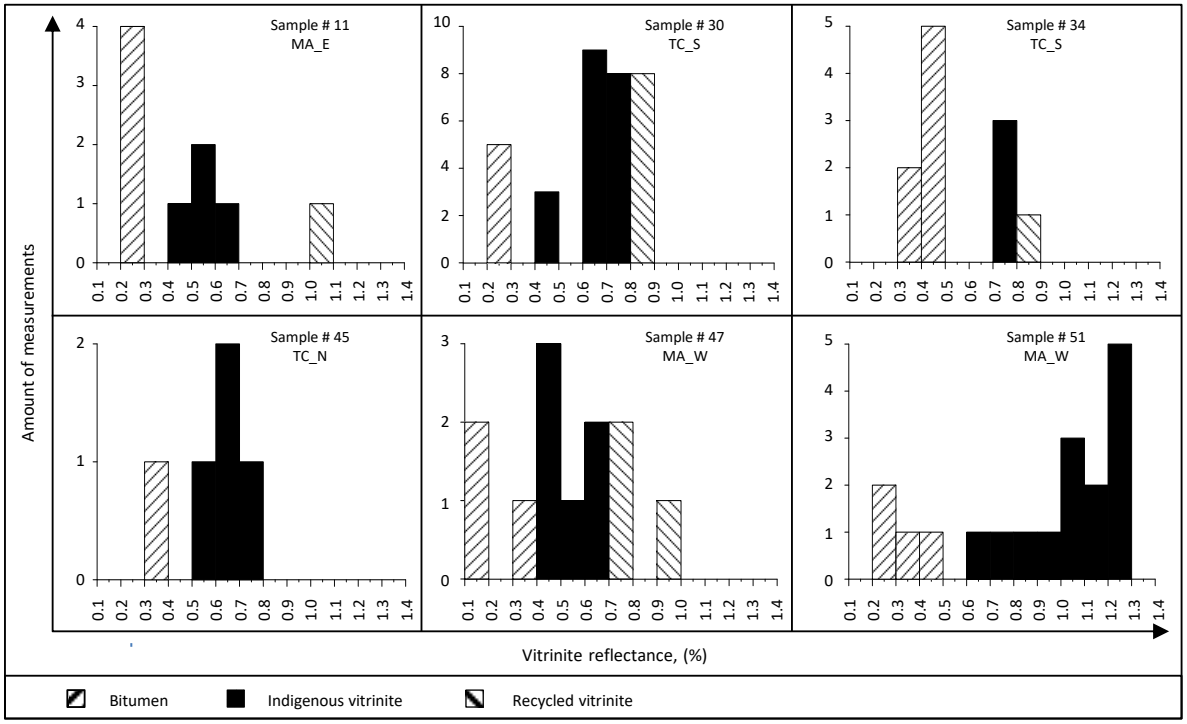

Fig. 4.3. Histograms of the vitrinite reflectance (%Ro) measurements on whole-rock samples of the Yacoraite Fm. from Tres Cruces (TC) and the Metán-Alemanía (MA) sub-basins. The individual sectors where samples were collected are north, south (N, S); east and west (E, W).

Based on these values, the samples from the Yacoraite Fm. analyzed here are at the onset of hydrocarbon generation in the Tres Cruces and the Metán-Alemanía sub-basins. The burial history of those outcrop samples is unknown. Therefore, the thermal maturity is expected to be higher in the deeper parts of the basin.

In sample (#51) a higher vitrinite reflectance of 1.07%Ro was measured, which agrees with a higher inferred thermal maturity indicated by T_{max} of 458 °C. Since the measured distance between this sample and sample #47 is less than 80 m (vertical distance in the stratigraphic succession <80 m), the difference in vitrinite reflectance cannot be caused by burial depth. Some parameters, including vitrinite reflectance, are affected by inorganic influences and are discussed in section 4.3.

As already mentioned, there is the presence of bitumen in the rock samples of the Yacoraite Fm. (difference in the pyrolysis curves before and after extraction in Fig. 4.2). Bitumen impregnation can cause vitrinite suppression of vitrinite reflectance. With the highest HI (1015 mg HC/g TOC), sample #30 is a candidate for vitrinite-reflectance suppression caused by its hydrocarbon richness. A vitrinite-reflectance value of 1.4 %Ro is found for this sample when the correction of Lo (1993), based on HI is applied. At this value, the fluorescence would have already disappeared. However, this sample exhibits a yellowish fluorescence (Fig. 3.11c), which agrees with the original vitrinite value of 0.66 %Ro and contradicts the corrected value. Both the vitrinite reflectance and the fluorescence are similar to other values in the southern sector of the Tres Cruces sub-basin (Table 4.1). Therefore, the vitrinite

reflectance in samples #30 is not affected by suppression nor were T_{max} values. Vitrinite-reflectance values here are reliable, and it is indicative that HI alone is not a reliable indicator for vitrinite suppression.

4.2 Mineral diagenesis

Analcime in amounts of < 9 % were detected by X-ray diffraction (XRD) in samples from the southern and northern sectors of the Tres Cruces sub-basin and the western sector of the Metán-Alemanía sub-basin. In the eastern sector of the Metán-Alemanía sub-basin, this mineral was not detected (Table 2, appendix). The presence of analcime constrains maximum burial conditions for the Yacoraite Fm. to less than 200 °C and pressures below 3 kbar (approx. 10 km depth). At 200 °C, the calculated vitrinite-reflectance values are close to 2.2 % using the Barker and Pawlewicz (1994) formula ($\%Ro = e^{(T*0.0124)-1.68)}$), which corresponds to the upper limit of organic-matter catagenesis (Mukhopadhyay, 1994).

Smectite was detected in all studied sub-basins in variable amounts from 9 % up to 90 % in the fraction smaller than 2 μm (Table 3, appendix). Because of its low thermal stability (Velde, 1992), smectite is used to constrain in more detail the temperature reached by the Yacoraite Fm. during burial. Fully expandable smectite becomes unstable at temperatures around 120 °C (op. cit.). Therefore, the Yacoraite Fm. likely did not reach higher temperatures than ≈120 °C. This temperature corresponds to a vitrinite reflectance of 0.8 % calculated with the formula $\%Ro = e^{(T*0.0124)-1.68}$ (Barker and Pawlewicz, 1994). XRD analysis furthermore shows that illite/mica is present in samples analyzed from all sectors and sub-basins. The measurement of illite crystallinity (IC) and/or Kübler Index is expressed as the Crystallinity Index Standard, (CIS) after Warr and Ferreiro-Mählmann (2015). Illite crystallinity is used to define mineral diagenetic stages with direct application in oil exploration (Jaboyedoff et al., 2001).

Although mineral transformation and organic-matter maturation are independent of one another mechanistically, they have been compared from diagenesis to epizone with vitrinite reflectance from 0.5-4 %Ro (Merriman, 2005). Illite crystallinity can accurately define the anchizone, which is the metamorphic grade between diagenesis and low-grade metamorphism and whose limits define the transition from dry-gas to overmature rocks. It is useful only in diagenetic studies in cases where biases due to the presence of detrital mica can be ruled out (Kübler and Jaboyedoff, 2000). CIS was only measured on the set of samples collected in the Valle del Tonco (Fig. 4.4) with the goal to have an additional parameter to evaluate diagenesis because of the unusual T_{max} and Ro values in sample #51.

The fraction smaller than 2 μm in sample #51 is exclusively composed of illite. In this sample, illite is interpreted to be authigenic due to lack of detrital minerals, e.g., quartz, feldspars, microcline, or albite (Fig. 3.2), and its wide FWHM. The detrital association is observed in the other samples (#47, #48, and #50). Besides, it is not possible to relate differences in FWHM between those samples and sample #51 to burial as the distance between the farthest samples (#47 & #51) is less than 80 m (vertical distance <80 m). Therefore, the Crystallinity Index (CIS) of samples #47, #48 and #50 reflect the

inherited crystallinity of detrital illite related to their pre-depositional history (recycling) and not the change of crystallinity due to *in situ* thermal stress.

The CIS value for the authigenic illite in sample #51 suggests that burial temperatures for the Yacoraite Fm. were between 100 °C and 200 °C (Fig. 4.4). The values of temperatures defining limits between metapelitic zones provided by Merriman and Frey (1999), do not provide a scale to calculate temperatures based on the Kübler Index. As mere exercise, in this study a burial temperature of the Yacoraite Fm. of 127 °C was calculated for sample #51 after interpolation of the Kübler values (CIS scale) vs. temperature (Inset Fig. 4.4) using the values that delimit the metapelitic zones. This value is only considered as indicative and not as a calibrated paleotemperature.

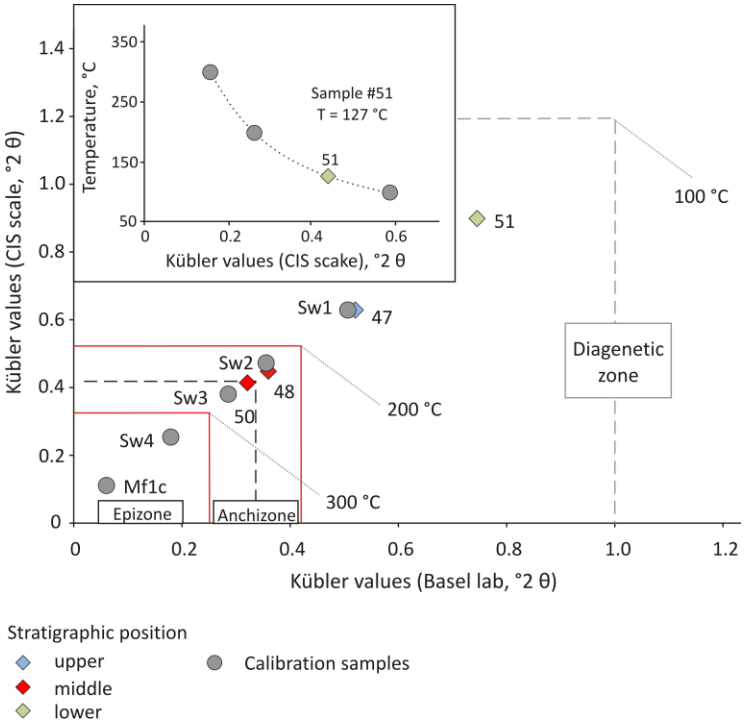

Fig. 4.4. Mineral diagenesis-metamorphism for samples of the Yacoraite Fm. collected in the Valle del Tonco (western sector of the Metán-Alemanía sub-basin). Metapelitic zones according to the revised Crystallinity Index Standard (CIS) after Warr and Ferreiro-Mählmann. (2015). Temperatures that define limits between metapelitic zones after Merriman and Frey (1999). New limits for the Anchizone are 0.32°2θ and 0.52°2θ on the Y-axis. MF1c and Sawn are samples for the last standardization exercise (Warr and Ferreiro-Mählmann, 2015). Inset: Temperature of the limits of metapelitic zones (blue dots) vs. Kübler Index (CIS scale). This plot provides an estimation of 127 °C as maximum temperature conditions for sample #51 (green dot), the only sample in which illite is considered to be authigenic. This is only used to have an estimate and should not be regarded as an exact paleotemperature determination.

Other clay minerals, such as kaolinite and chlorite, were not used to evaluate the burial temperature of the Yacoraite Fm. because they are thermally more stable (Kübler and Jaboyedoff, 2000) than the temperature range that this formation was probably exposed to. Kaolinite is stable up to the end of the dry gas window, and chlorite is stable even in the epizone in which potential source rocks are already overmature. Gypsum was also found in some samples (#10, #11, #39, #47, #48 & #50) in bulk XRD-analyses (Table 2, appendix). This mineral could have been originally deposited or precipitated after burial, uplift, and erosion. Gypsum becomes unstable at temperatures in excess of 42 °C, and it is expected to be transformed into anhydrite (Murray, 1964). Gypsum is not stable at temperatures around 120 °C as those calculated for the analyzed samples of the Yacoraite Fm. from organic thermal maturity and mineral diagenesis. Therefore, the presence of this mineral is likely due to the effect of surface waters after or during the uplift of tectonic inversion (e.g., Mon and Salfity,

1995). The possible effect of the surface waters did not affect the organic matter appreciably as indicated by its good preservation and presence of pyrite.

4.3 Inorganic controls of organic chemical composition

During the kerogen evaluation in the set of samples collected in the western sector of the Metán-Alemanía sub-basin some inconsistencies arose that affect kerogen typing and determination of thermal maturity (e.g., relatively low Hydrogen Index, higher vitrinite reflectance, higher T_{max}, exclusive generation of low-molecular hydrocarbons in the gas range (C_1-C_5), benzene and toluene in Py-GC). In the following sections, the role of mineral-matrix effect (MME) and radiation on those properties are discussed.

4.3.1 The role of minerals on kerogen properties

The role of minerals on kerogen classification

According to Rock-Eval pyrolysis results, the kerogen in sample #51 is classified as Type IV, namely S2 and HI are low (0.15 mg HC/g rock and 11 mg HC/g TOC, respectively) (Fig. 3.8, Fig. 3.9 and Table 6, appendix). Such characteristics might correspond to the abundance of inertinite (Peters and Cassa, 1994), maturity (Cornford et al., 1998) or reworked organic matter. Organic petrography revealed that no inertinites, but alginites with minor terrigenous input are the main organic constituents in this sample (Fig. 3.11f). This was further supported by Pr/n-C_{17} vs. Ph/n-C_{18} on its extract (Fig. 3.12). Although T_{max} values and vitrinite reflectance initially supported high maturity for this sample, these parameters are affected by mineral-matrix effect and radiation, as explained below.

During the pyrolysis of whole-rock samples, interaction with minerals can potentially influence the values of different parameters, which can lead to erroneous interpretations. The adsorption of hydrocarbons on the mineral fabric is called mineral-matrix effect (MME), it is known to reduce HI (Peters, 1986) and depends on the amount and type of minerals. MME is stronger for illite and smectite, followed by calcite and kaolinite (Espitalié et al., 1980; Dembicki et al., 1983). The lower the TOC content, the higher is the MME susceptibility (Espitalié et al., 1980).

Because of the relatively high illite/mica ratio varying from 37.6 % up to 100 %, as well as the presence of smectite (samples #47 & #50), MME was suspected to affect the measurements particularly in samples with low TOC (samples # 48 & #50). To further test this hypothesis, an additional set of Rock-Eval analyses were carried out on kerogen concentrates. The results show that HI values were higher in kerogen concentrates compared to whole-rock samples (Fig. 4.5a and Table 4.2). The difference in HI between whole-rock and kerogen concentrate (ΔHI) was found to correlate with illite/mica content in the clay fraction (<2 μm) (Fig. 4.5b and Table 4.2) for the three samples in question. With similar illite/mica content in samples #48 (97 %) and #51 (100 %) and the absence of smectite in both of these samples, ΔHI between whole-rock samples and their corresponding kerogen concentrates was expected to be similar. However, HI in the kerogen concentrate for sample #51 is still

lower than expected if MME were the only factor affecting this sample. MME alone cannot account for the difference in HI between whole-rock and kerogen concentrate in sample #51.

Table 4.2. Kerogen type and thermal maturity parameters in whole-rock samples and kerogen concentrates of the Yacoraite Formation and their relation to clay mineral composition.

Sample	TOC, %	Uranium (ppm)	U/TOC	HI			Tmax, °C			Ro, %	Clay minerals, %		
				WR	ker	Δ	WR	ker	Δ		smectite	chlorite	I/M
47	3.36	7	2	266	377	111	424	425	1	0.54	62.4		37.6
48	0.34	10	29	206	538	332	433	426	7	0.52		3	97
50	0.25	13	52	68	222	154	426	423	3		44.7		55.3
51	1.35	4440	3289	11	18	7	458	406	52	1.09			100

HI: Hydrogen Index, mg HC/g TOC; WR: Whole-rock; ker: kerogen concentrate, Δ: the difference between the parameter measured in whole-rock and kerogen concentrates. Measured vitrinite reflectance (Ro); clay mineral amount in clay fraction <2µm; I/M: illite/mica.

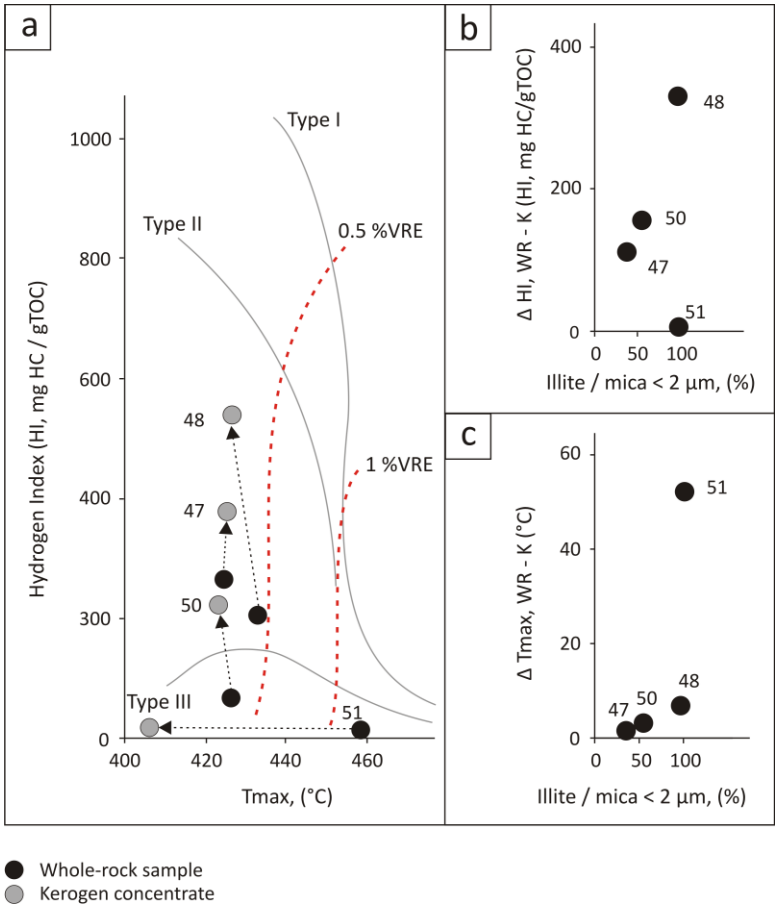

Fig. 4.5. Comparison of Rock-Eval parameters between whole-rock and kerogen concentrates. (a) Comparison of Hydrogen Index (HI) vs. T_{max} of whole-rock samples and their respective kerogen concentrates of the Yacoraite Fm. samples from the Valle del Tonco (western sector of the Metán-Alemanía sub-basin) for classification of kerogen types and thermal maturity assessment. Kerogen concentrates show higher HIs. (b) Illite/mica vs. the difference (Δ) in HI and (c) Illite/mica vs. the difference (Δ) in T_{max} of whole-rock samples and the respective kerogen concentrates. ΔHI and ΔT_{max} correlate with illite/mica content except for sample #51. The mineral matrix effect (MME) does not explain the difference in HI between the whole-rock and the kerogen concentrate of sample #51. The MME enhances T_{max} of the whole-rock sample and therefore partially explains the high ΔT_{max} of sample #51.

The role of minerals on the thermal maturity assessment

The organic matter in a whole-rock sample and its kerogen concentrate is qualitatively the same both having the same composition and structure and, therefore, a similar activation energy is required for their thermal transformation. As a consequence, T_{max} values before and after demineralization should be similar if controlled by thermal stress only (Rahman et al., 2017). This is the case for samples #47, #48, #50, whose differences in T_{max} (+/- 5°C) for whole-rock samples and kerogen extracts are small

and fall within the limits of the method's accuracy. Only T_{max} values of the whole-rock sample and the kerogen extract of sample #51 differ significantly being 458 °C and 406 °C, respectively (Fig. 4.5a; 4.6 and Table 4.2). Initially, the high T_{max} of 458 °C of the whole-rock sample # 51 was interpreted to indicate a higher maturity than other samples in close proximity having a T_{max} close to 429 °C. However, the vertical distance to the most distant sample is less than 80 m and therefore, burial is ruled out to have caused greater thermal maturity. No evidence for other geological processes was observed in the field that would have affected only this sample, i.e., intrusions or mineralization caused by hot fluids.

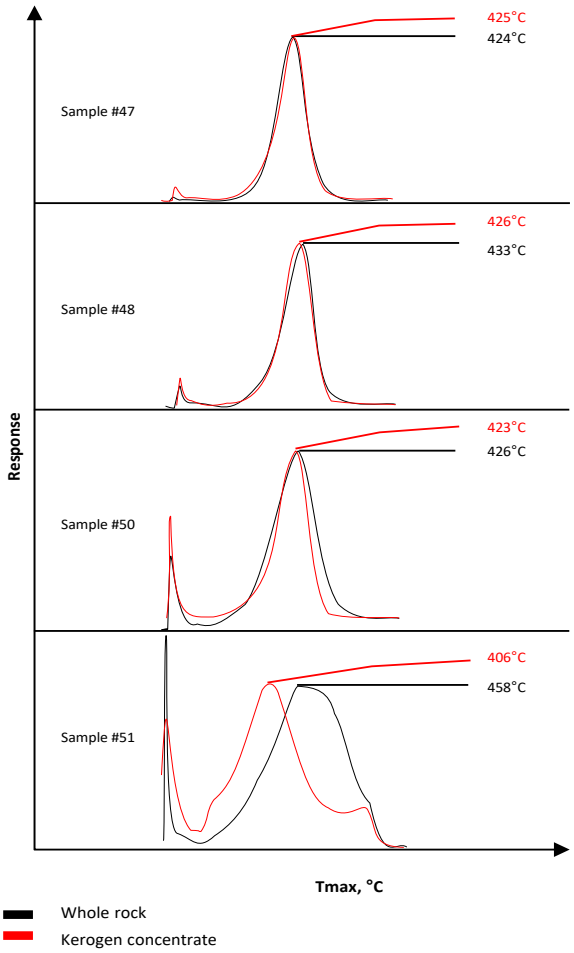

Fig. 4.6. Reconstructed Rock-Eval pyrograms of whole-rock samples (black lines) and kerogen concentrates (red lines) of the Yacoraite Fm. in samples collected in the Valle del Tonco (western sector of the Metán-Alemanía sub-basin). Except for sample #51, whole-rock samples and their respective concentrates have similar T_{max} values. That difference is partially explained as a consequence of the mineral-matrix effect. An additional process causing the T_{max} difference between the whole-rock and the kerogen concentrate of sample #51 is discussed in section 4.3.2. For better comparison, whole-rock intensities were multiplied by a factor of ≈60 for samples #47 and #48. For samples #50 and #51, the factors were ≈8 and ≈2, respectively.

Higher proportions of recycled organic matter can also increase T_{max} (Peters, 1986), however, this factor is discarded here as organic petrography showed alginite to be the main organic component (up to 85 %). One reason for the high T_{max} values might be the mineral matrix effect. An illite-enriched mineral matrix can retain up to 85 % of otherwise released hydrocarbons causing carryover into the S2 peak (Barker, 1974; Peters, 1986 and references therein), which results in a higher T_{max} compared to the one at which hydrocarbons were generated.

The effect of minerals on T_{max} became evident after removing them by concentrating the kerogen and repeating the pyrolysis experiment (Fig. 4.5a and Table 4.2). The difference in T_{max} was found to correlate with illite/mica content in the fraction smaller than 2µm (Fig. 4.5c and Table 4.2). Illite is the only clay mineral in sample #51 in the fraction (< 2µm) (Fig. 3.2). The adsorption on the

surface of minerals is proportional to the surface of the adsorptive particles (Espitalié et al., 1984). The surface of these particles increases exponentially with decreasing particle size. Therefore, strong adsorption of hydrocarbons generated during pyrolysis is expected in samples containing large portions of adsorptive clay minerals as in this case in sample #51. This will require higher temperature to release hydrocarbons and resulting in a higher T_{max}. Recent studies have shown that differences in T_{max} between whole-rock and kerogen concentrate can be as high as 30°C for Type II kerogen in cases where organic matter is intimately associated with clay minerals (Rahman et al., 2017). The T_{max} of kerogen concentrate from sample #51 was expected to be similar to T_{max} of kerogen concentrate in sample #48 with comparable illite/mica content and low TOC. However, the bigger difference suggests that MME alone is insufficient to account for the T_{max} difference between whole-rock and kerogen concentrate.

4.3.2 The effect of radiation on kerogen properties

Uranium enrichment has been reported in the Yacoraite Fm. in the western sector of the Metán-Alemanía sub-basin (Salfity and Marquillas, 1999; Ferreira et al., 2013). Quantitative analysis showed an extremely high uranium content (4400 ppm) in sample #51 while the uranium content of marine shales is typically below 10 ppm (Lewis et al., 2010; Lippmaa et al., 2011). Uranium was sourced from the Precambrian/Paleozoic granitic basement and incorporated into the regressive facies of the Yacoraite Fm. generated as a local consequence of the uplift of the Traspampean Arch (Salfity and Marquillas, 1999). The syngenetic uranium mineralization in the Yacoraite Fm. of the western sector of the Metán-Alemanía sub-basin indicates that the organic matter of sample #51 has been exposed to radiation for 60 Myr. Because of the high U/TOC ratio in sample #51, there is potentially a radiation effect on the organic matter similar to the one observed in the Middle Cambrian to Early Ordovician marine Alum Shale of Scandinavia (Lecomte, 2017; Yang et al., 2018) exhibiting a uranium content of not more 300 ppm (Lewan and Buchardt, 1989) (Fig. 4.7).

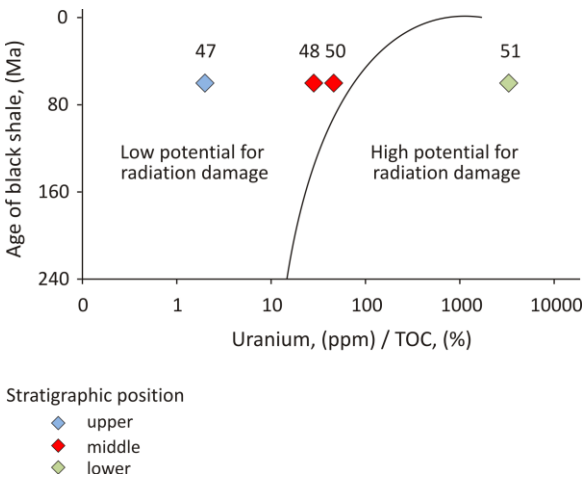

Fig. 4.7. Uranium / total organic carbon ratio (TOC) vs. age of the Yacoraite Fm. in samples collected in the Valle del Tonco (western sector of the Metán-Alemanía sub-basin) after Lewan and Buchardt (1989). Susceptibility and potential damage caused by radiation depend on uranium content, TOC, and time of exposition (age of the geological formation). The possible effect of radiation on organic matter increases in the following order: #47<#48<#50<<#51.

The role of radiation on kerogen classification and hydrocarbon generation

Py-GC results revealed a shortening in the hydrocarbon chain-length distribution in the pyrolysates following the order: sample #47<#48<#50<#51 with a predominant generation of hydrocarbons in the gas range for sample #51 (Fig. 4.8). These changes are accompanied by an increase in aromatic moieties, e.g., meta/paraxylene and orthoxylene (not detected in sample #51) (Fig. 4.8). An increase in aromaticity (%) as evaluated from the relative increase of orthoxylene compared to nonene and 2,3-dimethylthiophene was also observed and attributed to radiation in samples of the Alum Shale (Yang et al., 2018) (Fig. 4.9). However, the uranium content of these samples is too low (<15 ppm) to cause the observed increasing aromaticity in these samples (in the order: sample #47 < #48 < #50; Fig. 4.9 inset), but rather reflects the organofacies composition.

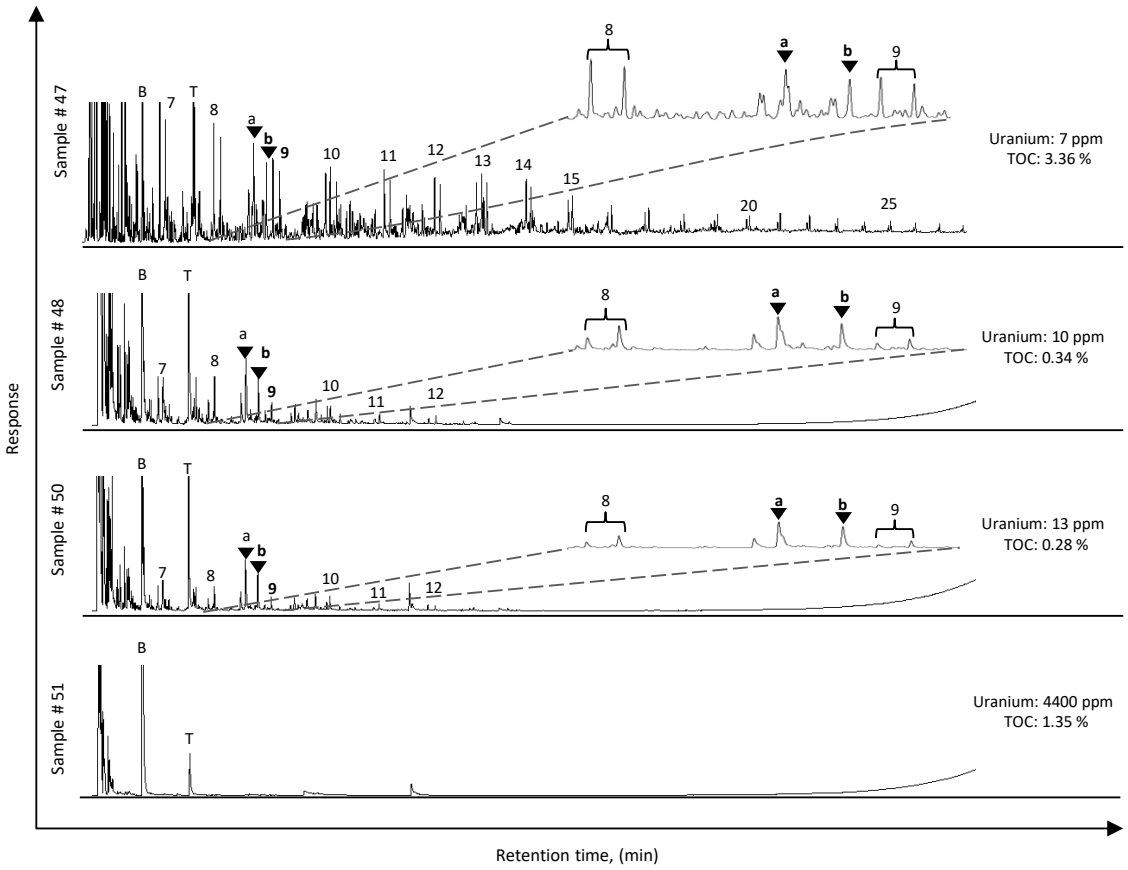

Fig. 4.8. Py-GC chromatograms of whole-rock samples of the Yacoraite Fm. (Valle del Tonco, western sector of the Metán-Alemanía sub-basin). The removal of most hydrocarbons in sample #51 is likely due to its high uranium content while the relative low uranium content in samples #47, #48, #50 suggests that hydrocarbon chain length shortening and increasing aromaticity are more likely caused by organofacies composition. Numbers indicate the number of carbon atoms in normal alkanes and alkenes. B: Benzene, T: Toluene, a: meta- and paraxylene, b: orthoxylene.

The uranium concentration of sample #51 is one order of magnitude higher compared to the Alum Shale samples (Yang et al., 2018). Pyrolysates in sample #51 are exclusively composed of low-molecular aromatic moieties (benzene and toluene) and gas hydrocarbons. No hydrocarbons at retention times higher than toluene, e.g., meta-, para-, ortho-xylene, were detected after chromatographic

separation, and therefore the aromaticity is not calculated. This was already observed in the organic-rich lenticular nodules the Alum Shale (Yang et al., 2019) known as "Kolm" with high uranium contents of up to 2289 ppm. This part of the Alum Shale has been exposed to uranium over longer times (≈500 Myr) compared to sample #51, but only to half the uranium concentration. The stability of aromatic compounds to radiation decreases with an increasing number of n-alkyl groups (Sevast'yanov et al., 1962), which explains the absence of meta-, para-, ortho-xylene in the highly irradiated sample #51, while the more stable toluene and benzene are present.

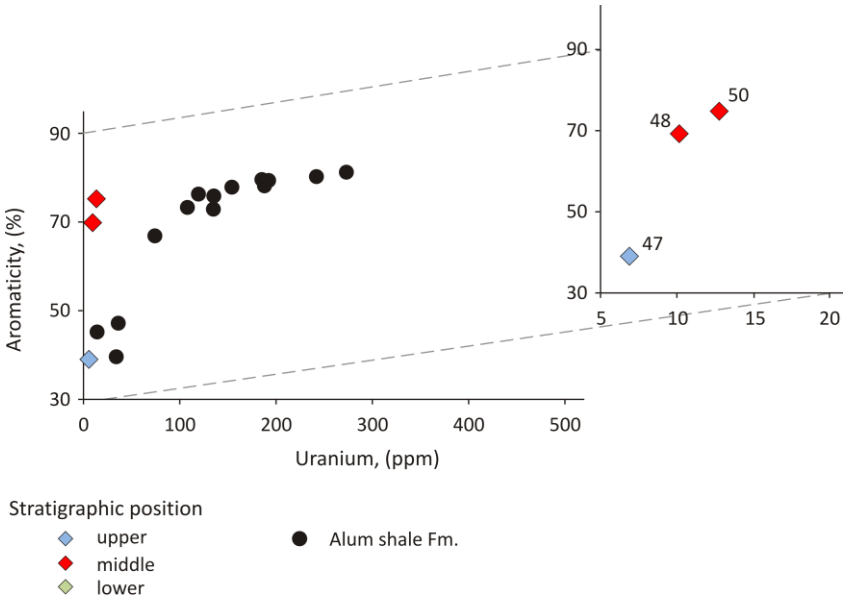

Fig. 4.9. Aromaticity (% o-xylene compared to *n*-non-1-ene and 2,3-dimethylthiophene) vs. uranium concentration (ppm) in whole-rock samples. As comparison, the plot shows the results obtained for the Middle Cambrian-Early Ordovician Alum Shale (black dots), after (Yang et al., 2018). Inset: samples of the Yacoraite Fm. (Valle del Tonco, western sector of the Metán-Alemanía sub-basin). Aromaticity increases with uranium content. However, as the uranium content in these samples is relatively low, the increase in aromaticity is more likely due to organofacies composition. Sample #51 is not shown because o-xylene and *n*-non-1-ene were not detected (see Fig. 4.8). The removal of these compounds and most of the other hydrocarbons is more likely due to the radiation effect.

Sample #47 generates Paraffinic-Naphthenic-Aromatic Low Wax Oils. In agreement with the increase in aromaticity, the generation of gas and condensates increases in the order: sample #47 < #40 < #50, which is interpreted to be controlled by organofacies composition. Sample #51 mainly generates gas hydrocarbons (Fig. 4.10) as expected from the Py-GC chromatograms (Fig. 4.8). Recent studies have shown similar behavior in samples from the Alum Shale in which increasing gas-prone character and aromaticity positively correlate with uranium content (Yang et al., 2018). Aromatization results in the removal of non-aromatic carbons, thereby increasing the abundance of aromatic moieties, and the lowering of hydrogen content independent of organic-matter type (Kelemen et al., 2007). As aromatic moieties have comparatively less hydrogen than paraffin/olefins hydrocarbons, aromaticity induced by radiation in sample #51 reduces the hydrogen content. As a consequence, low amounts of pyrolytic hydrocarbons are generated during Rock-Eval analysis (Fig. 3.9b), and therefore has low HI (Fig. 3.8 and Table 4.2). The extractable organic matter in sample #51 (0.035 mg HC/gr of rock), is one order in

magnitude lower compared to sample #48 (0.16 mg HC/gr of rock) and is likely another consequence of radiation (Lewan and Buchardt, 1989).

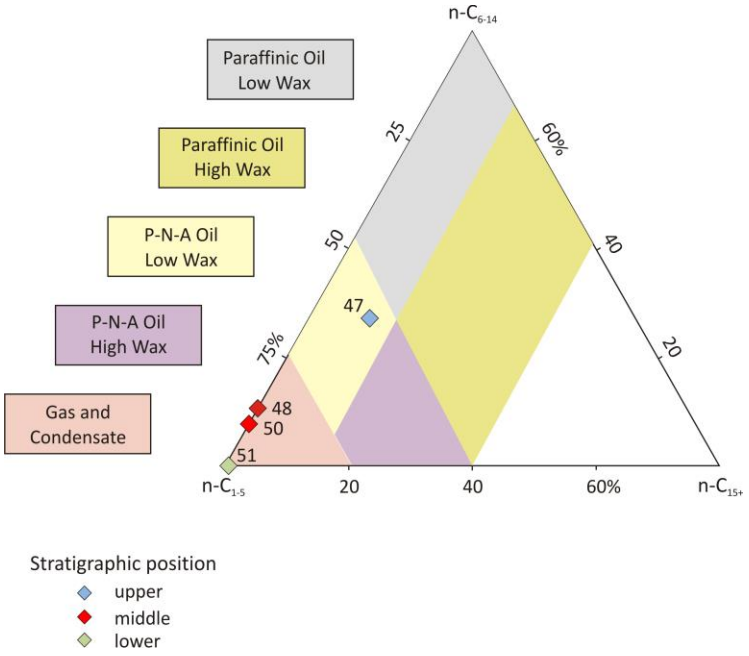

Fig. 4.10. Ternary plot of hydrocarbon chain-length distribution of pyrolysates (Py-GC) in samples of the Yacoraite Fm. (Valle del Tonco, western sector of the Metán-Alemanía sub-basin). Organofacies, according to Horsfield (1997), indicate that the sample from the lower sectors of the Yacoraite Fm. generate gas/condensates. A decrease in the gas/condensate generation is observed through the middle sector of the Yacoraite Fm. (samples #50 #48). Upper Yacoraite Fm. (sample #47) generates P-N-A Low Wax Oil.

The radiolysis hypothesis allows to reconcile Rock-Eval classification with organic petrography results. Sample #51 predominantly consists of alginite qualitatively and quantitatively it is similar to samples #47 and #48. The reduction of HI is expected in any kerogen type with increasing thermal maturity. By reducing HI, radiolysis effects can resemble thermal transformation (e.g., Sassen, 1984). The depositional environment of sample #51 was a freshwater lacustrine setting. While some sulphur might have been removed by redox reactions involving uranium, it is unlikely that the process was quantitatively significant. Any pyrite altered by such reactions would have yielded Fe-III oxides (Eglizaud et al., 2006), but low iron content in sample #51 similar to the other samples (#47 & #50) (Table 4, appendix) argues against this. Had the latter been quantitatively significant, strong mineral-matrix effects resulting in CO_2 generation would have occurred during pyrolysis (Espitalié et al., 1980., Alcañiz et al., 1989). Radiation not only alters the organic matter, but also induces the formation of oxygen-bearing functional groups such as OH- and peroxides (Gebicki and Gebicki, 1993; Eglizaud et al., 2006; Jaraula et al., 2015) that are also capable of oxidizing the organic matter.

The role of radiation on thermal maturity parameters

Previous investigations (Dahl et al., 1988) and more recent studies by Yang et al. (2018) have shown that T_{max} inversely varies with uranium content in whole-rock samples; this can be explained by the effect of radioactive decay over a long exposure time (Lewan and Buchardt, 1989; Yang et al., 2018). The presence of aromatic moieties in the kerogen can cause the weakening of the chemical bonds in the β position of their alkyl substituents (Claxton et al., 1993), which require a low amount of energy

to break them and, therefore, low T_{max} values are recorded. The high uranium content, suggests that sample #51 should have the lowest T_{max} value in the set of samples analyzed which is not the case. The high T_{max} in whole-rock fraction can be the result of combination effects of oxidation of the organic matter caused by oxygen-bearing compounds generated by radiation and adsorptive effects of the mineral matrix (Fig. 4.6). The adsorptive effects that mask the decrease of T_{max} in whole-rock were removed during acid treatment used in kerogen concentration and a lower T_{max} was measured in this last preparation. The low Tmax of the kerogen extract which separated the organic matter from the mineral matrix suggests that the high T_{max} of the whole rock may be caused by the mineral matrix effect.

Increasing vitrinite reflectance is the consequence of chemical and structural changes such as an increase in aromatization and polycondensation with increasing thermal stress (Carr and Williamson, 1990; Hatcher et al., 1994). These chemical changes are expressed by direct correlation between aromatic stretching bands and vitrinite reflectance as revealed by μ-FTIR spectroscopy studies (Hartkopf-Fröder et al., 2015). If radiation can cause an increase in aromatization, then high vitrinite reflectance (1.07 %Ro) in sample #51 could be the result of increased aromatization induced by radiation. Measurements of the aromatic ring size or their orientations were not available for this study and therefore a further evaluation of this process was not possible. Vitrinite reflectance was influenced by the uranium content neither in outcrop samples of Alum Shale from central Sweden and Öland nor well samples from the Baltic Sea (Lewan and Buchart, 1989) with Type II kerogen as their main organic constituent. However, in samples collected at the Poison Canyon Mine (New Mexico) mainly consisting of vitrinite, Sassen (1984) observed that uranium content positively correlated with vitrinite reflectance and inversely to fluorescence, which mimics an increase in thermal maturity.

Uranium in the Alum Shale is either syngenetic or early diagenetic therefore, those samples have been affected by radiation for at least 500 Myr (Lewan and Buchart, 1989; Yang et al., 2018). The samples studied by Sassen (1984) have been exposed to radiation for at least 60 Myr, and the uranium concentration today is three orders of magnitude higher (2.95-19.5 %) than those reported for Alum Shale (0.01-0.044 %). This indicates a predominant role of uranium concentration over the time of exposure to radiation.

4.3.3 The overlapping effects of mineral matrix and radiation

The radiolytic T_{max} suppression in sample #51 is masked by a strong mineral-matrix effect (MME). Sample #51 has similar illite content than sample #48, although in sample #51 illite is likely of authigenic origin. Therefore, if a higher T_{max} in sample #51 was solely the consequence of MME, a similar T_{max} would be expected in both whole-rock samples which is not the case here. This suggests an additional mechanism of adsorption, which, together with MME, must have enhanced T_{max} in sample #51 to 458 °C. Hydrocarbon adsorption also takes place on the surface of organic matter (Cheng and Huang, 2004; Ross and Bustin, 2009; Gasparik et al., 2014). It can be higher than adsorption on mineral surfaces (Wang and Reed, 2009; Collell et al., 2014) and increase with aromaticity of kerogen (Ziegs

et al., 2017; Mahlstedt and Horsfield, 2019). This mechanism provides an additional hydrocarbon-retention capacity (adsorption) in the kerogen structure of sample #51. Its enhanced vitrinite reflectance (Table 4.2) and the extinction of its fluorescence (Fig. 3.11f) support the higher degree of aromatization. The high abundances of benzene and toluene in sample #51 indicate the aromatic character of its kerogen (Fig. 4.8).

The increase in oxygen compounds in bitumen of some samples of the Alum Shale was attributed to radiation (Yang et al., 2018). Because those compounds do not easily degrade into low-molecular weight compounds, an increase of OI would not be observed which may explain the low OI of sample #51 (9 mg CO_2/g TOC). Acid treatment during kerogen concentration causes loss of the oxygen functional groups such as O-C=O, C=O and decrease in the condensed aromatic rings (Wang et al., 2016). If such compounds were formed in the kerogen of sample #51 due to radiation, the acid treatment used to get the kerogen concentrate, would have removed them affecting the 3-D structure of the kerogen, its pore space, and, therefore, its hydrocarbon-retention capacity. In the Therefore, kerogen concentration of sample #51 significantly reduced the hydrocarbon retention capacity on minerals and kerogen which can explain the lower T_{max} of the kerogen concentrate (406 °C) compared to the whole-rock aliquot (458 °C). In addition, the T_{max} of the kerogen concentrate of sample #51 is also lower than the T_{max} values of the kerogen concentrates of the other samples of the Yacoraite Fm. in the same stratigraphic succession, (Table 4.2). indicating that the T_{max} suppression of the kerogen concentrate is caused by the exposure to radiation.

4.4 Conclusions

Based on organic geochemical parameters, the samples from the Yacoraite Fm. in the Tres Cruces and the Metán-Alemanía sub-basins are at the onset of petroleum generation. This thermal maturity assessment is in accordance with the presence of smectite in samples from these sub-basins and with the interpreted diagenesis based in the Kübler Index on authigenic illite (sample #51) for the western sector of Metán-Alemanía sub-basin. Due to the low thermal maturity of the samples of the Yacoraite Fm., the organic parameters used to interpret depositional environments, e.g., pristane and phytane, are not affected by thermal maturity and are therefore considered reliable. As the burial history of those outcrop samples is unknown, higher thermal maturity and mineral diagenesis can be expected in deeper parts of the basin.

In the set of samples collected in the western sector of Metán-Alemanía sub-basin, the mineral-matrix effect (MME) is mainly caused by illite/mica content. The consequence is a lowering of the Hydrogen Index. MME and radiolysis-induced aromaticity in kerogen explain the strong adsorption of hydrocarbons during pyrolysis, which causes a high T_{max} in whole-rock. The increase of vitrinite reflectance and the fluorescence extinction are also consequences of radiolysis-induced aromaticity.

Primary oils generated from the Yacoraite Fm. are predominantly composed of low-sulphur Paraffinic-Naphthenic-Aromatic Low Wax Oil generated from marine organofacies and Paraffinic High

Wax Oil generated from lacustrine organofacies, with a minor contribution of Paraffinic Low Wax Oil and gas/condensates.

5. Characteristics and origin of produced oils and oil seep samples

This chapter presents geochemical parameters measured in oil seeps and produced oils to constrain properties of the source rock and for further comparison with source rocks in the area. Based on these interpretations, source rock-oil and oil-oil correlations are suggested. The biomarkers parameters used throughout this chapter are shown in Tables 7 and 8, appendix).

5.1 Inferences regarding source characteristics from produced oils and oil seep samples

Organic geochemical parameters are used to characterize the depositional environment of the oil from the oil seep samples and retrieved from produced oils. The following abbreviations are used through the text:

Barro Negro mud-oil mixture:	(BN_M-O) (samples a & b)
Laguna de la Brea water-oil mixture:	(LB_W-O) (sample c)
Laguna de la Brea mud-oil mixture:	(LB_M-O) (samples d & e)
Tar collected in the Tres Cruces sub-basin in its north sector:	(tar)
Fresh oil seep:	(sample f)

Samples from Laguna de la Brea were collected in the Lomas de Olmedo sub-basin where no rock samples were available. In addition, five samples of produced oils from the same basin, provided by Geomark and three samples provided by Prof. Dr. E. Rossello were examined in this study. The rest of the samples were collected in the Tres Cruces sub-basin.

5.1.1 Evolution of redox conditions

Pristane and phytane are used here for assessing the redox-condition prevailing at the time the source rocks of the oils were deposited. Pristane occurs in higher quantities than phytane (Fig. 5.1a and Table 7, appendix) in all the samples of produced oils, and in general, these differences are small. However, in oil samples from the Caimancito-30 and Río Pescado wells the amount of pristane is about twice that of phytane. Thus, the sample from Well-11 (Ramos X-11 oil field) has a ratio of 2.41. Differences in ratios are found in samples from the same oil field, as is the case in Caimancito. With the exception of the LB_W-O sample (c), all oil seep samples are essentially devoid of those isoprenoids (Table 7, appendix).

Slightly higher pristane compared to phytane concentration in all produced oils (Fig. 5.1a) suggests that their source rocks were deposited under moderately oxic conditions or alternatively to the presence of terrigenous organic matter (Peters et al., 2005a). The similar $\delta^{13}C$ values for pristane and phytane indicate that these isoprenoids shared a common precursor in all produced oil samples analyzed

in this study (Fig. 5.1b). Therefore, variations in pristane, phytane, and their ratios are reliable as parameters to assess redox conditions developed during the deposition of the sedimentary strata from which these oils were generated. These isoprenoids were not detected in the produced oils from Well-11 (the Ramos X-11 oil field) and the Río Pescado well. Regarding oil seep samples, the isoprenoids that were typical for the produced oils were only detected in sample LB_W-O in similar concentrations of 0.37 mg/g and 0.29 mg/g extract for phytane and pristane, respectively. The slightly higher phytane concentration suggests minor oxygen depletion in the former depositional environment (Peters et al., 2005a). Additional phytane input from precursors other than phytol such as archaebacterial lipids (Risatti et al., 1984) can also increase the phytane concentration. However, this sample was not selected for $\delta^{13}C$ analysis preventing further investigation of this possibility.

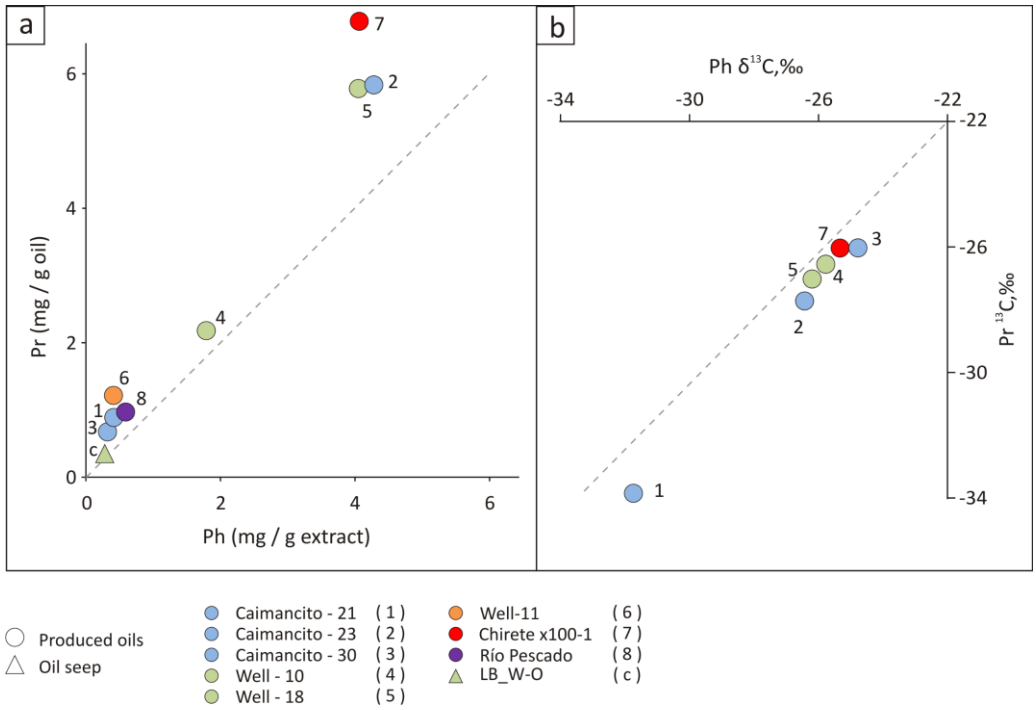

Fig. 5.1. Variation in Pristane vs. phytane in the aliphatic fraction in produced oil samples and one oil seep sample from the Lomas de Olmedo sub-basin. (a) Pristane vs. phytane predominance indicates that these samples were sourced from a rock deposited under slightly oxic environments. Pristane and phytane concentrations were calculated as mg/g oil for produced oils and mg/g extract for the oil seep sample. (b) Similar pristane and phytane $\delta^{13}C$ concentrations indicate a common precursor. Therefore, their use as a proxy to assess redox conditions is reliable in this set of produced oil samples, except for the Río Pescado in which no carbon isotopes were detected.

5.1.2 Source lithofacies

Inferences regarding the lithology of the possible source rocks come from steroidal hydrocarbon abundances. The catalytic effect of clay minerals facilitates the transformation of steranes to diasteranes (Moldowan et al., 1994a). Therefore, the extent of this transformation can be used to discriminate between a source-rock lithology comprised of shales or carbonates, which in conjunction with pristane and phytane (cf. section 3.2.5) allows redox conditions at the time of deposition to be evaluated (op. cit.). Pr/(Pr+Ph) ratios equal to or less than 0.65 and C_{27} diasteranes/(diasteranes + regular steranes)

ratios between 0.21 and 0.65 indicate that the petroleum samples were generated from a source rock deposited under anoxic conditions (Moldowan et al., 1986; Moldowan et al., 1994a). Well-11 (sample #6) from the Ramos X-11 oil field is an exception as it appears to have been generated by a source rock deposited under suboxic conditions as suggested from Pr/(Pr+Ph) ratio ≈0.7 and (C_{27} diasteranes/(diasteranes + regular steranes) ratio of 1 (Fig. 5.2 and Table 7 & 8, appendix).

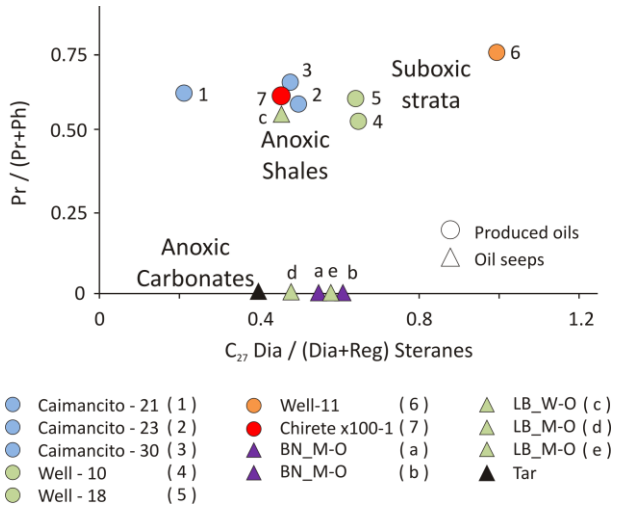

Fig. 5.2. Cross plot of pristane/ (pristane + phytane) ratios vs. C_{27} diasteranes/(diasteranes + regular steranes) for produced oil samples from the Lomas de Olmedo sub-basin. The Caimancito-21 oil (sample #1) was generated from a carbonate source rock. The other produced oils shown were generated from a shale source rock. The source rock for well-11 from the Ramos X-11 oil field sample (#6) was deposited under suboxic conditions (After Moldowan et al., 1994a). Sterane data were not available for the oil sample from Río Pescado and the fresh oil seep.

Oils generated from carbonate source rocks have a C_{27} diasteranes to regular steranes ratio of ≈0.2. Higher values characterize oils derived from shale source rocks (Moldowan et al., 1994a). Based on its ratios of C_{27} diasteranes to regular steranes close to 0.2, the Caimancito-21 oil (sample #1) was generated from a carbonate source rock. Higher ratios than 0.4 indicate that the other oil samples were generated from a shalier source rock (Fig. 5.2), like most of the oil seep samples with C_{27} diasteranes to regular steranes ratios ≥0.4 (Fig. 5.2). The source rock of the oil seep sample (c) was deposited in an anoxic environment. The rest of the oil seep material lack pristane and phytane and therefore no inferences are made regarding the redox conditions of the depositional environment of their source rock. No data were available for samples from Río Pescado and the fresh oil seep. The difference between inferred lithologies for the source rock in samples from the Caimancito oil field, i.e., Caimancito-21 (sample #1) and Caimancito-30 (sample #3) vs. Caimancito-23 (sample #2) suggests lateral and vertical variability of lithofacies in the source rock or contribution from different source rocks. The second possibility is discarded, however, because the oil in the Caimancito oil field is produced from the naturally fractured Yacoraite Fm. (Grosso et al., 2013).

5.1.3 Water-column stratification

Oxygen depletion in water during deposition with possible development of anoxic conditions may be the result of stratification related to salinity (cf. section 3.2.6). Gammacerane is a biomarker indicative of water-column stratification due to salinity or temperature gradient (cf. section 3.2.6). Gammacerane was only detected in samples of Caimancito-21, Caimancito-30, and Well-10 (Fig. 5.3).

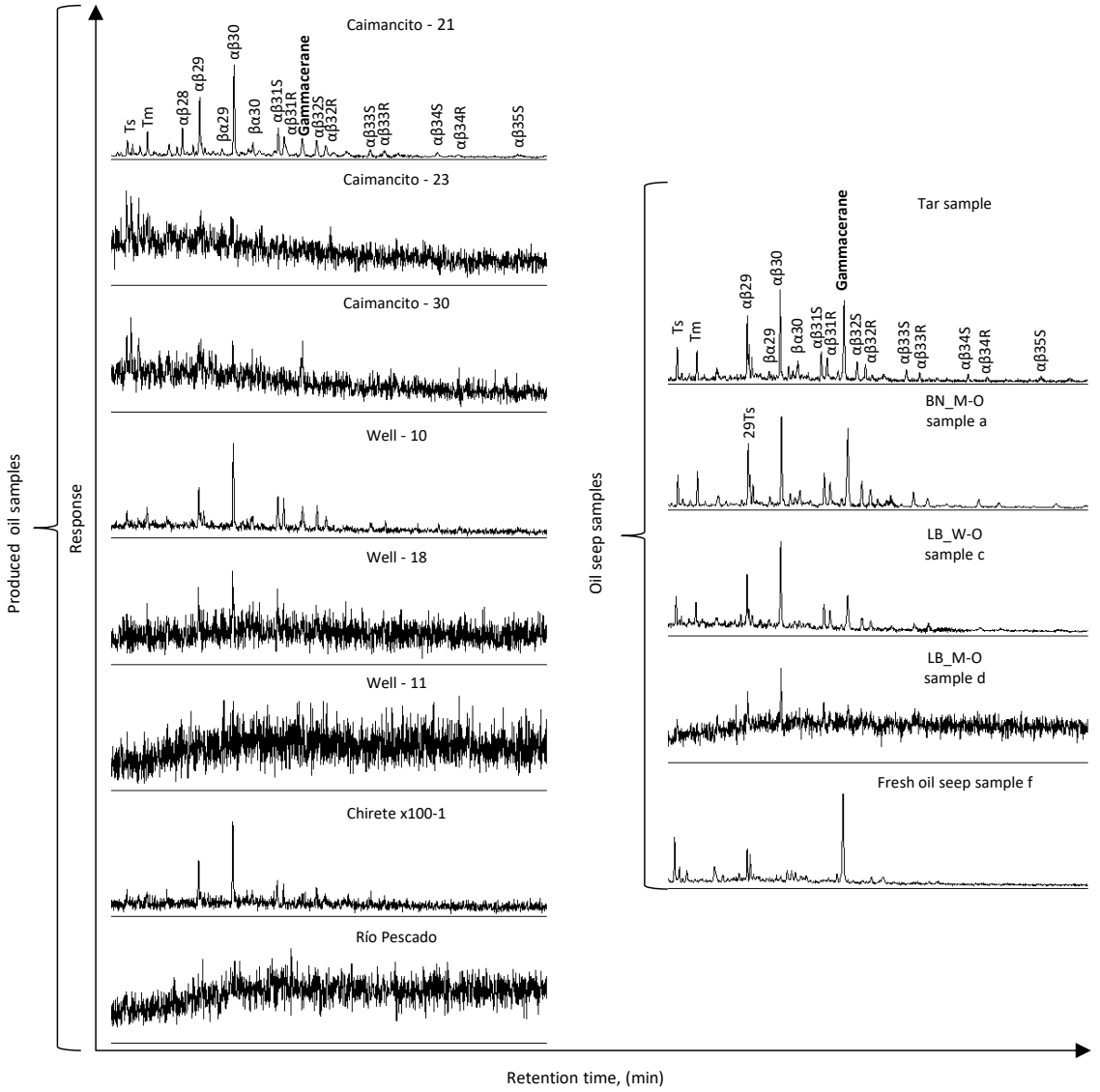

Fig. 5.3. GC-MS mass chromatograms of hopane distribution m/z=191 in the saturated fraction of produced oil samples from the Lomas de Olmedo sub-basin and representative oil seep samples collected in the Tres Cruces and the Lomas de Olmedo sub-basins. The full range from trisnorneohopane (27TS) up to αβC_{35}S hopane was detected in the produced oil of Caimancito-21, partially detected in the produced oils of Well-10 and Chirete x100-1, but were not detected in the rest of the produced oils. The same range of hopanes was detected in tar and the Barro Negro oil seep samples, partially detected in the oil seep/water mixture and the fresh oil seep. Some hopanes in this range were detected in the oil seep/mud from Laguna de la Brea locality. Oleanane, a biomarker indicative of angiosperms in the source rock, was not detected in any of the samples. The presence of gammacerane is an indicator of water-column stratification due to hypersalinity or temperature gradients (Sinninghe Damsté et al., 1995).

In the gammacerane-bearing samples, the Gammacerane Index (10*gammacerane /(gammacerane + C_{30}αβ-hopane) has values of 2, 5, and 2, respectively (Table 7, appendix). Gammacerane was not detected in Well-18 and Chirete x100-1 samples. The Gammacerane Index could not be calculated for these produced oil samples. According to the Gammacerane Index (Fig. 5.4), water stratification was developed during the deposition of the source rock of Caimancito-21 (sample #1), Caimancito-30 (sample #3), and Well-10 (sample #4) oil samples. The absence of gammacerane in samples obtained from Caimancito-23, Well-18, Well-11, Chirete x100-1, and Río Pescado indicate that they were sourced from a rock deposited in an environment where water stratification was not

developed. Both samples from the Barro Negro oil seep/mud (a & b) and the tar sample have similar Gammacerane Index values, which are close to 5. At the Laguna de la Brea location, the Gammacerane Index could be calculated only for the oil seep/water (c) with a value of 3. Neither gammacerane nor hopanes were detected in the oil seep/mud samples (d & e) at that same location (Fig. 5.3). The fresh oil sample has a Gammacerane Index of 10.

According to the Gammacerane Index (Fig. 5.4), Barro Negro oil seep/mud (samples a & b), the tar sample and the oil seep/water from the Laguna de la Brea (sample c) were sourced from a rock deposited in an environment where water-column stratification must have existed. This condition did not exist during the deposition of the rock that generated the oil seep/mud (samples d & e) from the Laguna de la Brea location since they lack gammacerane. Sample (c) was sourced from a different rock or different organofacies than samples (d) and (e), based on the presence of gammacerane in the sample (c) and its absence in the other two samples. Influences of the present environment on the Gammacerane Index cannot be discarded because they were collected in the shoreline environment of the present-day lagoon. However, the Gammacerane Index for sample (c) is in the range of other oil seep samples, e.g., samples (a) and (b). The Gammacerane Index for the fresh oil seep (sample f) indicates that water-column stratification also developed during the deposition of its source rock. Gammacerane is biodegraded at severe levels of biodegradation (at least 8 degree of biodegradation) and Gammacerane Index is no longer useful for the assessment of depositional environments (Huang, 2017).

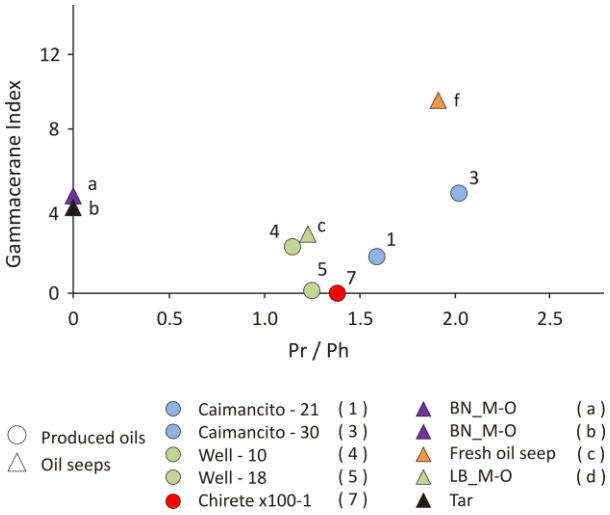

Fig. 5.4. Gammacerane Index vs. Pristane (Pr)/phytane (Ph) of produced oil samples from the Lomas de Olmedo sub-basin (circles) and oil seep samples collected in the Tres Cruces and the Lomas de Olmedo sub-basins (triangles). Except for samples of Well-18 (#5) and Chirete x100-1 (#7), the other produced oils and oil seep samples were sourced from a rock deposited where water-column stratification existed. Samples of Caimancito-23 (#2), Well-11 (#6), Río Pescado (#8), and the oil seep samples (d & e) are not shown, because they lack both gammacerane and hopanes. Modified from Peters et al. (2005a).

5.1.4 Marine versus lacustrine depositional setting

Oils generated from marine source rocks can be differentiated from oils with a lacustrine origin by their enrichment in organic sulphur, which is evaluated by the dibenzothiophene (DBT) content and its ratio to phenanthrene (P), as indicated by Hughes et al. (1995). Interpretations should be furthermore supported by additional parameters, as discussed in section 3.2.6. Except the oil sample of Well-11, that contains phenanthrene where DBT was not detected, the rest of the produced oils have a DBT/P equal to (sample of Chirete x100-1) or lower than 0.1. DBT/P ratios are variable in the oil seep samples (Table

7, appendix). This ratio is close to 0.5 for the Barro Negro oil seep/mud (sample b) and the oil seep/mud collected in Laguna de la Brea (sample e). For the other Barro Negro oil seep/mud (sample a), the oil seep/water of Laguna de la Brea (sample c), and the other oil seep/mud (d) in the same location, DBT/P ratios are 0, 1.41 and 0.16, respectively.

The fresh oil seep lacks DBT and P. Except for the oil seep sample (c), the rest of oil seep samples lack pristane and phytane. A Pr/Ph ratio of zero was used to plot them in Fig. 5.5. According to DBT/P ratios, all of the produced oils were sourced from low-sulphur marine or lacustrine shales (Fig. 5.5). The low DBT/P ratio of the oil sample from Caimancito-21 suggests it was sourced from an argillaceous shale, however the low C_{27} diasteranes to regular steranes ratio (Fig. 5.2) indicates a carbonate composition of its source rock. Except for the oil seep/water (LB_W-O, sample c) and the fresh oil seep, the remainder of the oil seep samples were sourced from a lacustrine low-sulphur source rock. Sample (c) collected from surface waters in the Laguna de la Brea plots outside of any specific field, likely reflecting a DBT contribution from the present-day lacustrine environment where this sample was collected.

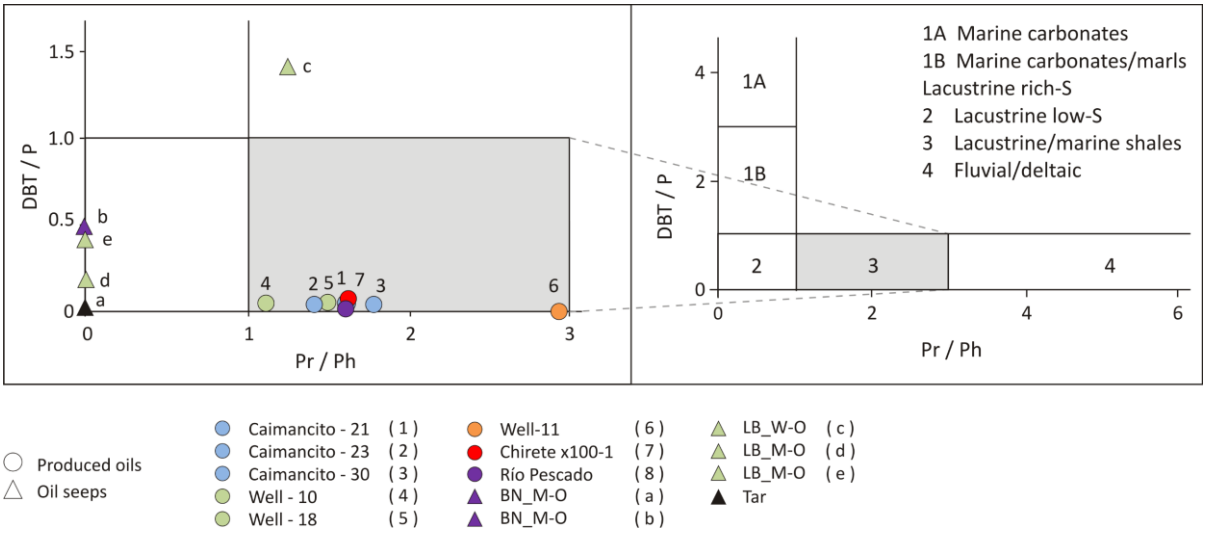

Fig. 5.5. Pristane (Pr)/Phytane (Ph) ratio vs. Dibenzothiophene (DBT)/Phenanthrene (P) ratio in produced oils (circles) from the Lomas de Olmedo sub-basin and oil seep samples collected in the Tres Cruces and the Lomas de Olmedo sub-basins (triangles). All produced oils were sourced from a rock deposited in a marine or lacustrine environment with low sulphur availability. Except the oil seep sample (c), the rest of the oil seep samples lack pristane and phytane. A Pr/Ph ratio of zero was used to plot them in the figure. The fresh oil seep sample (f) lacks those isoprenoids, phenanthrene, and dibenzothiophene, and therefore is not shown here. The oil seep samples were sourced from a rock deposited in a low-sulphur lacustrine environment. After Hughes et al. (1995).

To further support the assessment of the depositional environment, the combination of C_{26}/C_{25} tricyclic terpanes and $C_{31}R/C_{30}$ hopanes is used here using the same criteria previously discussed in section 3.2.6. Regarding the produced oil samples, C_{26}/C_{25} tricyclic terpanes were only detected in samples from Caimancito-21 (sample #1) and Caimancito-23 (sample #2) (Fig. 5.6). However, these peaks are too small in the sample from Caimancito-23 to provide a reliable C_{26}/C_{25} tricyclic terpanes ratio. The produced oil from Caimancito-23, Well-11, and Río Pescado have neither $C_{31}R$ nor C_{30}

hopanes (Fig. 5.3). Samples from Well-10 and Chirete x100-1 have $C_{31}R/C_{30}$ hopane ratios of 0.39 and 0.35, respectively. In the Well-18 and Caimancito-30 samples, C_{30} hopane was detected, but not $C_{31}R$.

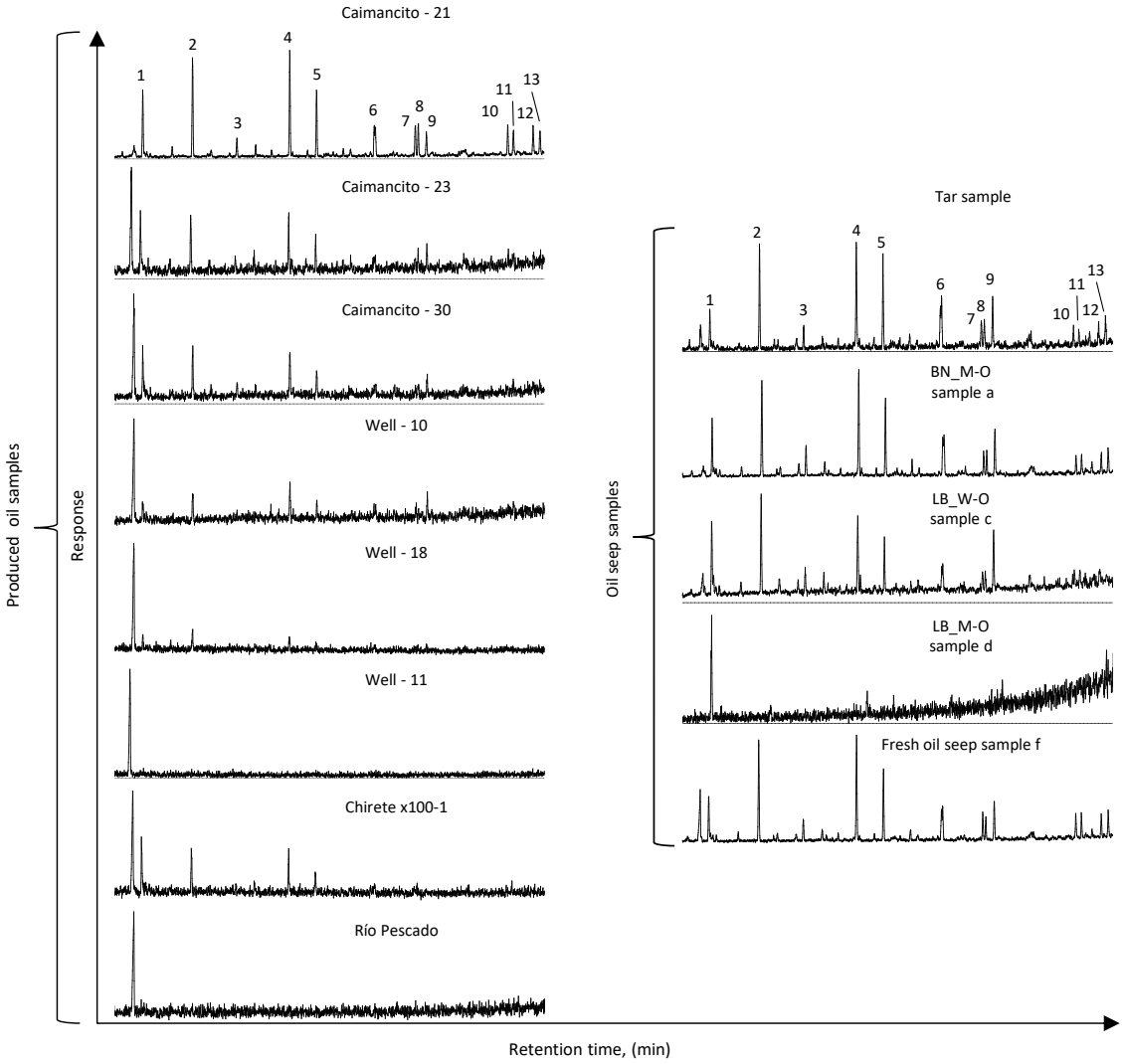

Fig. 5.6. GC-MS chromatograms of tricyclic terpane distribution m/z=191 in the saturate fraction of produced oil from the Lomas de Olmedo sub-basin and representative oil seep samples collected in the Tres Cruces and the Lomas de Olmedo sub-basins. The full range of C_{20} to C_{29} tricyclic terpanes was only detected in the produced oils of Caimancito-21 and Caimancito-23, partially detected in samples of Caimancito-30, Well-10, Well-18, and Chirete x100-1, and not detected in the samples of Well-11 and Río Pescado. The same tricyclic terpane distribution was detected in all oil seep samples, except in the oil seep/water mixture from Laguna de la Brea. Specific compounds: 1: C_{20}-Triterpane; 2: C_{21}-Triterpane; 3: C_{22}-Triterpane; 4: C_{23}-Triterpane; 5: C_{24}-Triterpane; 6: C_{25}R+S-Triterpane; 7: C_{26}R-Triterpane; 8: C_{26}S-Triterpane; 9: C_{24}-Tetraterpane; 10: C_{28}R-Triterpane; 11: C_{28}S-Triterpane; 12: C_{29}R-Triterpane; 13: C_{29}S-Triterpane.

The C_{26}/C_{25} tricyclic terpane ratios vary from 1.1 to 1.5, and $C_{31}R/C_{30}$ hopane ratios vary from 0.2 to 0.3 in oil seep samples tar, a, b, and c. The two oil seep/mud samples of Laguna de la Brea (d & e) lack $C_{31}R$ hopanes and tricyclic terpanes (C_{26}, C_{25}). The fresh oil seep sample has a C_{26}/C_{25} tricyclic terpane ratio of 1.5, but lacks hopanes ($C_{31}R$, C_{30}). Based on the C_{26}/C_{25} tricyclic terpane ratio of 2.1 and $C_{31}R/C_{30}$ hopane ratio of 0.2, the Caimancito-21 (sample #1) was sourced from a lacustrine source rock (Fig. 5.7). The absence of hopanes ($C_{31}R/C_{30}$) and the C_{26}/C_{25} tricyclic terpane ratio of 1.3 do not allow a clear distinction between marine and lacustrine settings for the sample of Caimancito-23.

The produced oils of Well-10 and Chirete x100-1 lack C_{26}/C_{25} tricyclic terpanes (Fig. 5.6). Their $C_{31}R/C_{30}$ hopane ratio of 0.39 and 0.35, respectively, suggests they were generated by a marine source rock. Well-18 and Caimancito-30 samples also lack C_{26}/C_{25} tricyclic terpanes. In these samples, C_{30} hopane was detected, but not $C_{31}R$. Depositional environment interpretations based only on the presence of C_{30} hopane is not conclusive. Due to the absence of $C_{31}R/C_{30}$ hopanes (Fig. 5.3) and C_{26}/C_{25} tricyclic terpanes (Fig. 5.6) in the produced oils of Well-11 (sample #6) and Río Pescado (sample #8), it is not possible to interpret depositional environments in this context.

With C_{26}/C_{25} tricyclic terpane ratios between 1 to 1.3 and $C_{31}R/C_{30}$ and hopane ratios between 0.2 to 0.3, the Barro Negro oil seep (sample b) and the tar sample plot in a region that does not allow the discrimination between marine and lacustrine environments. The other Barro Negro oil seep (sample a), LB_W-O (sample c), and the fresh oil seep were sourced from a rock deposited under lacustrine conditions. Due to the absence of C_{26}/C_{25} tricyclic terpanes and $C_{31}R/C_{30}$ hopanes in the other two oil seep/mud from Laguna de la Brea (d & e) and the mentioned hopanes in the fresh oil seep (sample f), it is not possible to interpret depositional environments in this context.

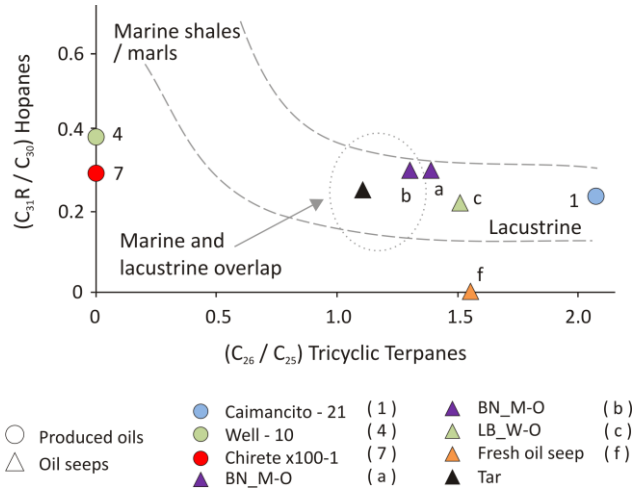

Fig. 5.7. Cross plot of $C_{31}R/C_{30}$ hopane vs. C_{26}/C_{25} tricyclic terpanes in produced oils samples from the Lomas de Olmedo sub-basin and oil seep samples collected in the Tres Cruces and the Lomas de Olmedo sub-basins. Oil seep samples (b & tar) plot in a zone between marine and lacustrine environments, which does not allow to unambiguously distinguish these environments. The produced oil of Caimancito-21 (#1) and the oil seep samples (a & c and fresh-oil) were sourced from a rock deposited under lacustrine conditions. The $C_{31}R/C_{30}$ hopane ratio of samples from Well-10 and Chirete x100-1 suggest that their source rock was deposited in a marine environment. Modified from Peters et al. (2005a).

5.1.5 Terrigenous versus aquatic organic-matter types

Steranes are considered products of the transformation of sterols (Volkman, 1988). It was originally suggested by Huang and Meinschein (1979) that C_{27}, C_{28}, and C_{29} sterols could be used to characterize the organic material deposited in recent sediments. This approach was extended to C_{27}, C_{28}, and C_{29} steranes (Moldowan et al., 1985), and it is routinely used to this day (Fang et al., 2019). Regular $\alpha\alpha\alpha C_{27}R$ to $\alpha\alpha\alpha C_{29}R$ steranes were detected only in Caimancito-21 (sample #1). Caimancito-23 (sample #2), Caimancito-30 (sample #3), and Well-10 (sample #4) lack $\alpha\alpha\alpha C_{29}$ steranes. Only $\alpha\alpha\alpha C_{27}R$ steranes were detected in the sample of Well-18. None of the $\alpha\alpha\alpha C_{27}R$ to $\alpha\alpha\alpha C_{29}R$ steranes were detected in samples of Well-11 (Ramos X-11 oil field, sample # 6), Chirete x100-1 (sample # 7) and the Río Pescado (sample # 8). (Table 8, appendix).

Oil seep samples collected in Barro Negro (a & b), and two of the oil seep samples from Laguna de la Brea (c & e) have similar abundances of αααC_{27}R and αααC_{28}R steranes, but they lack the αααC_{29}R sterane. The other oil seep collected at the Laguna de la Brea locality (sample d) only contains the αααC_{27}R sterane. None of these steranes were detected in the fresh oil seep sample. All of the three steranes were detected in the tar sample (Table 8, appendix). The lack or negligible amounts of αααC_{29}R steranes relative to αααC_{27}R and αααC_{28}R steranes indicates minor terrigenous input to the source rocks of the oil samples from the Caimancito (samples 1-3) and Martinez del Tineo (samples #4 & #5) oil fields and most of the oil seep samples analyzed (except the fresh oil seep). Comparative higher terrestrial input is suggested for the source rock of Caimancito-21 and the tar sample because of the relative higher abundance of αααC_{29}R sterane (Fig. 5.8), and in consideration of the likely Mesozoic age of the source rock.

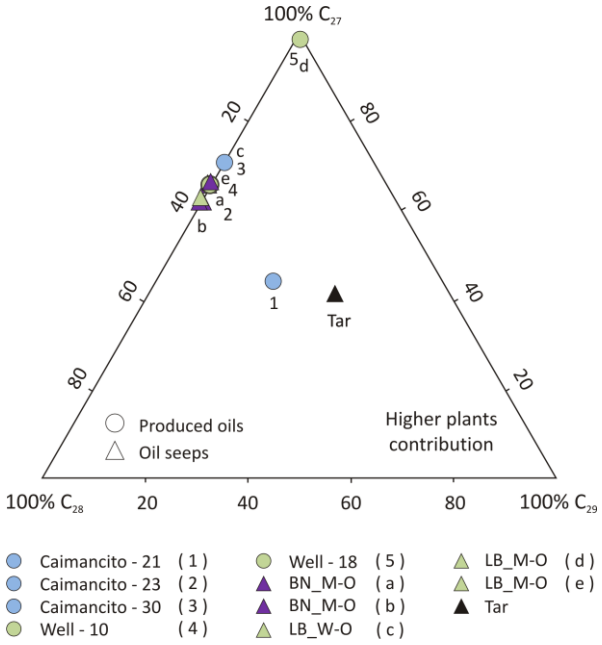

Fig. 5.8. Ternary plot of αααC_{27}R, αααC_{28}R and αααC_{29}R steranes in produced oil samples from the Lomas de Olmedo sub-basin and oil seep samples collected in the Tres Cruces and the Lomas de Olmedo sub-basins. Higher relative amounts of αααC_{29}R sterane in samples of Caimancito-21 (#1) and the tar indicate the input of terrigenous plants in their source rock. The other produced oils and oil seep samples were generated from a source rock with no or negligible plant-matter input.

The abundance of C_{29} steranes is considered to reflect the predominant contribution of higher plants. However, their predominance in an environment of high algal productivity (Volkman, 1988) in Paleozoic or older crude oils (Grantham and Wakefield, 1988) suggested that their presence is not reliable regarding the input of higher plants. Therefore, interpretations of depositional environments and type of organic input must be supported by other, more adequate parameters. More sensitivity in analyses of biomarkers was reached with multiple reaction monitoring mass spectrometry (MRM-GC/MS). This allowed steranes to be detected in samples from Well-11 (Ramos X-11 oil field, sample # 6) and Chirete x100-1 (Sample #7). This data was not available for the produced oil of Río Pescado (sample #8). Samples from Caimancito and Martinez del Tineo oil fields (Well-10 & Well-18) show a C_{29}/C_{27} regular steranes ratio between 1 and 2 (Table 8, appendix). Although the produced oil of Chirete x100-1 has C_{27} steranes, it lacks C_{29} (Fig. 5.9). The opposite is observed in the produced oil of Well-11 (Ramos X-11 oil field, sample # 6).

The analysis of C_{29}/C_{27} regular steranes in the material from oil seep samples also shows variations. A ratio of 0.96 and 1.01 was calculated for the two Barro Negro oil seep samples (a & b). Higher values characterize the oil seep samples collected in Laguna de la Brea (samples c, d & e). These are 1.7 and 2.2 for the oil seep/mud, and 1.5 for the oil seep/water, respectively. The tar sample lacks both C_{27} and C_{29} regular steranes, while this data was no measured for the fresh oil seep. C_{29}/C_{27} regular sterane ratios confirm the low terrigenous input for the source rocks of the Caimancito and Martinez del Tineo oil fields (Well-10 & Well-18) (Fig. 5.9 and Table 7 & 8 appendix). The same is interpreted now for the produced oil of Chirete x100-1 based on the presence of C_{27} regular steranes and the absence of C_{29} steranes. The sample obtained from Well-11 was sourced from a rock with significant terrestrial plant input as suggested by the presence of C_{29} regular steranes and the absence of C_{27} steranes (Not shown in Fig. 5.9). Except for tar and the fresh oil seep sample, C_{29}/C_{27} regular sterane ratios confirm limited land-plant input for the source rocks of the oil seep samples.

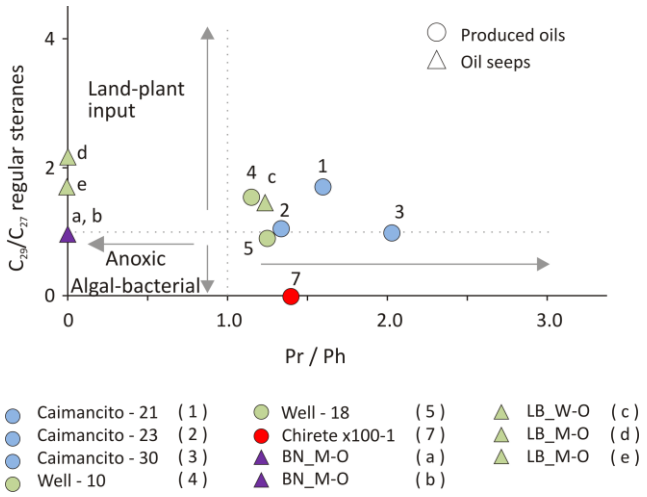

Fig. 5.9. C_{29}/C_{27} regular steranes ratio vs. Pristane (Pr)/ phytane (Ph) ratio of produced oil samples from the Lomas de Olmedo sub-basin and oil seep samples collected in the Tres Cruces and the Lomas de Olmedo sub-basins. Samples of Caimancito-23 (#2), -30 (#3), Well-18 (#5) from Martinez del Tineo oil field, and oil seep samples collected in Barro Negro (a, b) were sourced from a rock with limited or no land-plant input. Samples of Caimancito-21 (#1), Well-10 (Martinez del Tineo oil field) and the oil seep samples collected at the Laguna de la Brea locality (c, d, & e) were sourced from a rock with slightly higher land-plant input. Because of the presence of C_{29} and the absence of C_{27} regular sterane in the sample of Well-11 (#6), the C_{29}/C_{27} ratio is not calculated and therefore it is not shown. The presence of C_{29} steranes in this sample suggest a significant input of terrestrial plant material for its source rock. No results are available for the Río Pescado sample (#8), the tar sample, and the fresh oil

The Pristane/n-C_{17} and Phytane/n-C_{18} ratios indicate a source rock mainly comprised of Type II/III kerogen deposited under reducing conditions; this is the case for the produced oils of the Caimancito and Martinez del Tineo sites (Well-10 & Well-18), Well-11, Chirete x100-1, the Río Pescado oil fields (Fig. 5.10). This indicates Type II algal kerogen with some Type III kerogen input in agreement with low amounts of plant-material input as interpreted from sterane analysis. Higher Pr/n-C_{17} and Ph/n-C_{18} ratios in the produced oil of Well-11 (#6) indicate higher contribution of Type III kerogen to its source rock, which agrees with a presence of f C_{29} regular steranes and absence of C_{27} regular steranes.

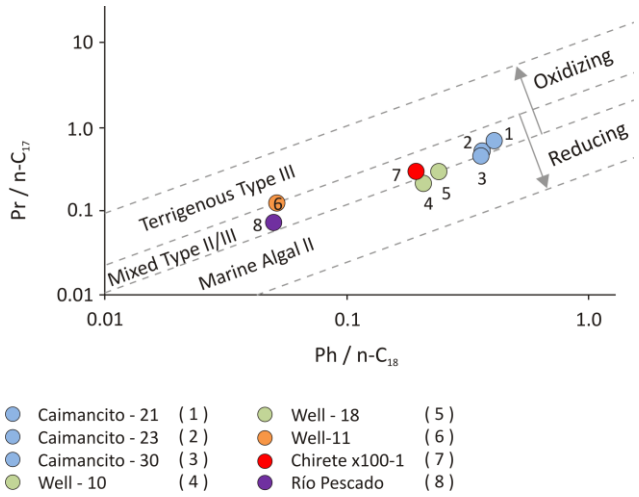

Caimancito - 21 (1)
Caimancito - 23 (2)
Caimancito - 30 (3)
Well - 10 (4)
Well - 18 (5)
Well-11 (6)
Chirete x100-1 (7)
Río Pescado (8)

Fig. 5.10. Pristane/n-C_{17} vs. Phytane/n-C_{18} ratios in produced oil samples from the Lomas de Olmedo sub-basin. These oils were sourced from a Type II kerogen-bearing rock with some Type III kerogen input as suggested by II/III kerogen mixtures deposited under reducing conditions. The source rock of the sample of Well-11 had higher contribution of Type III kerogen and was deposited under slightly oxic conditions.

In addition to their main use as maturity indices, diamondoids (adamantanes and diamantanes) can be used to infer the possible kerogen type of the source rock. Diamondoids are not of biological origin (Moldowan et al., 2015). However, their carbon-frame is thought to be the result of the re-arrangement of biogenic precursors (Araujo et., 2012) catalyzed by minerals (Katz et al., 2008; Wei et al., 2006a). Their distribution is source dependent (Moldowan et al., 2015) and has been used to infer the kerogen type in the source rocks (Schulz et al., 2001). Because of their high thermal stability (Dahl et al., 1999; Wei et al., 2006a; Moldowan et al., 2015), diamondoids can preserve such genetic information even under temperatures conducive to oil cracking, where biomarkers are not suitable anymore (Moldowan et al., 2015). In this study, two indexes were calculated based on adamantanes and diamantanes according to Schulz et al. (2001):

Ethyladamantane index (EAI) = 2-EA/(2-EA+1-EA). Where 2-EA is 2-ethyladamantane and 1-EA is 1-ethyladamantane.

Dimethyldiamantane index-1 (DMDI-1) = 3,4-DMD/ (3,4-DMD + 4,9-DMD). Where 3, 4-DMD is 3-, 4-dimethyldiamantane and 4, 9-DMD is 4-, 9-dimethyldiamantane.

With EAI lower than 80 % and DMDI-1 equal or lower than 75 % (Fig. 5.11), all produced oils analyzed in this study fall into the region defined for typical Type II marine source rocks such as the Spekk Formation (Schultz et al., 2001), for example. This suggests that the organic matter of the source rock from which these produced oils were generated was predominantly Type II kerogen (Fig. 5.11). The oil seep samples did not contain measurable adamantanes. As adamantanes are generated with the increase in thermal maturity (Araujo et al., 2012; Wei et al., 2007), their absence in the oil seep samples in this study suggests that these compounds were never present in these samples. Diamondoids can be biodegraded at severe levels of this process (degree 8; Grice et al., 2000). The level of biodegradation in the oil seep samples studied here is <7 (cf. 5.4.2); therefore, this does not explain the absence of adamantanes in the oil seep samples.

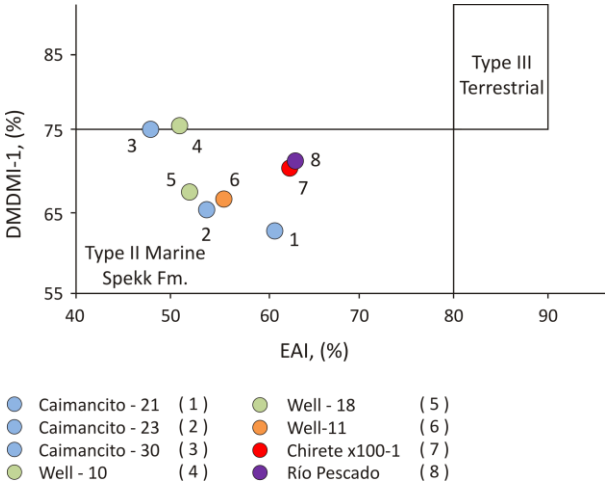

Fig. 5.11. Dimethyldiamantane index-1 (DMDI-1) vs. Ethyladamantane index (EAI) of produced oil samples from the Lomas de Olmedo sub-basin. These oils were sourced from a Type II kerogen-bearing rock similar to a Type II marine Spekk Formation. After Schulz et al. (2001).

5.2 Age-related biomarkers in produced oils and oil seep samples

5.2.1 General considerations

The Cretaceous Yacoraite and the Devonian Los Monos formations are the main source rocks in the Olmedo sub-basin, where the produced oil samples in this study come from. Because of their very different age, the oils generated from these formations should easily be differentiated based on age-related biomarkers. Oleanane is a biomarker derived from angiosperms (Riva et al., 1988; Moldowan et al., 1994b) which first appeared during the Cretaceous (Martin et al., 1989; Doyle and Donoghue, 1993), and is therefore well suited to help assess the age of generative source rocks. Oleanane was not detected in any of the produced oil or oil seep samples of this study (Fig. 5.3) but it was also not detected in the rock extracts of the Cretaceous Yacoraite Formation either. Thus, its mere absence is not conclusive for age assignment in this case (also see Peters et al., 2005a).

Ratios of 24-norcholestanes or 24-nordiacholestanes (presumably linked to diatoms) to their corresponding 27-norcholestanes and 27-nordiacholestanes (likely algal-sourced) have been used as age-constraining biomarkers differentiating Jurassic from Cretaceous or younger oils (e.g., Holba et al., 1998). This ratio was not calculated because all the produced oils in this study lack 24-nordiacholestanes and 24-norcholestanes while 27-nordiacholestanes were only detected in the produced oil of Caimancito-23 and Well-10.

5.2.2 Age assignment based on steranes ratios

The C_{28}/C_{29} steranes ratio was observed to change from Precambrian to Paleogene times in oils derived from marine source rocks without a strong influence of land-plant or lacustrine organic matter (Grantham and Wakefield, 1988). The C_{28}/C_{29} steranes ratio is suitable to differentiate Late Cretaceous/Cenozoic from Paleozoic oils, but it is not suitable to provide age assignments with more accuracy. In oils generated from Early Paleozoic source rocks, the C_{28}/C_{29} steranes ratio is <0.5. It increases up to 0.7 for oils sourced from Early Jurassic source rocks and has values >0.7 is oils generated from Late Jurassic to Miocene source rocks (op. cit.). As indicated in section 5.1.5 steranes are not

highly specific for certain organic input, particularly C_{29} steranes, which indicates that additional contributions from different organisms can influence the C_{28}/C_{29} sterane ratio. Additionally, factors such as biodegradation and thermal maturity can change the amount of the different steranes, and therefore their ratios (Seifert et al., 1984).

The period covered by the C_{28}/C_{29} sterane ratio makes it suitable to differentiate oils generated from the Devonian Los Monos Fm. and the Cretaceous Yacoraite Fm. All samples from the Caimancito oil field in this study and the Well-10 from Martinez del Tineo oil field have C_{28}/C_{29} sterane ratios between 0.9 and 1.1. The sterane ratio is therefore consistent with generation from a Cretaceous source rock (Fig. 5.12a) and no connectivity or at least not large influence of Devonian source rocks. C_{29} steranes were detected in the sample from Well-18, but no C_{28} steranes. C_{28} and C_{29} steranes were not detected in the produced oils of Well-11 (Ramos X-11 oil field), Chirete x100-1, and Río Pescado. Except for one oil seep/mud from the Laguna de la Brea (sample d), all the other oil seep samples have both, C_{28} and C_{29} steranes with ratios varying between 0.74 and 1.8, respectively. C_{29} steranes were detected in the sample (d), but no C_{28}.

The oil seep samples in this study were generated from a source rock whose steranes ratios are consistent with a Cretaceous age assignment (Fig. 5.12a). The C_{28}/C_{29} steranes ratio of the tar sample (0.74) puts this sample at the limit of the oils generated from the Late Jurassic source rocks and Cretaceous source rocks. This is likely due to the inaccuracy of the C_{28}/C_{29} steranes ratio in the age assignment. Sedimentation in the Salta rift basin started in the Early Cretaceous (Marquillas et al., 2005). Therefore, the Cretaceous is most likely the age of the source rock of the tar sample. Due to the absence of C_{28} steranes in the oil seep/mud sample from the Laguna de la Brea (sample d), it was not possible to infer the age of its source rock. But based on the overall distribution of the Los Monos Formation in NW Argentina it appears unlikely that this unit may have influenced the steranes in the Yacoraite Formation in the western part of the study region.

The ratio of C_{28}/C_{29} steranes in the extract of the middle section of the Yacoraite Fm. (sample #42) is 0.9 (black dot in Fig. 5.12a), which indicates it that it is of Cretaceous age. This supports the use of this ratio in age assignments of oils generated from this formation. A better location of the Yacoraite Fm. sample (#42) was obtained here when the $C_{28}\alpha\beta\beta S/C_{29}\alpha\beta\beta S$ steranes ratio was used (Fig. 5.12b), and the same criteria used for age assignment based on C_{28}/C_{29} steranes were followed. The ratio of $C_{28}\alpha\beta\beta/C_{29}\alpha\beta\beta$ steranes in the rock extract of sample #42 is 1.67 (black dot in Fig. 5.12b). All samples from the Caimancito oil field in this study and the Well-10 from the Martinez del Tineo oil field have $C_{28}\alpha\beta\beta S/C_{29}\alpha\beta\beta S$ steranes ratios between 1.2 and 1.5. In the sample from Well-18, $C_{29}\alpha\beta\beta$ sterane was detected, but not $C_{28}\alpha\beta\beta$ sterane. Neither $C_{28}\alpha\beta\beta$ nor $C_{29}\alpha\beta\beta$ steranes were detected in the produced oils from Well-11 (Ramos X-11 oil field), Chirete x100-1, and Río Pescado. The lack of one or both of the $C_{28}\alpha\beta\beta$ and $C_{29}\alpha\beta\beta$ steranes prevented the age assignment for samples of Well-18, Well-11, Chirete x100-1, Río Pescado, the oil seep/mud sample from the Laguna de la Brea (sample d), and the fresh oil seep sample.

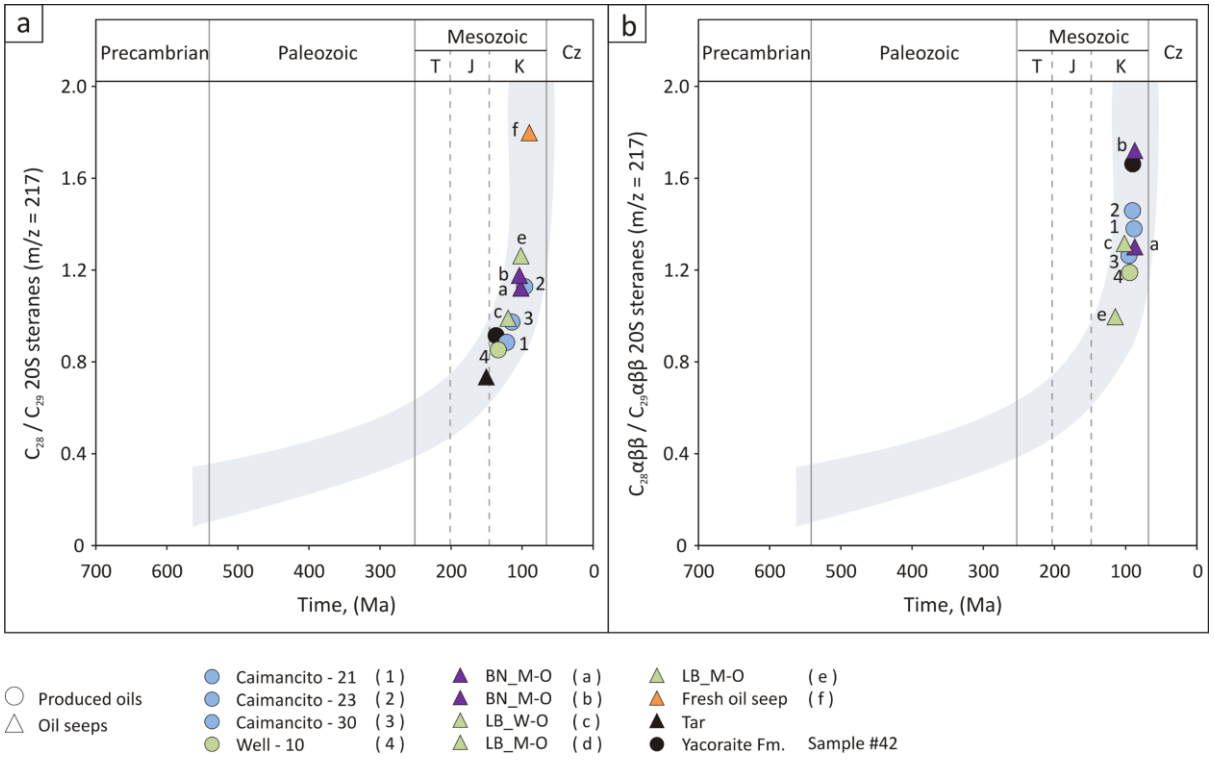

Fig. 5.12. Evolution of C_{28}/C_{29} steranes ratio used to the assessment of the age of produced oil samples from the Lomas de Olmedo sub-basin and oil seep samples collected in the Tres Cruces and the Lomas de Olmedo sub-basins. (a) C_{28}/C_{29} steranes ratio for produced oils, oil seep samples, and one sample of the Yacoraite Fm. Produced oils and oil seep samples were generated from a Cretaceous source rock. The inferred age of the source rock of the tar sample is at the limit between the Late Jurassic and Cretaceous-age materials. During the Devonian there was no deposition in the Salta rift basin. Therefore, the Cretaceous is the most likely age for the source rock of the tar sample. The inferred age for rock extract (black dot, sample # 42) collected from the middle section of the Yacoraite Fm. in the Tres Cruces sub-basin agrees with its deposition during the Cretaceous, which validates this parameter for this set of samples. (b) C_{28} αββS/C_{29}αββ sterane ratios for the same samples as plotted in (a) also show that the source rock for the samples was deposited during the Cretaceous. However, the position of the samples allows to assign their age more robustly than using C_{28}/C_{29} ratios. Samples were plotted approximately in the center of the interpreted age trend (shaded area). T: Triassic, J: Jurassic, K: Cretaceous, Cz: Cenozoic undifferentiated. After Grantham and Wakefield (1988) and Peters et al. (2005a).

The inferred age based on C_{28}αββS/C_{29}αββS steranes in sample #42 is consistent with the Yacoraite Fm. being the source rock of the oils studied here. Except for one oil seep/mud from the Laguna de la Brea (sample d) and the fresh oil seep samples, all other oil seep samples have both, C_{28}αββS and C_{29}αββS steranes, with ratios varying between 1 and 1.7, respectively. Sample (d) has the C_{29}αββS sterane but lacks the C_{28}αββS sterane. The opposite was found in the fresh oil seep sample. Based on the above interpretations and the similar C_{28}/C_{29} ratios it thus can be concluded that samples from the Caimancito oil field, Well-10, and the oil seep samples (except d) all were generated from a Cretaceous source rock (Fig. 5.12b). In this plot the sample from the Yacoraite Fm. and most of the produced oils and oil seep samples are allocated in a clearer Cretaceous position compared to Fig. 5.12a. Therefore C_{28}/C_{29} steranes ratio seems to be useful to discriminate oils generated from the Yacoraite Fm. from an older source rock, e.g., the Devonian Los Monos Fm. To verify this, oil samples proven to be sourced from this formation would be required.

5.3 Maturity of produced oils and oil seep samples

Increasing thermal maturity in source rocks and their genetically related petroleum causes structural changes at C_{22} in hopanes and in C_{20} steranes biomarkers (Mackenzie and McKenzie, 1983). (R)-isomers in living organisms are transformed into the (S) configuration during thermal maturation (Peters et al., 2005a). Additionally, there is a change in the configuration of (αα) towards the (ββ) form at C_{14} and C_{17} positions in steranes (Seifert and Moldowan, 1986). As a consequence of these transformations, the ratios of 20S/(20S+20R) and ββ/(αα+ββ) isomers increase with thermal maturity (op. cit.). Thermal maturity of oils and oil seep samples can be used to infer likely source rocks and, therefore, it is useful in source-oil and oil-oil correlations and recognizing oil mixing (Ten Haven et al., 1993; Picha and Peters., 1998; Curiale, 2008; Moldowan et al., 2015).

5.3.1 Maturity assessment based on hopanes and sterane isomerization

The conversion of one stereoisomer into another reaches an equilibrium at certain levels of thermal maturity. For example, for C_{31} and C_{32} hopanes the equilibrium of the transformation of (R) into (S) isomers is reached at a 22S/(22S+22R) ratio of ≈60 % (Seifert and Moldowan, 1980; Van Duin et al., 1997). Ratios of these isomers in the range from 50-54% suggest a thermal maturity that corresponds to the onset of the oil window. Ratios between 57-62% correspond to the main phase of oil generation and higher thermal levels (op. cit.). For C_{29} steranes, the conversion of (R) into (S) isomers reaches the equilibrium at 20S/(20S+20R) ratios between 52-55%. Ratios of (ββ)/(αα+ββ) between 67-71% indicate the equilibrium in the conversion from (αα) into (ββ) sterane isomers (Grantham, 1986; Seifert and Moldowan, 1986). The equilibrium of these reactions is reached at peak oil-window conditions. Ratios of the biomarker isomerization are useful for thermal assessments, but vitrinite-reflectance values cannot be inferred from them (Peters et al., 2005a).

The (S) and (R) isomers of C_{31} and C_{32} hopanes were only detected in the produced oils of Caimancito-21 (sample #1), Well-10 (sample #4) and Chirete x100-1 (sample #7) (Fig. 5.3). The S/(S+R) ratios of these isomers in C_{31} and C_{32} hopanes are approximately 60% in sample Caimancito-21 and Well-10 (Fig. 5.13). In the produced oil of Chirete x100-1, the ratio for the conversion of (R) into (S) isomers of C_{31} hopanes is 50% while the corresponding transformation in C_{32} hopane is complete with a value of 100% (Fig. 5.13). These hopanes were detected in most of the oil seep samples, with the exception of the two samples from oil seep/mud mixtures retrieved from Laguna de la Brea (sample d & e) and the fresh oil seep (Fig. 5.3). In the oil seep samples in which these C_{31} and C_{32} hopane isomers were detected, the hopanes were found with similar ratios of approximately 60% (Fig. 5.13).

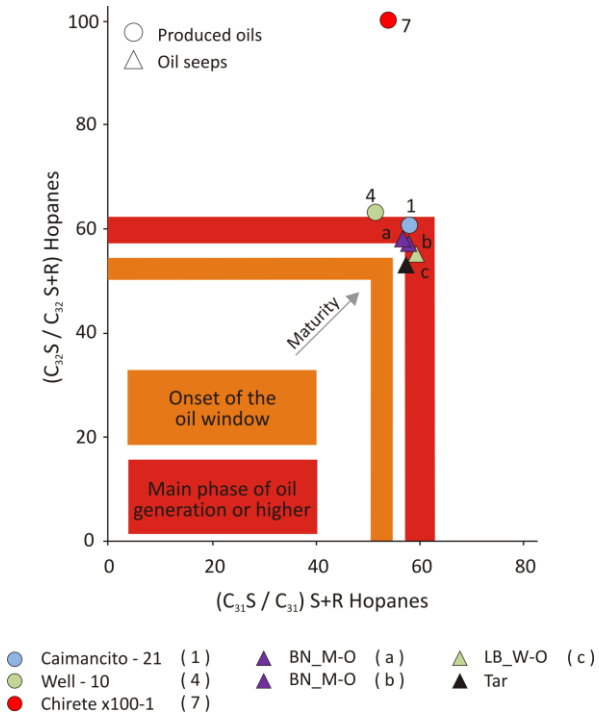

Fig. 5.13. Hopane isomerization based on (S)/(S+R) isomer ratio in produced oil samples from the Lomas de Olmedo sub-basin and oil seep samples collected in the Tres Cruces and the Lomas de Olmedo sub-basins. Produced oil samples and oil seep samples have experienced thermal conditions related to the main phase of oil generation. Limits of the thermal maturity zones after Peters et al. (2005a).

Hopane isomerization has already reached equilibrium in the conversion of (R) to (S) isomers in the produced oils of Caimancito-21 (sample #1) and Well-10 (sample #4) from the Martinez del Tineo oil field. The same conditions can be observed for the oil seep samples of Barro Negro (samples a, b), the water-oil mixture of the Laguna de la Brea (sample c), and the tar (Fig. 5.13). Based on hopane isomerization, these samples (except the produced oil of Chirete x100-1) have experienced thermal conditions related to the main phase of oil generation. In the produced oil of Chirete x100-1 (7), biodegradation could be responsible for the depletion of the (R) isomer of the C_{32} hopane, consequently leading to the interpretation of its higher conversion into the (S) isomer. However, this process is probably not the cause, because such behavior is not observed for the C_{31} hopane. The absence of gammacerane in this sample does not support hypersalinity (which causes water-column stratification) as a factor for (S) isomer enrichment. The contrasting interpretation based on C_{31} and C_{32} hopane isomerization is likely due to the original composition of the organic matter.

Sterane isomerization can provide additional support for the thermal maturity assessment in produced oils and oil seep samples that were analyzed in this study (Fig. 5.14). However, C_{29} steranes were not detected in the produced oil of Chirete x100-1, Well-11, and Río Pescado. In the fresh oil seep, only the C_{29} ααα (S) sterane was detected. In produced oils and oil seep samples the C_{29} sterane conversion from the (R) the (S) isomer configuration reaches values between ≈49-65 % while the conversion from (αα) to (ββ) reaches values between ≈60-80% (Fig. 5.14). The C_{29} sterane (R)-to-(S)-conversion has reached equilibrium in the sample Caimancito-21 (#1) and it is close to this condition in the samples from Caimancito-30 (#3), Well-10 (#4), and Well-18 (#5). The S/(S+R) ratio in samples from Caimancito-23 (sample #2) and the oil seep samples (except the tar) is higher than the equilibrium ratio (Fig. 5.14).

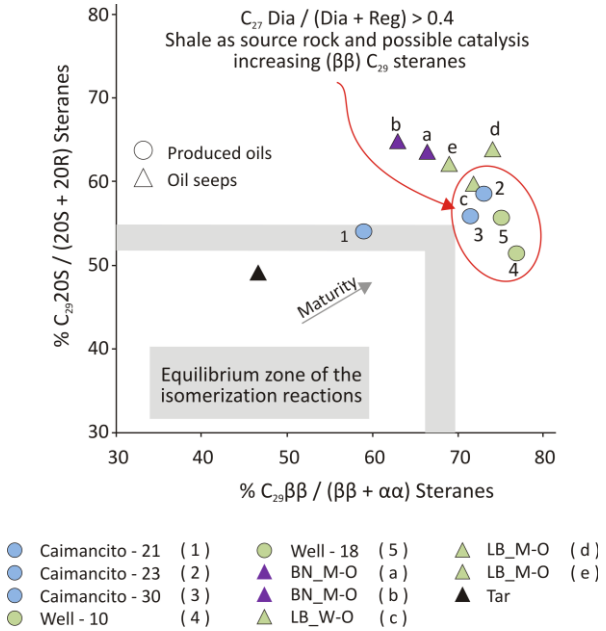

Fig. 5.14. Sterane isomerization based on ratios of (ββ) to (αα) steranes and (S) to (R) C_{29} steranes in produced oil samples from the Lomas de Olmedo sub-basin and oil seeps samples collected in the Tres Cruces and Lomas de Olmedo sub-basins. Except for the produced oil of Caimancito-21 (#1) and the tar oil seep, the rest of the samples are out of the equilibrium zone. Therefore, except for the tar sample, all produced oils and oil seep samples are mature at least within the peak of the oil window or higher. The thermal maturity of the tar sample is below the peak-oil window. (After Grantham, 1986; Seifert and Moldowan, 1986).

The percentage of the conversion from (αα) to (ββ) is lower than the equilibrium ratio in the sample of Caimancito-21 (sample #1), and the oil seep samples (b) and tar (Fig. 5.14). This isomerization has reached the equilibrium in oil seep samples (a) and (e). Higher percentages above the equilibrium are observed in samples from the Martinez del Tineo oil field (samples 4 & 5), Caimancito-23 (#2), -30 (#3) and the oil seep samples (c) and (d). In produced oil and oil seep samples (Fig. 5.14) (except tar), the isomerization from (R) to (S) C_{29} steranes suggests that they are mature, at least in the peak-oil window. In the same figure, the (αα) to (ββ) isomerization suggests the same, except for oil seep samples of Barro Negro (a, b), the tar sample and the Caimancito-21 samples. These samples were likely generated at thermal conditions between the onset and the peak of the oil window. Those (ββ)/(αα+ββ) ratios that are higher and out of the equilibrium zone indicate the influence of factors other than thermal maturity.

Maturity, however, is not the only controlling factor. Certain isomers may be enriched in the original organic material (Moldowan et al., 1992). Higher amounts of (S) and (ββ) are related to hypersaline environments (Ten Haven et al., 1986). Biodegradation preferentially eliminates (R) isomers (Rullkötter and Wendisch, 1982). Mineral catalysis increases the amount of (S) and (ββ) isomers (Huang et al., 1990). Produced oils in Fig. 5.14 are not or only slightly biodegraded (Well-10) (section 5.4), therefore, it is not the cause for the depletion of the (R) or (αα) isomers and the corresponding enrichment in (S) and (ββ) isomers.

Gammacerane was detected in samples of Caimancito-30, Well-10, and the oil seep samples (a, b, c). Therefore, hypersalinity could have contributed to the increase in (ββ) sterane isomers in these samples. The oil seep samples are biodegraded, which contributes to the depletion of (αα) and (R) isomers with the consequent relative increase in (ββ) and (S) isomers. In the produced oils with C_{29}

steranes (ββ)/(αα+ββ) ratios higher and beyond equilibrium, the ratio of C_{27} diasteranes/regular steranes is higher than 0.4 (Fig. 5.2), suggesting that they were generated from a shale source rock, in which an increase of the (ββ) isomers can be caused by clay catalysis (Huang et al., 1990). The absence of all or certain hopanes and steranes in the produced oils Well-11, Chirete x100-1, Río Pescado, and the fresh oil seep sample, prevented their maturity assessment. Hopanes are ubiquitously found in oils and extracts (Van Graas, 1990), so presumably, these oils could be more mature than the range for which hopanes and steranes are usually applicable. At thermal maturities higher than 1%Ro, the biomarker quantities are too low due to their thermal degradation that occurs before oil cracking (Moldowan et al., 2015), and measurements of their concentration become inaccurate (Van Graas, 1990).

5.3.2 Maturity assessment based on aromatic hydrocarbons

Additional assessment of the thermal maturity in this set of samples was carried out by using a proportion of aromatic moieties. The relative proportions of phenanthrene (P) and its methylated homologs systematically change with thermal maturity (Radke et al., 1982a, b). These changes were attributable to the alkylation of phenanthrene and structural reorganization of its methylated homologs (methylphenanthrenes, MP) causing the increase of 2-MP and 3-MP at expenses of their homologues with methyl groups located at 1- and 9- positions in the phenanthrene structure (Radke et al., 1982a, b). The methylphenanthrene Index (MPI-1) reflects such changes and is little influenced by kerogen type and provides an estimation of thermal maturity at higher maturities than hopane and sterane isomerization (Radke et al., 1982b).

MPI-1 is calculated as 1.5*(2-MP + 3-MP)/(P + 1-MP + 9-MP), where P is phenanthrene; M, stands for the methyl-group substituents and the number indicates its position in the phenanthrene structure. MPI-1 covers from the early stage of oil generation (≈0.6 %Ro) up to the condensate/wet gas stage. It shows a good positive linear correlation with vitrinite reflectance up to late stage of oil generation (≈1.35 %Ro) with the equation: %Ro=0.60* MPI-1 + 0.37 (Radke et al., 1982b) and shows good negative correlation further up to ≈2 %Ro with the equation: %Ro=-0.6*MPI-1+2.3 (Radke and Welte, 1981). Phenanthrene and its methyl-substituted homologs 1-, 2-, 3-, 9-methylphenanthrenes were detected in all samples of the produced oils in this study (Fig. 5.15). In the oil seep samples, except sample d, those phenanthrenes are absent or occur in low amounts (Fig. 5.15), likely due to their severe biodegradation (section 5.4).

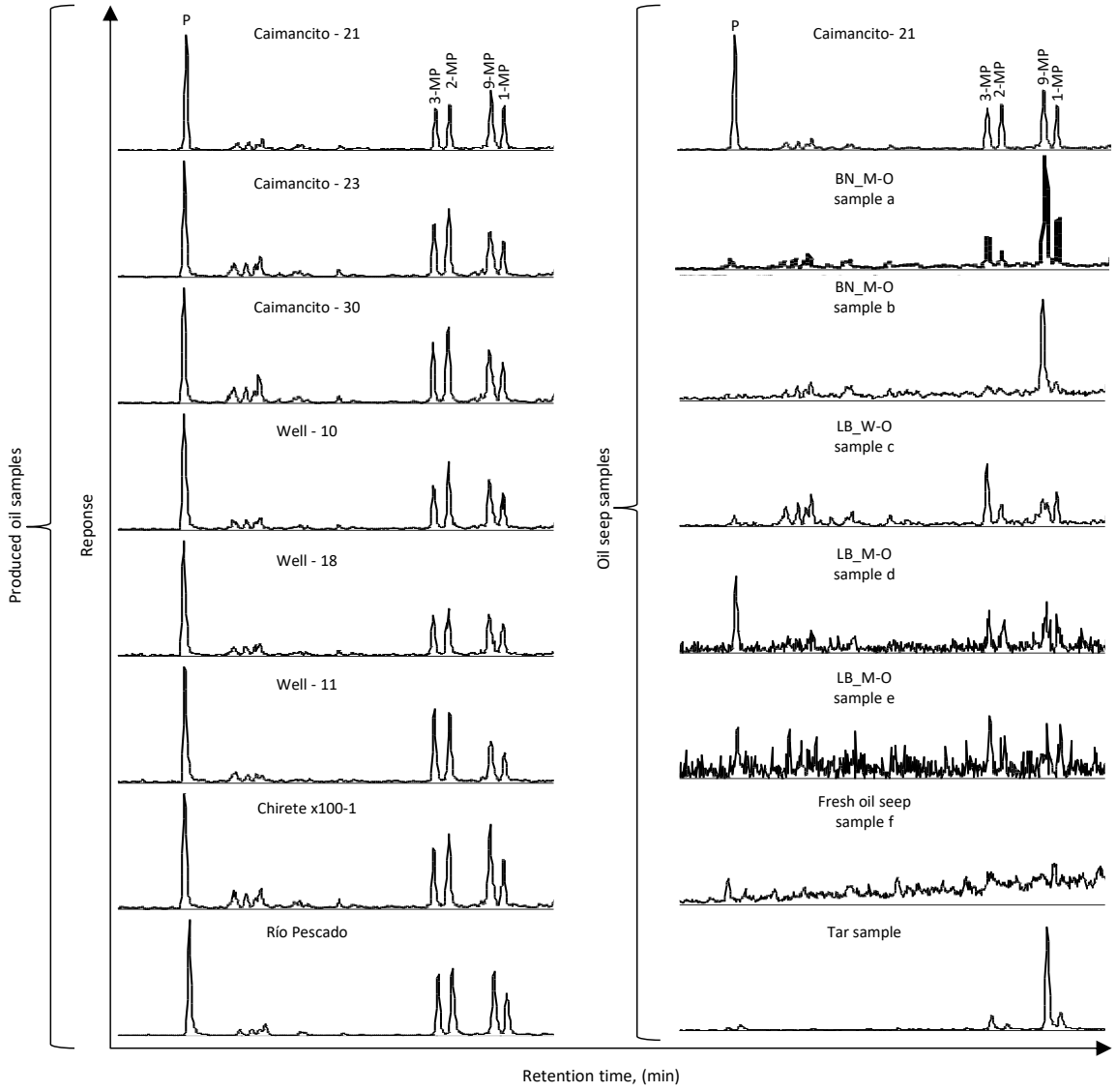

Fig. 5.15. GC-MS chromatograms of phenanthrenes m/z=178+192 in the aromatic fraction of produced oil from the Lomas de Olmedo sub-basin and oil seep samples collected in the Tres Cruces and the Lomas de Olmedo sub-basins. P: phenanthrene, MP: methylphenanthrene with the number indicating the position of the methyl group in the phenanthrene structure.

Table 5.1 displays the MPI-1 values and the corresponding calculated vitrinite reflectance for the produced oils in this study. MPI-1 was calculated only for the oil seep sample (d) because the other samples had too low phenanthrene concentrations. Due to the positive correlation up to 1.35 %Ro and negative correlation at higher thermal maturities ≈2 %Ro, two different vitrinite-reflectance values are obtained from one single MPI-1 value.

Table 5.1. The methylphenanthrene Index (MPI-1) and the calculated maturity expressed as vitrinite reflectance (Ro, %) for the produced oils and one oil seep in this study.

sample type	Sample ID	Short ID	MPI_1	Ro (%) _MPI_1%	Ro (%)_MPI_1%
Produced oils	Caimancito-21	1	0.58	0.72	1.95
	Caimancito-23	2	0.91	0.92	1.75
	Caimancito-30	3	0.97	0.95	1.72
	Well-10	4	0.82	0.86	1.81
	Well-18	5	0.68	0.78	1.89
	Well-11	6	1.12	1.04	1.63
	Chirete x100-1	7	0.81	0.86	1.81
	Río Pescado	8	0.86	0.89	1.78
oil seeps	LB_M-O	d	0.79	0.84	1.83

MPI-1= 1.5 (3-MP + 2-MP)/(P + 9-MP + 1-MP). Where (P) is phenanthrene and (MP), methylphenanthrene. Numbers indicate the position of the methyl group in the phenanthrene structure. After Radke et al., 1982a and Radke et al., 1982b. %RoMPI-1: calculated vitrinite reflectance, %Ro obtained from MPI-1 through the equations: %Ro=0.60*MPI-1 + 0.37 (%Ro value from 0.65 % to 1.35 %) and %Ro= -0.6*MPI-1+2.3 (%Ro value from 1.35 % to 2.00 %). After Radke et al. (1982b) and Radke and Welte (1981).

The thermal maturity of all produced oils and the oil seep sample has been based on the lower, rather than the higher calculated vitrinite-reflectance values. From the hopane and sterane isomerization it is clear that the lower calculated vitrinite-reflectance values reflect better the thermal maturity for produced oils from Caimancito, Martinez del Tineo oil fields (Well-10 & Well-18), Chirete x100-1, and the oil seep sample (d). The thermal maturity of produced oil samples of Well-11 and Río Pescado is not constrained by hopanes and steranes due to the lack of these compounds. However, at higher calculated vitrinite-reflectance values (Table 4.1) severe oil cracking would be expected and there is no evidence for that. Calculated vitrinite-reflectance values indicate that the produced oils of Caimancito-21, Well-10, Well-18, Chirete x100-1, and the oil seep sample (d) have a thermal maturity that corresponds to the main phase of oil generation, an assessment which agrees with the interpretation based on hopane isomerization for the first two samples (Fig. 5.13).

The produced oil from Caimancito-21 has the lowest degree of maturity, which agrees with previous interpretations based on sterane isomerization (Fig. 5.14). Based on the calculated vitrinite reflectance, the other two samples from the Caimancito oil field, i.e., the Caimancito-23 and Caimancito-30 samples, were generated at the peak-oil window. The absence of biomarkers in the produced oil of Río Pescado with lower thermal maturities compared to the produced oils from Caimancito-23 and -30 more likely reflects the nature of its source rock. Compared to the same samples from the Caimancito oil field, the slightly higher thermal maturity of the produced oil from Well-11, partially explains the absence of biomarkers due to their thermal cracking, and additionally suggests it was generated from a source rock initially depleted in these biomarkers.

5.3.3 Maturity assessment based on diamondoids

At thermal maturities higher than ≈1 %Ro, the concentration of biomarkers decreases while the concentration of the more thermally resistant compounds, such as diamondoids (adamantanes,

diamantanes), increases (Dahl et al., 1999; Wei et al., 2006b; Wei et al., 2007; Moldowan et al., 2015). Based on pyrolysis experiments Wei et al. (2006b) suggested that diamondoids are stable at least up to thermal maturities of 4 % vitrinite reflectance. The progressive decrease in biomarkers and the increase in diamondoids is exemplified here by comparing the concentrations of stigmastane and methyldiamantanes (3- + 4-) in the produced oils (Fig. 5.16).

Produced oils from Well-10 and Well-18 (Martinez del Tineo oil field) have relative concentrations of stigmastane of 246 ppm and 23 ppm, respectively. Samples from the Caimancito oil field have a narrow range of relative stigmastane concentration of 138-152 ppm. Produced oils from Chirete x100-1 and Río Pescado lack stigmastane. No steranes were detected in the produced oil from Well-11, using full-scan mass-spectra mode. Some steranes, including stigmastane, could only be detected by using metastable reaction monitoring (GC-MRM-MS) analysis for this sample. Therefore, no sterane peaks were available in TIC (where the sample standard was added) to calculate the stigmastane concentration in this sample.

In the produced oils from the Caimancito and Martinez del Tineo oil field (Well-10 & Well-18), the sum of 3- + 4- methyldiamantanes concentration is between 1.4-2 ppm and 2.8 ppm in the produced oil of Chirete x100-1. Produced oils of Río Pescado and Well-11 display comparatively higher concentrations of 5 and 7 ppm, respectively. The relative higher concentrations in the oil sample of Well-11 are attributable to its slightly higher thermal maturity. If the increase in 3- + 4-methyldiamantanes is only related to increasing thermal maturity, similar or even lower concentrations of these compounds are expected in the produced oil from Río Pescado compared to the produced oil from the Caimancito-23 and Caimancito-30 sites, because of the higher maturity of these last two samples (Table 5.1). This, however, is not the case. In addition, if this sample were generated from the same source rock as the produced oils from the Caimancito oil field, its methyldiamantanes concentrations (3- + 4-) should be located in between that of the produced oil from Caimancito-21 and the produced oil of Caimancito-23/-30. This suggests a relationship with a different source rock for the produced oil of Río Pescado and the produced oil from the Caimancito oil field.

The presence of stigmastane, along with the low concentrations of 3- + 4-methyldiamantanes, indicates that samples from Caimancito and Martinez del Tineo oil fields were not or insignificantly mixed with more-mature oils (Fig. 5.16 and Table 8, appendix). Conversely, the absence of stigmastane in Río Pescado (sample #8) suggests no mixing with less mature oils has occurred. For the produced oil of Well-11 (sample #6), the presence of stigmastane (concentration not calculated), along with the 3- + 4-methyldiamantanes suggests that this sample contains a mixture of two oils with different thermal maturity.

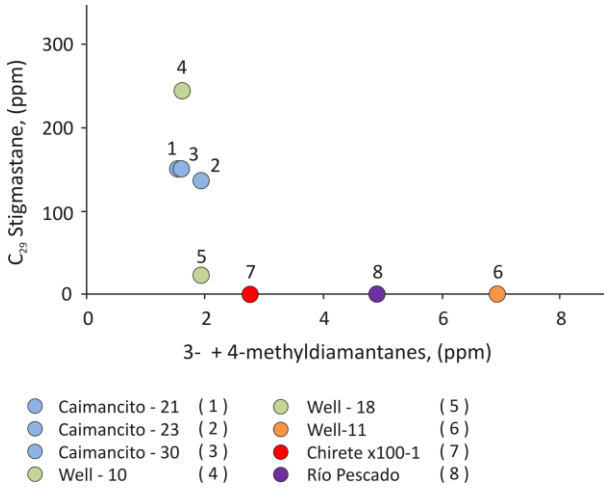

Fig. 5.16. Concentrations of C_{29} stigmastane vs. concentration of 3- + 4-methyldiamantanes in produced oil samples from the Lomas de Olmedo sub-basin. The higher concentrations of 3- + 4-methyldiamantanes in the produced oil of Well-11 from the Ramos X11 oil field (sample #6) are due to its higher thermal maturity as indicated by MPI-1 (Table 5.1). The less mature samples of the Caimancito, Martinez del Tineo (Well-10 & Well-18) and Chirete x100-1 have relative lower concentrations of these compounds. In comparison with the produced oil of Caimancito-23 and Caimancito-30, the lower mature sample from the Río Pescado well has higher methyldiamantanes (3- + 4-) concentrations. This indicates for this sample that the amount of these compounds is not due to thermal maturity only and suggests a different source rock. In the produced oil of Well-11, C_{29} stigmastane was detected, but could not be measured (see text). It was plotted as zero. Adapted from Moldowan et al. (2015).

The ratio between (1- + 2-methyladamantanes)/(3- + 4-methyldiamantanes) is source dependent and remains relatively constant during maturation and oil cracking (Moldowan et al., 2015). This ratio in the produced oils analyzed in this study plots along a trend line, which suggests they were generated from source rocks with similar organofacies and not necessarily the same source rock (Fig. 5.17). Produced oils from the Caimancito oil field and Well-10 plot together with the produced oils of Chirete X-11-1 and Well-18 close together and in the lower left of the diagram (Fig. 5.17), which corresponds to the lower concentrations of methyladamantanes (1- + 2-) and methyldiamantanes (3- + 4-). Produced oils from Río Pescado and Well-11 plot separately in the upper right of the diagram (Fig. 5.17), corresponding to the higher concentrations of these compounds.

The relatively higher maturity explains the higher adamantane and diamantane concentration in the produced oil of Well-11. The produced oil of Río Pescado has a higher adamantanes concentration than the more mature produced oil from the Caimancito-23 and -30 wells. This suggests that these samples from the Caimancito oil field and the produced oil from Río Pescado well were generated from a different source rock. It is inferred that a similar/same source rock that generated the sample from Río Pescado well generated the produced oil from Well-11 at higher maturities. This agrees with the information from the providers of those samples who indicated they were sourced from the Devonian Los Monos Fm.

Compared to the established ratio for the sample set, the deviation in the (3- + 4-methyldiamantanes)/(1- + 2-methyladamantanes) ratio for Chirete x100-1 produced oil (sample #7) is likely due to evaporative fractionation. Methyladamantanes (1- + 2-) are more susceptible to be removed in the gas phase due to evaporative fractionation than methyldiamantanes (3- + 4-), which produces an oil enriched in the latter compounds (Moldowan et al., 2015). The oil seep samples lack methyladamantanes (1- + 2-) and therefore, are not shown in Fig. 5.17. Both of the mud-oil mixture samples (d & e) and the fresh oil seep sample also lack 3- + 4-methyldiamantanes. The rest of the oil seep samples have 3- + 4-methyldiamantanes concentrations between 0.7-3 ppm (Table 8, appendix).

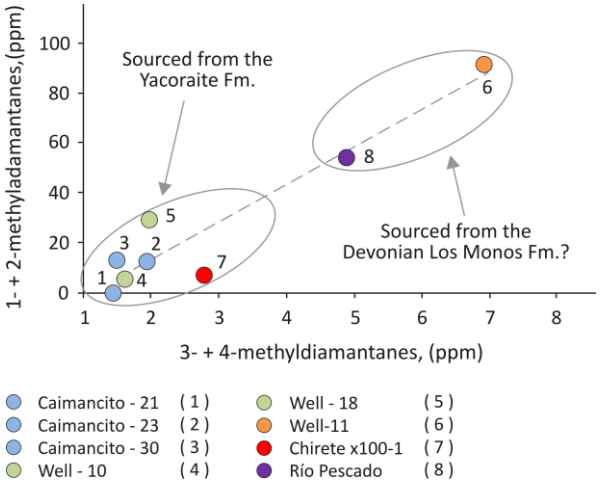

Fig. 5.17. Concentrations of methyladamantanes (1- + 2-) vs. methyldiamantanes (3- + 4-) in produced oil samples from the Lomas de Olmedo sub-basin. Produced oil are split in two main groups, which may be related to their different source rocks. The produced oil of Well-11 and Río Pescado were sourced from the Devonian Los Monos Fm. according to the providers. This explains why the produced oil of Río Pescado (#8) has higher concentrations of methyladamantanes and methyldiamantanes even though according to MPI it is less mature than samples of Caimancito-23 and Caimancito-30 (Table 5.1). The highest concentrations of these compounds in the produced oil of Well-11 is due to its highest thermal maturity. The deviation Chirete x100-1 from the trend line is possible due to evaporative fractionation of its oil. Modified from Moldowan et al. (2015).

In samples of the Yacoraite Fm. from the Pozo Escondido well in the Lomas de Olmedo sub-basin, hydrocarbons in fluid inclusions were trapped at temperatures in the range from 121-137 °C (Cesaretti et al., 2000). If those hydrocarbons were trapped immediately after having been generated, the temperature at which they were generated and the temperature at which they were trapped in fluid inclusions are approximately the same. In this study, using the temperature range of the hydrocarbon-bearing fluid inclusions, the thermal maturity of the Yacoraite Fm. was calculated to be in the range between 0.8-1 %Ro, applying the Barker and Pawlewicz (1994) formula:

V-calc. $=e^{(T*0.0124)-1.68}$, where

V-calc. is calculated vitrinite reflectance (%), and T is paleotemperature (°C).

Although Cesaretti et al. (2000) did not report kerogen type, here it is assumed that the Type II-III kerogen reported by Hernández et al. (2008) represents the general composition in the sub-basin and therefore in samples from Pozo Escondido. The calculated maturity of the Yacoraite Fm. (vitrinite reflectance values between 0.8-1 %Ro), represents the peak of the oil generation for Type II and III kerogens (Tissot and Welte, 1984). This indicates that oils trapped in fluid inclusions were probably generated at the peak of the oil window. These conditions of thermal stress agree with the maturity of the produced oils from Caimancito-23, Caimancito-30, Well-10, and Chirete x100-1 (Table 5.1).

5.4 Biodegradation of produced oils and oil seep samples

Depending on their carbon skeletons and functionality, organic compounds display differences in their resistance to biodegradation and some are therefore selectively removed from produced oils and oil seep samples (Seifert et al., 1984; Wenger et al., 2002). The resistance to biodegradation increases in the order n-alkanes <phenanthrene and dibenzothiophene <regular steranes <C_{30}-C_{35} hopanes <tricyclic terpanes (Wenger et al., 2002). Diamondoids, compounds that are not biomarkers but are increasingly generated during thermal maturity, are more resistant to biodegradation than most biomarkers. Adamantanes and diamantanes are part of the group of diamondoids. While the concentration of adamantanes decreases with the degree of biodegradation of three to six, diamantanes

are resistant to a degree of biodegradation of eight (Zhibing et al., 2007). The alkyl substitution in the adamantane structure also affects its resistance to biodegradation. Methyladamantanes (1- + 2-) are more resistant to biodegradation than adamantane. Therefore, the ratio of methylated adamantanes to adamantane increases with advancing biodegradation (Grice et al., 2000).

5.4.1 Biodegradation in produced oils

Assessments of the extent of biodegradation based on selected geochemical ratios and compound abundances are summarized in Table 5.2.

Table 5.2. Some parameters used to determine the extent of biodegradation in produced oils and oil seep samples.

Type of sample	Sample ID	Short ID	n-C_{17} (mg/g oil)	n-C_{18} (mg/g oil)	Pri (mg/g oil)	Phy (mg/g oil)	Pri/n-C_{17}	Phy/n-C_{18}	DBT (mg/g oil)	Phen. (mg/g oil)	DBT / Phen.	Biodegradation rank
Produced oil	Caimancito-21	1	1.4	1.5	0.9	0.6	0.66	0.4	1.3	31.1	0.0	0
	Caimancito-23	2	12.4	11.4	5.9	4.1	0.48	0.36	2.4	104.8	0.0	0
	Caimancito-30	3	1.4	1.0	0.7	0.4	0.46	0.36	2.2	80.1	0.0	0
	Well-10	4	8.2	9.0	2.1	1.9	0.26	0.21	1.8	42.4	0.0	1
	Well-18	5	19.8	16.4	5.9	4.0	0.3	0.24	1.6	39.0	0.0	0
	Well-11	6	10.5	8.3	1.3	0.4	0.12	0.05	NI	49.0	0.0	0
	Chirete x100-1	7	24.0	21.1	6.7	4.1	0.28	0.19	5.3	55.5	0.1	1-2
	Río Pescado	8	13.2	11.9	1.0	0.6	0.07	0.05	3.4	132.5	0.0	0
Oil seep	BN_M-O	a	NI	NI	NI	NI	NC	NC	0.8	3.3	0.0	4-5
	BN_M-O	b	NI	NI	NI	NI	NC	NC	0.4	0.8	0.5	5
	LB_W-O	c	0.2	0.0	0.4	0.3	NC	NC	2.1	1.5	1.4	4-5
	LB_M-O	d	NI	NI	NI	NI	NC	NC	0.2	1.0	0.2	4-5
	LB_M-O	e	NI	NI	NI	NI	NC	NC	0.9	2.2	0.4	5
	Fresh oil	f	0.0	0.0	NI	NI	NC	NC	NI	NI	NC	5
	M-O	Tar	NI	NI	NI	NI	NC	NC	NI	0.2	0.0	5

Abundance: Pri: pristane; Phy: phytane; DBT: dibenzothiophene; Phen: phenanthrene. NI: not identified. NC: ratio not calculated due to the absence of isoprenoids. Biodegradation rank: based on the compiled biodegradation scale after Wenger et al. (2002).

Produced oils from the Caimancito oil field, Río Pescado, and Well-11 (Ramos X-11 oil field), because they contain a high abundance of low-molecular weight paraffins, do not exhibit any signs of biodegradation (Fig. 5.18). In the Martinez del Tineo oil field, the presence of petroleum with signs of biodegradation has been indicated (Disalvo et al., 2002). In this study the produced oils from Well-10 and Well-18 are from the Martinez del Tineo oil field. The sample from Well-10 shows slight biodegradation as indicated by depletion of lighter hydrocarbons (<n-C_{10}), while the sample of Well-18 does not. The produced oil from Chirete x 100-1 is slightly to moderately biodegraded, as indicated by the absence of alkanes lighter than n-C_{10} (Fig. 5.18).

The produced oils are either unbiodegraded or only slightly biodegraded. Therefore, this is not the cause for the total or partial absence of biomarkers as explained below in the context of DBT, regular steranes, hopanes and tricyclic terpanes:

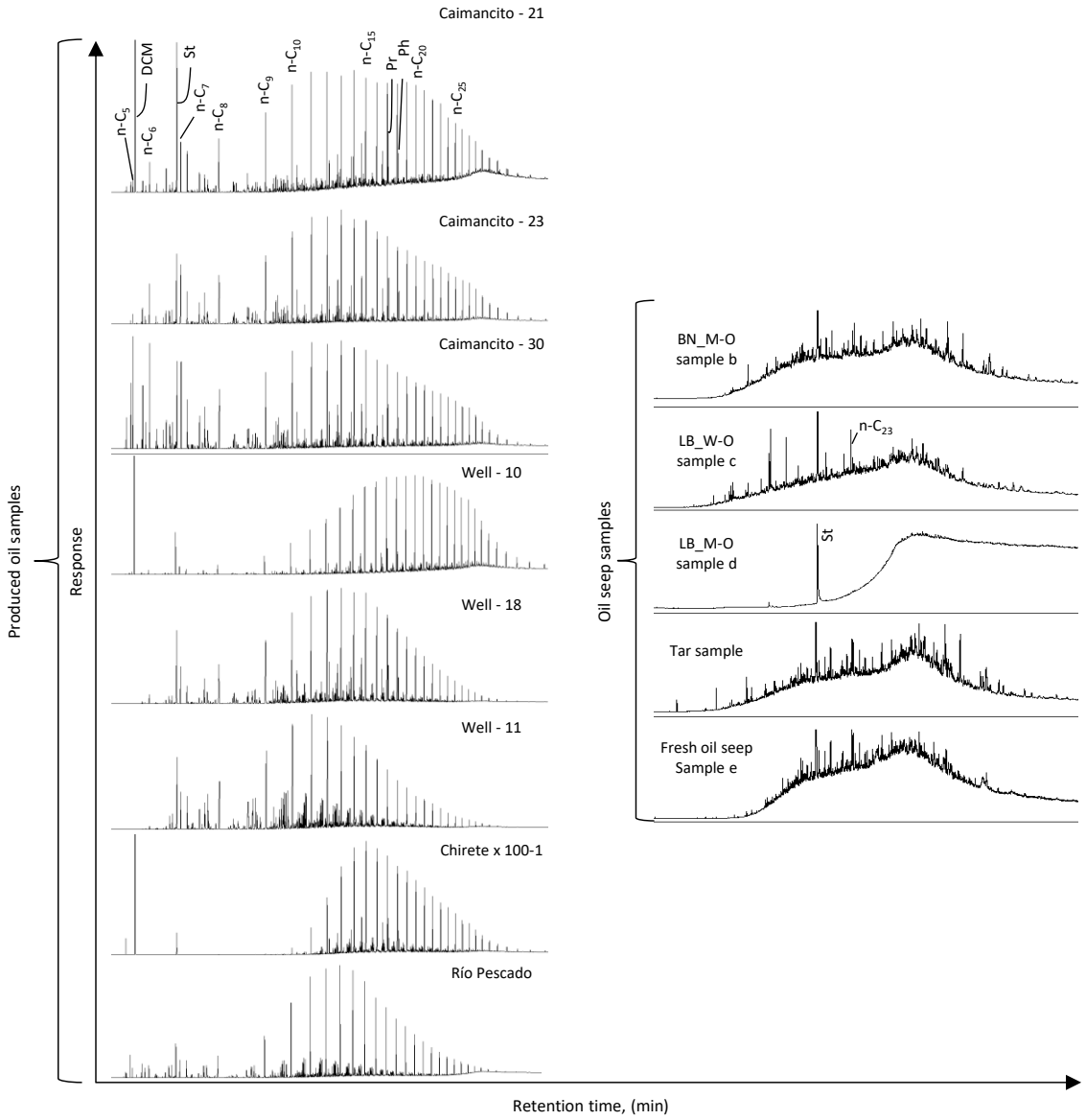

Fig. 5.18. GC-FID chromatograms of produced oils from the Lomas de Olmedo sub-basin and representative oil seep samples collected in the Tres Cruces and the Lomas de Olmedo sub-basins. The produced oils are not or slightly biodegraded (Well-10, Chirete x100-1). The rising baseline in the chromatograms of the oil seep samples (b, c, d, tar, and f) indicates that heavy biodegradation. Whole oil chromatography results are shown for produced oils. Chromatograms of the aliphatic fraction are shown for oil seep samples. St: standard (compound of known concentration). For produced oils, 2,2,4 trimethyl isopentane was added as standard. For oil seep samples, the standard was 5-α-androstan.

Dibenzothiophene (DBT) and phenanthrene (P):

Higher abundances of phenanthrene compared to dibenzothiophene could be detected for most of the produced oil samples (Table 7, appendix), which is reflected by low DBT/P ratios with values between 0.02-0.1. In the produced oil of Well-11 (sample #6) DBT was not detected, only phenanthrene. According to n-alkanes <n-C_{10} content, this sample does not show effects of biodegradation. Depletion of DBT starts at a moderate biodegradation level (Wenger et al., 2002). Therefore, the lack of this compound in the analyzed sample is probably not due to biodegradation but may reflect the lack of incorporation of sulfur into the organic matter from which this sample was originally generated.

Regular steranes:

The full range of steranes was detected in the produced oils of the Caimancito and Martinez del Tineo oil fields (Well-10 & Well-18). Steranes could not be detected in the Río Pescado sample, but to some extent in the produced oils of Well-11 and Chirete x100-1. Depletion of regular steranes starts at heavy biodegradation levels, where the complete elimination of n-alkanes is expected (Wenger et al., 2002). Given the presence of n-alkanes in produced oil samples lacking steranes, heavy biodegradation is ruled out as the cause of their absence. In the produced oil from Well-11 the thermal maturity (1.04 %Ro, Table 5.1) is likely responsible for the absence of some steranes. This is not the case for samples from Chirete x100-1 and Río Pescado with lower thermal maturities of 0.86%Ro and 0.89%Ro, respectively (Table 5.1). The absence of steranes in those samples is probably due to the original composition of their source rock.

Hopanes and tricyclic terpanes:

The full range from trisnorneohopane (27TS) to αβC_{35}S hopane was detected in the produced oil from Caimancito-21, partially detected in the samples of Well-10 and Chirete x100-1, and not detected in the rest of the produced oils (See hopanes distribution Fig. 5.3). Tricyclic terpanes are completely absent in the produced oils of Well-11 and Río Pescado, and significant amounts of tricyclic terpanes were detected in the rest of the samples. The full range of tricyclic terpanes was only detected in the samples from Caimancito-21 and Caimancito-23 (See distribution of tricyclic terpanes Fig. 5.6).

The depletion of hopanes and tricyclic terpanes occurs at severe biodegradation levels (Wenger et al., 2002). Given the presence of n-alkanes in produced oil samples that lack hopanes, heavy biodegradation is ruled out as the cause of their absence.

Terpanes and hopanes are commonly found in oils and extracts (Van Graas, 1990), and their absence in the produced oil Well-11 is probably related to higher thermal maturity. The absence of these biomarkers in the range of less mature produced oils is probably related to the absence of their precursors in the original organic matter composition.

5.4.2 Biodegradation in oil seep samples

Heavy biodegradation is observed in the oil seep samples according to gas chromatography of the aliphatic fraction (Fig. 5.18). This is shown by the rise of the baseline of the chromatograms (Killops and All-Juboori, 1990). The absence of isoprenoids in all of the samples suggests at least a level of 4 on the biodegradation scale (Wenger et al., 2002). Complete removal of hopanes and steranes indicates a severe degree of biodegradation (rank 7). Since hopanes were detected in all oil seep samples (Fig. 5.3), the degree of biodegradation is constrained to values < 7. Table 5.2 summarizes the parameters used to estimate the extent of biodegradation.

The tar, the two oil seep/mud mixtures (sample b from Barro Negro, sample e from Laguna de la Brea), and the fresh oil seep sample lack methyl-, dimethyl- and trimethylnaphthalenes (Fig. 5.19). Since these compounds are eliminated at a biodegradation level of 5, their absence and the absence of

isoprenoids (Fig. 5.18) indicates a biodegradation rank of 5. The rest of the oil seep samples have some trimethylnaphthalenes (Fig. 5.19), indicating a biodegradation rank lower than 5 (Fisher et al., 1998). The absence of isoprenoids in these oil seep samples (Fig. 5.18 and Table 7, appendix) suggests a biodegradation rank of at least 4 (Fisher et al., 1998; Wenger et al., 2002). Therefore, a biodegradation rank between 4 and 5 is interpreted for these samples.

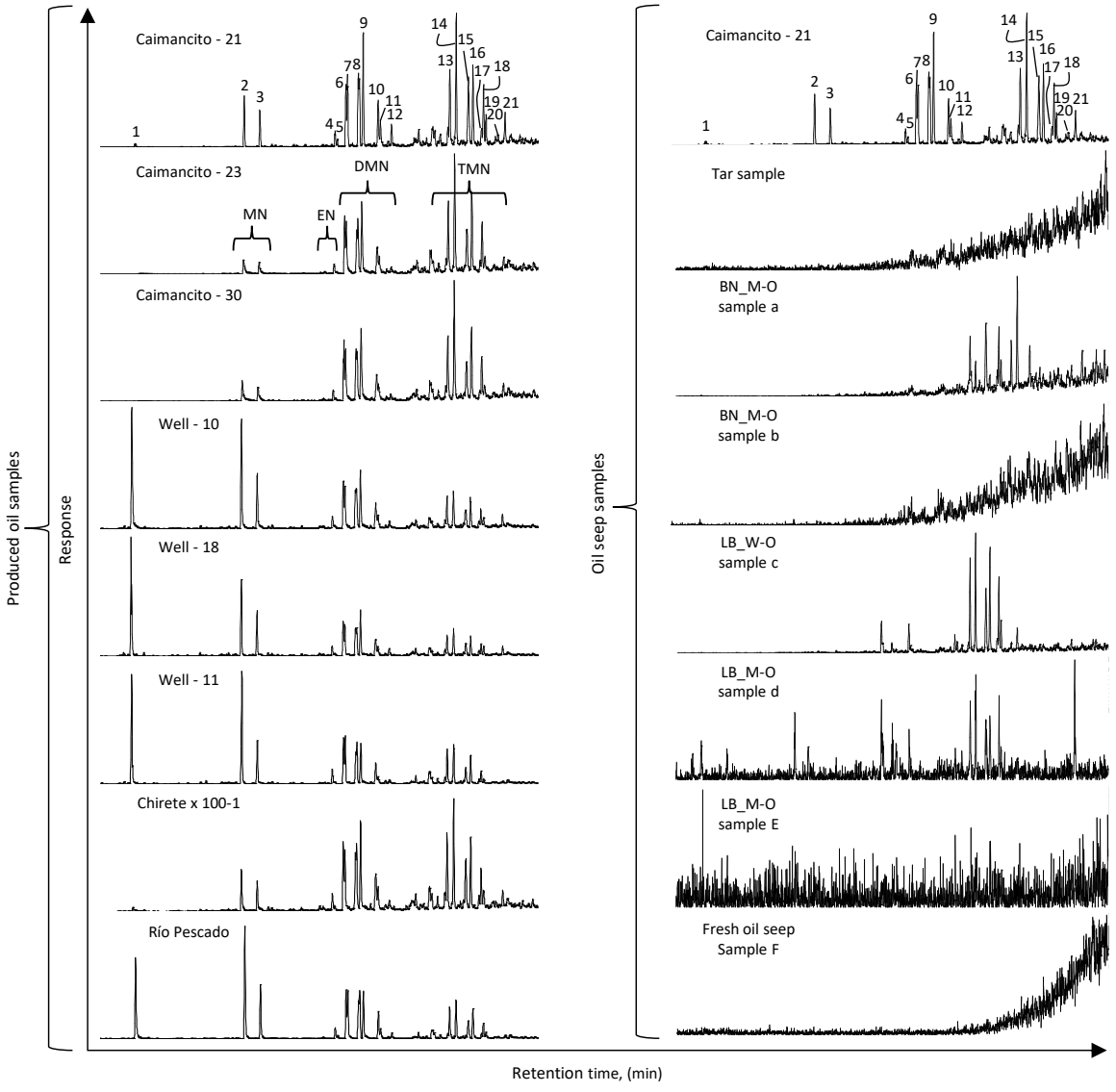

Fig. 5.19. GC-MS chromatograms of naphthalenes m/z = 128, 142, 156, 170 for produced oils from the Lomas de Olmedo sub-basin and representative oil seep samples collected in the Tres Cruces and the Lomas de Olmedo sub-basins. Naphthalenes are present in the produced oils because they are either not or slightly/moderately biodegraded. Oil seep samples are heavily biodegraded. A level of 5 in the biodegradation rank (Fisher et al. 1998; Wenger et al., 2002) is interpreted for oil-seep samples: tar, b, e, f based on the absence of methylnaphthalenes. Because some methylnaphthalenes are present in the rest of the oil seep samples, a biodegradation rank between 4-5 is inferred for them. Compound classes: MN: methylnaphthalenes, DMN: dimethylnaphthalenes, TMN: trimethylnaphthalenes, EN: ethylnaphthalene. Specific compounds: 1: Naphthalene; 2: 2-MN; 3: 1-MN; 4: 2-EN; 5: 1-EN; 6: 2,6-DMN; 7: 2,7-DMN; 8: 1,3-DMN+1,7-DMN; 9: 1,6-DMN; 10: 1,4-DMN+2,3-DMN; 11: 1,5-DMN; 12: 1,2-DMN; 13: 1,3,7-TMN; 14: 1,3,6- TMN; 15: 1,3,5-TMN + 1,4,6-TMN; 16: 2,3,6-TMN; 17: 1,2,7-TMN; 18: 1,6,7-TMN; 19: 1,2,6-TMN; 20: 1,2,4-TMN; 21: 1,2,5-TMN.

5.5 Source rock - oil correlations

In this study the source rock-oil correlations are based on the character of the depositional environment, the kerogen type, and the age of the Yacoraite Fm. in the Tres Cruces and the Metán-Alemanía sub-basins compared to the produced oils from the Lomas de Olmedo sub-basin and the oil seep samples collected in the Lomas de Olmedo and the Tres Cruces sub-basins. No source-rock samples were available from the Lomas de Olmedo sub-basin. Therefore, the source rock-oil correlations assume similar depositional environments and kerogen type in the Lomas de Olmedo sub-basin as described for the Yacoraite Fm. in the Tres Cruces and the Metán-Alemanía sub-basins in the literature and in this study.

5.5.1 Correlations based on depositional environment and kerogen type

The Yacoraite Fm. was deposited in anoxic, low-sulphur marine and lacustrine environments (see chapter 3 for detailed discussion). In these environments, predominantly Type II kerogen composed of alginites was the main organic material deposited, along with higher terrestrial input in the western sector of the Metán-Alemanía and the south sector of the Tres Cruces sub-basin. The source rock of the produced oil of Well-11 was deposited in a suboxic environment according to a (Pr/Pr+Ph) ratio ≈0.7. The rest of the produced oil samples were sourced from rocks deposited under anoxic conditions with a (Pr/Pr+Ph) lower than 0.65 (Fig. 5.2). According to the degree of transformation of C_{27} steranes to diasteranes (Fig. 5.2), the produced oil of Caimancito-21 was generated from a carbonate source rock, while the rest of these produced oils (except Río Pescado) and the oil seep samples (except the fresh oil) were sourced from a shale source rock. These data were not available for the produced oil of Río Pescado and the fresh oil seep. Therefore, no further inferences could be drawn for these samples.

Shales and marls of the Yacoraite Fm. were deposited in anoxic environments (Fig. 3.12 & 3.14) and have a variable carbonate content of up to 70 % (Fig. 3.1 and Table 2, appendix) in the Tres Cruces and the Metán-Alemanía sub-basins. If this formation was also deposited in the Lomas de Olmedo sub-basin under similar conditions, it could be the source rock for these produced oils. Suboxic or anoxic conditions may develop as a result of increasing salinity, thereby decreasing oxygen solubility (Lange et al., 1972). Gammacerane is an indicator for water-column stratification, commonly caused by hypersalinity.

The presence of gammacerane in the produced oils from Caimancito-21, -30, and Well-10 with Gammacerane Indexes in the range from 3 to 6 (Fig. 5.4), suggests a hypersaline depositional environment. The absence of this biomarker may suggest a freshwater depositional environment for the source rocks of the produced oils of Caimancito-23, Well-11 (Ramos X-11 oil field), Well-18, Río Pescado and Chirete x100-1. A removal of gammacerane by biodegradation in these samples is not a likely scenario, because the complete elimination of this biomarker occurs only at severe levels of biodegradation (Wenger et al., 2002), for which none of the wells shows any evidence (cf. section 5.4).

A depositional environment in which water-column stratification occurred is also interpreted for the oil seep samples of Barro Negro, tar, fresh oil seep, and the water-oil mixture of Laguna de la Brea with Gammacerane indexes between 3 and 5. Gammacerane was not detected in any of mud-oil mixtures from Laguna de la Brea, probably due to their severe biodegradation (see discussion in section 5.4.2). Gammacerane indices between 2 and 6 were measured in the Yacoraite Fm. rock samples (inset in Fig. 3.16). The Yacoraite Fm. was deposited in shallow water depths, where the development of a temperature gradient would have been unlikely and therefore, the water-column stratification more likely developed as a consequence of hypersalinity conditions. The range of Gammacerane indices in the Yacoraite Fm. samples is similar to that calculated for the produced oils of Caimancito-21, Caimancito-30, and Well-10, and the gammacerane-bearing oil seep samples. The absence of gammacerane in rock samples #35, #41 & #51 and the source rock of the rest of the produced oils and oil seep samples suggests their deposition in a freshwater environment.

According to the C_{26}/C_{25} tricyclic terpane ratio of 2 and the $C_{31}R/C_{30}$ hopane ratio of 0.2 (Fig. 5.7), the source rock of Caimancito-21 was deposited in a lacustrine environment. In contrast, marine environments were interpreted for Well-10, and Chirete x100-1 samples with $C_{31}R/C_{30}$ hopane ratios of 0.39 and 0.35, respectively. Due to the partial (produced oils of Well-18, Caimancito-23 and Caimancito-30) or total lack of the diagnostic tricyclic terpanes and hopanes (produced oil of Well-11, Río Pescado and oil seep samples d & e), interpretations concerning the depositional environments for these samples remain inconclusive or could not be carried out at all. No further differentiation of the depositional environment was possible for Barro Negro (sample b), and the tar oil seep samples, because their characteristics plot in the overlapping zone of marine and lacustrine environments. Their tricyclic terpane (C_{26}/C_{25}) ratios are from 1 to 1.5 and hopane ratios ($C_{31}R/C_{30}$) are between 0.22 and 0.31 (Fig. 5.7). The other Barro Negro oil seep (sample a), the LB_W-O (sample c), and the fresh oil seep samples were sourced from a rock deposited in a lacustrine setting.

The Yacoraite Fm. was initially deposited in a predominantly marine environment as indicated by the predominance of n-C_{15} hydrocarbons and a $C_{31}R/C_{30}$ hopane ratio higher than 0.25. With $C_{31}R/C_{30}$ hopane and C_{26}/C_{25} tricyclic terpane ratios between 1 and 1.4, some of the samples from the Yacoraite Fm. plot within the overlapping zone of marine and lacustrine environments, and therefore, no clear distinction between these depositional settings is possible. Lacustrine environments, however, had developed during deposition of the middle and upper sections of the formation, as indicated by the increasing predominance of n-C_{6-14} hydrocarbons (Fig. 3.10) which is also supported by an increasing C_{26}/C_{25} tricyclic terpane ratio of 1-2 (Fig. 3.16). In addition, the similar hydrocarbon chain-length distribution of pyrolysates of the tar sample compared to the ones of nearby outcropping shales (samples #39 & #40, Fig. 3.10c) indicate common or similar organic precursors suggesting a genetic relation.

The source rock of the produced oils and oil seep samples in this study was deposited in an environment with low sulphur content as indicated by dibenzothiophene (DBT)/phenanthrene (P) ratios lower than 1 (Fig. 5.5). DBT/P ratios lower than one were also calculated for the extracts of the

Yacoraite Fm., regardless of their geographic or stratigraphic location (Fig. 3.15). Additional support for the source rock-oil correlation is provided by the C_{31}-C_{35} homohopane distribution (Picha and Peters, 1998), which depends on their precursors (e.g., higher plants, bacteria) (Peters and Moldowan, 1991). The majority of homohopanes were detected in samples of Caimancito-21, Well-10, and Chirete x100-1, and the Barro Negro oil seep samples (a & b, Fig 5.3). The rest of the produced oils and oil seep samples lack homohopanes. The Yacoraite Fm. has organofacies with similar homohopane distributions to those of the produced oils and oil seep samples (a & b, Fig. 5.20).

Similar homohopane distribution between the produced oil of Chirete x100-1 and samples #34 and #47 suggests this produced oil was sourced from organofacies like those found in the lower and upper sections of the Yacoraite Fm. The produced oil of Caimancito-21 and the two Barro Negro oil seep samples were generated from similar organofacies as those found in the upper (sample #37) and the lower sections of the Yacoraite Fm. (sample #29). The intermediate homohopane distribution between the produced oils from Camancito-21 and Chirete x100-1 suggest that the sample from Well-10 is an oil mixture from different organofacies. This indicates the occurrence of similar organofacies with similar homohopane distributions in the Yacoraite Fm. in the Lomas de Olmedo sub-basin compared to those found in the same formation in the Tres Cruces and the Metán-Alemanía sub-basins.

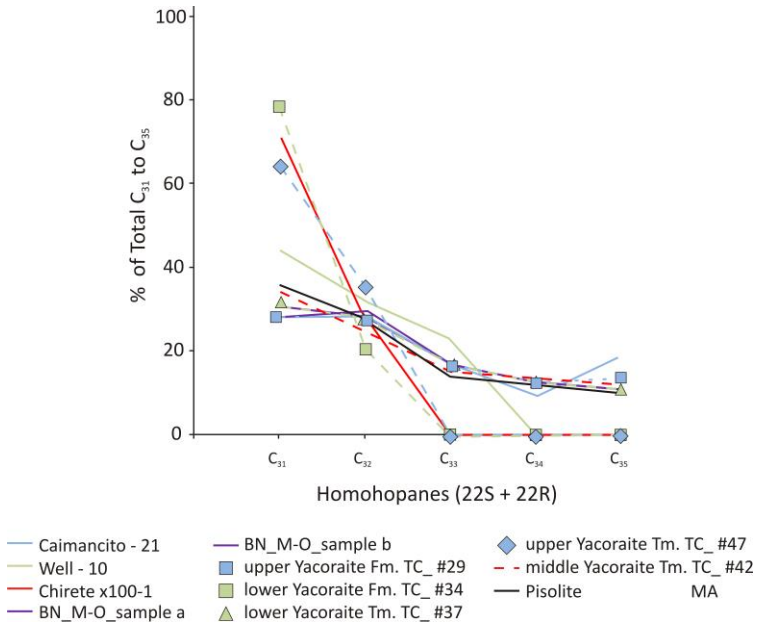

Fig. 5.20. Relative amount of C_{31} to C_{35} homohopane (%) in rock extracts of the Yacoraite Fm. from the Tres Cruces and Metán-Alemanía sub-basins, produced oils from the Lomas de Olmedo sub-basin and oil seep samples collected in the Tres Cruces and the Lomas de Olmedo sub-basins. Similar homohopane distributions suggest genetic correlations. Caimancito-21, Chirete x100-1, and the Barro Negro oil seep samples were generated from similar organofacies compared to those retrieved from the upper and the lower sections of the Yacoraite Fm. The produced oil of Well-10 is interpreted here as a mixture of oils generated from different organofacies, e.g., similar to material from the lower and upper sections of the Yacoraite Fm. in the Tres Cruces sub-basin. The rest of the produced oils and oil seep samples is not shown due to partial or total lack of homohopanes (Fig. 5.3). BN_M-O: Barro Negro mud-oil mixture. TC: The Tres Cruces sub-basin. MA: The Metán-Alemanía sub-basin. After Picha and Peters (1998).

Pr/n-C_{17} ratios between 0.07 and 0.66, Ph/n-C_{18} ratios between 0.05 and 0.4 (Fig. 5.10), Ethyladamantane Index <80%, and dimethyldiamantane index-1 <75% (Fig. 5.11) indicate that all produced oil samples were sourced from a source rock mainly composed of Type II kerogen with low land-plant input. C_{29}/C_{27} regular sterane ratios lower than 2 (Fig. 5.9) also support minor land-plant input for the source rock of the produced oils of Caimancito and Martinez del Tineo (Well-10 & Well-18) oil fields, Chirete x100-1, and the oil seep samples (except the tar and the fresh oil seep). A higher

land-plant contribution was interpreted for the Well-11 sample based on the presence of C_{29} steranes and the absence of C_{27} regular steranes. No steranes were detected in the Río Pescado sample and the fresh oil seep. The rock samples from the Yacoraite Fm. are mainly composed of alginites (see examples in Fig. 3.11) with some contribution of terrigenous plants. This is supported by Pr/n-C_{17} ratios between 0.43-4.89 and Ph/n-C_{18} ratios between 0.31-3.98 (Fig. 3.12).

5.5.2 Correlations based on diamantanes

The advantage of diamantanes for the current study is that they were detected in all oil samples, from which representative samples are shown in Fig. 5.21. Concentrations of different diamantanes in the aliphatic fraction are between 1-5 ppm in the analyzed produced oils (Fig. 5.22a). Higher concentrations were measured in the produced oils of Río Pescado and Well-11 (Ramos X-11 oil field).

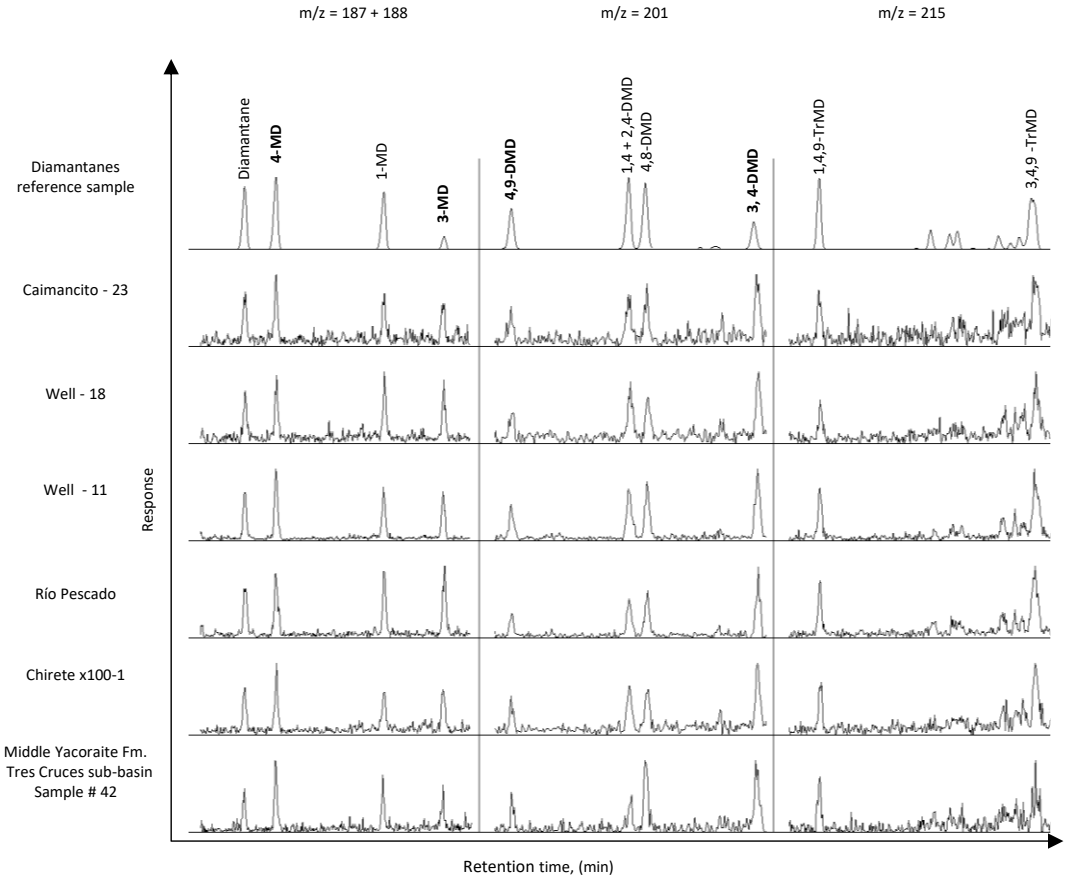

Fig. 5.21. GC-MS chromatograms of diamantanes in the saturate fraction of produced oils from the Lomas de Olmedo sub-basin and one representative rock extract of the Yacoraite Fm. from the Tres Cruces sub-basin. MD: methyldiamantanes; DMD: dimethyldiamantanes; TrMD: trimethyldiamantanes. The number indicate the position of the methyl group in the diamantane structure. The sum of 3- + 4-methyldiamantanes concentrations (Moldowan et al, 2015) and its ratio to 4,9-dimethyldiamantane (Schulz et al., 2001) have been suggested to be source-rock dependent and potentially useful in source rock - oil correlations. MD: dimethyldiamantanes, TrMD: Trimethyldiamantanes.

Diamantanes were also detected in several oil seep samples in this study: two samples (a & b) collected at Barro Negro, the tar sample, and the water/oil mixture collected at Laguna de la Brea (sample c, Fig. 5.22a). The diamantane concentrations in the tar sample and the water-oil mixture (sample c) have diamantane concentrations between 2-4 ppm being in the range of most produced oils of this study. The two Barro Negro oil seep samples a & b are variable, ranging between 1.6-11.5 ppm in the aliphatic fraction have higher diamantane concentrations lying between the diamantane concentration of the produced oils of Río Pescado and Well-11 (Ramos X-11 oil field) (Fig 5.22a).

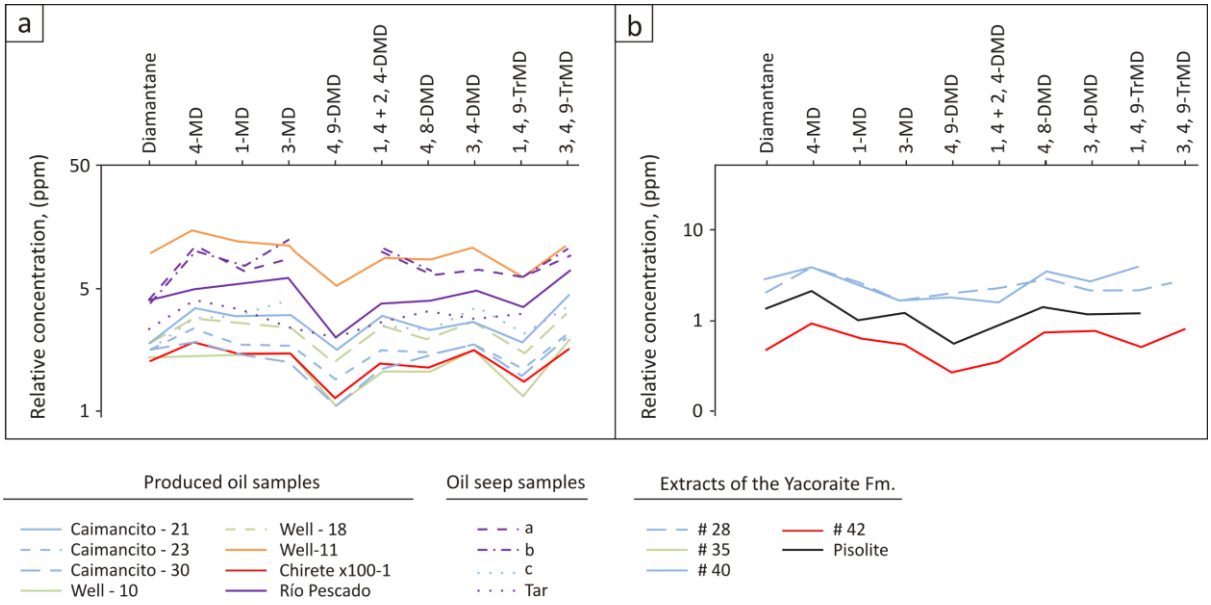

Fig. 5.22. Distributions of the relative concentrations of diamantanes (referred to 5-α-androstan, 5 mg/ml) in the aliphatic fraction of (a) produced oils from the Lomas de Olmedo sub-basin, oil seep samples collected in the Tres Cruces and the Lomas de Olmedo sub-basins and (b) source-rock extracts from the Yacoraite Fm. The Well-10 and Well-18 samples come from the Martinez del Tineo oil field, the Well-11 sample is from the Ramos X-11 oil field. Similar distributions of the relative concentrations of diamantanes between the lower and middle sections of the Yacoraite Fm. extracts and produced oil samples suggest they were generated from similar source rocks. MD: methyldiamantanes, DMD: dimethyldiamantanes TrMD: Trimethyldiamantanes. Pis: pisolite.

Diamantanes were detected in most source-rock extract samples (Table 8, appendix) from the Yacoraite Fm. in its different stratigraphic levels (Fig. 5.21 & 5.22b), e.g., the lower (sample #35), the middle (sample #42 & pisolite), and the upper sections of this unit (sample #28 & sample #40). They differ in up to one order of magnitude, with sample #42 having the lowest concentration between 0.5-1.0 ppm, and sample #35 having the highest diamantanes concentration in the range of 2.5-14 ppm (Fig. 5.22b). Similar distributions of the relative concentrations of diamantanes are observed in extracts of the lower (sample #35) and the middle (sample #40) sections of the Yacoraite Fm. (Fig. 5.22b) and the produced oils and oil seep samples of this study (Fig. 5.22a). For example, relatively high concentrations of 4-MD exist in all produced oils, with the exceptions of Río Pescado and Well-10 samples; relatively high concentrations of 3-MD occur in all samples, except for the sample from Well-18; relatively low concentrations of 4,9-DMD and relative high concentrations of 4,8-DMD and 3,4-DMD exist in all produced oils.

The concentrations of diamantanes were found to depend on source rock (Moldowan et al., 2015) and kerogen type (Schulz et al., 2001) from which the oils were originated. These characteristics thus potentially support source rock-oil correlations. The distributions of the relative concentrations of diamantanes suggests similarities between the Yacoraite Fm. in the different sectors of the Tres Cruces and the Metán-Alemanía sub-basins and the source rock of the produced oils in the Lomas de Olmedo sub-basin. The deposition of the main source rocks in the NW Argentina, i.e., both the Devonian Los Monos Fm. and the Cretaceous Yacoraite Fm. occurred under marine conditions (Marquillas et al., 2005; di Pasquo, 2007; Cruz et al., 2008; Troth et al., 2011; di Pasquo et al., 2015) with the development and predominance of lacustrine settings at the end of deposition of the Yacoraite Fm. (cf. section 3.2.6). Source rock-oil correlations based on the characterization of depositional environment are insufficient to differentiate oils generated from these formations because similar environments were developed during their deposition.

5.5.3 Oil-source correlations in the context of source-rock age

The significant difference in age between the Devonian Los Monos Fm. and the Cretaceous Yacoraite Fm. can be used for source-rock correlations based on age-related biomarkers. As explained in section 5.2 in the context of the age of petroleum, the presence of oleanane (indicative of angiosperm plants) would corroborate a Middle Jurassic or younger age of the oils and rock extracts (Moldowan et al., 1994b). However, this biomarker was not detected in the produced oils and oil seep samples analyzed in this study (Fig. 5.3). Their source rock could be older than Middle Jurassic, or it is younger but lacked the oleanane precursor. Alternatively, thermal maturation or biodegradation could destroy and eliminate this biomarker.

Biodegradation can be excluded to explain the absence of this biomarker in the oil seep samples. Oleanane is resistant to levels of biodegradation comparable to those in the oil seep samples of this study (Wenger et al., 2002), interpreted to reach a rank of 4-5 (cf. section 5.4.2). The produced oils are either unaffected or only slightly biodegraded (e.g., Well-10, Chirete x100-1). The absence of oleanane in the sample of Well-11 can result from its thermal maturity of ≈1 %Ro, but a source rock older than Middle Jurassic or a younger one lacking an oleanane precursor cannot be excluded as possible explanation.

The absence of oleanane in extracts of the Yacoraite Fm. from the Tres Cruces and the Metán-Alemanía sub-basins (Fig. 5.23), demonstrates the existence of source rocks younger than Middle Jurassic in NW Argentina that lack oleanane. Therefore, similar oleanane-depleted organofacies of the Yacoraite Fm. may occur in the Lomas de Olmedo sub-basin as source rocks of oleanane-depleted produced oils. During the deposition of the Devonian Los Monos Fm., angiosperms did not yet exist.

Therefore, the oils generated from this formation would not contain oleanane. The mere absence of oleanane is not a decisive criterion to distinguish between oils originating from these two formations.

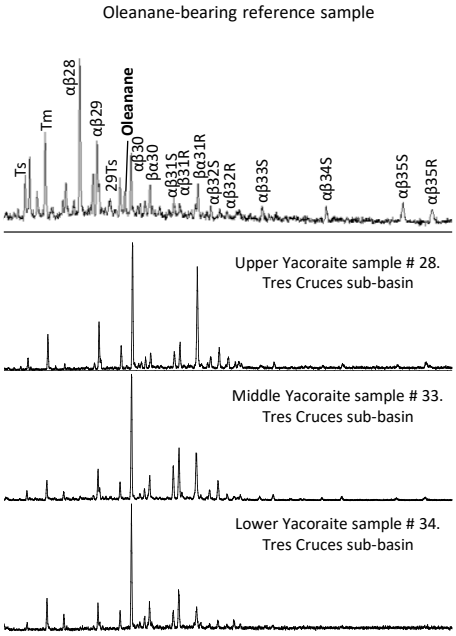

Fig. 5.23. GC-MS chromatograms of hopanes distribution m/z=191 in the saturate fraction of rock extracts of representative samples of the Yacoraite Fm. in the Tres Cruces sub-basin. The homohopane series from $\alpha\beta C_{29}$ to $\alpha\beta C_{32}R$ is observed. The age-related biomarker oleanane was not detected in any of the rock extracts. This biomarker is indicative of the input of angiosperms, which already existed by the time when the Yacoraite Fm. was deposited (Maastrichtian-Danian); therefore, the absence of this biomarker indicates that the Yacoraite Fm. lacks the oleanane precursor. Due to its absence, this biomarker cannot be used to constrain the age of produced oil or oil seep samples.

The ratio of C_{28}/C_{29} steranes is age-dependent (Grantham and Wakefield, 1988). This ratio is lower than 0.5 in oils that are older than Early Paleozoic. It increases up to ≈0.7 for Late Paleozoic to Early Jurassic oils. In oils sourced from Late Jurassic to Miocene, the ratio is higher than ≈0.7.

With C_{28}/C_{29} steranes between 0.9 and 1.8, the produced oils of the Caimancito oil field, Well-10 from the Martinez del Tineo oil field, and the oil seep samples (except sample d) were generated from a Cretaceous source rock (Fig. 5.12a). The tar sample with a C_{28}/C_{29} steranes ratio of 0.74 plots within the limit between the Late Jurassic and Early Cretaceous. The sedimentation in the Salta rift basin started during Early Cretaceous. Therefore, this is a more likely age for the source rock of the tar sample. The absence of C_{28}, C_{29} steranes prevented an age determination for the produced oils of Well-18, Well-11, Chirete x100-1, Río Pescado and the oil seep (d). The C_{28}/C_{29} steranes ratio of 0.9 in sample #42 of the middle section of the Yacoraite Fm. in the Tres Cruces sub-basin (Fig. 5.12a), suggests it was deposited during the Cretaceous (Grantham and Wakefield, 1988; Peters et al., 2008). This agrees with the stratigraphic position of the middle section and strongly indicates its genetic correlation with the Cretaceous oils discussed above.

5.6 Oil-oil correlations

5.6.1 Correlations based on diamondoids

Unlike biomarkers, adamantanes were detected in all produced oils (Fig. 5.24), and therefore, are potentially suitable for correlation purposes. As in the case of diamantanes (Fig. 5.22a), similar distributions of relative concentrations of adamantanes (0.32-250 ppm) are observed in the aliphatic fraction of all produced oils (Fig. 5.25).

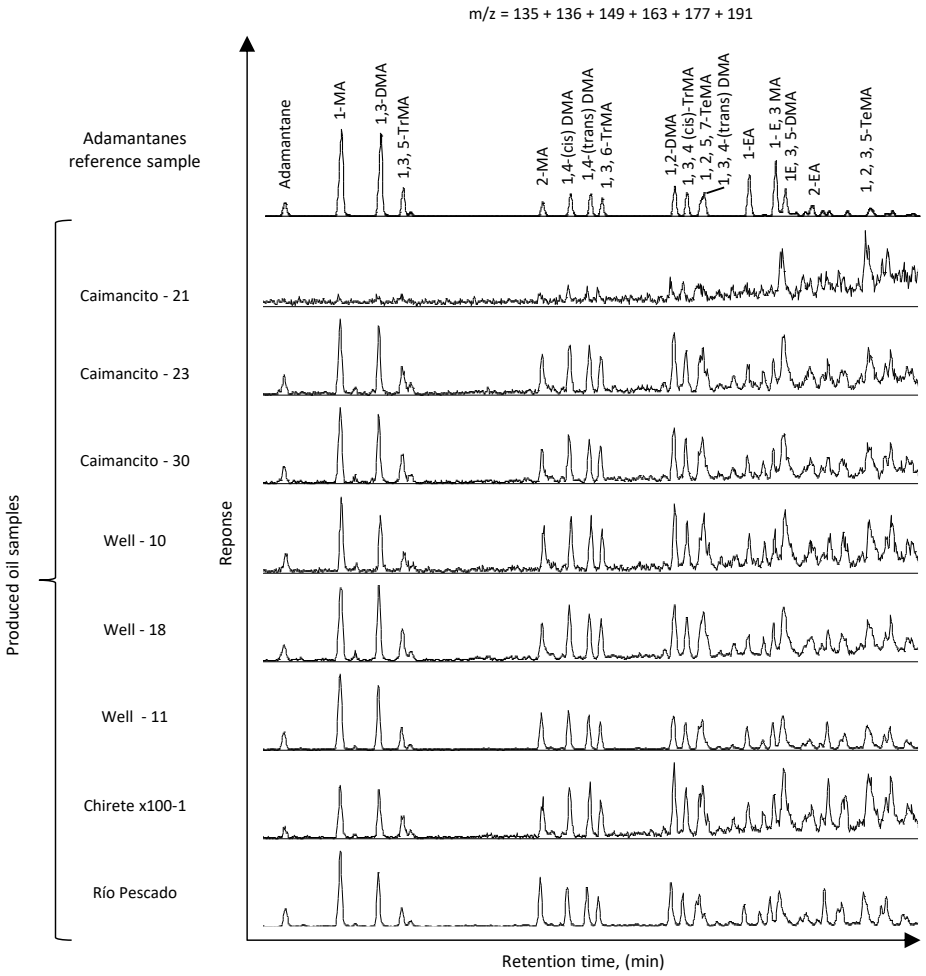

Fig. 5.24. GC-MS chromatograms of adamantanes in the saturate fraction of produced oils from the Lomas de Olmedo sub-basin. Adamantanes were detected in all the produced oils but were not detected in any extracts of the Yacoraite Fm. The proportion of 2-ethyladamantane to 1-ethyladamantane has been found to correlate with kerogen type (Schulz et al., 2001). MA: methyladamantanes, DMA: dimethyladamantanes, TrMA: trimethyladamantanes, EA: ethyladamantanes. Numbers indicate the position of the methyl group in the adamantane structure. Cis y trans refer to geometric isomerism. Cis: functional groups are on the same side of the carbon chain; trans: the functional groups are on opposing sides of the carbon chain.

The proportion of the sum of concentrations of methyladamantanes (1- + 2-) vs. the sum of methyldiamantanes (3- + 4-) suggest that produced oils in this study were generated from similar source rocks (Fig. 5.17). The ethyladamantane index and the dimethyldiamantane index-1 suggest that all oils were generated from a Type II kerogen source rock (Fig. 5.11). Different concentrations of methyldiamantanes (3- + 4-) vs. methyladamantanes (1- + 2-), allowed a discrimination of the oils, presumably as a consequence of their different source rocks (Fig. 5.17). One group comprised of the produced oils of Caimancito, the Martinez del Tineo oil fields, and Chirete x100-1 are characterized by the Yacoraite Fm. as the source rock. The other group, which is composed of the produced oils of Well-11 and Río Pescado, is likely sourced from the Devonian Los Monos Fm.

The presence of stigmastane along with 3- + 4-methyldiamantanes (Fig. 5.16) suggests, that the oil sample of Well-11 may represent a mixture of oils with different degrees of maturity. Additionally,

based on C_{28}/C_{29} sterane ratio (Fig. 5.12), the produced oils from Caimancito-21, Caimancito-23, and Well-10 (from the Martinez del Tineo oil field) have been generated by a Cretaceous source rock.

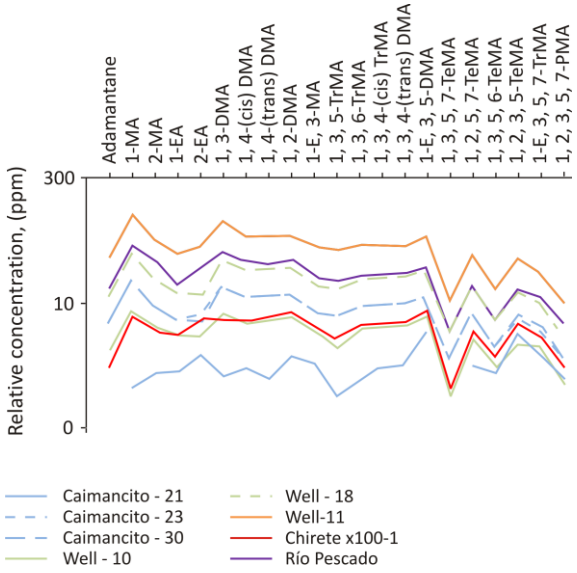

Fig. 5.25. Distribution of relative concentrations of adamantanes (referred to 5-α-androstan, 5 mg/ml) in the aliphatic fraction of produced oil samples from the Lomas de Olmedo sub-basin. Similar distributions of relative concentrations of adamantanes confirm their usefulness as an oil-oil correlation parameter. MA: methyladamantanes, DMA: dimethyladamantanes, TrMA: trimethyladamantanes, EA: ethyladamantanes. Cis y trans refer to geometric isomerism; Cis: functional groups are on the same side of the carbon chain; trans: the functional groups are on opposing sides of the carbon chain.

The similar distribution pattern of relative adamantane concentrations (Fig. 5.25) suggest that these produced oils originate from a similar source rock in agreement with the previous interpretation based on diamantanes (Fig. 5.22a). The different distribution of relative concentrations of adamantanes in the sample from Caimancito-21 compared to the other produced oils is likely due to differences in the depositional environment of its source rock as indicated by different $C_{31}R/C_{30}$ hopane, C_{26}/C_{25} tricyclic terpane ratios (Fig. 5.7), and $\alpha\alpha\alpha C_{27}R$-$C_{29}R$ steranes (Fig. 5.8).

5.6.2 Correlations based on light hydrocarbons

In addition to adamantanes, specific oil-oil correlation parameters based on light hydrocarbons (e.g., Halpern, 1995) were calculated for all samples, except Chirete x100-1, which lacks these hydrocarbons. These parameters are labeled consecutively from C1 to C5 corresponding to the relative proportion of each of the following compounds to the sum of all five): 2,2-dimethylpentane, 2,3-dimethylpentane, 2,4-dimethylpentane, 3,3-dimethylpentane, 3-ethylpentane. The distribution of these five parameters for samples of the produced oils of Martinez del Tineo (Well-10 & Well-18) and the Caimancito oil field (Caimancito-23 & Caimancito-30) are quite similar (Fig. 5.26), which suggests they were generated from the same or very similar source rocks (Halpern, 1995), i.e., the Yacoraite Fm., as discussed in section 5.5.

The oil sample from Well-11 appears to a mixture of oils; while its C1 to C4 parameters correlate well with Caimancito-23, Caimancito-30, and the two samples from the Martinez del Tineo oil fields (Well-10 & Well-18), its C5 parameter correlates with Caimancito-21. Alternatively, this may also suggest that Caimancito-21 represents a mixture of oils in which one of the components is similar to the sample of Well-11. The presence of stigmastane and comparatively higher methyldiamantane (3-

+ 4-) concentrations (Fig. 5.16) suggests that the sample of Well-11 is composed of two oils with different thermal maturity.

The component with the higher degree of maturity may have been derived from the Devonian Monos Fm. Stigmastane was also detected in the Caimancito-21 sample, but its comparatively lower concentrations of methyldiamantanes (3- + 4-) do not support mixtures of oils with different thermal maturity. Light hydrocarbon parameters from C1 to C5 in the produced oil of Río Pescado are very different from those calculated for the other produced oils. This indicates that it is not related to any of them, which agrees with previous interpretations in this study, based on concentrations of methyldiamantanes (3- + 4-) and stigmastane (see section 5.3.3, Fig. 5.16).

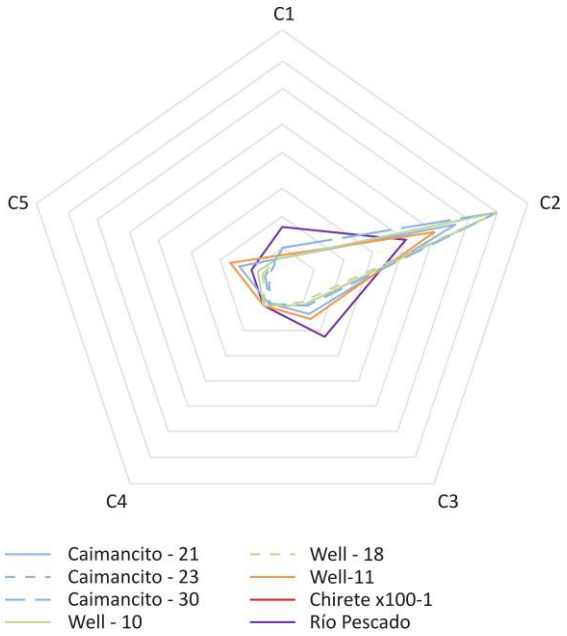

Fig. 5.26. Light hydrocarbon star diagrams for produced oil samples from the Lomas de Olmedo sub-basin. C1 to C5 are calculated parameters corresponding to the ratios of each of the following compounds to the sum of all: 2,2-dimethylpentane; 2,3-dimethylpentane; 2,4-dimethylpentane; 3,3-dimethylpentane; 3-ethylpentane after Halpern (1995). Good correlations are observed in samples of Caimancito-23, Caimancito-30, Well-10, and Well-18. A good correlation is observed between the produced oils from Caimancito-21 and Well-11 (from Ramos X-11 oil field). Based on the results of the shown ratios the sample of Río Pescado does not correlate with any of the other produced oils See text for discussion and implications.

5.7 Conclusions

5.7.1 Characteristics of the source rock for produced oil and oil seep samples as inferred from source-rock correlations.

Based on DBT/P ratios, the source rocks for the produced oils and oil seep samples were deposited in an environment with low-sulphur availability/incorporation into organic matter. Type II kerogen with some terrigenous plant contribution characterizes the source rock for the produced oils according to C_{29}/C_{27} regular steranes ratios, the predominance of C_{27} and C_{28} over C_{29} steranes, Pr/n-C_{17} and Ph/n-C_{18} ratios. Based on the same steranes parameters, the source rock of the oil seep samples also reflects low terrestrial plant input. It was slightly higher for the source rock of the samples from Caimancito-21 and the tar oil seep, and it is more pronounced for the sample of Well-11. No biomarkers indicative of kerogen type were found in the fresh oil seep. According to C_{28}/C_{29} ratios, oil samples from Caimancito and the Martinez del Tineo (Well-10 & Well-18) oil fields were sourced from a Cretaceous rock for which Pr/(Pr+Ph) ratios indicate deposition under anoxic conditions. C_{27} diasteranes to regular steranes ratio and C_{26}/C_{25} tricyclic terpane ratio indicate that the oil sample of

Caimancito-21 was generated from a lacustrine carbonate source rock. C_{27} diasteranes to regular steranes ratios for the remainder of the analyzed samples indicate their source rock was a shale. The source rock for Well-10 and Chirete x100-1 was deposited in a marine environment as suggested by $C_{31}R/C_{30}$ hopane ratios. The presence of gammacerane indicates that water-column stratification developed during the deposition of the source rock of Caimancito-21, Caimancito-30, and Well-10. The depositional environment was either not clearly distinguished based on C_{26}/C_{25} tricyclic terpanes and $C_{31}R/C_{30}$ hopanes or not defined due to the absence of these biomarkers. In addition, the absence of the C_{28}/C_{29} steranes in the oils from Well-11 and Río Pescado prevented their age assessment.

Based on the age-dependent biomarkers C_{28}/C_{29} steranes, all oil seeps with the exception of sample (d), lacking C_{28}/C_{29} steranes, were sourced from a Cretaceous shale which deposited in a lacustrine environment (samples a, c and the fresh oil seep) according to C_{27} diasteranes to regular steranes and C_{26}/C_{25} tricyclic terpane ratios. For the rest of the samples, the depositional environment was not defined either due to unclear identification of or the absence of C_{26}/C_{25} tricyclic terpanes and $C_{31}R/C_{30}$ hopanes. The presence of gammacerane in the oil seep samples (except for samples d, e), indicates that water-column stratification had developed during the deposition of their source rock.

The oil-source correlations are tentative because no rock samples were available from the Lomas de Olmedo sub-basin from which the analyzed samples of produced oils were retrieved. Therefore, they are based on the inference that a source rock in the Lomas de Olmedo sub-basin exists which has similar characteristics compared to those of the Yacoraite Fm. in the Tres Cruces and the Metán-Alemanía sub-basins. My results combined with published accounts support such an inference (cf. sections 1.6 and 1.7).

The Yacoraite Fm. shares the characteristic of deposition in an environment with low-sulphur incorporation into organic matter and Type II kerogen as the main organic constituent with the source rock of the produced oil and the oil seep samples. A good correlation based on age and depositional environment exists between the samples of the Yacoraite Fm. and the three produced oils of the Caimancito oil field, Well-10, as well as oil seep samples a, b, c, e, tar, and the fresh oil seep. A similar hydrocarbon chain-length distribution of pyrolysates of the tar sample and a shale sample retrieved from the nearby upper Yacoraite Fm. also suggests their genetic relation. A partial correlation based on characteristics of the depositional environment was found between the Yacoraite Fm. and samples of Well-18, Chirete x100-1, and the oil seep (d). Weak correlations between produced oils from Well-11 and Río Pescado and the Yacoraite Fm. suggest they were generated from a different source rock, likely the Los Monos Formation.

Based on the isomerization of hopanes and steranes and the methylphenanthrene index (MPI-1) oil samples from Caimancito-23, Caimancito-30, Well-10, and Chirete x100-1 experienced thermal stress associated with peak-oil window conditions. The thermal maturity of these produced oils agrees with the calculated maturity of the Yacoraite Fm. (0.8-1%Ro) based on entrapment temperatures of fluid inclusions (Cesaretti et al., 2000). The produced oils with lower maturity retrieved from

Caimancito-21 (0.72%Ro) and Well-18 (0.78%Ro) were likely generated from the Yacoraite Fm. during earlier stages of thermal maturity.

Compared to produced oils from Caimancito-23 and -30, the slightly lower mature produced oil from Río Pescado has higher concentrations of methyladamantanes (1- + 2-) and methyldiamantanes (3- + 4-). This suggests that its lack of biomarkers is not due to its thermal maturity, but most likely related to a source rock depleted of these compounds. The same is interpreted for the oil sample of Well-11 that is most mature is this set of samples whose higher maturity would explain the decrease of some biomarkers, but not their near complete absence. This source rock was likely similar or even identical to the source rock of the Río Pescado sample and likely was the Los Monos Fm. Age-based biomarkers suggest that the analyzed oil seep samples were generated from a Cretaceous source rock (except sample d, which lacks C_{28} steranes) most likely the Yacoraite Fm. The higher thermal maturity of the oil seep samples compared to the outcrop samples of the Yacoraite Fm. indicates that this formation is more mature at greater depth.

5.7.2 Biodegradation of produced oils and oil seep samples

The absence of low-molecular hydrocarbon in the Chirete x 100-1 and Well-10 samples suggests they are slightly biodegraded. The rest of the produced oil samples show no signs of biodegradation. Therefore, the absence of biomarkers is probably related to the composition of original material. The oil seep samples are severely biodegraded. This can be the cause for the selective removal of the (S) isomers in hopanes and steranes and (αα) isomers in steranes. Consequently, they may have experienced less thermal stress than they appear to.

5.7.3 Oil - oil correlations

The produced oils share the characteristic of a low-sulphur source rock that is mainly composed of Type II kerogen. Similar distributions of relative concentrations of adamantanes and diamantanes indicate that the produced oils were sourced from rocks with similar organofacies, but not necessarily the same source rock. The genetically most related produced oils according to the light-hydrocarbons star diagrams are the samples from the Martinez del Tineo oil field (Well-10 & Well-18), Caimancito-23, and Caimancito-30. The produced oil from Well-11 is more mature than the produced oil from Caimancito-21, but both correlate well. The sample of Well-11 partially correlates also with the other samples from the Caimancito and Martinez del Tineo oil fields. A mixture of two oils of different levels of thermal maturity is interpreted for the Well-11 sample, based on the presence of stigmastane and higher concentrations of methyldiamantanes (3- + 4-). The sample with a lower degree of maturity may have been generated from the Yacoraite Fm., whereas the more-mature sample may have been sourced by the Devonian Los Monos Fm. The sample from Río Pescado does not correlate with any of the other produced oils suggesting it was generated from the Los Monos Fm.

6. Petroleum generating properties of the Yacoraite Fm.

The primary goal of this chapter is to document how organofacies and thermal maturity control the transformation of organic matter in the Yacoraite Fm. into hydrocarbons. The changing bulk and detailed primary oil composition during maturation, and inferred associated physical properties are also presented.

6.1 Organofacies and primary oil composition

The type of kerogen and its thermal maturity determine the type of petroleum that a source rock generates (as reviewed by Tissot and Welte, 1984; Dembicki, 2009). Algal material of Type I kerogen with high initial H/C and low initial O/C atomic ratios (Tissot et al., 1978), deposited mainly in lacustrine environments, generates paraffinic (Béhar and Vandenbroucke, 1987), waxy oil (Horsfield, 1989; Dembicki, 2009). Type II kerogen deposited in marine environments under reducing conditions has lower H/C and higher O/C atomic ratios (Béhar and Vandenbroucke, 1987) generating mainly naphthenic or aromatic oil (Horsfield, 1989). Type III kerogen derived predominantly from terrestrial plant input and some aquatic organic matter altered by oxidizing conditions has low initial H/C and high initial O/C atomic ratios (Tissot et al., 1978) generating mainly gas (e.g., Tissot et al., 1974; Béhar and Vandenbroucke, 1987) but also some waxy oil (Horsfield, 1989 and references therein). Type IV kerogen is inert and without hydrocarbon-generation potential.

Horsfield (1989) pointed out that the schemes to classify kerogen, e.g., from Rock-Eval pyrolysis, are insufficient to derive information regarding petroleum composition. Earlier, Horsfield (1984) noted that hydrogen deficiency (Type III kerogen) is not unequivocally synonymous with inferior oil potential and that molecular characterization of kerogen is needed to predict petroleum compositions. In nature, associations of different types of organic matter, e.g., higher plants, bacteria, phytoplankton, and zooplankton are mixed in different proportions in the different depositional environments. Therefore, a particular depositional environment is not expected to be uniformly characterized by a single type of organic matter. Higher amounts of higher plant debris are expected to be deposited nearby the river mouth of lacustrine or marine environments. This explains why in lacustrine environments not only the classical Type I kerogen but also Type II and III kerogens are found (Carrol and Bohacs, 2001).

Horsfield (1989) defined petroleum type organofacies based on chain-length distributions from Py-GC that linked kerogen composition to bulk petroleum composition; by following this definition he showed that the facies were independent of elementally based classification schemes. In his study he correlated pyrolysates of well-characterized source rocks with their genetically related petroleum. The rock pyrolysates were split according to their chain-length distribution of total C_1-C_5 resolved pyrolysates, C_6-C_{14} n-alkanes plus n-alk-1-enes, and C_{15+} n-alkanes plus n-alk-1-enes. This correlation established the link between depositional environment, petroleum precursors and composition.

Marine environments are characterized by their richness in n-alkanes and n-alkenes of short to intermediate chain length and define the Paraffinic Oil Low Wax zone (Fig. 6.1). Other marine shales rich in aromatic hydrocarbon, producing significant amounts of hydrocarbons in the gas range and low in wax components define the Paraffinic-Naphthenic-Aromatic Low Wax zone. Pyrolysates of lacustrine environments rich in long-chain n-alk-1-enes and n-alkanes defined the Paraffinic Oil High Wax zone. Pyrolysates of one coal sample representing deltaic environments were used to define the Paraffinic-Naphthenic-Aromatic High Wax zone**.** Pyrolysates of vitrinites and sporinites, representing terrestrial kerogen are characterized by a short length in n-alkyl moieties. Their chain-distribution indicates that they are rich in hydrocarbon in the C_1 to C_5 range, therefore gas-prone, and plot in the apex of gas and condensates region Horsfield (1989).

The classification scheme was further refined by di Primio and Horsfield (1996) by distinguishing high- and low-sulphur varieties of crude oils generated from mainly marine organic matter. The refined concept of organofacies (di Primio and Horsfield, 2006) integrated the characterization of the organic precursors with the prediction of petroleum type generated by thermal maturation. Following Horsfield's (1989) organofacies approach, the bulk composition of the first-formed petroleum that can be generated from the Yacoraite Fm. is discussed here. The Yacoraite Fm. predominantly generates Paraffinic-Naphthenic-Aromatic Low Wax Oil and Paraffinic High Wax Oil both from Type II and II/III kerogens (Rock-Eval). Minor contributions of Paraffinic Low Wax Oil are generated from Type II and II/III kerogens. Type III kerogen generate gas/condensates (Fig. 6.1).

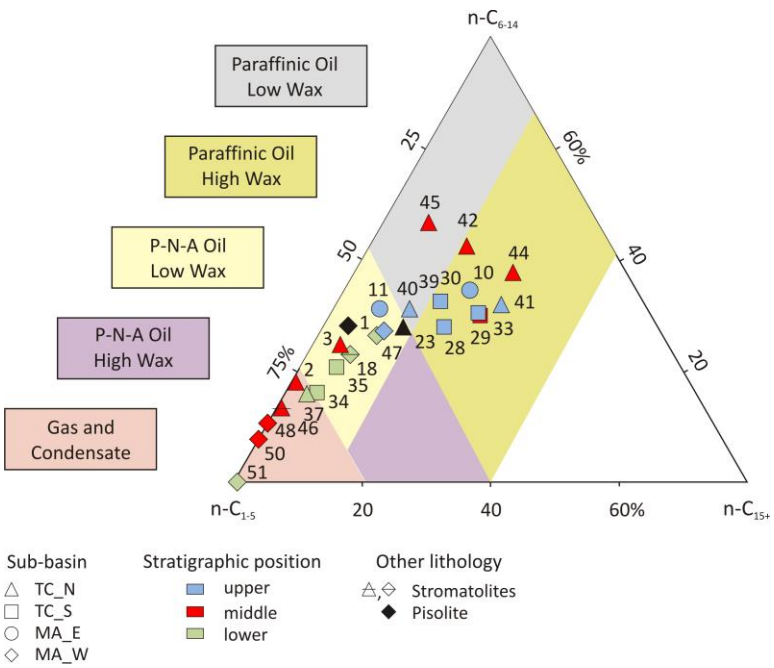

Fig. 6.1. Ternary plot of hydrocarbon chain-length distribution (Py-GC) of total C_1-C_5 resolved pyrolysates, C_6-C_{14} n-alk-1-enes plus n-alkanes, and C_{15+} n-alk-l-enes plus n-alkanes in samples of the Yacoraite Fm. Organofacies of the Yacoraite Fm. predominantly generate the following types of oils: P-N-A Low Wax Oil (Marine), Paraffinic High Wax Oil (Lacustrine), and minor contributions of Paraffinic Low Wax Oil, and Gas/Condensates. (TC) Tres Cruces, (MA) Metán-Alemanía sub-basins. The sectors where samples were collected are north, south (N, S) and east and west (E, W).

Lower Yacoraite Formation

According to the hydrocarbon chain-length distribution, the marine facies deposited in the south sector of the Tres Cruces sub-basin represented by samples #34, #35 & #37 (Fig. 6.1) generate P-N-A

Oil Low Wax. The same types of hydrocarbons are generated by the marine facies in the western sector of the Metán-Alemanía sub-basin represented by stromatolite samples #1 & #18. The same sub-basin registers differences in the Valle del Tonco. Sample #51 generates hydrocarbons in the gas range (C_1-C_5) due to either predominant terrestrial input or, less commonly, radiogenically altered organic matter (Horsfield et al., 1992a; Yang et al., 2018), putting this sample in the left corner apex (Fig. 6.1). This sample is predominantly composed of alginites (Fig. 3.11f), and therefore, a predominant terrestrial input can be ruled out as the cause of its gas-prone character. A higher thermal maturity is an alternative explanation for the predominant gas generation from sample #51. However, the difference in T_{max} between the whole-rock sample (458 °C) and its kerogen concentrate (406 °C) does not support this interpretation and suggests the effect of artefacts during pyrolysis. Section 4.3 addresses the factors affecting the kerogen typing and thermal maturity assessment of this sample.

Middle Yacoraite Formation

In the northern sector of the Tres Cruces sub-basin, marine organofacies of the Yacoraite Fm. generate P-N-A Low Wax Oil (sample #3) and Paraffinic Oil Low Wax (sample #45). The lacustrine organofacies represented by samples #42 & #44 generate Paraffinic Oil High Wax oil as well as sample #33 from the southern sector in the same sub-basin. Stromatolite sample #46 plots in the Gas and Condensate zone with a relatively higher abundance of gas hydrocarbons (C_1-C_5). This does not mean that the stromatolite is composed of terrestrial organic matter, but as explained in section 3.2.1, stromatolites can be composed of mucopolysaccharides of cyanobacteria, whose elemental compositions are similar to terrestrial organic matter. The shale sample #2 is the most gas-prone sample in the Tres Cruces sub-basin. In the western sector of the Metán-Alemanía sub-basin, the middle section of the Yacoraite Fm. (sample #50) becomes more gas-prone. This suggests this sample had comparatively higher terrestrial input as indicated by its Type III kerogen (Fig. 6.1).

Upper Yacoraite Formation

The lacustrine organofacies in the Tres Cruces sub-basin generates Paraffinic Oil with High Wax content. This is observed in the southern sector of this sub-basin represented by samples #23, #28, #29 #30, as well as samples #39 & #41 collected in the northern sector. In this sector, sample #40 plots within the limit of three petroleum compositions, i.e., the Paraffinic Oil Low Wax/ High Wax, and the P-N-A Low Wax Oil. This reflects the development of lacustrine settings that were still under some marine influence. For this time, the transition from marine to lacustrine depositional environments is also inferred for the Metán-Alemanía sub-basin. In the eastern sector, marine organofacies represented by sample #11 generate P-N-A Oil Low Wax. This sample plots close to the borders of the Paraffinic Oil Low Wax zone. The lacustrine organofacies in sample #10 generates oils characterized by long hydrocarbon chains; thus, Paraffinic Oil with High Wax content is expected to be generated.

The tar sample collected in the Tres Cruces sub-basin plots in an intermediate position between the Paraffinic oils, the P-N-A oil with high wax content, and P-N-A oils with low wax content (Fig.

6.1). In addition, the similar hydrocarbon chain-length distribution of pyrolysates of the tar sample compared to the ones of the nearby shales in the field from the upper section of the Yacoraite Fm. (samples #39 & #40) suggests a genetic relation. Genetic relations between asphaltenes and kerogen have been established based on their similar composition and structure, as revealed by Py-GC. This was shown by comparison of a naturally matured sequence from catagenesis up to metagenesis (0.48-1.45%Ro) in samples from the Jurassic Posidonia Shale of Germany, with asphaltenes separated from crude oils and whole-rock pyrolysates of their source rock (Muscio et al., 1991; Lehne et al., 2009). Of special interest is the similar to each other gas to oil ratio of asphaltenes and whole-rock pyrolysates that indicates they have similar chain-length distribution (Horsfield et al., 1993).

In the western sector of the Metán-Alemanía sub-basin, the upper section of the Yacoraite Fm. (sample #48) generates hydrocarbons in the gas range (C_1-C_5). This suggests relatively higher terrigenous input compared to sample #47 representing the marine organofacies from which P-N-A Low Wax Oil can be generated. The transformation of organic matter into hydrocarbons is facilitated by the incorporation of sulphur into the organofacies. This is because C-S bonds require lower activation energy compared to C-C (Schenk et al., 1997) to be broken under thermal stress.

As a consequence, hydrocarbons can be generated at relatively low thermal maturities. 2,5-dimethylthiophene is one alkylthiophene pyrolytic product that represents sulphur moieties in the kerogen structure. It is indicative of labile C-S bonds in the kerogen structure (Orr, 1986; di Primio and Horsfield, 1996), and its amount is proportional to elemental sulphur content (Eglinton et al., 1990). Primary oils generated from the Yacoraite Fm. have a low sulphur content, as indicated by the small proportion of 2,5-dimethylthiophene (Fig. 6.2). This agrees with the analysis of rock extracts shown earlier where dibenzothiophene to phenanthrene ratios lower than 0.4 suggested low sulphur incorporation into organic matter (Fig. 3.15).

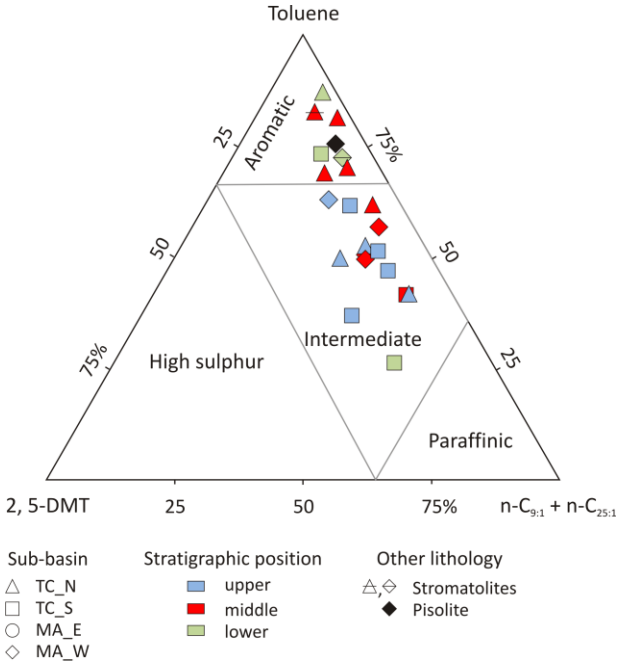

Fig. 6.2. Kerogen classification of samples from the Yacoraite Fm. using specific compounds (after di Primio and Horsfield, 1996). In the apexes the relative proportions of n-C_9 alkene plus n-C_{25}, toluene and 2, 5-dimethylthiophene (2,5-DMT) are shown. Samples of the Yacoraite Fm. exhibit a low sulphur content. (TC) Tres Cruces, (MA) Metán-Alemanía sub-basins. The sectors where samples were collected are north, south (N, S) and east and west (E, W).

The compounds determined via thermovaporisation essentially represent the composition of the S1 peak measured in Rock-Eval pyrolysis although the C_1-C_5 range of hydrocarbons is significant lost during sampling collection and handling (Larter, 1988). Fig. 6.3 shows the relative abundances of short, intermediate, and long-chain lengths in thermovaporised compounds for a sample set of the Yacoraite Fm. but this bulk composition does not totally represent the in-situ subsurface composition due to the loss of light ends.

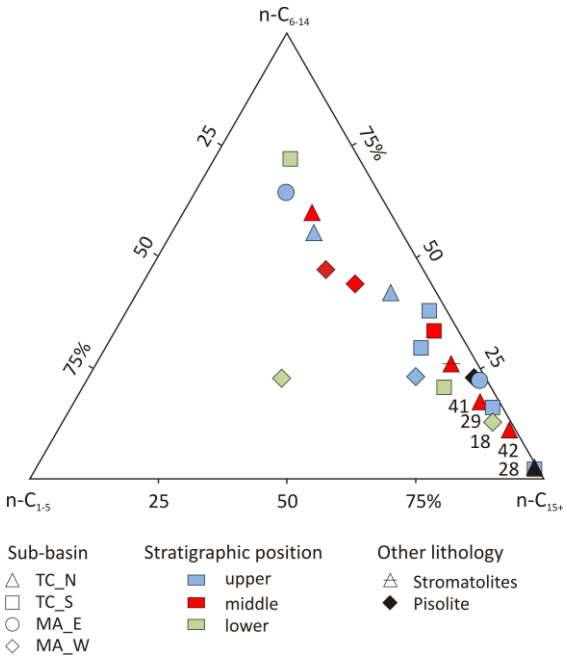

Fig. 6.3. Ternary plot of hydrocarbon chain-length distribution of mobile hydrocarbons fraction by Thermo vaporization (T-vap) in samples of the Yacoraite Fm. (TC) Tres Cruces, (MA) Metán-Alemanía sub-basins. The sectors where samples were collected are north, south (N, S) and east and west (E, W).

The petroleum already generated and potentially ready to migrate is characterized by ranges of compounds of C_6-C_{14} and C_{15+} hydrocarbons. Those ranges dominate and vary between 25 % and 75 % of the chain-length distributions. In a few samples the C_{15+} fraction predominates with amounts higher than 75 % (samples #18, #29, #41, #42) up to 100 % (sample #28 and tar) of the chain-length distributions These variations do not show a relation to the stratigraphic position where the samples were taken. In only one sample (#51), a predominance in the n-C_1 to n-C_5 range was observed, which agrees with its gas-generation potential evaluated from Py-GC.

The chain-length distributions are different in retained hydrocarbons (analyzed by T-vap) and the pyrolysates (Py-GC). This is revealed by the ratio of n-C_{15+} n-alkanes over C_6-C_{14} n-alkanes calculated from both analyses (Fig. 6.4). In the majority of the samples, long-chain hydrocarbons (C_{15+}) are preferentially generated over C_6-C_{14} in Py-GC compared to T-vap, but in samples #18, #42, #44, and pisolite, the opposite is observed. The composition of the hydrocarbons generated from kerogen depends upon kerogen type and thermal maturity. The set of samples analyzed is at the onset of petroleum generation. Sample #18 has a higher T_{max} of 445 °C suggesting a higher maturity but due to its low TOC (0.09 %), this result is likely increased by the mineral-matrix effect.

High values of the ratio between 4 and 8 are not related to oil-stained samples. This factor is assessed here by using the production index (PI) from Rock-Eval pyrolysis as (S1/S1+S2). The pisolite and sample #42 have a relatively high production index of 0.32 and 0.4, while the other two samples #18 and #44 have values of 0.07 and 0.09, respectively. On the other hand, sample #35 with a relatively high PI of 0.35, has a $C_{15+}(C_6\text{-}C_{14})$-Tvap ratio of 0.16 closer to samples with lower PI. All of this information suggests that the ratio between 4 and 8 in this set of samples does not change due to thermal maturity or stagnation, but it is related to the specific kerogen type of each sample.

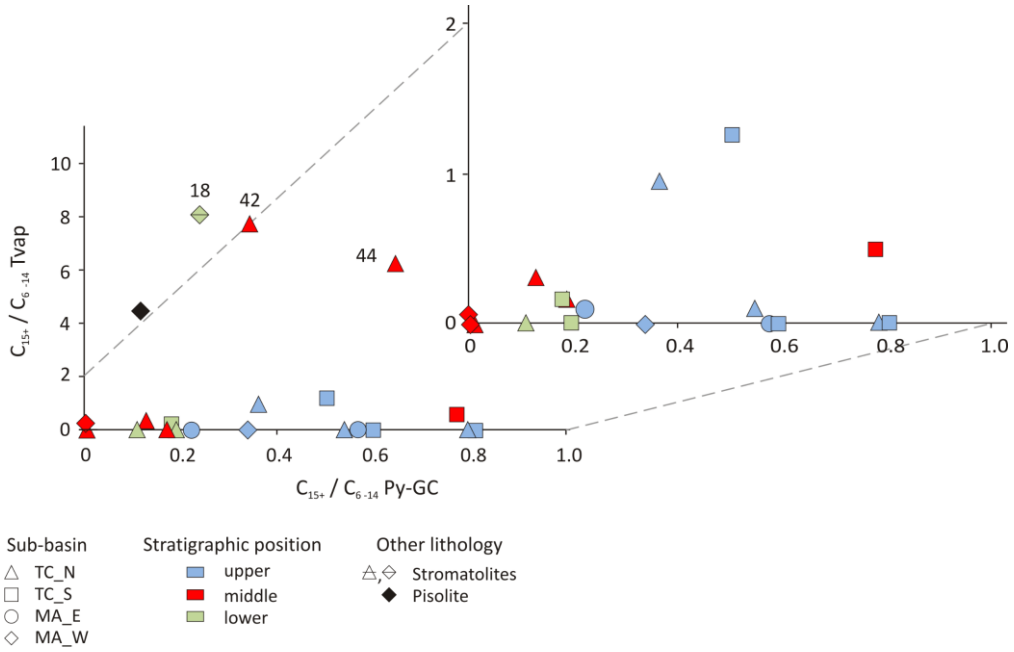

Fig. 6.4. The ratio of $C_{15+}/C_6\text{-}C_{14}$ n-alkanes as calculated from Py-GC (X-axes) and T-vap (Y-axes) for samples of the Yacoraite Fm. Since these samples are at the onset of hydrocarbon generation, and because no relation is observed to the production index, differences in the observed $C_{15+}(C_6\text{-}C_{14})$ ratios are attributed to the specific kerogen composition. (TC) Tres Cruces, (MA) Metán-Alemanía sub-basins. The sectors where samples were collected are north, south (N, S) and east and west (E, W).

6.2 Bulk kinetics of kerogen to hydrocarbon conversion of the Yacoraite Fm.

Thermal stress causes kerogen breakdown through a large number of chemical reactions (Tissot and Welte, 1984). Instead of trying to describe every reaction, the bulk kinetics approach provides the extent of kerogen breakdown and hydrocarbon generation as a whole (Pepper and Corvi, 1995 and references therein). The conversion of organic matter in sediments into hydrocarbons depends on its composition and structure, and it is controlled by temperature exposure over geological time. The different structure and chemical bond strength in the organic matter determine the activation energy distribution (Ea), which is the energy required for kerogen to be broken down into hydrocarbons, and the frequency factor representing the frequency of possible collisions between molecules for the reaction to take place. The relatively simple structure of many Type I kerogens generates a narrow activation energy distribution (Espitalié, 1986) with dominant Ea at 56 kcal/mol and a high-frequency factor in the case of the Eocene Green River Shale of the western U.S. (Schenk et al., 1997).

Broader unimodal distributions of activation energies have been noted for some Type I kerogens (Horsfield et al., 1994), but are usually characteristic of Type II (exemplified by the Toarcian Posidonia Shale in NW Germany) and Type III kerogens (illustrated by an Indonesian coal) (Schenk et al., 1997; Schenk and Horsfield, 1998). This wide distribution of activation energies indicates the existence of chemical bonds with different energy requirements to be broken and, therefore, the heterogeneous kerogen structure. Geological heating rates are much lower (up to 12 orders in magnitude) than experimental heating rates in the laboratory (Pepper and Corvi, 1995). Kinetics experiments are carried out on aliquots of the samples in order to establish parameters that will enable conversions under laboratory conditions to be extrapolated to geological heating rates (Ungerer and Pelet, 1987).

Calculated activation energy (Ea) distributions and frequency factors (A) of the kinetic models determined for low-maturity samples of the Yacoraite Fm. are shown in Fig. 6.5. Activation energy distributions for the samples are between 42 kcal/mol and 62 kcal/mol with frequency factors from 1.76 $10^{12}s^{-1}$ up to 7.35 $10^{13}s^{-1}$ except for sample #3 and tar which have frequency factors one order of magnitude higher, being 1.38 $10^{14}s^{-1}$ and 1.19 $10^{14}s^{-1}$, respectively (Table 9, appendix). The kinetic parameters of the set of samples are similar to published data on source rocks containing Type II kerogen (Braun and Burnham, 1992; Dieckmann et al., 1998; di Primio and Horsfield, 2006; Tan et al., 2013). The tar sample has an activation energy distribution that closely resembles that from a nearby shale (sample #40). This indicates a similar structure/composition of their organic matter and suggests that they are genetically linked. The frequency factor for the bulk reaction of the tar sample is one order of magnitude higher than sample #40 (Fig. 6.5), which suggests that its conversion to hydrocarbons proceeds more rapidly. Genetically related asphaltenes share the molecular characteristic of their parent source rocks (Horsfield, 1997) and similar structural character (Béhar and Vandenbroucke, 1987), which explains why genetically immature asphaltenes exhibit similar thermal behavior as their parent kerogen.

Neither activation energy distribution nor the dominant activation energies were found to be related to any specific relative position in the stratigraphic succession (Fig. 6.5). Samples #29 and #47 have the lowest dominant activation energy close to 48 kcal/mol that accounts for most of the bulk reaction. More than 60 % of the total bulk reaction takes place at around 50 kcal/mol for samples #30, #33, #35, #40, and tar. For samples #3 and #44, dominant activation energies are close to 53 kcal/mol. It is slightly higher and close to 54 kcal/mol for samples #23 and #39.

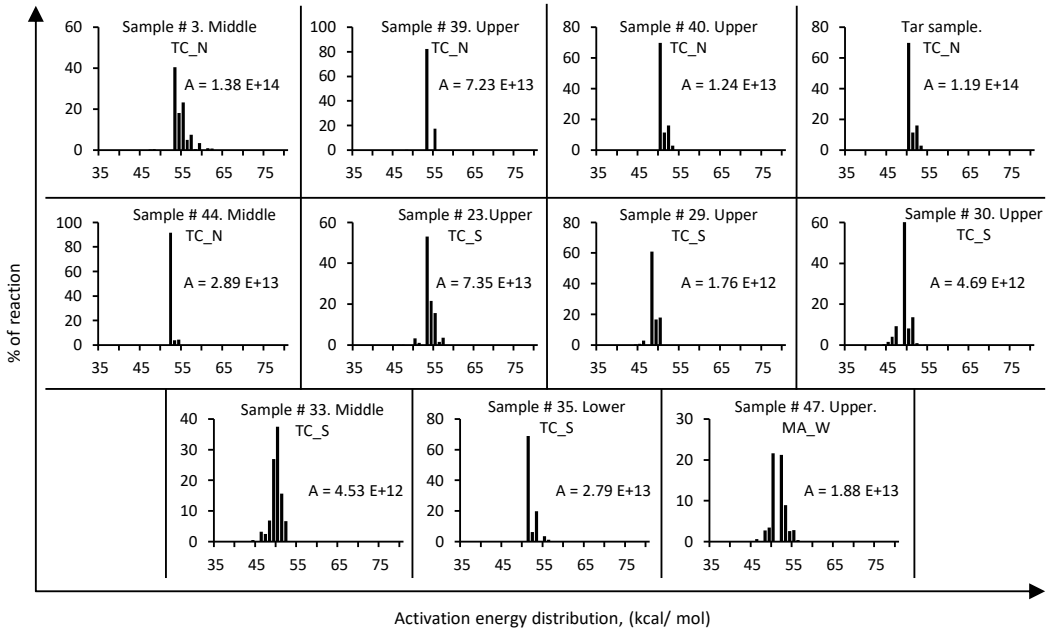

Fig. 6.5. Activation energy distribution (kcal/mol) and the frequency factor (A, 1/s) calculated for selected whole-rock samples from the Yacoraite Fm. see text for discussion

The activation energy distributions do not correlate with the depositional environment. Except for samples #3, #35, #40, #47 and tar, the rest of the samples were deposited in lacustrine environments according to their hydrocarbon chain-length distribution (Fig. 3.10b, c). The interpretation of a lacustrine depositional setting is supported by C_{26}/C_{25} tricyclic terpanes ratios >1 (Zumberge, 1987) for samples #23, #33, and #44 (Fig. 3.16). Narrow activation energy distributions are considered to be typical of lacustrine Type I kerogen and indicate a relatively homogeneous kerogen type with a limited number of chemical bonds that break down within a relatively small temperature window (Ungerer and Pelet, 1987). The lacustrine samples #39 and #44 show narrow activation energy distributions, but samples #23 and #33 don't. Sample #39 has an activation energy distribution similar to that reported for immature kerogen of the same formation in the western sector of the Metán-Alemanía sub-basin (Romero-Sarmiento et al., 2019).

Sample #30 with Type I kerogen (HI=1015 mgHC/g TOC) has a wide activation energy distribution, which indicates its heterogeneous structure. Differences in the distribution of the activation energies in lacustrine samples were reported for the Type I kerogen of the Green River Shale of the Washakie Basin in Wyoming (Horsfield et al., 1994). While the freshwater member of this formation shows the "typical" lacustrine narrow energy distribution, the alkaline Laney Shale member exhibits a broad activation energy distribution indicating its heterogeneous, rather than homogeneous structure (Horsfield et al., 1994). This indicates that the kinetic assessment should be done case-by-case, instead of using kinetics parameters according to the type of kerogen (di Primio and Horsfield, 2006).

Samples #40, and #47 plot in the border of the region delimiting lacustrine and marine depositional environments according to the hydrocarbon chain-length distribution (Fig. 3.10c).

$C_{31}R/C_{30}$ hopane ratio of 0.59 suggest that sample #47 was deposited in a marine environment. Sample #47 exhibits a pseudo bimodal pattern in which both energy-distribution populations create a "mirror" image around 51 kcal/mol. The sample's relative broad activation energy distribution is likely caused by a mixture of Type II and III kerogen.

The kinetic data can be used to model the onset of hydrocarbon generation and its further development as a function of temperature. Organofacies variability causes the Yacoraite Fm. to generate petroleum over a broad range of temperatures of up to 60 °C from ≈108 °C (sample #30, upper Yacoraite Fm.) to 170°C for sample #3 (middle Yacoraite Fm.) (Fig. 6.6a). The higher temperature indicates higher energy requirements to break the chemical bonds (Tissot and Welte, 1984) and suggests the presence of very stable organic matter of sample #3, which requires activation energies of up to 63 kcal/mol and a frequency factor of $1.38x\ 10^{14}s^{-1}$ for thermal cracking (Fig. 6.5 and Table 9, appendix.

As a consequence of organofacies variability, the onset of petroleum generation (TR 10%) is different even at similar stratigraphic position (Fig. 6.6a). For lower temperatures, this is exemplified by samples #33 (middle) and sample #29 (upper) with the same temperature for the onset of petroleum generation of 115°C. They reach almost complete generation (TR=90%) at 149°C and 144°C, respectively. For higher temperatures, this is exemplified by sample #44 (middle) and sample #39 (upper) having similar temperatures for onset (TR=10%) of hydrocarbon transformation of 130°C and 133°C, respectively. Near complete conversion (TR=90%) is reached at 150°C and 157°C, respectively.

Transformation ratios do not depend on specific organofacies in the analyzed set of samples. For example, some organofacies generating paraffinic oil with high wax content (Fig. 6.1a) require low temperatures (samples #29, #30 & #33), others require high temperatures for petroleum generation (samples #23, #39 & #44). P-N-A low-wax organofacies (samples #35 & #47) plot in the middle of the transformation ratios distributions in Fig. 6.6a. However, sample #3 has one of the highest onsets of petroleum generation (TR=10%) of 132°C (Fig. 6.6a) and at 90%TR requires 170°C for petroleum generation.

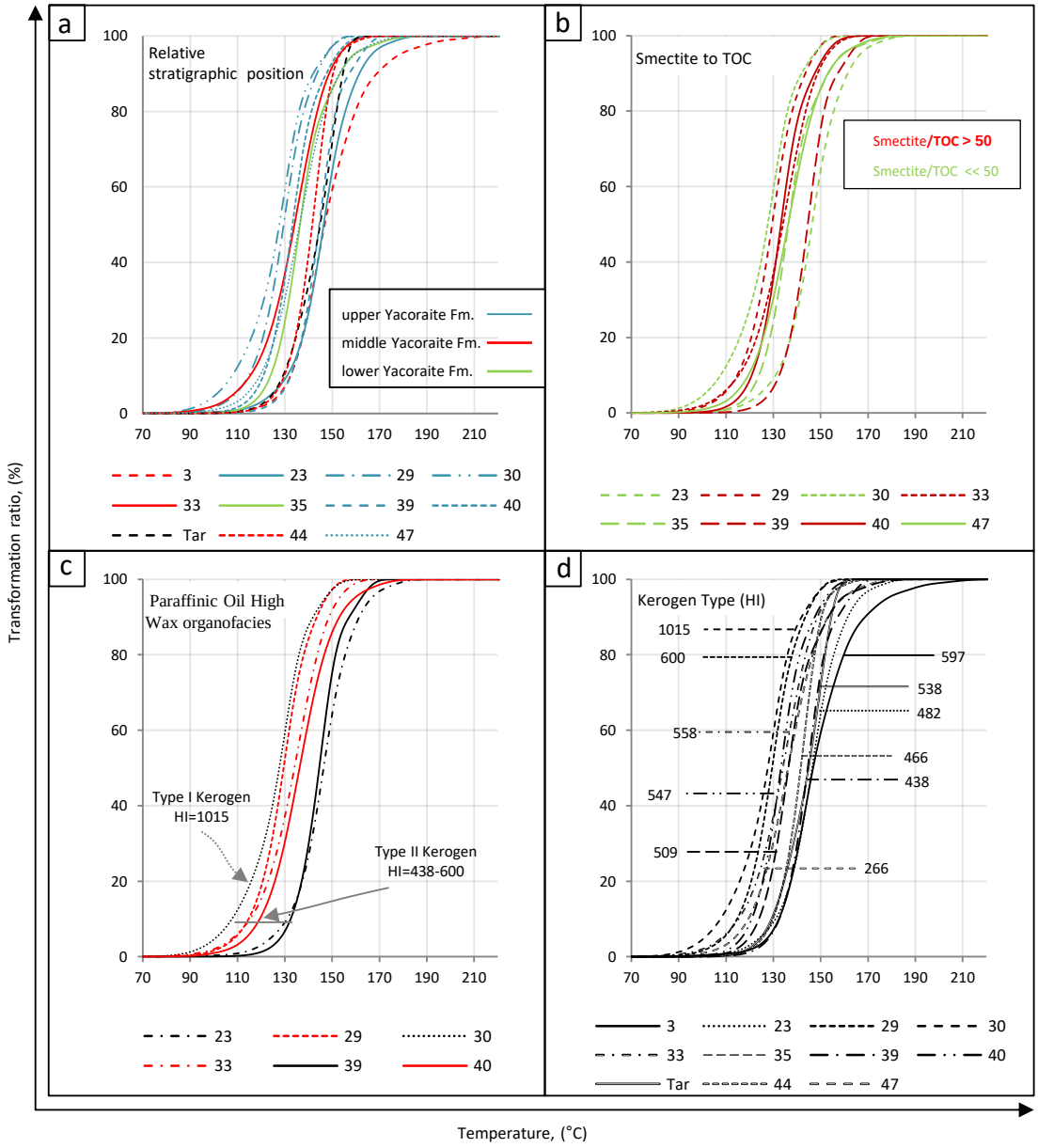

Fig. 6.6. Calculated geological temperatures (X-axes) at which different transformation ratios (Y-axes) are reached for kerogen to petroleum transformation in samples of the Yacoraite Fm. for a heating rate of 3 K/Myr. (a) The range of the geological temperatures for petroleum generation was found to be independent of the relative stratigraphic position. (b) Smectite content or its proportion to TOC does significant influence on the transformation ratios. This is exemplified by sample #39 with 54 % smectite (Sm) and Sm/TOC=59, with the highest temperatures for hydrocarbon generation and sample #30 with the lowest smectite content (9 %) and Sm/TOC ratio=2 and has the lowest temperatures for hydrocarbon generation. Samples #35 and #44 are not shown because smectite was not identified. (c) Temperatures of petroleum generation were found to be dependent on organofacies type (Horsfield, 1997). Paraffinic Oil High Wax organofacies have differences up to 24°C (sample #30 and #39) for the onset of petroleum generation. Differences up to 19 °C, are observed at TR=90 % between samples #23 and #30. Numbers in brackets are the smectite/TOC ratio. (d) Hydrogen-rich organofacies e.g., samples #29, #30, #33 with lower thermal requirements to be transformed into hydrocarbons exist in the Tres Cruces sub-basin. Numbers in brackets correspond to Hydrogen Index (mg HC/g TOC).

Organofacies in the southern sector of the Tres Cruces sub-basin have slightly lower thermal requirements for the onset of petroleum generation (TR=10%). These temperatures are in the range of 108°C (sample #30) to 131°C (sample #23). In the north these temperatures are in the range of 121°C

(sample #40) to 132°C (samples #3 & #39). The complete transformation of organic matter to hydrocarbons (TR=90%) occurs at lower temperatures in the southern sector of the Tres Cruces sub-basin compared to its counterpart in the north. In the southern sector these temperatures are in the range from 142°C (sample #30) to 161°C (sample #23), while in the north these temperatures range from 148°C (sample #40) to 170°C (sample #3). The onset of petroleum generation (TR=10%) from the tar sample starts at 129°C and terminates (TR=90%) at 154°C in a similar temperature range as a shale collected nearby (sample #40).

Chemical reactions can occur at lower temperatures by decreasing activation energies through catalysts. The role of catalysis of smectite on thermal kerogen cracking has previously been reported in pyrolysis experiments (Espitalié et al., 1980). For Type II kerogen of the Miocene Monterey Fm. of California Rahman et al. (2018) reported a reduction in the onset of petroleum generation attributable to smectite content in the whole-rock samples. Samples #29, #33, and #40 with higher smectite to TOC ratios (>50, red lines in Fig. 6.6b) consistently have lower temperatures of petroleum generation than samples with ratios of less than 50 (green lines in Fig. 6.6b). However, samples #30 and #39 behave differently. Sample #30, with a smectite/TOC ratio of 2, which is the lowest value in this set of samples, generates petroleum at the lowest temperatures compared to all samples. Sample #39, with a high smectite/TOC ratio of 59, generates petroleum at the highest temperatures (except for sample #23 at 90 %TR). It was shown that not only content but also the degree of association between smectite and organic matter controls the catalytic behavior of organic matter under laboratory heating conditions (Rahman et al., 2018). Under geological heating rates, however, clay catalysis does not play a significant role in controlling petroleum composition (Yang and Horsfield, 2016). Although the role of smectite cannot be ruled out in our samples, it appears not to affect hydrocarbon generation.

Figure 6.6c shows samples which organofacies are predominantly composed by Type II kerogen and only one sample (#30) with Type I kerogen (HI=1015 mg HC/g TOC) and generate petroleum with Paraffinic Oil with High Wax composition (Fig. 6.1). Sample #30 generates hydrocarbons at around 20 °C lower temperatures than its organofacies counterparts. Other hydrogen-rich samples (e.g., #29, #33, #40), with relatively lower thermal requirements to be transformed into hydrocarbons, also occur in the Tres Cruces sub-basin (Fig. 6.6d).

6.3 Physical properties-PVT of the primary petroleum

Compositional kinetic models predict the relative amount of gas and heavier components generated from kerogen as a function of transformation ratio. The PhaseKinetics model predicts bulk petroleum composition through thermal maturity in a PVT-compatible format and considers only primary reactions (di Primio and Horsfield, 2006). Thermal cracking of retained oils and refractory kerogen is not considered (secondary cracking). Retained oils can be expected when the source rock is not an efficient expeller due to factors such as low TOC content and lithology.

Oil to gas thermal cracking can proceed in the source rocks or in reservoirs through reactions that generally require more energy than those that transform kerogen into oil (Horsfield et al., 1992b; Dieckmann et al., 1998). As a consequence, there is little or no overlapping between thermal requirements for oil and secondary gas generation in the case of source rocks. By extrapolation of laboratory experiments to natural conditions, it was found that the main oil generation occurs between 90-140 °C. The primary gas generation occurred between 110-165 °C, and the main generation of secondary gas occurred between 150-180 °C (Dieckmann et al., 1998), but depends on the geological heating rates; its onset can occur at higher temperatures of up to 190 °C (Horsfield et al., 1992b). Pepper and Dodd (1995) suggested a broader range of temperatures varying from 115 °C (onset, 10 %TR) to 205 °C (90 %TR), as the corresponding thermal requirement for the secondary cracking of the more labile and more stable end members in oils.

The variety of individual reactions that occur during secondary cracking is addressed with first-order kinetic models in which the rate of reaction is proportional to the concentration of oil. These models have shown to be a convenient approximation of natural processes and have a predictive application (Horsfield et al., 1992b; Pepper and Dodd, 1995; Dieckmann et al., 1998). In these models the different thermal requirements to break chemical bonds of the different chemical species are represented by the activation energy distributions and assume a single pre-exponential factor as a bulk property for the oil to gas conversion. The quite narrow activation energy distributions found in the oil to gas thermal cracking (Horsfield et al., 1992b; Pepper and Dodd, 1995; Dieckmann et al., 1998), indicate the relatively homogeneous structure of oils compared to kerogen. This does not imply a uniform oil composition, and consequently the oil to gas conversion depends on the type and subsequent stability of oils as well as the heat-flow history (Horsfield et al., 1992b). Secondary cracking yields can be evaluated by using high temperatures (final temperatures of 560 °C and 700 °C) in closed GC-pyrolysis (Mahlstedt and Horsfield, 2012) and using a modified GORFit - model (Mahlstedt et al., 2013).

The PVT-datasets for each transformation ratio allows characterizing the physical properties of the fluids, i.e., properties such as saturation pressure (Psat) and formation volume factor (Bo) can be calculated. Psat is the pressure below which the gas and liquid phases separate from a petroleum mixture. Bo is defined as the ratio between the oil volume at reservoir conditions compared to surface conditions. Compositional kinetics indicate the presence of moieties that break at different activation energies to mainly generate liquid hydrocarbons in which predominate boiling ranges $C_{7\text{-}15}$ and $C_{16\text{-}25}$. Gases are mostly dominated by n-C_1, followed by n-C_2 and n-C_3 (Fig. 6.7).

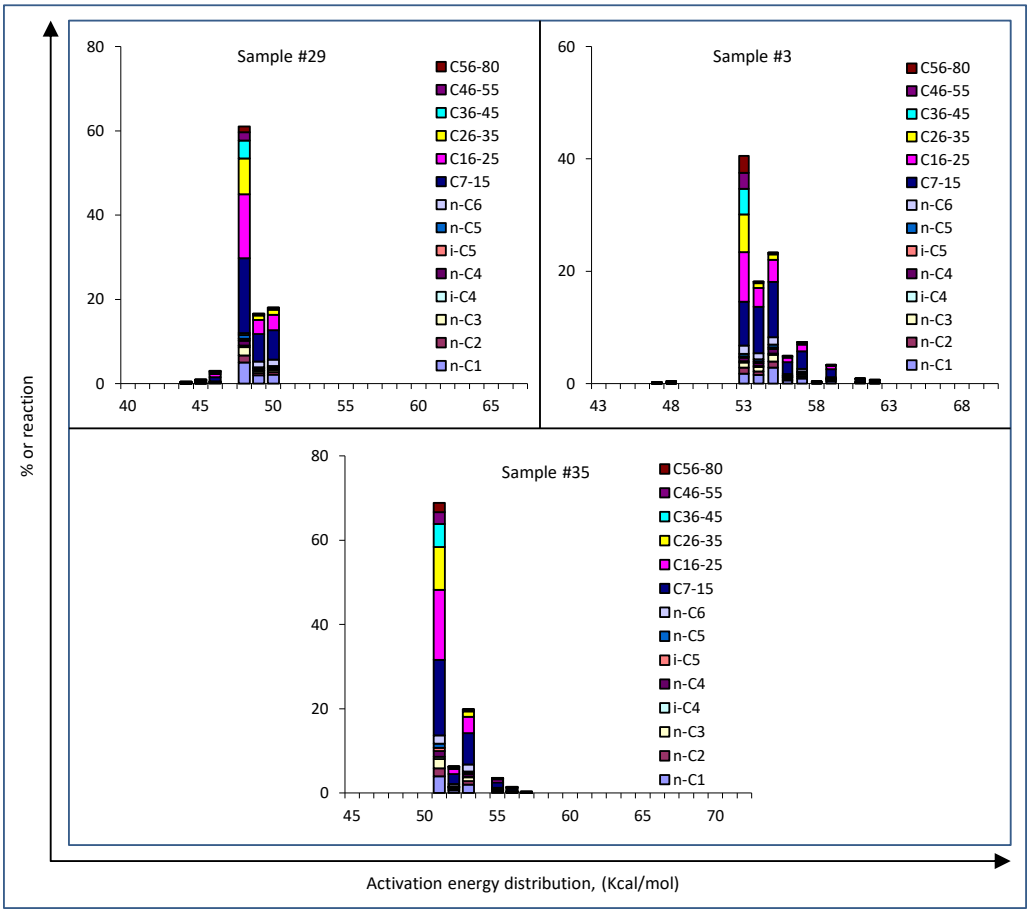

Fig. 6.7. PhaseKinetics 14-compounds models for selected samples of the Yacoraite Fm. Generated fluids are mainly composed of liquid hydrocarbons. These samples were chosen to cover the range of different transformation ratios (Fig. 6.6).

With subtle differences, GORs increase in all samples with the degree of transformation (%TR) (Fig. 6.8) as previously reported (di Primio and Horsfield, 2006; Hartwig et al., 2012; Tan et al., 2013). GOR evolution with TR is similar in P-N-A Low Wax organofacies (sample #35) and Paraffinic Oil High organofacies (sample #29). For these samples, GORs vary from 100 Sm^3/Sm^3 at 10 %TR up to ≈234 Sm^3/Sm^3 at 90 %TR. Sample #3 with P-N-A Low Wax has a similar GOR at 10 %TR. At 30 %TR, GOR decreases likely due to a decrease in the density of the C_{7+} fraction (oil). With further increasing transformation ratios, GOR increases again like in the other samples, but reaching a higher value of 288 Sm^3/Sm^3 at the end of petroleum generation (TR=90 %). With GORs lower than 350Sm^3/Sm^3, these organofacies from the Yacoraite Fm. are expected to mainly generate black oil over their entire thermal maturation.

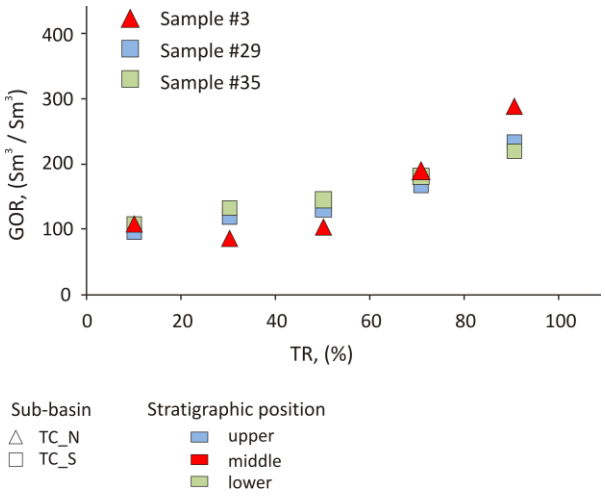

Fig. 6.8. Calculated Gas/Oil ratio (GOR) as a function of kerogen transformation (TR) in samples of the Yacoraite Fm. Black oil is expected to be generated from these samples over their entire maturation (kerogen cracking), as indicated by GORs <350 Sm^3/Sm^3. (TC) Tres Cruces sub-basins. The sectors where samples were collected are north, south (N, S).

The saturation pressure (Psat) increases as a function of thermal maturity, defined by TRs in agreement with previous studies (di Primio and Horsfield, 2006; Hartwig et al., 2012; Tan et al., 2013). Fluids generated for these three samples do not exceed a Psat of 200 bar (Fig. 6.9), which suggests no predominant generation of volatile components during kerogen cracking in agreement with P-N-A Low Wax and Paraffinic High Wax organofacies content. Psat gradually increases from ≈134 bar at the onset of petroleum generation (TR=10 %) up to ≈188 bar in the end of petroleum generation (TR=90 %).

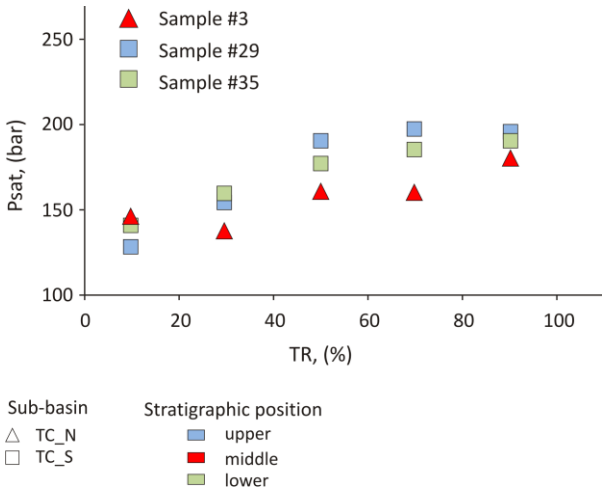

Fig. 6.9. Calculated saturation pressure (Psat) as a function of kerogen transformation ratio (TR) in samples of the Yacoraite Fm. In general, an increase of Psat without exceeding 200 bars observed in P-N-A Low Wax organofacies (samples #3 & #35) and Paraffinic Oil High organofacies (sample #29). Samples collect in (TC) Tres Cruces sub-basins in its north and south (N, S) sector.

Psat evolution behaves quite similar for different organofacies, i.e., for P-N-A Low Wax (Sample #35) and Paraffinic High Wax (sample #29). Psat gradually increases from ≈134bar at the onset of petroleum generation (TR=10%) up to ≈190bar at TR=70%. In the end of petroleum generation (TR=90%), Psat still increases in sample #35 but decreases for sample #29. Methane proportion is the main factor controlling Psat. The volumetric proportion of methane (gas dryness) likely decreases in comparison to the one at 70%. Alternatively, it is also possible that an increase in the miscibility presumably occurs due to the increasing proportion of light vs. heavy liquid components. The same occurs in sample #3 in which Psat decreases at 30%TR compared to 10%TR and slightly remain constant from 50%-70%TR.

As Bo and Psat directly co-vary in genetically related petroleum (di Primio et al., 1998), similar behavior is expected for artificially matured samples. In fluids generated from selected samples of the Yacoraite Fm. collected in the Tres Cruces sub-basin, Psat and Bo directly co-vary, although not in a linear way (Fig. 6.10). The Psat and Bo in the Yacoraite Fm. samples analyzed here fall into the region defined for natural petroleum fluids as compiled by di Primio and Horsfield (2006). Generation of such fluids starts (onset, TR=10%) at temperatures of 108-131 °C and continues up to temperatures of 143-170°C (TR=90%). (Fig. 6.6a).

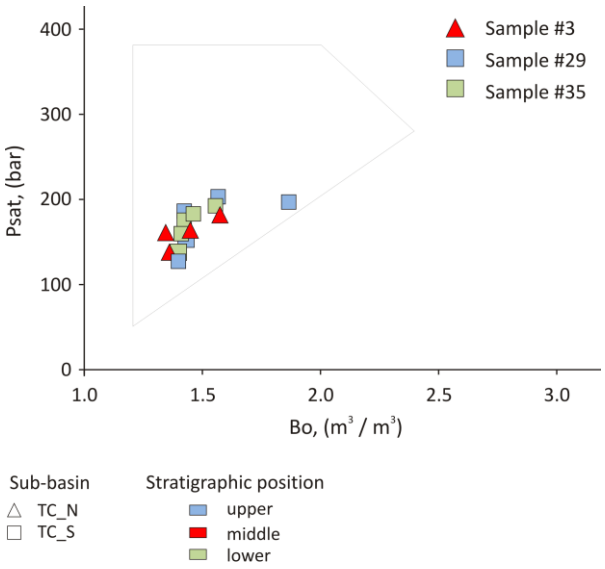

Fig. 6.10. Calculated saturation pressure (Psat) and volume factor (Bo) in samples of the Yacoraite Fm. Fluids generated from this set of samples plot within the region defined for natural petroleum. (TC) Tres Cruces sub-basins. The sectors where samples were collected are north, south (N, S).

Maximum burial paleotemperatures were calculated to be 76°C and 87°C for samples #29 and #35 from the southern sector of Tres Cruces sub-basin, according to their vitrinite-reflectance values of 0.48%Ro and 0.55%Ro:

$T = (\ln \%Ro + 1.68)/0.0124$

(%Ro: vitrinite reflectance (%), T: maximum burial temperature (°C); Barker and Pawlewicz, 1994).

Vitrinite-reflectance could not be measured for sample #3 from the north sector of the Tres Cruces sub-basin but was calculated from its T_{max} (427°C) (Jarvie et al. (2001):

$\%Ro = (0.018 * T_{max}) - 7.16$

The calculated vitrinite reflectance of 0.53%Ro for sample #3 is considered reliable, because it is similar to the measured ones for samples #39 (Ro=0.50%) and sample #40 (Ro=0.55%) collected in the same sector. A paleotemperature of 84°C was estimated for sample #3 based on its calculated vitrinite-reflectance value. The maximum burial depth of the samples #3, #29 and #35; was estimated using 30°C/km as the global average of the thermal gradient (Tissot and Welte, 1984), and 8°C as the mean annual surface temperature for the Tres Cruces locality (Entrocassi et al., 2014). The maximum burial depth was calculated to be ≈2.5 km, ≈2.3 km and ≈2.6 km respectively, for samples #3, #29 and #35.

Phase separation occurs at lower pressures than Psat. Hydrostatic pressure is considered here the threshold for phase separation, because it is typically lower than lithostatic pressure (Tissot and Welte, 1984). Using a representative average hydrostatic gradient of 109 bar/km (op. cit.), the hydrostatic pressure at the maximum burial depth is 276 bar, 247 bar and 287 bar, respectively for samples #3, #29 and #35. Saturation pressures for the primary fluids generated from all three samples (<200 bar) are lower than the estimated hydrostatic pressures. Therefore, no phase separation occurred in the source rocks under those burial conditions. Phase separation from the petroleum admixtures is expected at shallower depth than ≈1.8 km as calculated using the hydrostatic gradient mentioned above.

6.4 Conclusions

Activation energy distributions for the transformation of organic matter of the Yacoraite Fm. to hydrocarbons range between 42-62 kcal/mol with frequency factors from 1.76 x $10^{12}s^{-1}$ up to 7.35 x $10^{13}s^{-1}$, respectively. Consequently, the Yacoraite Fm. generates petroleum over a range of temperatures of up to 60°C from ≈108°C to 170°C. Organofacies in the southern sector of the Tres Cruces sub-basin have slightly lower thermal requirements for the onset (TR=10%) and the complete transformation to hydrocarbons (90%) by 13°C and 5-9°C, respectively compared to organofacies of the northern sector. In the Metán-Alemanía sub-basin, sample #47 has an onset of petroleum generation at 119°C and shows almost complete transformation of hydrocarbon at 153°C.

Under thermal stress, selected samples representing P-N-A Low Wax and P-N-A High wax organofacies were found to mainly generate black oil (GOR <350 Sm^3/Sm^3) in which boiling ranges C_{7-15} and C_{16-25} predominate. Gas-range hydrocarbons are also generated with predominantly methane composition. Saturation pressure of the fluids generated from these selected samples does not exceed 200 bar, which suggests no main generation of a volatile product from kerogen under thermal stress at any transformation ratio. The Psat is lower than the hydrostatic pressure at the maximum burial depth. Therefore, no phase separation occurred in the source rocks under those burial conditions.

7. Petroleum generation in space and time – basin modeling

A 1-D model was created in Petromod 2012 to study the burial history, the thermal maturity of Yacoraite Fm., and to explain the presence of the oil seep samples in the Tres Cruces sub-basin. Since there are differences in the lithology, thickness, and the erosion in the stratigraphic succession compared to the Metán-Alemanía and the Lomas de Olmedo sub-basins, the thermal modeling only applies to the Tres Cruces sub-basin. One important characteristic feature of the Tres Cruces basin is the nearly continuous sedimentation from the onset of rifting in the Early Cretaceous until approximately the Middle Miocene (Monaldi et al. 2008, Siks and Horton, 2011).

Thermal modeling requires the definition of properties and values to be assigned as input data, boundary conditions and calibration data. As input data the lithology and thickness were provided by published accounts as well as the interpreted cross-section which served as a framework to consider the

tectonic activity in the area. The classification of the units in the framework of the petroleum system is based on the literature (sections 1.7 and 1.8) and also inferred from lithological data. The bulk-kinetics parameters correspond to specific measurements on outcrop samples collected for this research.

Regarding the boundary conditions, the basal heat-flow value was constrained considering geological events and regional heat-flow data. The lithology and the interpretation of depositional environments compiled from the literature were used to assign paleo-water depths. The software calculated the temporal evolution of sediment-water-interface temperature (SWIT) for the study area, considering the paleolatitude of the study area.

7.1 Input parameters for the 1D model

An interpreted cross section (Salazar De Langer et al., 2008, 2009; Salazar De Langer, unpublished), of the seismic line 1225 traced in NW-SE direction and ≈5 km north of the sampling location provides information regarding the geometry of the sediments at depth (Fig. 7.1). The seismic line is part of a set acquired in 1990 by a consortium led by Texaco-Argentina (op. cit.). They were recorded at 25 m intervals with a Sercel 368-E instrument using dynamite as seismic source. The seismic information was collected with 240 data channels and processed using a post-stack migration approach. The seismic information was converted in time using seismic stacking velocities.

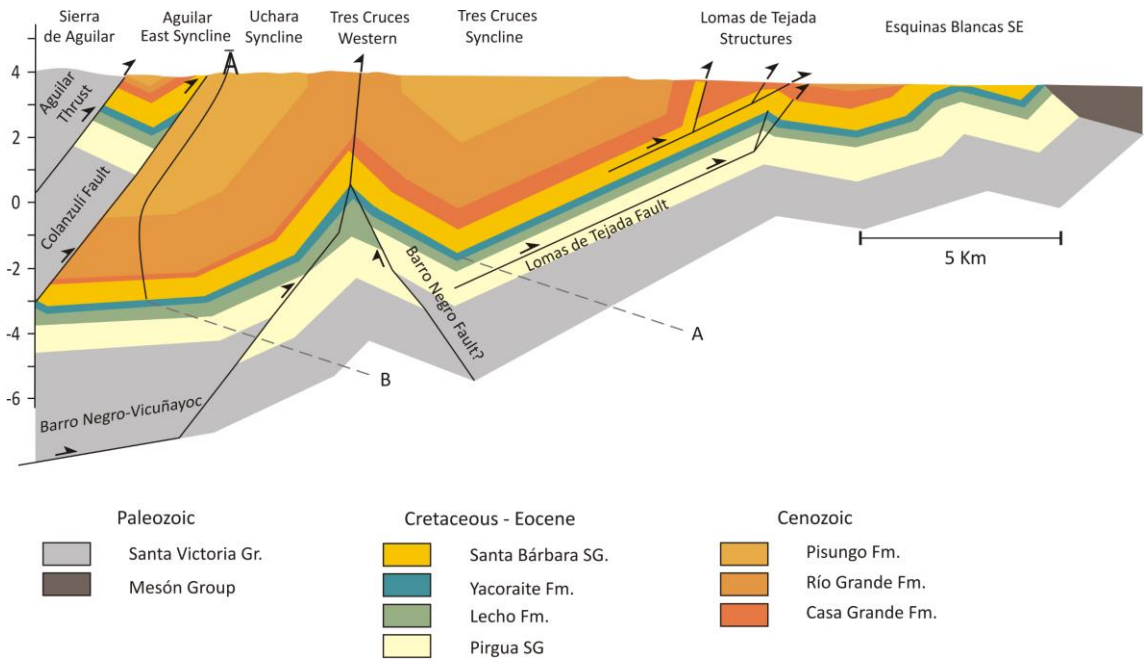

Fig. 7.1. Sketch of the interpreted cross-section based on seismic line 1225 showing the present-day configuration of the sediments at depth. The Yacoraite Fm. is at different depths due to thrust faulting. Thermal modeling assesses the thermal maturity and transformation ratio of the Yacoraite Fm. at points A and B (Salazar De Langer et al., 2008, 2009; Salazar De Langer, unpublished).

The profile (Fig. 7.1) shows tectonic deformation of the sediments, which is younger than the Pisungo Fm. of ≈Late Oligocene to Early Miocene age, likely caused by the last deformation phase of the Andean orogen, which is ongoing. The layers in the stratigraphic succession show significant dip

caused by tectonic processes. In the northwestern part of the profile in Fig. 7.1. (left side), the overburden was eroded, and presently, the Yacoraite Fm. lies under a cover of ≈7 km of sediments of the Ordovician Santa Victoria Group and younger strata. On the SE (right side), the overburden was eroded, and the Yacoraite Fm. is still found in outcrops.

Lithology

The lithology of each formation was customized, mixing standard lithologies of the Petromod 2012 library (Table 7.1). The type of lithology and its percentages were assigned according to stratigraphic descriptions reported for the Tres Cruces sub-basin (Boll and Hernández, 1986; Coutand et al., 2001; Marquillas et al., 2005; Sánchez and Marquillas, 2010).

Table 7.1. Customized lithological composition for the stratigraphic succession in the Tres Cruces sub-basin.

Group	sub-group	Formation	Lithological composition, %				
			Conglomerate	Sandstone	Siltstone	Shale	Limestone
Orán	Jujuy	Pisungo	100				
	Metán	Río Grande	60	40			
		Casa Grande	70	30			
Salta	Santa Bárbara	Lumbrera	20	40	40		
		Maíz Gordo		100			
		Mealla	30	30	30		10
	Balbuena	Yacoraite		45		15	40
		Lecho		20	80		
	Pirgua	undifferentiated					
		undifferentiated		100			
		undifferentiated					
Santa Victoria						100	

Lithologies selected from the library of Petromod 2012: Conglomerate (quarzitic), Sandstone (quartzite, typical), Siltstone (organic lean), Shale (typical), Limestone (Chalk, 75 % calcite).

The vertical depth and the true thickness (perpendicular to bedding) were measured on the interpreted cross-section of the seismic line 1225 (Fig. 7.1) and agree with other reports (Boll and Hernández, 1986). The difference between vertical depth and the true thickness is the additional burial due to tectonics, which is simulated by the rapid deposition of an extra layer called Pisungo_art. The thickness, age and the paleo-water depth assigned to the stratigraphic units are shown in Table 7.2.

Table 7.2. Thickness, age, and paleo-water depth of the deposition in the Tres Cruces sub-basin used as input data for 1-D modeling. This model assumes no erosion but thickness correction due to the dip of the stratigraphic layers caused by tectonics.

Layer	Top (m)	Base (m)	Thickness (m)	Deposition		PSE	PWD (m)
				From (Myr)	to (Myr)		
Pisungo_art	0	750	750	11.63	0	Overburden Rock	0
Pisungo Fm.	750	2750	2000	23.03	11.63	Overburden Rock	5
Río Grande Fm.	2750	4750	2000	33.9	23.03	Overburden Rock	5
Casa Grande Fm.	4750	5550	800	37.8	33.9	Overburden Rock	5
Lumbrera Fm.	5550	5750	200	50	37.8	Seal Rock	5, 10, 5
Maíz Gordo Fm.	5750	5850	100	59.2	50	Reservoir Rock	5
Mealla Fm.	5850	6090	240	61.6	59.2	Seal Rock	5, 10
Yacoraite Fm.	6090	6300	210	68	61.6	Source Rock	5, 20, 10
Lecho Fm.	6300	6700	400	70	68	Underburden Rock	2
Pirgua SG	6700	7600	900	129.4	70	Underburden Rock	5
Santa Victoria Group	7600	9600	2000	485	458.4	Underburden Rock	30

The lithological composition was customized (Table 7.1). PWD: Paleo-water depth as inferred from the lithology and the description of the depositional environment in the literature. The role of every unit as petroleum system element (PSE) is based on the literature (sections 1.7 and 1.8) and inferred from their descriptions.

Paleo-water depth (PWD)

Paleo-water depth was inferred from the lithologies of the different layers, the depositional environment described in sections 1.5, 1.6, and descriptions in Boll and Hernández (1986), Coutand et al. (2001), Marquillas et al. (2005), Sánchez and Marquillas (2010). The Pirgua sub-group was deposited in alluvial-fan environments, which evolved during the rifting climax to lacustrine settings, and later to fluvial environments during the syn-rift phase (Sánchez and Marquillas, 2010). After rifting, the Balbuena Sub-group was deposited consisting of the Lecho and Yacoraite Fm. (Marquillas et al., 2005). The Lecho Fm. was initially deposited in a lacustrine environment that later evolved into a distal braided-river setting (Sánchez and Marquillas, 2010). The onset of deposition of the Yacoraite Fm. was in a marine environment, which later became lacustrine (cf. Chapter 3). Later the strata of the Santa Bárbara Sub-group, namely the Mealla Fm., the Maíz Gordo Fm., and the Lumbrera Fm. were deposited Marquillas et al., 2005. The deposition of the Mealla Fm. occurred in anastomosing rivers, which evolved to more organized fluvial channels of higher energy and changed to a semi-arid, muddy-sandy plain environment (op.cit.). Subsequently, as a consequence of Cenozoic Andean mountain building, the development of a foreland basin began (e.g., Montero-López et al., 2020). Under these new conditions, the Casa Grande Fm. was deposited in alluvial fans and ephemeral rivers. With further topographic changes, braided rivers developed during the deposition of the Río Grande Fm. and the Pisungo Fm. (Boll and Hernández, 1986).

Source rock kinetic parameters

For modeling of the hydrocarbon generation, specific bulk-kinetics parameters were measured and assigned. They were determined for samples #23, #29, #30, and #33 collected in the southern sector

of the Cres Cruces sub-basin at the site of the Barro Negro oil seep. They encompass kinetic parameters of different organofacies of the Yacoraite Fm. (Fig. 6.5).

7.2 Boundary conditions

The simulation of geological processes, in particular the non-linear set of equations describing the pressure and temperature evolution in sedimentary basins, uses numerical models for which boundary conditions have to be defined. The most important ones are the lower and upper boundary conditions for temperature. The upper boundary condition is the temperature at the surface of the earth or as used in the program PetroMod, the sediment-water-interface-temperature (SWIT). The lower boundary condition represents the heat input or heat flow from the underlying basement defined as basal heat flow. Both boundary conditions vary on geological timescales, and therefore, have to be reconstructed considering all geological information available from the study area.

Basal heat flow

The basal heat-flow evolution defines the heat input into the model, which strongly controls the thermal maturity and the transformation rate of the organic matter into hydrocarbons. The exact heat-flow evolution of the study area is unknown. The lack of calibration data in the study area, e.g., present-day heat flow, thermal gradient, thermal maturity indicators such as vitrinite reflectance, or bottom-hole temperatures (BHT), makes its determination uncertain. However, it can be reconstructed with some confidence within the geological framework of the area (Moretti et al., 1996 and references therein). In particular, the Cretaceous rifting event and the presence of the oil seep samples in the area provide a framework to reconstruct the paleo heat-flow evolution of the study area. The vitrinite-reflectance data measured on outcrop samples (Section 4.1.2) provides additional calibration data to validate the paleo heat-flow evolution. Two paleo heat-flow histories were tested. The first one assumes a heat-flow peak of 90 mW/m² due to Cretaceous rifting, which decreases to a present-day heat flow of about 45mW/m² (black line in Fig. 7.2). This was considered as a minimum heat-flow scenario.

The second scenario (red line in Fig. 7.2) considers a higher heat flow based on the increase in the geothermal gradient in the Puna region (Springer and Förster, 1998; Springer 1999). This high heat flow is a consequence of the Cenozoic volcanism whose most intense expression occurred in the Late Miocene-Pliocene (Coira and Kay, 1993; Petrinovic et al., 2017). The impact of this additional source of heat was included as an additional heat-flow peak of up to 70mW/m^2 in the Late Miocene-Pliocene similar in magnitude to the present-day heat-flow of the volcanic arc in the central Andes (Springer, 1999). After the Cenozoic volcanism, the model considers an exponential decrease in heat-flow up to 55mW/m² at present-day, which is based on the regional published data in the range from 45-55mW/m^2 (Moretti et al., 1996 and references therein). Higher heat-flow values of up to 94mW/m^2 are reported in the Bolivian Puna at the border to Argentina (Henry and Pollack, 1988). To the north at ≈21°S, the heat-flow in the Altiplano reaches values up to 180mW/m^2 (Springer and Förster, 1998; Springer 1999).

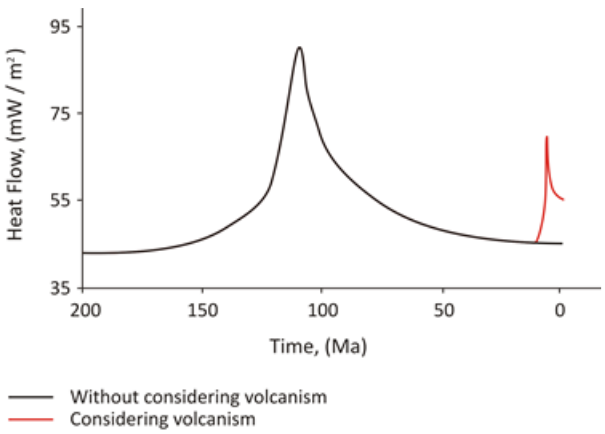

Fig. 7.2. Paleo heat-flow histories used in thermal modeling for the stratigraphic succession in the Tres Cruces sub-basin. The black line represents the heat-flow evolution with minimum values. The high heat-flow scenario considers the intense volcanic activity that occurred during the Late Miocene-Pliocene represented by the red line.

The comparison of the heat flow in southern Bolivia and NW Argentina is considered valid because these areas share a similar geological evolution:

- Similar tectonic regime during the formation of the Cretaceous rift (Monaldi et al., 2008).
- Similar lithospheric response to the orogenic load that started during the Paleocene (DeCelles et al., 2011).
- The development of a combined foreland basin in southern Bolivia and northern Argentina (DeCelles et al., 2011).
- These zones were affected by the Andean orogeny with younger signs of deformation in south Bolivia and active deformation at present-day (Marret et al., 1994).
- Neogene volcanism in Bolivia is contemporary to the "Altiplano-Puna Volcanic Complex" formed during the intense volcanism stage in the Late Miocene–Pliocene (Petrinovic et al., 2017).

Sediment-water interface temperature

The upper boundary condition was defined using a tool provided within PetroMod (Wygrala, 1989) to calculate the average surface-temperature history for the study area. The sediment-water-interface-temperature (SWIT) is automatically corrected for paleo-water depth.

7.3 Calibration data

Vitrinite reflectance analyses were carried out on ten outcrop samples of the Yacoraite Fm. collected in the Tres Cruces sub-basin (c.f. 4.1.2). A vitrinite-reflectance value of 0.58 %Ro was used for calibration which is the average of the values of samples #23, #29, #30, #34 & #35 (Table 4.1) collected in the south sector where the oil seep samples retrieved in the Tres Cruces sub-basin. Besides, the presence of these oil seeps suggests a source rock in the area, which is in the oil window and, therefore, mature enough to generate and expel hydrocarbons. Based on age- and depositional environment-related biomarkers, the oil seep samples collected in the Tres Cruces sub-basin were likely generated from the Yacoraite Fm. (section 5.2). This indicates that this formation is more mature at greater depth compared to vitrinite reflectance measured on outcrop samples.

7.4 The conceptual model

Thermal modeling focuses on the study area in the Tres Cruces sub-basin where the oil generation is documented by the oil seeps and uses the interpreted cross-section (Fig. 7.1). Two burial histories were modeled. The first burial history assumes continuous sedimentation without significant additional burial and erosion, representing the minimum burial history of the region. The second burial history includes additional burial caused by Andean shortening resulting in folding and thrusting and the subsequent erosion to the present-day burial-depth. This scenario is considered here the most likely because of the significant erosion that occurred in this area after faulting.

7.5 Results

7.5.1 The effects of burial and heat-flow evolution on the Yacoraite Fm.

No erosion and regional heat-flow scenario

This scenario uses the stratigraphic succession at point A in Fig. 7.1 and considers additional burial due to folding and faulting by the Andean orogeny, but no subsequent erosion. The age, lithology and thickness of the different layers are shown in Tables 7.1 and 7.2. The burial history assuming continuous sedimentation and no erosion is shown in Fig. 7.3a. At point A in Fig. 7.1, the thermal model predicts that the Yacoraite Fm. reached a vitrinite reflectance of 0.64%Ro (red bar in the inset in Fig. 7.3a) when a heat-flow evolution (black line Fig. 7.2) with a minimum present-day value of 45mW/m^2 is used. That vitrinite reflectance value is close to 0.58%Ro measured in the outcrop samples of the same formation. At point B in Fig. 7.1, that represents the deepest location chosen for modeling, a higher thermal maturity of 0.71%Ro is predicted, which is consistent with its deeper burial.

Regional heat-flow scenario with erosion

The occurrence of oil seeps documents oil generation in the area. Therefore, additional burial due to folding and thrusting and subsequent erosion was used to meet thermal conditions for oil generation. At point A in Fig. 7.1, thermal modeling estimates the erosion of ≈3km of thrusted layers during the Andean orogeny in the Late Pleistocene for the Yacoraite Fm. to reach a thermal maturity that corresponds with the oil window with a vitrinite reflectance of 0.82%Ro (inset in Fig. 7.3b). The heat-flow evolution used in this scenario assumes a present-day value of 45mW/m² after decreasing from 90mW/m² due to Cretaceous rifting (black line in Fig. 7.2).

Additional heat input due to volcanism

This scenario assumes continuous deposition, and it considers additional burial due to the effects of the Andean orogeny, but no subsequent erosion at point A in Fig. 7.1. Its burial history is shown in Fig. 7.3a. The extra heat flow caused by the high-intensity volcanic activity during the Late Miocene-Pliocene increased the thermal maturity of the Yacoraite Fm. up to the oil window with a vitrinite reflectance of 0.80%Ro at point A and 0.86%Ro at point B in Fig. 7.1.

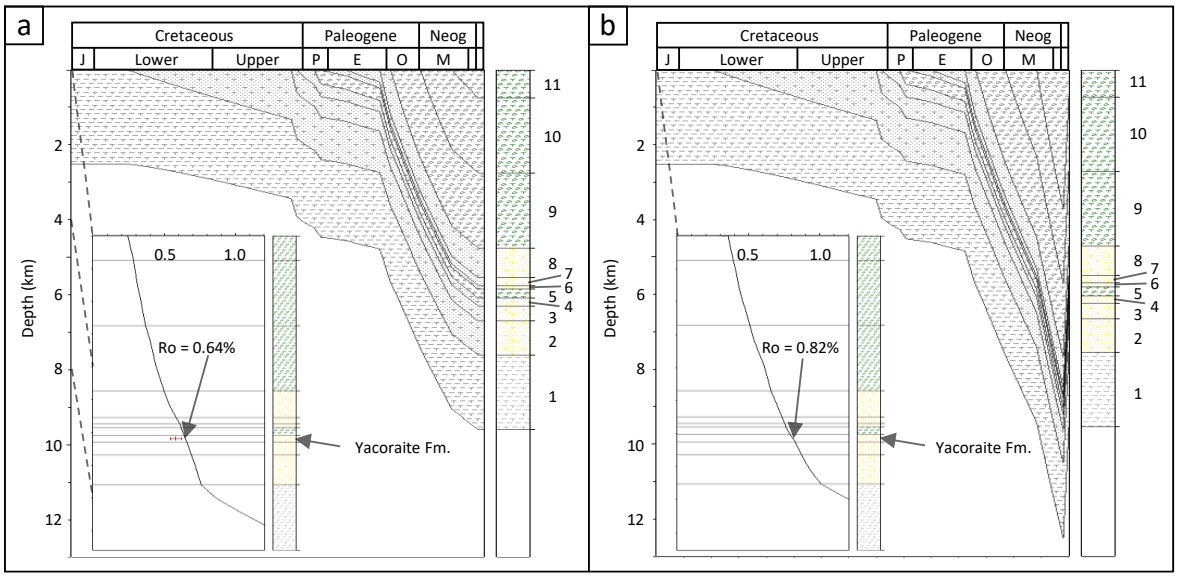

Fig. 7.3. Burial histories of the stratigraphic succession in the Tres Cruces sub-basin and their impact on the thermal maturity of the Yacoraite Fm. (a). Scenario of continuous deposition, additional burial due to Andean orogeny but no subsequent erosion. Inset: In this scenario, the model predicts a thermal maturity of the Yacoraite Fm. of 0.64%Ro at point A in Fig. 7.1. This value is close to 0.58%Ro measured in outcrop samples. (b). Scenario considering additional burial at point A in Fig. 7.1; caused by the Andean compression resulting in folding, thrusting and the subsequent erosion to the present-day burial-depth. Inset: Under these circumstances, the Yacoraite Fm. reached the oil window with a vitrinite reflectance of 0.82%Ro. For both models, the paleo heat-flow evolution considers a heat-flow peak of 90mW/m² during the Early Cretaceous due to rifting, which decreases to present-day heat flow of about 45mW/m² (black line in Fig. 7.2). J: Jurassic, P: Paleocene, E: Eocene, O: Oligocene, M: Miocene. The stratigraphic succession: Santa Victoria Group. (1), Pirgua Sub-group (2), Lecho Fm. (3), Yacoraite Fm. (4), Mealla Fm. (5), Maíz Gordo Fm. (6), Lumbrera Fm. (7), Casa Grande Fm. (8), Río Grande Fm. (9), Pisungo Fm. (10) and Pisungo_art. (11), which simulates the rapid deposition of an additional layer to account for the additional burial due to overthrusting.

7.5.2 Modeling hydrocarbon generation using source rock-specific kinetics

No erosion and regional heat-flow scenario

In this scenario the present-day transformation ratios (TR) of the Yacoraite Fm. at point A in Fig. 7.1 are approximately 1%, 8%, 15% & 8% for samples #23, #29, #30 & #33, respectively (continuous lines in Fig. 7.4). At point B in Fig. 7.1, the model predicts TRs between ≈4-25 %. Although the petroleum expulsion may occur with these transformation ratios, they are low to allow the migration towards the surface. Therefore, this model does not fully explain the presence of oil seeps.

Regional heat-flow scenario with erosion

When the additional burial caused by the Andean orogeny and the subsequent erosion is considered at point A in Fig. 7.1, thermal modeling predicts higher transformation ratios than the previous model. In this model, the onset (TR 10%) of petroleum generation was reached between ≈10-≈9 Ma for samples #29, #30 & #33. Sample #23 reached this TR later at ≈4 Myr ago. Hydrocarbon generation is still active with present-day TR of ≈20%, 75%, 75% & 56% for samples #23, #29, #30 & #33, respectively (dotted lines in Fig. 7.4). With the highest TRs, not only the expulsion should occur, but the migration towards the surface is more likely than in the previous model.

Additional heat input due to volcanism

Under these conditions at point A (Fig. 7.1), samples of the Yacoraite Fm., namely #29, #30 & # 33 reached the onset of hydrocarbon generation at ≈8-6Ma (dashed lines in Fig. 7.4). Sample #23 reached the same TR at c.a. 4Ma. As a consequence of the remaining heat, the present-day TRs are high and similar, but lower by approximately 5% compared to the ones reached in the model with erosion. As a consequence of extra heat due to volcanism, the Yacoraite Fm. at point B buried deeper than in point A (Fig. 7.1) and reached the onset of hydrocarbon generation ≈1My earlier. Their present-day TRs are 84% for samples #30 & #33 and 68% & 25% for samples #29 and #23, respectively.

From the above models, the model involving erosion is considered here to be the more likely scenario. This is because due the Andean orogeny the sediments in the Tres Cruces sub-basin were uplifted, tectonically deformed and exposed to erosion after faulting. For example, the Yacoraite Fm. now outcrops at ≈4000 m.a.s.l. in the study area. The eroded sediments increased thermal maturity of the underlying units with additional contribution by the tilt of the layers caused by tectonism. Contribution of additional heat sources due to volcanism cannot be ruled out, though. Calibration data at depth is needed to constrain the effect of these factors on thermal maturity.

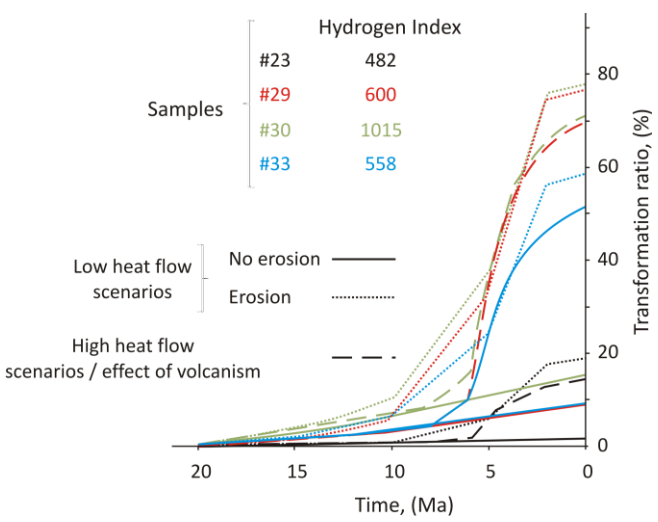

Fig. 7.4. Transformation ratios (TR) of the kerogen in hydrocarbons under different scenarios considered in the thermal modeling for the stratigraphic succession in the Tres Cruces sub-basin. Specific kinetic parameters were used for the samples. All TRs shown were calculated for the Yacoraite Fm. at point A (Fig. 7.1). TRs are represented by continuous lines in the model that does not consider erosion, dotted lines for the model that considers erosion, and discontinuous lines in the model with high heat flow due to the high-intensity Late Miocene-Pliocene volcanism. In the first model, present-day TRs are lower than 15%. Therefore, hydrocarbon expulsion and migration towards the surface is unlikely. The model that considers erosion predicts higher present-day TRs between ≈60-75% for the three samples with higher HI. These TRs are similar but higher by ≈5% compared to the model with higher heat flow due to volcanism. In both of these models, the present-day TR of sample #23 is ≈20 %TR. Hydrogen Index: mg HC/g TOC.

Fig. 7.4 shows the presence of hydrogen-rich samples with a comparatively higher TR, e.g., samples #29 & #30 with HI of 600 mg HC/g TOC and 1015 mg HC/g TOC, respectively. With these TRs, petroleum expulsion is likely, and the possible migration occurs as indicated by the oil seep samples found in the region. The higher TR for the hydrogen-rich samples #29, #30 & #33 compared to sample #23 results from their lower activation energy required in the thermal degradation of their kerogen. Sample #23 has a higher activation energy distribution with 54 kcal/mol as its main activation energy. The main activation energies for the other three samples fall between 48-50 kcal/mol (Fig. 6.5).

7.5.3 The petroleum system elements and exploration risks

In the study area exist all lithological units that represent the elements of the petroleum system, i.e., the stratigraphic traps involve the Yacoraite Fm. as the source rock, the Mealla Fm. is the carrier rock, and the Maíz Gordo Fm. deposited in fluvial channels is the reservoir. The lateral extent and the continuity of those channels needs to be estimated and taken into consideration. In addition, the siltstones of the Lumbrera Fm. are considered a regional seal (Disalvo et al., 2002). In the Tres Cruces sub-basin this formation is composed by siltstones (Sánchez and Marquillas, 2010), which could compromise its effectiveness as a seal. Carbonates and shales within the Yacoraite Fm. would provide a more effective seal (Disalvo et al., 2002; Hernández et al., 2008; Sánchez and Marquillas, 2010).

Traps formed as the results of tectonism play an important role in the hydrocarbon accumulation. Therefore, they are the potential targets for exploration. Potential traps could have been generated as a consequence of the late Cenozoic tectonic evolution of the Andes. This ongoing phase has been an important tectonic episode, with the potential to overprint the characteristics of the previous deformation phases (Salfity and Marquillas, 1999). Thermal modeling predicts that between ≈50-65% of the hydrocarbon was generated before or during such structural traps were formed. The amount of hydrocarbon generated after those possible traps formed, accounts for ≈10 %. The integrity of such traps is uncertain, which represents a risk to be considered during hydrocarbon exploration. Consequently, the traps leaked the oil to the surface through a network of faults, e.g., the Colanzulí, the Barro Negro, and the Barro Negro-Vicuñayoc faults (Fig. 7.1) that directly connect the source rock and the potential reservoir rocks with the surface. This explains the presence of oil seeps in the study area and the traces of limited amounts of petroleum found in drilled wells in this sub-basin (Alvarez, 1999).

7.6 Conclusions

When continuous sedimentation, no erosion, but additional burial due to shortening and tectonic loading is assumed, thermal modeling predicts that the Yacoraite Fm. is in the oil window with vitrinite-reflectance values between 0.64-0.71%Ro in the Tres Cruces sub-basin. Under these conditions, the Yacoraite Fm. reached transformation ratios of up to 25% which is low to allow migration of hydrocarbons towards the surface.

However, the presence of oil seeps in the area indicates that the Yacoraite Fm. is more mature in some parts of this sub-basin. Therefore, a model in which this formation reaches higher maturities is required. Thermal maturities in the range of the oil window with a vitrinite reflectance of ≈0.80-0.85%Ro were reached with two different scenarios. One included ≈3km of additional burial caused by Andean compression and subsequent erosion to present-day burial-depth. The other scenario considered the potential of thermal influences exerted by volcanism that occurred during Late Miocene-Pliocene.

With the range of thermal maturities, the calculated present-day TRs vary between ≈20-80%, depending on the specific bulk-kinetics parameters measured for four analyzed samples. At these TRs not only expulsion occurs, but migration towards stratigraphic or structural traps is likely and leakage

to the surface is possible. Because of the significant deformation and erosion in the study area, the model that considers erosion is the most likely scenario bringing the Yacoraite Fm. up to the oil window.

Petroleum generated from the Yacoraite Fm. can be stratigraphically trapped in the Maíz Gordo Fm. and the Yacoraite Fm. itself. Seals are provided by carbonate intervals within the Yacoraite Fm. and possibly and with less efficacy, by the Lumbrera Fm. The structural traps were formed after or during most of the hydrocarbons were generated. Their integrity is questionable, as indicated by the presence of oil seeps. A regional study is needed to ultimately clarify the uncertainties described before.

8. Summary and perspectives

Depositional environment assessment and petroleum potential of the Yacoraite Fm.

Variations in organic and mineral composition within the Cretaceous Yacoraite Fm. including tricyclic terpanes, hopanes, sulphur, gammacerane, bulk, and mineral composition help to track changes in depositional environments during its deposition. The onset of deposition was associated with the existence of marine environments in the Tres Cruces and Metán-Alemanía sub-basins of north-western Argentina during a phase of post-rift thermal subsidence. Despite these marine conditions, lacustrine environments became predominant towards the end of deposition of the Yacoraite Fm. in the Tres Cruces sub-basin. However, this transition is not observed in the Metán-Alemanía sub-basin, but this may be due to a lesser number of samples analyzed for organic geochemistry. During the deposition of the Yacoraite Fm. the incorporation of sulphur into the organic matter was low. Sustained anoxic conditions allowed the good preservation of organic matter, which consists predominantly of oil-prone Type II kerogen. During deposition, changes in environmental conditions can be inferred from clay mineralogy. For example, the predominance of smectite vs. illite/mica indicates changes in weathering conditions in the upper section of the Yacoraite Fm, presumably due to climate variations that affected the Tres Cruces sub-basin. Rock samples from the Lomas del Olmedo sub-basin farther to the east were not available for this study.

All analyzed outcrop samples of the Yacoraite Fm. are at the onset of hydrocarbon generation and therefore did not experience the thermal requirements for the transformation of significant amounts of kerogen into hydrocarbons. Hydrocarbon expulsion is unlikely at this level of thermal maturity, and therefore does not to explain the existence of oil seeps. From these oil seeps the presence of more-mature source rocks in the Tres Cruces sub-basin can be inferred. Organic geochemistry parameters suggest that the Yacoraite Fm. is the source rock of all of these oil seeps. Their C_{28}/C_{29} steranes ratio clearly indicate that they were generated from a Cretaceous source rock. Similar characteristics including tricyclic terpanes, hopanes, and gammacerane in the oil seeps and organofacies from the middle and upper sections of the Yacoraite Fm. indicate their genetic relation. This suggests that the Yacoraite Fm. has more maturity at depth, an assessment, which is predicted and further supported by thermal modeling, but which remains to be proven, though.

Thermal modeling predicts that the Yacoraite Fm. reached the oil window due burial by Cenozoic sediments and additional effects exerted by tectonic loading due to Andean shortening and associated with folding and thrusting with subsequent erosion. Most of the kerogen-to-hydrocarbon transformation occurred before or during the formation of structural traps. These hydrocarbons could have migrated to the surface through a network of faults that connect the source rock and possible reservoirs with the surface (e.g., the Barro Negro and the Colanzulí faults). The amount of hydrocarbons that were generated following trap formation accounts for not more than ≈10% of the generation potential. Regional studies aiming to improve the knowledge about thermal maturity and thickness of the Yacoraite Fm., changes in thickness and lithology of the Cenozoic sediments, and knowledge of calibration data at depth, will eventually help to improve thermal modeling efforts.

Variability in organofacies, as evaluated in the relatively low-maturity organofacies of the Yacoraite Fm. account for the differences in activation energy distribution that range from 45 kcal/mol and 62 kcal/mol with frequency factors from $1.76 \times 10^{12} s^{-1}$ up to $7.35 \times 10^{13} s^{-1}$, respectively. The obvious consequence is the different requirements of thermal energy for the transformation of kerogen in hydrocarbons. It is anticipated that under thermal stress, the Yacoraite Fm. generates black oil (GOR <350 Sm^3/Sm^3) mainly composed of Paraffinic-Naphthenic-Aromatic Low Wax and Paraffinic High Wax Oils with a minor contribution of Paraffinic Low Wax Oil and gas/condensates. In addition, the low TOC content limits the hydrocarbon potential. PhaseKinetics (di Primio and Horsfield, 2006) predicts the separation of gas and liquid phases that occurred at pressures lower than 200 bar ≈1.8 km when the average hydrostatic gradient pressure gradient is considered.

This dissertation also highlights the biases caused by inorganic influence in the assessment of the fundamental organic parameters such as kerogen typing and thermal maturity of the Yacoraite Fm. This is not only interesting from a pure research focus, but this also has practical importance with respect to hydrocarbon exploration. Samples of the Yacoraite Fm. with low TOC contents (<0.5 %) are especially susceptible to the mineral-matrix effect. This effect leads to an overestimation of the terrestrial input and the gas-prone character.

In this study, some inconsistencies in the assessment of kerogen type and thermal maturity of the Yacoraite Fm. were explained to be the consequence of radiation effects. Radiation alters the organo-geochemical properties based on kerogen in whole-rock analysis (Rock-Eval pyrolysis, Py-GC, organic petrography), which may result in an overestimation of the terrestrial organic-matter input, the gas-prone character, and thermal maturity. Despite the lower amount of bitumen compared to kerogen, the study highlighted the presence of n-alkyl moieties and isoprenoids in the bitumen fraction (GC-FID) that were not detected in kerogen (Py-GC). Kerogen typing based on pristane/n-C_{17} and phytane/n-C_{18} ratios provided results in agreement with the organic-matter composition, as seen by the results of organic petrography. In this study the ratios of Pr/n-C_{17} vs. Ph/n-C_{18} in the highly-irradiated sample are in the range of immature to early mature samples. This suggests the utility of Pr/n-C_{17} vs. Ph/n-C_{18}

ratios in the assessment of kerogen type of samples highly-affected by radiation and to constrain their thermal maturity.

For the assessment of the Yacoraite Fm. in the context of hydrocarbon exploration, the radiation effect on organo-geochemical parameters is of minor importance, but one sample at the base of the Yacoraite Fm. deserves special attention in this regard due the pronounced effects caused by a high uranium content of 4400 ppm. The results obtained have important practical implications in petroleum exploration, particularly in evaluations regarding the organic-matter behavior in samples that have been exposed to high amounts of radiation. Further work needs to be done to understand the mechanisms and the response of different portions of organic matter (bitumen and kerogen) with respect to radiation.

Contributions to the understanding of the petroleum system in the Lomas de Olmedo sub-basin

Today, the Lomas de Olmedo sub-basin is the most productive sub-basin in the Salta rift basin, with the Cretaceous Yacoraite Fm. and the Devonian Los Monos Fm. as the main source rocks. Based on the interpretation of the depositional environment and age assignment, the produced oils from the Caimancito oil field and Well-10 (Martinez del Tineo oil field) and the oil seep samples (except d), were sourced from the Yacoraite Fm. Partial correlation with this formation was established for the produced oils of Well-18 and Chirete x100-1, as well as the oil seep sample (d).

The absence of depositional environment-, age-, and thermal maturity- diagnostic biomarkers did not allow for an assessment of the produced oils of Well-11 and Río Pescado. Samples from these locations were differentiated from the other oils based on their higher concentrations of the thermally resistant methyladamantanes (1- + 2-) and methyldiamantanes (3- + 4-). The use of these compounds enables ones to deconvolve oil mixtures and provide additional information to improve the estimation concerning the oil-budget in NW Argentina. The Well-11 sample serves as a model for this purpose. Initially, its stigmastane content and the comparatively higher concentrations of methyldiamantanes (3- + 4-), suggested the presence of two oils with different thermal maturity. Light hydrocarbon parameters (Halpern, 1995) indicate the affinity of the low-maturity member to the produced oil of Caimancito-21 and therefore its genetic link to the Yacoraite Fm. The produced oil of Well-11 has higher concentration of the mentioned methyladamantanes and methyldiamantanes compared to any of the produced oils from the Caimancito block in this study. Therefore, it is unlikely that the Yacoraite Fm. was the source rock of the relatively high-mature oil member. This member was sourced from a more-mature source rock than the Yacoraite Fm. which likely was the Devonian Los Monos Fm. The results of this dissertation contribute to the establishment of the specific baseline of methyldiamantanes (3- + 4-) concentrations of produced oils in NW Argentina. More data is needed, however, to define an accurate baseline and to identify possible oil mixtures. This also provides a framework to re-evaluate the thermal maturity of the highly biodegraded oil seep samples. Future contributions to the differentiation of the oils generated from different source rocks will allow to better understand their contributions to the oil-budget.

9. References

Abas, N., Kalair, A., Khan, N., 2015. Review of fossils fuels and future energy technologies. Futures 69, 31-49.

Acharya, S.S., Chakrabarti, R., 2019. Variations in trace metal concentrations and Sr, Nd isotopic compositions in sediments from two contrasting settings in the Eastern Arabian Shelf: Implications for provenance and paleoclimate reconstruction. Chemical Geology 509, 134-151.

Alcañiz, J., Romera, J., Comellas, L., Munne, R., Puigbo, A., 1989. Effects of some mineral matrices on flash pyrolysis-GC of soils humic substances. The science of the Total Environment 81/82, 81-90.

Allmendinger, R.W., Ramos, V.A., Jordan, T.E., Palma, M., Isacks, B.L. 1983., Paleogeography and Andean structural geometry, northwest Argentina. Tectonics 2, 1-16.

Alonso, R.N., 1980. Icnitas de dinosaurios (Ornithopoda, Hadrosauridae) en el Cretácico Superior del Norte de Argentina. Argentina. Acta Geologica Lilloana 15, 55-63.

Alonso, R., 2018. 'Lola Mora y su filosofía del esquisto'. *El Tribuno newspaper*, Salta, April 23.

Alvarez, L.A., 1999. Geología de hidrocarburos en el noreste Argentino. Contribución para el relatorio del XIV congreso geológico argentino. Tema: Hidrocarburos Tomo II, pp. 27-36. Salta, Argentina.

Araujo, P.L.B., Mansoori, G.A., Araujo, E.S., 2012. Diamondoids: occurrence in fossil fuels, applications in petroleum exploration and fouling in petroleum production. A review paper. Int. J. Oil, Gas and Coal Technology 5, 316-367.

Arnous, A., Zeckra, M., Venerdini, A., Alvarado, P., Arrowsmith, R., Guillemoteau, J., Landgraf, A., Gutiérrez, A., Strecker, M.R., 2020. Neotectonic activity in the low-strain broken foreland (Santa Bárbara System) of the north-western Argentinean Andes, (26S). Lithosphere, 1-25.

Barker, C.E., 1974. Pyrolysis techniques for source rock evaluation. AAPG Bulletin 58, 2349-2361.

Barker, C.E., Pawlewicz, M.J., 1994. Calculation of vitrinite reflectance from thermal histories and peak temperatures. A comparison of methods, In: Mukhopadhyay, P.K., Dow, W.G. (Eds.), Vitrinite reflectance as a maturity parameter: Applications and limitations. American Chemical Society, Symposium Series 570, Chicago, Illinois, pp. 216-229.

Becker, T., Summa, L., Ducea, M., Karner, G., 2015. Temporal growth of the Puna Plateau and its bearing on the post-Salta Rift system subsidence of the Andean foreland basin at 25°30'S, In: DeCelles, P.G., Ducea, M.N., Carrapa, B., Kapp, P.A. (Eds.), Geodynamics of a Cordilleran Orogenic System: The Central Andes of Argentina and Northern Chile. Geological Society of America Memoir 212, pp. 407-433.

Béhar, F., Vandenbroucke, M., 1987. Chemical modelling of kerogens. Organic Geochemistry 11, 15-24.

Berner, R.A., Raiswell, R., 1984. C/S method for distinguishing freshwater from marine sedimentary rocks. Geology 12, 365-368.

Boll, A., Hernández, R., 1986. Interpretación estructural del área Tres Cruces. Boletín de Informaciones Petroleras 7, 2-14.

Bohacs, K.M., Carroll, A.R., Neal, J.E. and Mankiewicz, P.J., 2000. Lake-basin type, source potential, and hydrocarbon character: an integrated-sequence-stratigraphic-geochemical framework, In: Gierlowski-Kordesch, E.H., Kelts, K.R. (Eds.), Lake Basins through Space and Time. AAPG Studies in Geology 46, 3-34.

Bond, M., López, G.M., 1995. Los mamíferos de la Formación Casa Grande (Eoceno) de la Provincia de Jujuy, Argentina. Ameghiniana 32, 301-309.

Braun, R.L., Burnham, A.K., 1992. PMOD: A flexible model of oil and gas generation, cracking, and expulsion. Organic Geochemistry 19, 161-172.

Brooks, J.D., Gould, K., Smith, J.W., 1969. Isoprenoid hydrocarbons in coal and petroleum. Nature 222, 257-259.

Burke, K., Dewey, J., 1973. Plume-generated triple junctions: Key indicators in applying plate tectonics to older rocks. Journal of Geology 81, 406-433.

Canuel, E.A., Hardison, A.K., 2018. Carbon Cycle, In: White, W.M., Casey, W.H., Marty, B., Yurimoto, H. (Eds.), Encyclopedia of Geochemistry Vol.1, pp. 191-194.

Carr, A.D., Williamson, J.E., 1990. The relationship between aromaticity, vitrinite reflectance and maceral composition of coals: Implications for the use of vitrinite reflectance as a maturation parameter. Adv. in Org. Geochem. 16, 313-323

Carrera, N., Muñoz, J.A., Sàbat, F., Mon, R., Roca, E., 2006. The role of inversion tectonics in the structure of the Cordillera oriental (NW Argentinean Andes). Journal of Structural Geology 28, 1921-1932.

Carrol, A.R., Bohacs, K.M., 2001. Lake-type controls on petroleum source rock potential in nonmarine basins. AAPG Bulletin 85, 1033-1053.

Casanova, J., 1986. East African rift stromatolites, In: Frostick, L.E., Renault, R.W., Reid, I., Tiercelin, J.J (Eds.), Sedimentation in the African rifts. Geological Society Special Publication 25, Blackwell, Oxford, pp 201-210.

Cesaretti, N.N., Parnell, J., Dominguez, E.A., 2000. Pore fluid evolution within a hydrocarbon reservoir: Yacoraite Formation (Upper Cretaceous), northwest Basin, Argentina. Journal of Petroleum Geology 23, 375-398.

Chamley, H., 1989. Clay Sedimentology. Springer-Verlag, Berlin, 623 pp.

Cheng, A.L., Huang, W.L., 2004. Selective adsorption of hydrocarbons gases on clays and organic matter. Organic Geochemistry 35, 413-423.

Claxton, M., Patience, R., Park, P., 1993. Molecular modelling of bond energies in potential kerogen subunits. Conference paper. Extended abstracts of the 16th International meeting on organic geochemistry Falch Hurtigtrykk. Oslo, Stavanger, pp. 198-201.

Clementz, D.M., 1979. Effect of oil and bitumen saturation on source-rock pyrolysis: AAPG Bulletin 63, 2227-2232.

Cohen, A.S., Talbot, M.R., Awramik, S.M., Abell, P., 1997. Lake level and paleoenvironmental history of Lake Tanganyika, Africa, as inferred from Late Holocene and modern stromatolites. Geological Society of America Bulletin 109, 444-460.

Coira, B., Kay, S.M., 1993. Implications of Quaternary volcanism at Cerro Tuzgle for crustal and mantle evolution of the Puna Plateau, Central Andes, Argentina. Contributions to Mineralogy and Petrology 113, 40-58.

Collell, J., Ungerer, P., Galliero, G., Yiannourakou, M., Montel, F., Pujol, M., 2014. Molecular simulation of bulk organic matter in Type II shales in the middle of the oil formation window. Energy & Fuels 28, 7457-7466.

Cónsole-Gonella., Griffin, M., Cione, A., Gouiric Cavalli, S., Aceñolaza, F.G., 2012. Paleontología de la Formación Yacoraite (Maastrichtiano-Daniano) en el ámbito de la Subcuenca de Tres Cruces, Cordillera Oriental de la Provincia de Jujuy, Argentina. XIII Reunión Argentina de Sedimentología, Relatorio. Salta, pp. 45-56.

Cónsole-Gonella, C.A, Marquillas, R.A., 2014. Bioclaustration trace fossils in epeiric shallow marine stromatolites: The Cretaceous-Palaeogene Yacoraite Formation, Northwestern Argentina. Lethaia 47, 107-119.

Cónsole-Gonella, C.A, de Valais, S., Marquillas, R.A., Sánchez, M,C., 2017. The Maastrichtian-Danian Maimará tracksite (Yacoraite Formation, Salta Group), Quebrada de Humahuaca, Argentina: environments and ichnofacies implications. Palaeogeography, Palaeoclimatology, Palaeoecology 468, 327-350.

Cornford, C., Gardner, P., Burges, C., 1998. Geochemical truths in large data sets, I: geochemical screening data. Organic Geochemistry 29, 519-530.

Coutand, I., Cobbold, P.R., Urreiztieta, M., Gautier, P., Chauvin, A., Gapais, D., Rossello, E., López-Gamundi, O., 2001. Style and history of Andean deformation, Puna plateau, northwestern Argentina. Tectonics 20, 210-234.

Cristallini, E., Cominguez, A.H., Ramos, V.A., 1997. Deep structure of the Metan-Guachipas region: tectonic inversion in Northwestern Argentina. Journal of South American Earth Sciences 10, 403-421.

Cruz, C.E., Sylwany, C.A., Villar, H.J., 2002. La cuenca de Tarija, Bolivia y noroeste de Argentina: ¿sistema petrolero único o múltiples sistemas petroleros?, In: Instituto Argentino del petróleo y del gas. (Ed.), V Congreso de exploración y desarrollo de hidrocarburos, pp. 1-19.

Cruz, C.E., Veramendi, J.O., Benedetto, M.D., Pereira, M., Villar, H.J., 2008. Los sistemas petroleros Devónicos del subandino sur y pie de monte de la cuenca de Tarija, Bolivia, In: Cruz, C.E., Rodríguez,

J.F., Hechem, J.J., Villar, H.J. (Eds.), VII Congreso de exploración y desarrollo de hidrocarburos. Instituto Argentino del petróleo y del gas. Buenos Aires, pp. 159-187.

Curiale, J.A., 2008. Oil-source rock correlations – Limitations and recommendations. Organic Geochemistry 39, 1150-1161.

Dahl, B., Bojesen-Koefoed, J., Holm, A., Justwan, H., Rasmussen, E., Thomsen, E., 2004. A new approach to interpreting Rock-Eval S_2 and TOC data for kerogen quality assessment, Organic Geochemistry 35, 1461-1477.

Dahl, J., Hallberg, R., Kaplan, I., 1988. The effects of radioactive decay of uranium on elemental and isotopic ratios of Alum Shale kerogen. Applied Geochemistry 3, 583-589.

Dahl, J.E., Moldowan, J.M., Peters, K.E., Claypool, G.E., Rooney, M.A., Michael, G.E., Mello, M.R., Kohnen, M.L., 1999. Diamondoid hydrocarbons as indicators of natural oil cracking. Nature 399, 54-57.

D'Ambrosio, A., Lipparini, L., Bigi, S., Cassola, T., Bambridge, V.R., Derks, J.F., Trippetta, F., 2021. Structural restoration and basin modelling of the central apennine orogen/foredeep/foreland system: New insights on the regional petroleum system. Marine and Petroleum Geology 127, 1-20.

Danesh, A., 1998. PVT and phase behavior of petroleum reservoir fluids. First edition, Elsevier, Amsterdam 400 pp.

DeCelles, P.G., Carrapa, B., Horton, B.K., Gehrels, G.E., 2011. Cenozoic foreland basin system in the central Andes of northwestern Argentina: Implications for Andean geodynamics and modes of deformation. Tectonics 30, 1-30.

De Groot, K., 1965. Inorganic Precipitation of calcium carbonate from sea-water. Nature 207, 404-405.

de Leeuw, J.W., Largeau, C., 1993. A review of macromolecular organic compounds that comprise living organisms and their role in kerogen, coal and petroleum formation, In: Engel, M.H., Macko, S.A. (Eds.), Organic Geochemistry, Principles and Applications. Plenum Press, New York, pp. 23-72.

del Papa, C.E., Salfity, J.A., 1999. Non-marine Paleogene sequences, Salta Group, Northwest Argentina. Acta Geológica Hispánica 34, 105-121.

Delvaux, D., Martin, H., Leplat, P., Paulet, J., 1989. Comparative Rock-Eval pyrolysis as an improved tool for sedimentary organic matter analysis. Organic Geochemistry 16, 1221-1229

Demaison, G.J., Moore, G.T., 1980. Anoxic environments and oil source bed genesis. AAPG Bulletin 64, 1179-1209.

Dembicki, H., 2009. Three common source rock evaluation errors made by geologists during prospect or play appraisals. AAPG Bulletin 93, 341-356.

Dembicki, H., Horsfield, B., Ho, T.T.Y., 1983. Source rock evaluation by pyrolysis-gas chromatography. AAPG Bulletin 67, 1094-1103.

Deschamps, R., Rohais, S., Hamon, Y., Gasparrini, M., 2020. Dynamic of a lacustrine sedimentary system during late rifting at the Cretaceous–Palaeocene transition: Example of the Yacoraite Formation, Salta Basin, Argentina. The Depositional Record 6, 1-4.

di Pasquo, M., 2007. Asociaciones palinológicas en las formaciones Los Monos (Devónico) e Itacua (Carbonífero Inferior) en Balapuca (Cuenca Tarija), sur de Bolivia. Parte 1. Formación Los Monos. Revista Geológica de Chile 34, 97-137.

di Pasquo, M., Noetinger, S., Isaacson, P., Grader, G., Starck, D., Morel, E., Folnagy, H.A., 2015. Mid-Late Devonian assemblages of herbaceous lycophytes from northern Argentina and Bolivia: Age assessment with palynomorphs and invertebrates and paleobiogeographic importance. Journal of South American Earth Sciences 63, 70-83.

di Primio., R., Horsfield, B., 1996. Predicting the generation of heavy oils in carbonates/evaporitic environments using pyrolysis methods. Organic Geochemistry 24, 999-1016.

di Primio, R., Horsfield, B., 2006. From petroleum-type organofacies to hydrocarbon phase prediction. AAPG Bulletin 90, 1031-1058.

di Primio, R., Dieckmann, V., Mills, N., 1998. PVT and phase behavior analysis in petroleum exploration. Organic Geochemistry 29, 207-222.

Dieckmann, V., Schenk, H.J., Horsfield, B., Welte, D.H., 1998. Kinetics of petroleum generation and cracking by programmed-temperature closed-system pyrolysis of Toarcian Shales. Fuel 77, 23-31.

Disalvo, A., 2002. Cuenca del Noroeste: Marco geológico y reseña histórica de la actividad petrolera., In: Schiuma, M., Hinterwimmer, G., Vergani, G. (Eds.), Rocas reservorio de las cuencas productivas de la Argentina. V Congreso de exploración y desarrollo de hidrocarburos, pp. 663-677.

Disalvo, A., Rodríguez- Schelotto, M.L., Gómez-Omil, R., Hoffman, C., Benítez, J., Hurtado, S., 2002. Los reservorios de la Formación Yacoraite, In: Schiuma, M., Hinterwimmer, G., Vergani, G. (Eds.), Rocas reservorio de las cuencas productivas de la Argentina. V Congreso de exploración y desarrollo de hidrocarburos, pp. 717-738.

Do Campo, M., Bauluz, B., del Papa, C., White, T., Yuste, A., Mayayo, M.J., 2018. Evidence of cyclic changes recorded in clay minerals assemblages from a continental Paleocene-Eocene sequence, northwestern Argentina. Sedimentary Geology 368, 44-57.

Dow, W.G., 1977. Kerogen Studies and Geological Interpretations. Journal of Geochemical Exploration 7, 77-99.

Doyle, A., Donoghue, M.J., 1993. Phylogenies and angiosperm diversification. Paleobiology 19, 141-167.

Durand, B., Monin, J.C., 1980. Elemental analysis of kerogens (C, H, 0, N, S, Fe), In: Durand, B. (Ed.), Kerogen. Editions Technip, Paris, pp. 113-142.

Eglinton, T.I., Sinninghe-Damsté, J.S., Kohnen, M.E.L., de Leeuw, J.W., Larter, S.R., Patience, R.L., 1990. Analysis of maturity-related changes in the organic sulphur composition of kerogens by flash pyrolysis-gas chromatography, In: Orr, W.L., White, C.M. (Eds.), Geochemistry of sulfur in Fossils Fuels. American Chemical Society, Chicago, Illinois, pp. 529-565.

Eglizaud, N., Miserque, F., Simoni, E., Schlegel, M., Descostes, M., 2006. Uranium (VI) interaction with pyrite (FeS_2): Chemical and spectroscopic studies. Radiochimica Acta 94, 651-656.

Entrocassi, G.S., Hormigo, D.F., Gavilán, R.G., Sánchez-Mata, D., 2014. Bioclimatic typology of Jujuy Province (Argentina). LAZAROA 35, 7-18.

Eseme, E., Littke, R., Krooss, B.M., Schwarzbauer, J., 2007. Experimental investigation of the compositional variation of petroleum during primary migration. Organic Geochemistry 38, 1373-1397.

Espitalié, J., 1986. Use of Tmax as a maturation Index for different types of organic matter. Comparison with vitrinite reflectance, In: Burrus, J. (Ed.), Thermal Modelling in Sedimentary Basins. Editions Technip, Paris, pp. 475-496.

Espitalié, J., Deroo, G., Marquis, F., 1985. La pyrolyse Rock-Eval et ses applications. Deuxieme partie. Rev. Inst. Fr. Pétr. 40, 775-784.

Espitalié, J., Laporte, J.L., Madec, M., Marquis, F., Leplat, P., Paulet, J., Boutefeu, A., 1977. Méthode rapide de caractérisation des roches méres, de leur potential pétrolier et de leur degré d'évolution. Rev. Inst. Fr. Pétr. 32, 23-42.

Espitalié, J., Madec, M., Tissot, B., 1980. Role of mineral matrix in kerogen pyrolysis: influence on petroleum generation and migration: AAPG Bulletin 64, 59-66.

Espitalié, J., Makadi, K.S., Trichet, J., 1984. Role of the mineral matrix during kerogen pyrolysis. Organic Geochemistry 6, 365-382.

Fang, R., Littke, R., Zieger, L., Baniasad, A., Li, M., Schwarzbauer, J., 2019. Changes of composition and content of tricyclic terpane, hopane, sterane, and aromatic biomarkers throughout the oil window: A detailed study on maturity parameters of Lower Toarcian Posidonia Shale of the Hils Syncline, NW Germany. Organic Geochemistry 138, 1-19.

Ferreira, L.C., Molina-Castillo, J.I., Alfaro, L., Gorustovich, S., Guidi, F., 2013. Geología y metalogenia del uranio en la comarca Acosta, departamento Guachipas, Salta. Revista de la Asociación Argentina 70, 366-376.

Fisher, S.J., Alexander, R., Kagi, R.I., Oliver, G.A., 1998. Aromatic hydrocarbons as indicators of biodegradation in north Western Australian reservoirs, In: Purcell, P. G., Purcell, R.R. (Eds.), Sedimentary Basins of Western Australia: West Australian Basins Symposium. Petroleum Exploration Society of Australia, pp. 185-194.

França, A.B., Milani, E.J., Schneider, R.L., López-Paulsen, O., López, M.J., Suárez-Soruco, R., Santa-Ana, H., Weins, F., Ferreiro, O., Rossello, E.A., Bianucci, H.A., Aramayo-Flores, R.F., Vistalli, M.C., Fernández-Seveso, F.A., Fuenzalida, R.P., Muñoz, N., 1995. Phanerozoic correlations in Southern South America, In: Tankard, A.J., Suárez-Soruco, R., Welsink, H.J. (Eds.), Petroleum basins of South America. AAPG Memoir 62, Tulsa, pp. 129-161.

Galliski, M.A., Viramonte, J.G., 1988. The Cretaceous paleorift in northwestern Argentina: A petrologic approach. Journal of South American Earth Sciences 63, 329-342.

Garzione, C.N., McQuarrie, N., Perez, N.D., Ehlers, T.A., Beck, S.L., Kar, N., Eichelberger, N., Chapman, A.D., Ward, K.M., Ducea, M.N., Lease, R.O., Poulsen, C.J., Wagner, L.S., Saylor, J.E., Zandt, G., Horton, B.K., 2017. Tectonic evolution of the Central Andean plateau and implications for the growth of plateaus. Annual Review Earth Planetary Sciences 45, 529‑559.

Gasparik, M., Bertier, P., Gensterblum, Y., Ghanizadeg, A., Kross, B.M., Littke, R., 2014. Geological controls on the methane storage capacity in organic-rich shales. International Journal of Coal Geology 123, 34-51.

Gebicki, S., Gebicki, J.M., 1993. Formation of peroxides in amino acids and proteins exposed to oxygen free radicals. Biochememical Journal 289, 743-749.

Gomes, J.P., Bunevich, R.B., Tonietto, S.N., Alves, D.V., Santos, J.F., Whitaker, F.F., 2020. Climatic signals in lacustrine deposits of the Upper Yacoraite Formation, Western Argentina: Evidence from clay minerals, analcime, dolomite and fibrous calcite. Sedimentology 67, 2282-2309.

Grantham, P.J., 1986. Sterane isomerisation and moretane/hopane ratios in crude oils derived from Tertiary source rocks. Organic Geochemistry 9, 293-304.

Grantham, P.J., Wakefield, L.L., 1988. Variations in the sterane carbon number distributions of marine source rock derived crude oils through geological time. Organic Geochemistry 12, 61-73.

Grice, K., Alexander, R., Kagi, R.I., 2000. Diamondoid hydrocarbon ratios as indicators of biodegradation in Australian crude oils. Organic Geochemistry 31, 67-73.

Grier, M.E., Salfity, F.A., Allmendinger, R.W., 1991. Andean reactivation of the Cretaceous Salta rift, northwestern Argentina. Journal of South American Earth Sciences 4, 351-372.

Grosso, S., López, R., Vergani, G., O'Leary, S., 2013. Reservorios carbonáticos naturalmente fracturados en el yacimiento Caimancito (Formación Yacoraite), cuenca Cretácica del noroeste Argentino. Revista de la Asociación Geológica Argentina 7, 53-69.

Halpern, H.I., 1995. Development and applications of light-hydrocarbon-based star diagrams. AAPG Bulletin 79, 801-815.

Han, Y., Mahlstedt, N., Horsfield, B., 2015. The Barnett Shale: Compositional fractionation associated with intraformational petroleum migration, retention, and expulsión. AAPG Bulletin 99, 2173-2202.

Hartkopf-Fröder, C., Königshof, P., Littke, R., Schwarzbauer, J., 2015. Optical thermal maturity parameters and organic geochemical alteration at low grade diagenesis to anchimetamorphism: A review. International Journal of Coal Geology 150-151, 74-119.

Hartley, A.J., 1993. Sedimentological Response of an Alluvial System to Source Area Tectonism: The Seilao Member of the Late Cretaceous to Eocene Purilactis Formation of Northern Chile. Spec. Pub. Int. Ass. Sediment. 17, 489-500.

Hartwig, A., di Primio, R., Anka, Z., Horsfield, B., 2012. Source rock characteristics and compositional kinetic models of Cretaceous organic rich black shales offshore southwestern Africa. Organic Geochemistry 51, 17-34.

Hatcher, P.G., Wenzel, K.A., Cody, G.D., 1994. Coalification reactions of vitrinite derived from coalified wood, In: Mukhopadhyay, P.K., Dow, W.G. (Eds.), Vitrinite Reflectance as a Maturity Parameter: Applications and Limitations. American Chemical Society, Series 570, Chicago, Illinois, pp. 112-135.

He, C., Ji, L., Su, A., Wu, Y., Zhang, M., Zhou, S., Li, J., Hao, L., Ma, Y., 2019. Source-rock evaluation and depositional environment of black shales in the Triassic Yanchang Formation, southern Ordos Basin, north-central China. Journal of Petroleum Science and Engineering 173, 899-911.

Henry, S., Pollack, H.N., 1988. Terrestrial heat flow above the Andean subduction zone in Bolivia and Peru. Journal of Geophysical Research 93, 15.153-15.162.

Herlinger, R.JR., Zambonato, E.E., De Ros, L.F., 2017. Influence of diagenesis on the quality of lower Cretaceous Pre-Salt lacustrine carbonate reservoirs from northern Campos Basin, offshore Brasil. Journal of Sedimentary Research 87, 1285-1313.

Hernández, R., Gómez-Omil, R., Boll, A., 2008. Estratigrafía, tectónica y potencial petrolero del rift Cretácico en la Provincia de Jujuy, In: Coira, B., Zappettini, E. (Eds.), Geología de la Provincia de Jujuy, Relatorio del XVII Congreso Geológico Argentino, pp. 207-232.

Herrera, C.M., Powell, J., del Papa., 2012. Un nuevo Dasypodidae (Mammalia, Xenarthra) de la Formación Casa Grande (Eoceno) de la Provincia de Jujuy, Argentina. Ameghiniana 49, 267-271.

Hillaire-Marcel, C., Carro, O., Casanova, J., 1986. ^{14}C and Th/U Dating of Pleistocene and Holocene stromatolites from east African paleolakes. Quaternary Research 25, 312-329

Holba, A.G., Dzou, L.I.P., Masterson, W.D., 1998. Application of 24-norcholestanes for constraining source age of petroleum. Organic Geochemistry 29, 1269-1283.

Hongn, F., del Papa, C., Powell, J., Payrola, P., Petrinovic, I., & Mon, R.., 2011. Fragmented Paleogene foreland basin in the Valles Calchaquíes, NW of Argentina, In: Salfity, J.A., Marquillas, R.A. (Eds.), Cenozoic Geology of the Central Andes of Argentina. Salta: SCS Publisher, pp. 189-209.

Horsfield, B., 1984. Pyrolysis studies and petroleum exploration. Adv. in Petrol. Geochem 1, 247-298.

Horsfield, B., 1989. Practical Criteria for Classifying Kerogens: Some observations from pyrolysis-gas chromatography, Geochimica et Cosmochimica Acta 53, 891-901.

Horsfield, B., 1997. The bulk composition of first-formed petroleum in source rocks, In: Welte, D.H., Horsfield, B., Baker, D.R. (Eds.), Petroleum and basin evolution. Springer-Verlag, Berlin, pp. 335-402.

Horsfield B., Bharati S. and Larter S. R., 1992a. On the atypical petroleum-generating characteristics of alginite in the Cambrian Alum Shale, In: Schidlowski, M., Golubic, S., Kimberley, M.M., Sr, D.M.M., Trudinger P.A. (Eds.), Early Organic Evolution. Springer, Berlin Heidelberg, pp. 257-266.

Horsfield, B., Schenk, H.J., Mills, N. and Welte, D.H., 1992b. An investigation of the in-reservoir conversion of oil to gas: compositional and kinetic findings from closed-system programmed-temperature pyrolysis. Organic Geochemistry 19, 191-204.

Horsfield, B., Curry D.J., Bohacs, K., Littke, R., Rullkötter, J., Schenk, H.J., Radke, M., Schaefer, R.G., Carroll, A.R., Isaksen, G., Witte, E.G., 1994. Organic geochemistry of freshwater and alkaline lacustrine environments, Green River Shale of the Washakie Basin, Wyoming. Organic Geochemistry 22, 415-440.

Horsfield B., Düppenbecker, S.J., Schenk, H.J., Schaefer, R.G., 1993. Kerogen typing concepts designed for the quantitative geochemical evaluation of petroleum potential, In: Doré, A.G., Augustson J.H., Hermanrud C., Steward D.J., Sylta O. (Eds.), Basin modelling: Advances and applications. Norwegian Petroleum Society Special Publication 3, pp. 243-249.

Horsfield, B., Leistner, F., Hall, K., 2015. Chapter 7: Microscale sealed vessel pyrolysis, In: Grice, K. (Ed.), Principles and practice of analytical techniques in geosciences. Royal Society of Chemistry, Cambridge, pp. 209-241.

Horton, B.K., 2018. Tectonic regimes of the Central and Southern Andes: Responses to variations in plate coupling during subduction. Tectonics, 37, 402–429.

Hosseini, S.H., Horsfield, B., Poetz, S., Wilkes, H., Yalçın, M.N., Kavak, O., 2017. Role of maturity in controlling the composition of solid bitumens in veins and vugs from SE Turkey as revealed by conventional and advanced geochemical tools. Energy & Fuels 31, 2398-2413.

Huang, H., 2017. The effect of biodegradation on gammacerane in crude oils. Biodegradation 28, 313-326.

Huang, W.Y., Meinschein, W., 1979. Sterols as ecological indicators. Geochimica et Cosmochimica Acta 43, 739-745.

Huang, D., Li. J., Zhang, D., 1990. Maturation sequence of continental crude oils in hydrocarbon basins in China and its significance. Organic Geochemistry 16, 521-529.

Hughes, W.B., Holba, A.G., Dzou, L.P., 1995. The ratios of dibenzothiophene to phenanthrene and pristane to phytane as indicators of depositional environment and lithology of petroleum source rocks. Geochimica et Cosmochimica Acta 59, 3581-3598.

Iaffa, D.N., Sàbat, F., Bello, D., Ferrer, O., Mon, R., Gutierrez, A.A., 2011. Tectonic inversion in a segmented foreland basin from extensional to piggy back settings: The Tucumán basin in NW Argentina. Journal of South American Earth Sciences 31, 457-474.

Iaffa, D.N., Sàbat, F., Muñoz, J.A., Carrera, N., 2013. Basin fragmentation controlled by tectonic inversion and basement uplift in Sierras Pampeanas and Santa Bárbara System, Northwest Argentina, In: Nemčok, M., Mora, A., Cosgrove, J. W. (Eds.), Thick-Skin-Dominated Orogens: From Initial Inversion to Full Accretion. Geological Society, London, Special Publications 377, pp. 101-117.

Jaboyedoff, M., Bussy, F., Kübler, B., Thelin, Ph., 2001. Illite "cristallinity" revised. Clays and clay Minerals 49, 156-167.

Jaraula, C.M.B., Schwark, L., Moreau, X., Pickel, W., Bagas, L., Grice, K., 2015. Radiolytic alteration of biopolymers in the Mulga Rock (Australia) uranium deposit. Applied Geochemistry 52, 97-108.

Jarvie, D.M., Claxton, B.L., Henk, F., Breyer, J.T., 2001. Oil and Shale Gas from the Barnett Shale, Ft. Worth Basin, Texas. Abstract. AAPG National Convention, Denver, p. A100.

Jordan, T.E., Alonso, R.N., 1987. Cenozoic stratigraphy and basins tectonics of the Andes mountains, 20 °-28 ° south latitude: AAPG Bulletin 71, 49-64.

Jordan, T, E., Isacks, B., Allmendinger, R., Brewer, J., Ando, C., Ramos, V.A., 1983. Andean tectonics related to geometry of subducted plates. Geological Society America, Bulletin 94, 341-361.

Katz, B.J., 1983. Limitations of "Rock-Eval" pyrolysis for typing organic matter. Organic Geochemistry 4, 195-199.

Katz, B.J., Mancini, E.A., Kitchka, A.A., 2008. 'A review and technical summary of the AAPG Hedberg research conference on origin of petroleum biogenic and/or abiogenic and its significance in hydrocarbon exploration and production'. AAPG Bulletin 92, 549-556.

Kelemen, S.R., Afeworki, M., Gorbaty, M.L., Sansone, M., Kwiatek, P.J., Walters, C.C., Freund, H., Siskin, M., 2007. Direct Characterization of Kerogen by X-ray and Solid-State ^{13}C Nuclear Magnetic Resonance Methods. Energy & Fuels 21, 1548-1561.

Keller, G., Abramovich, S., 2009. Lilliput effect in late Maastrichtian planktic foraminifera: Response to environmental stress. Palaeogeography, Palaeoclimatology, Palaeoecology 284, 47-62.

Keller, G., Punekar, J., Mateo, P., 2016. Upheavals during the Late Maastrichtian: Volcanism, climate and faunal events preceding the end-Cretaceous mass extinction. Palaeogeography, Palaeoclimatology, Palaeoecology 441, 137-151.

Kelts, K., 1988. Environments of deposition of lacustrine petroleum source rocks: an introduction, In: Fleet, A.J., Kelts, K., Talbot, M.R. (Eds.), Lacustrine Petroleum Source Rocks, Geological Society Special Publication 40, pp. 3-26.

Killops, S.D., All-Juboori, M.A.H.A., 1990. Characterization of the unresolved complex mixture (UCM) in the gas chromatograms of biodegraded petroleums. Organic Geochemistry 15, 147-160.

Kley, J., Rossello, E.A., Monaldi, C.R., Habighorst, B., 2005. Seismic and field evidence for selective inversion of Cretaceous normal faults, Salta rift, northwest Argentina. Tectonophysics 399, 155-172.

Klinkhammer, G.P., Palmers. M.R., 1991. Uranium in the oceans: Where it goes and why Geochimica et Cosmochimica Acta 55, 1799-1806.

Kübler, B., Jaboyedoff, M., 2000. Illite crystallinity. Earth and Planetary Sciences 331, 75-89.

Lange, R., Staaland, H., Mostad, A., 1972. The effect of salinity and temperature on solubility of oxygen and respiratory rate in oxygen-dependent marine invertebrates. J. Exp, Mar. Biol. Ecol 9, 217-229.

Langford, F., Blanc-Valleron, M., 1990. Interpreting Rock-Eval pyrolysis data using graphs of pyrolizable hydrocarbons vs. total organic carbon. AAPG Bulletin 74, 799-804.

Larter, S., 1988. Some pragmatic perspectives in source rock geochemistry. Marine and Petroleum Geology 5, 194-204.

Leanza, A.F., 1969. Sistema de Salta, sue dad, sus peces voladores, su asincronismo con el horizonte calcáreo-dolomitico y con las calizas de Miraflores y la hibridez del Sistema subandino. Revista de la Asociación Geológica Argentina 4, 393-407.

Lecomte, A., Cathelineau, M., Michels, R., Peiffert, C., Brouand, M., 2017. Uranium mineralization in the Alum Shale Formation (Sweden): Evolution of a U-rich marine black shale from sedimentation to metamorphism. Ore Geology Reviews 88, 71-98.

Legarreta, L., Villar, H.J., 2011. Geological and geochemical keys of the potential shale resources, Argentina basins. Presentation at AAPG Geoscience technology workshop. unconventional resources: Basics, challenges and opportunities for new frontier plays. Buenos Aires, Argentina.

Lehne, E., Dieckmann, V., di Primio, R., Fuhrmann, A., Horsfield, B., 2009. Changes in gas composition during simulated maturation of sulfur rich type II-S source rock and related petroleum asphaltenes, Organic Geochemistry 40, 604-616.

Lewan, M.D., Buchardt, B., 1989. Irradiation of organic matter by uranium decay in the Alum Shale, Sweden. Geochimica et Cosmochimica Acta 53, 1307-1322.

Lewis, S., Henderson, R., Dickens, G., Shields, G., Coxhell, S., 2010. The geochemistry of primary and weathered oil shale and coquina across the Julia Creek vanadium deposit (Queensland, Australia). Mineralium Deposita 45, 599-620.

Li, L., Keller, G., 1998. Maastrichtian climate, productivity and fauna1 turnovers in planktic foraminifera in South Atlantic DSDP sites 525A and 21. Marine Micropaleontology 33, 55-86.

Linnert, C., Mutterlose, J., Herrle, J.O., 2011. Late Cretaceous (Cenomanian–Maastrichtian) calcareous nannofossils from Goban Spur (DSDP Sites 549, 551: Implications for the palaeoceanography of the proto North Atlantic. Palaeogeography, Palaeoclimatology, Palaeoecology 299, 507-528.

Lippmaa, E., Maremäe, E., Pihlak, A.T., 2011. Resources, production and processing of baltoscandian multimetal black shales. Oil Shale 28, 68-77.

Littke, R., Baker, D.R., Rullkötter, J., 1997. Deposition of petroleum source rocks, In: Welte, D.H., Horsfield, B., Baker, D.R. (Eds.), Petroleum and basin evolution. Springer-Verlag, Berlin, pp. 271-333.

Lo, H.B., 1993. Correction criteria for the suppression of vitrinite reflectance in hydrogen- rich kerogens: Preliminary guidelines. Organic Geochemistry 20, 653-657.

Mackenzie, A.S., McKenzie, D., 1983. Isomerization and aromatization of hydrocarbons in sedimentary basins formed by extension. Geological Magazine 120, 417-70.

Mackenzie, A.S., Hoffman, C.F., Maxwell, J.R., 1981. Molecular parameters of maturation in the Toarcian shales, Paris Basin, France. III. Changes in aromatic steroid hydrocarbons. Geochimica et Cosmochimica Acta 45, 2369-2376.

Magoon, L.B, Schmoker, J.W., 2000. The total petroleum system-the natural fluid network that constrains the assessment unit, In: U.S. Geological Survey (Ed.), USGS Digital Data series 60, Reston, 31 pp.

Mahlstedt, N., Horsfield, B., 2012. Metagenetic methane generation in gas shales I. Screening protocols using immature samples. Marine and Petroleum Geology 31, 27-42.

Mahlstedt, N., Horsfield, B., 2019. Thermovaporisation: A screening tool for the gas-sorptive properties of source rocks. Organic Geochemistry 131, 1-4.

Mahlstedt, N., Horsfield, B., di Primio, R., 2013. GORFit – From Liquids to Late Gas: Deconvoluting Primary from Secondary Gas Generation Kinetics. 26th International Meeting on Organic Geochemistry (IMOG), Tenerife, Canary Islands (Spain). Book of Abstracts, p. 193.

Mann, U., Hantschel, T., Schaefer, R.G., Krooss, B., Leythaeuser, D., Littke, R., Sachsenhofer, R.F., 1997. Petroleum Migration: Mechanisms, pathways, efficiencies, and numerical simulations, In: Welte, D.H., Horsfield, B., Baker, D.R. (Eds.), Petroleum and basin evolution. Springer-Verlag, Berlin, pp. 403-509.

Marengo, H.G., 2006, Micropaleontología y estratigrafía del Mioceno marino de la Argentina: las transgresiones de Laguna Paiva y del "Entrerriense-Paranense", PhD thesis, Universidad de Buenos Aires, 123 pp.

Marquillas, R.A., Salfity, J.A., 1988. Tectonic framework and correlations of the Cretaceous-Eocene Salta Group; Argentina, In: Bahlburg, H., Breitkreuz, Ch., Giese, P. (Eds.), The southern central Andes. Springer, Berlín Heidelberg, pp. 119-136.

Marquillas, R.A., del Papa, C., Sabino, I.F., 2005. Sedimentary aspects and paleoenvironmental evolution of a rift basin: Salta Group (Cretaceous–Paleogene), northwestern Argentina. International Journal of Earth Sciences 94, 94-113.

Marquillas, R., Sabino, I., Nobrega-Sial, A., del Papa, C., Ferreira, V., Matthews, S., 2007. Carbon and oxygen isotopes of Maastrichtian-Danian shallow marine carbonates: Yacoraite Formation, northwestern Argentina. Journal of South American Earth Sciences 23, 304-320.

Marquillas, R.A., Salfity, J.A., Matthews, S.J., Matteini, M., Dantas, E., 2011. U-Pb zircon age of the Yacoraite Formation and its significance to the Cretaceous-Tertiary boundary in the Salta Basin, Argentina, In: Salfity, J.A., Marquillas, R.A. (Eds.), Cenozoic geology of the Central Andes of Argentina, Salta. SCS Publ. pp. 227-246.

Marret, R.A., Allmendinger, R.W., Alonso, R.N., Drake, R.E., 1994. Late Cenozoic tectonic evolution of the Puna Plateau and adjacent foreland, northwestern Argentine Andes. Journal of South American Earth Sciences 7, 179-207.

Martin, W., Gierl, A., Saedler, H., 1989. Nature 339, 46-48. Molecular evidence for pre-Cretaceous angiosperm origins.

Martinod, J., Husson, L., Roperch, P., Espurt, N., 2010. Horizontal subduction zones, convergence velocity and the building of the Andes. Earth and Planetary Science Letters 299, 299-309.

McCarthy, K., Rojas, K., Niemann, M., Palmowski, D., Peters, K., Stankiewics, A., 2011. Basic petroleum geochemistry for source rock evaluation. Oilfield Review 23, 32-43.

McGroder, M.F., Lease, R.O., Pearson, D.M., 2015. Along-strike variation in structural styles and hydrocarbon occurrences, Subandean fold-and-thrust belt and inner foreland, Colombia to Argentina, In: DeCelles, P.G., Ducea, M.N., Carrapa, B., Kapp, P.A., (Eds.), Geodynamics of a Cordilleran Orogenic System: The Central Andes of Argentina and Northern Chile: Geological Society of America Memoir 212.

McKirdy, D.M., Hahn, J.H., 1982. The composition of kerogen and hydrocarbons in precambrian rocks, In: Holland, H.D., Schidlowski, M. (Eds.), Mineral deposits and the evolution of the biosphere. Springer-Verlag, Berlin, pp. 123-154.

McKirdy, D.M., McHugh, D.J., Tardi, J.W., 1980. Comparative analysis of stromatolitic and other microbial kerogens by pyrolysis-hydrogen-gas chromatography, In: Trudinger, P.A., Walter, B.J. (Eds.), Biogeochemistry of ancient and modern environments. Springer-Verlag, Berlin, pp. 187-200.

McQuarrie, N., Horton, B.K., Zandt, G., Beck, S., DeCelles, P.G., 2005. Lithospheric evolution of the Andean fold–thrust belt, Bolivia, and the origin of the central Andean plateau. Tectonophysics 399, 15-37.

Merriman, R.J., 2005. Clays and sedimentary basin history. European Journal of Mineralogy 17, 7-20.

Merriman, R.J., Frey. M., 1999. Patterns of very low-grade metamorphism in metapelitic rocks, In: Frey, M., Robinson, D. (Eds.), Low-Grade Metamorphism. Blackwell Science, Oxford, pp. 61-107.

Meyer, C.A., Hippler, D., Lockley, M.G., 2001. The Late Cretaceous vertebrate ichnofacies of Bolivia facts and implications. Asociación Paleontológica Argentina. Publicación Especial 7. VII International Symposium on Mesozoic Terrestrial Ecosystems. Buenos Aires, pp. 133-138.

Moldowan, J.M., Dahl, J., Zinniker, D., Barbanti, S.M., 2015. Underutilized advanced geochemical technologies for oil and gas exploration and production-1. The diamondoids. Journal of Petroleum Science and Engineering 126, 87-96.

Moldowan, J.M., Lee, C.Y., Sundararaman, P., Salvatori, T., Alajbeg, A., Gjukic, B., Demaison, G.J., 1992. Source correlation and maturity assessment of select oils and rocks from the Central Adriatic Basin (Italy and Yugoslavia), In: Moldowan, J.M., Albrecht, P., Philp, R.P. (Eds.), Biological Markers in Sediments and Petroleum. Prentice-Hall, Englewood Cliffs, NJ, pp. 370-401.

Moldowan, J.M., Peters, K.E., Carlson, R.M.K., Schoell, M., Abu-Ali, M.A., 1994a. Diverse applications of petroleum biomarker maturity parameters. Arabian Journal for Science and Engineering 19, 273-98.

Moldowan, J.M., Dahl, J., Huizinga, B.J., Fago, F.J., Hickey, L.J., Peakman, T.M., Taylor. D.W., 1994b. The molecular fossil record of oleanane and its relation to angiosperms. Science 265, 768-71.

Moldowan, J.M., Seifert, W. K., Gallegos, E.J., 1985. Relationship between petroleum composition and depositional environment of petroleum source rocks. AAPG Bulletin 69, 1255-1268.

Moldowan, J.M., Sundararaman, P., Schoell, M., 1986. Sensitivity of biomarker properties to depositional environment and/or source input in the Lower Toarcian of S.W. Germany. Organic Geochemistry 10, 915-26.

Mon, R., Salfity, J.A., 1995. Tectonic evolution of the Andes of northern Argentina, In: Tankard, A.J., Suárez-Soruco, R., Welsink, H.J. (Eds.), Petroleum basins of South America. AAPG Memoir 62, Tulsa, pp. 269-283.

Monaldi, C.R., Salfity, J.A., Kley, J., 2008. Preserved extensional structures in an inverted Cretaceous rift basin, nortwestern Argentina: Outcrop examples and implications for fault reactivation. Tectonics 27, 1-21.

Montero-López, C., Hongn, F., López Steinmetz, R.L., Aramayo, A., Pingel, H., Strecker, M.R., Cottle, J.M., Bianchi, C., 2020. Development of an incipient Paleogene topography between the present-day Eastern Andean Plateau (Puna) and the Eastern Cordillera, southern Central Andes, NW Argentina. Basin Research, 1-24.

Moore, D.M., Reynolds, R.C.Jr., 1997. X-Ray Diffraction and the Identification and analysis of clay minerals, second ed. Oxford, New York, 376 pp.

Moretti, I., Baby, P., Mendez, E., Zubieta, D., 1996. Hydrocarbon generation in relation to thrusting in the Sub Andean zone from 18 to 22°S Bolivia. Petroleum Geoscience 2, 17-28.

Mukhopadhyay, P.K., 1989. Characterization of amorphous and other organic matter types by microscopy and pyrolysis-gas chromatography. Organic Geochemistry 14, 269-284.

Mukhopadhyay, P.K., 1994. Vitrinite reflectance as maturity parameter. Petrographic and molecular characterization and its applications to basin modelling, In: Mukhopadhyay, P.K., Dow, W.G. (Eds.), Vitrinite reflectance as a maturity parameter: Application and Limitations. American Chemical Society, Symposium Series 570, Chicago, Illinois, pp. 1-25.

Muniz, M.C., Bosence, D.W.J., 2018. Lacustrine carbonate platforms: Facies, cycles, and tectonosedimentary models for the presalt Lagoa Feia Group (Lower Cretaceous), Campos Basin, Brazil. AAPG Bulletin 102, 2569-2597.

Murray, R.C., 1964. Origin and diagenesis of gypsum and anhydrite. Journal of Sedimentary Petrology 34, 512-523.

Muscio, G.P.A., Horsfield, B. and Welte, D.H., 1991. Compositional changes in the macromolecular organic matter (kerogens, asphaltenes and resins) of a naturally matured source rock sequence from northern Germany as revealed by pyrolysis methods, In: Manning D.A.C. (Ed.), Organic Geochemistry Advances and Applications in the Natural Environment. Manchester University Press, Manchester and New York, pp. 447-449.

Myrbo, A., 2012. Carbon cycle in lakes, In: Bengtsson L., Herschy R.W., Fairbridge R.W. (Eds.), Encyclopedia of Earth Sciences Series. Springer, Dordrecht, pp. 121-125.

Narváez, P.L., Volkheimer, W., 2011. Palynostratigraphy and paleoclimatic inferences of the Balbuena and Santa Bárbara Subgroups (Salta Group Basin, Cretaceous-Paleogene): Correlation with Patagonian basins, In: Salfity. J.A., Marquillas, R.A. (Eds.), Cenozoic geology of the Central Andes of Argentina. SCS Publisher, Salta, Argentina, pp. 283-300.

Nelson, B.W., 1967. Sedimentary phosphate method for estimating paleosalinities. Science 158, 917-920.

Nesbitt, H.W., Young, G.M., 1982. Early Proterozoic climates and plate motions interred from major element chemistry of lutites. Nature 299, 715-717.

Oncken, O., Hindle, D., Kley, J., Elger, K., Victor, P., Schemmann, K., 2006. Deformation of the central Andean upper plate system-facts, fiction, and constraints for plateau models, In: Oncken O., Chong, O., Franz, G., Giese, P., Götze, H-J., Ramos, V.A., Strecker, M.R., Wigger, P. (Eds.), The Andes: Active subduction orogeny. Springer-Verlag, Berlin, pp. 3-27.

Orr, W.L., 1986. Kerogen/asphaltene/sulfur relationships in sulfur-rich Monterrey oils. Organic Geochemistry 10, 499-516.

Pepper, A.S., Corvi, P.J., 1995. Simple kinetic models of petroleum formation. Part I. oil and gas generation from kerogen. Marine and Petroleum Geology 12, 291-319.

Pepper, A.S., Dodd, T.A., 1995. Simple kinetic models of petroleum formation. Part II: oil -gas cracking. Marine and Petroleum Geology 12, 321-340.

Peters, K.E., 1986. Guidelines for evaluating petroleum source rock using programmed pyrolysis. AAPG Bulletin 70, 318-329.

Peters, K.E., Cassa, M.R., 1994. Applied source rock geochemistry, In: Magoon, L.B., Dow, W.G. (Eds.), The petroleum system-from source to trap. AAPG Memoir 60, pp. 93-120.

Peters, K.E., Clifford, C.W., Moldowan, J.M., 2005a. The biomarker Guide. Vol. 2. Biomarkers and isotopes in petroleum exploration and earth history, second ed. Cambridge University Press, New York, 1155 pp.

Peters, K.E., Moldowan, J.M., 1991. Effects of source, thermal maturity, and biodegradation on the distribution and isomerization of homohopanes in petroleum. Organic Geochemistry 17, 47-61.

Peters, K.E., Ramos, L.S., Zumberge, J.E., Valin, Z.C., Bird, K.J., 2008. De-convoluting mixed crude oil in Prudhoe Bay Field, North Slope, Alaska. Organic Geochemistry 39, 623-645.

Peters, K.E., Walters, C.C., Mankiewicz, P.J., 2005b. Evaluation of kinetic uncertainty in numerical models of petroleum generation. AAPG Bulletin 90, 387-403.

Petrinovic, I.A., Grosse, P., Guzmán, S., Caffe, P.J., 2017. Evolución del volcanismo Cenozoico en la Puna Argentina. Conference paper. Relatorio del XX Congreso Geológico Argentino, pp. 469-483.

Picha, F.J. and Peters, K.E.,1998. Biomarker oil-to-source rock correlation in the Western Carpathians and their foreland, Czech Republic. Petroleum Geoscience 4, 289-302.

Poelchau, H.S., Baker, D.R., Hantschel, Th., Horsfield, B., Wygrala, B., 1997. Basin simulation and the design of the conceptual basin model, In: Welte, D.H., Horsfield, B., Baker, D.R. (Eds.), Petroleum and basin evolution Springer-Verlag, Berlin, pp. 3-70.

Pomar, L., Ward W.C., 1995. Sea-Level Changes, Carbonate Production and Platform Architecture: The Llucmajor platform, Mallorca, Spain, In: Haq, B.U. (Ed.), Sequence Stratigraphy and depositional response to eustatic, tectonic and climatic forcing. Coastal systems and continental margins. Vol. 1, Springer, Dordrecht, pp. 87-112.

Prinz, L., Zieger, L., Littke, R., McCann, T., Lokay, P., Asmus, S., 2017. Syn-and post-depositional sand bodies in lignite–the role of coal analysis in their recognition. A study from the Frimmersdorf Seam, Garzweiler open-cast mine, western Germany. International Journal of Coal Geology 179, 173-186.

Quattrocchio, M.E., Volkheimer, W., Marquillas, R.A., Salfity, J.A., 2005. Palynostratigraphy, palaeobiogeography and evolutionary significance of the Late Senonian and Early Palaeogene palynofloras of the Salta Group, northern Argentina. Revista Española de Micropaleontología 37, 259-272.

Quick, J.C., 1994. Iso-rank variation of vitrinite reflectance and fluorescence intensity, In: Mukhopadhyay, P.K., Dow, W.G. (Eds), Vitrinite reflectance as a maturity parameter: Application and Limitations. American Chemical Society, Symposium Series 570, Chicago, Illinois, pp. 64-75.

Radke, M., Welte, D.H., 1981. The Methylphenanthrene Index (MPI). A maturity parameter based on aromatic hydrocarbons, In: Bjorøy, M., Albrecht, C., Cornford, C, et al., (Eds.), Advances in organic geochemistry. John Wiley & Sons, New York, pp. 504-512.

Radke, M., Horsfield, B., Littke., R., Rullkötter, J., 1997. Maturation and petroleum generation, In: Welte, D.H., Horsfield, B., Baker, D.R. (Eds.), Petroleum and basin evolution. Springer-Verlag, Berlin, pp. 271-333.

Radke, M., Vriend, S.P., Schaefer, R.G., 2001. Geochemical characterization of lower Toarcian source rocks from NW Germany: interpretation of aromatic and saturated hydrocarbons in relation to depositional environment and maturation effects. Journal of Petroleum Geology 24, 287-307.

Radke, M., Willsch, H., Welte, D.H., 1980. Preparative hydrocarbon group type determination by automated medium pressure liquid chromatography. Analytical Chemistry 52, 406-411.

Radke, M., Willsch, H., Leythaeuser, D., 1982a. Aromatic components of coal: relation of distribution pattern to rank. Geochimica et Cosmochimica Acta 46, 1831-1848.

Radke, M., Welte, D.H., Willsch, H., 1982b. Geochemical study on a well in the Western Canada Basin: relation of the aromatic distribution pattern to maturity of organic matter. Geochimica et Cosmochimica Acta 46, 1-10.

Rahman, H.M., Kennedy, M., Löhr, S., Dewhurst, D.N., 2017. Clay-organic association as a control on hydrocarbon generation in shale. Organic Geochemistry 105, 42-55.

Rahman, H.M., Kennedy, M., Löhr, S., Dewhurst, D.N., Sherwood, N., Yang, S., Horsfield, B., 2018. The influence of shale depositional fabric on the kinetics of hydrocarbon generation through control of mineral surface contact area on clay catalysis. Geochimica et Cosmochimica Acta 220, 429-448.

Ramos, V., Alonso, R.N., Strecker, M., 2006. Estructura y neotectónica de las Lomas de Olmedo, zona de transición entre los sistemas subandino y de Santa Bárbara Provincia de Salta. Revista de la Asociación Geológica Argentina 61, 579-588.

Righi, D., Meunier, A., 1995. Origin of clays by rock weathering and soil formation, In: Velde, B. (Ed.), Origin and Mineralogy of Clays: Clays and the Environment. Springer-Verlag, Heidelberg, pp. 43-161.

Risatti J.B., Rowland S.J., Yan D.A., Maxwell J.R., 1984. Stereochemical studies of acyclic isoprenoids-XII. Lipids of methanogenic bacteria and possible contributors to sediments. Organic Geochemistry 6, 93-104.

Riva, A., Caccialanza, P.G., Quagliaroli, F., 1988. Recognition of 18β(H)-oleanane in several crudes and Tertiary-Upper Cretaceous sediments. Definition of a new maturity parameter. Organic Geochemistry 13, 671-675.

Rodrigues Duran, E., di Primio, R., Anka, Z., Stoddart, D., Horsfield, B., 2013. Petroleum system analysis of the Hammerfest Basin (Southwestern Barents Sea): comparison of basin modelling and geochemical data. Organic Geochemistry 63, 105-121.

Roemers-Oliveira, E., Fernandes, L.A., Freire, E.B., Amarante-Simões, L.S., 2015. Microbial filaments in stromatolites and laminites of Balbuena III Sequence (Maastrichtian/Danian) of Yacoraite Formation in Metán-Alemania Sub-basin, Salta region, Argentina, and its palaeoenvironmental significance. Brazilian Journal of Geology 45, 399-413.

Romer, R.L., Hahne, K., 2010. Life of the Rheic Ocean: Scrolling through the shale record. Gondwana Research 17, 236-253.

Romero-Sarmiento, M.F., Rohais, S., Littke, R., 2019. Lacustrine Type I kerogen characterization at different thermal maturity levels: Application to the Late Cretaceous Yacoraite Formation in the Salta Basin-Argentina. International Journal of Coal Geology 203, 15-27.

Ross, D.J.K., Bustin, M.R., 2009. The importance of shale composition and pore structure upon gas storage potential of shales gas reservoirs. Marine and Petroleum Geology 26, 916-927.

Rossello, E.A., Mozetic, M.E., 1999. Caracterización estructural y significado geotectónico de los depocentros Cretácicos continentales del centro-oeste argentino. Boletim do 50 Simpósio sobre o Cretáceo do Brasil, 107-113.

Rossello, E.A., López de Luchi, M., 2005. The Trans-Argentine corridor (Central Argentina): Cretaceous intracontinental rifting associated with Gondwana break-up. Congreso; Gondwana 12. Mendoza, Argentina, p. 313.

Rubiolo, D.G., 1999. Esquema de evolución tectonosedimentaria para las cuencas Cenozoicas de la Cordillera Oriental (22° a 23°), Argentina. Acta Geológica Hispánica 32, 77-92.

Rullkötter, J., Wendisch, D., 1982. Microbial alteration of 17α (H)-hopane in Madagascar asphalts: removal of C-10 methyl group and ring opening. Geochimica et Cosmochimica Acta 46, 1543-53.

Sabino, I., 2004. Estratigrafía de la Formación la Yesera (Cretácico): Base del relleno sinrift del Grupo Salta, noroeste argentino. Revista de la Asociación Geológica Argentina 59, 341-359.

Sachse, V.F., Littke, R., Heim, S., Kluth, O., Schober, J., Boutib, L., Jabour, H., Perssen, F., Sindern, S., 2011. Petroleum source rocks of the Tarfaya Basin and adjacent areas, Morocco. Organic Geochemistry 42, 209–227.

Salazar De Langer, L.J. Structural and seismic-stratigraphic analysis of the Tres Cruces Sub-Basin, Northwest Argentina. Thesis Dr. rer. nat. dissertation. Friedrich-Schiller-Universität Jena. Unpublished.

Salazar De Langer, L.J., Kley, J., Monaldi, C.R., Rossello, E.A., 2009. Orogen-parallel shortening in the central Andes: examples from NW Argentina and the role of normal faults reactivation, In: Wörner, G., Möller-McNett, S. (Eds.), Lateinamerika-Kolloquium. Abstracts and Program, LAK, Göttingen, pp. 252-253.

Salazar De Langer, L.J., Kley, J., Monaldi, C.R., Rossello, E.A., Monaldi, R., Wiegand, M., 2008. 3D structure of the Tres Cruces synclinorium from seismic data and serial balanced cross-sections, Eastern Cordillera, Argentina. 7th International Symposium on Andean Geodynamics. Extended Abstracts, Nice, pp. 477-480.

Sallet, A., Rushton, S., Buambua, L., Inman, K., Mcneil, R., Dickson, J.A.D., 2016. Presalt stratigraphy and depositional systems in the Kwanza Basin, offshore Angola: AAPG Bulletin 100, 1135-1164.

Salfity, J.A., Marquillas, R.A., 1994. Tectonic and sedimentary evolution of the Cretaceous-Eocene Salta Group basin, Argentina, In: Salfity, J.A. (Ed.), Cretaceous tectonics of the Andes. Earth Evolution Sciences Monograph Series. Vieweg & Sohn, Braunschweig/Wiesbaden, pp. 266-315.

Salfity, J.A., Marquillas, R.A., 1999. Chapter 19. La cuenca Cretácica del norte Argentino, In: Caminos, R. (Ed.), Geología Argentina**.** Instituto de geología y recursos minerales. Anales 29, Buenos Aires. pp. 613-626.

Sánchez, M.C., Marquillas, R.A., 2010, Facies y ambientes del Grupo Salta (Cretácico-Paleógeno) en Tumbaya, quebrada de Humahuaca, Provincia de Jujuy. Revista de la Asociación Geológica Argentina 67, 383-391.

Sassen, R., 1984. Effects of radiation exposure on indicators of thermal maturity. Organic Geochemistry 5, 183-186.

Schenk, H.J., Horsfield, B., 1998. Using natural maturation series to evaluate the utility of parallel reaction kinetics models: an investigation of Toarcian shales and Carboniferous coals, Germany. Organic Geochemistry 29, 137-154.

Schenk, H.J., Horsfield, B., Kroos, B., Schaefer, R.G., Schwochau, K., 1997. Kinetics of petroleum formation and cracking, In: Welte, D.H., Horsfield, B., Baker, D.R. (Eds.), Petroleum and basin evolution. Springer-Verlag, Berlin, pp. 231-324.

Schink, B., 2006. Microbially driven redox, reactions in anoxic environments: pathway, energies, and biochemical consequences. Eng. Life. Sci. Review 6, 228-233.

Schulz, L.K., Wilhelms, A., Rein, E., Steen, A.S., 2001. Application of diamondoids to distinguish source rock facies. Organic Geochemistry 32, 365-375.

Seifert, W.K., Moldowan, J.M., 1980. The effect of thermal stress on source-rock quality as measured by hopane stereochemistry. Physics and Chemistry of the Earth 12, 229-37.

Seifert, W.K., Moldowan, J.M., 1986. Use of biological markers in petroleum exploration, In: Johns, R.B. (Ed.), Methods in Geochemistry and Geophysics. Elsevier, Amsterdam, pp. 261-290.

Seifert, W.K., Moldowan, J.M., Demaison, G.J., 1984. Source correlation of biodegraded oils. Organic Geochemistry 6, 633-643.

Sempere, T., Butler, R.F., Richards, D.R., Marshall, L.G., Sharp, W., Swisher, C.C., 1997. Stratigraphy and chronology of Late Cretaceous-Early Paleogene strata in Bolivia and northwest Argentina. Geological Society of America Bulletin 109, 709-727.

Sevast'yanov, Y.G., Bulanov, L.A., Smirnov-Averin, A.P., Kaplan, E.P., Nefedov, O.M., Chel'tsova, M.A., Petrov, A.D., 1962. The thermal and radiation stability of some aromatic compounds. Soviet Atomic Energy 14, 578-81.

Siks, B., Horton, B., 2011. Growth and fragmentation of the Andean foreland basin during eastward advance of fold-thrust deformation, Puna plateau and Eastern Cordillera, northern Argentina, Tectonics 30, 1-27.

Simkiss, K., Wilbur, K.M., 1989. Biomineralization. First edition, Academic Press, New York, 377 pp.

Singer, A., 1984. The paleoclimatic interpretation of clay minerals in sediments, a review. Earth-Science Reviews 21, 251-293.

Sinninghe Damsté, J.S., Kenig, F., Koopmans, M.P., Köster, J., Schouten, S., Hayes, J.M., de Leeuw, J.W., 1995. Evidence for gammacerane as an indicator of water-column stratification. Geochimica et Cosmochimica Acta 59, 1895-900.

Snowdon, L.R., 1995. Rock-Eval Tmax suppression: Documentation and amelioration. AAPG Bulletin 79, 1337-1348.

Song, J., Littke, R., Maquil, R., Weniger, P., 2014. Organic facies variability in the Posidonia black shale from Luxembourg: implications for thermal maturation and depositional environment. Palaeogeography, Palaeoclimatology, Palaeoecology 410, 316-336.

Song, J., Littke, R., Weniger, P., Ostertag-Henning, C., Nelskamp, S., 2015. Shale oil potential and thermal maturity of the Lower Toarcian Posidonia. International Journal of Coal Geology 150, 127-153.

Springer, M.,1999. Interpretation of heat-flow density in the Central Andes. Tectonophysics, 306, 377-395.

Springer, M., Förster, A., 1998. Heat-flow density across the Central Andean subduction zone. Tectonophysics 291, 123-139

Stach, E., Mackowsky, M.TH., Teichmüller, M., Taylor, G.H., Chandra, D., Teichmüller, R., 1982. Stach's Textbook of Coal Petrology. Gebrüder Borntraeger, 535 pp.

Starck, D., 2011. Cuenca Cretácica-Paleógena del Noroeste Argentino. VIII Congreso de exploración y desarrollo de hidrocarburos. Simposio Cuencas Argentinas. Visión Actual, pp. 407-453.

Starck, D., Vergani, G., 1996. Desarrollo tecto-sedimentario del Cenozoico en el sur de la Provincia de Salta-Argentina. XIII Congreso Geológico Argentino y III Congreso de Exploración de Hidrocarburos, Actas I, pp. 433-452.

Stasiuk, L., 1994. Oil-prone alginite macerals from organic-rich Mesozoic and Palaeozoic strata, Saskatchewan, Canada. Marine and Petroleum Geology 11, 208-217.

Stinco, L., Barredo, S., 2014. Características geológicas y recursos asociados con los reservorios no convencionales del tipo shale de las cuencas productivas de la Argentina. Petrotecnia, 45-66.

Strecker, M.R., Cerveny, P., Bloom, A.L., Malizia, D., 1989. Late Cenozoic tectonism and landscape development in the Foreland of the Andes: Northern Sierras Pampeanas (26°-28°S), Argentina. Tectonics 8, 517-534.

Suarez-Ruiz, I., Iglesias, M.J., Jiménez, A., Laggoun-Défarge, F., Prado, J.G., 1994. Petrographic and geochemical anomalies detected in spanish Jurassic Jet, In: Mukhopadhyay, P.K., Dow, W.G. (Eds.), Vitrinite reflectance as a maturity parameter: Application and Limitations. American Chemical Society Symposium, Series 570, Chicago, Illinois, pp. 76-92.

Summa, L., Becker, T., Gray, G., Awwiller, D., 2015. Evolving genetic concepts and their influence on hydrocarbon system predictions, Suandean fold belt and deformed foreland, Argentina, In: DeCelles, P.G., Ducea, M.N., Carrapa, B., Kapp, P.A. (Eds.), Geodynamics of a Cordilleran Orogenic System: The Central Andes of Argentina and Northern Chile. Geological Society of America Memoir 212, pp. 435-487.

Tan, J., Horsfield, B., Mahlstedt, N., Zhang, J., di Primio, R., Vu, T.A.T., Boreham, C.J., Van Graas, G., Tocher, B.A., 2013. Physical properties of petroleum formed during maturation of Lower Cambrian shale in the upper Yangtze Platform, South Chine, as inferred from PhaseKinetics modelling. Marine and Petroleum Geology 48, 47-56.

Tarafa, M.E., Hunt, J.M., Ericson, I., 1983. Effect of hydrocarbon volatility and adsorption on source-rock pyrolysis. Journal of Geochemical Exploration 18, 75-85.

Taylor, G.H., Teichmüller, M., Davis, A., Diessel, C.F.K., Littke, R., Robert, P., 1998. Organic petrology. Gebrüder Borntraeger, Berlin-Stuttgart, 704 pp.

Tegelaar, E.W., Noble, R.A., 1994. Kinetics of hydrocarbon generation as a function of the molecular structure of kerogen as revealed by pyrolysis-gas chromatography. Organic Geochemistry 22, 543-574.

Ten Haven, H.L., Lafargue, E., Kotarba, M., 1993. Oil/oil and oil/source rock correlations in the Carpathian Foredeep and Overthrust, south-east Poland. Organic Geochemistry 20, 935-959.

Ten Haven, H.L., de Leeuw, J.W., Peakman, T.M., Maxwell, J.R., 1986. Anomalies in steroid and hopanoid maturity indices. Geochimica et Cosmochimica Acta 50, 853-855.

Terra, G.J.S., Rodrigues, E.B., Freire, E.B., Lykawka, R., Raja-Gabaglia, G.P., Hernández, J. I., 2012. Salta Basin, Argentina: A good analog for Phanerozoic lacustrine microbialite-bearing reservoirs. AAPG Hedberg Conference Microbial carbonate reservoir characterization, Houston, Texas.

Thompson, 1988. Gas-condensate migration and oil fractionation in deltaic systems. Marine and Petroleum Geology 5, 237-246.

Thorez, J., 1976. Practical identification of clay minerals. Editions G. Lelotte, Belgique, 91 pp.

Tissot, B.P., Welte, D.H., 1984. Petroleum formation and ocurrence. Second revised and enlarged edition, Springer-Verlag, Berlin, 699 pp.

Tissot, B., Deroo, G., Hood, A., 1978. Geochemical study of the Uinta Basin: formation of petroleum from the Green River Formation. Geochimica et Cosmochimica Acta 72, 1469-1485.

Tissot, B., Durand, B., Espitalie, J., Combaz, A., 1974. Influence of the nature and diagenesis of organic matter in the formation of petroleum: AAPG Bulletin 58, 499-506.

Tribovillard, N., Algeo, T.J., Lyons, T., Riboulleau, A., 2006. Trace metals as paleoredox and paleoproductivity proxies: An update. Chemical Geology 232, 12-32.

Troth, I., Marshall, J.E.A., Racey, A., Becker, R.T., 2011. Devonian sea-level change in Bolivia: A high palaeolatitude biostratigraphical calibration of the global sea-level curve. Palaeogeography, Palaeoclimatology, Palaeoecology 304, 3-20.

Turner, J.C.M., 1964. Descripción geológica de la Hoja 2c, Santa Victoria escala 1:200.000. Carta Geológico-Económica de la República Argentina. Provincias de Salta y Jujuy. Servicio Nacional Minero Geológico, Boletín 104.

Tyson, R.V., 2001. Sedimentation rate, dilution, preservation and total organic carbon: some results of a modelling study. Organic Geochemistry 32, 333-339.

Uliana, M.A., Legarreta, L., Laffitte, G.A., Villar, H., 2014. Estratigrafía y geoquímica de las facies generadoras de hidrocarburos en las cuencas petrolíferas de Argentina. Simposio de sistemas petroleros, IV Congreso de exploración y desarrollo de hidrocarburos, Mar del Plata, pp. 1-62.

Ungerer, P., Pelet, R., 1987. Extrapolation of the kinetics of oil and gas formation from laboratory experiments to sedimentary basins. Nature 327, 52-54.

Urien, C.M., Zambrano, J.J., Yrigoyen, M.M., 1995. Petroleum basins of Southern South America: an overview, In: Tankard, A.J., Suárez Soruco, R., Welsink, H.J. (Eds.), Petroleum Basins of South America. AAPG Memoir 62, 63-77.

Van Duin, A.C., Sinninghe Damsté, J.S., Koopmans, M.P., Van de Graaf, B., de Leeuw, J.W., 1997. A kinetic calculation method of homohopanoid maturation: applications in the reconstruction of burial histories of sedimentary basins. Geochimica et Cosmochimica Acta 61, 2409-2429.

Van Graas, G.W., 1990. Biomarker maturity parameters for high maturities: Calibration of the working range up to the oil/condensate threshold. Organic Geochemistry 16, 1025-1032.

Velde, B., 1992. Introduction to clay minerals: Chemistry, origins, uses and environmental significance. First edition, Chapman & Hall, London 198 pp.

Viramonte, J.G., Galliski, M.A., Saavedra, V.A., Aparicio, A. García-Cacho, L. Escorza, C.M., Parica, C. 1984. Edad, génesis y mecanismos eruptivos de las riolitas granatíferas de San Antonio de los Cobres, provincia de Salta. IX Congreso Geológico Argentino. Actas III, 216-233.

Volkman, J.K., 1988. Biological marker compounds as indicators of the depositional environments of petroleum source rocks. Geological Society, London, Special Publications 40, pp. 103-122.

Wang, F.P., Reed, R.M., 2009. Pore networks and fluid flow in gas shales. Proceedings of the SPE annual technical conference and exhibition, New Orleans, LA, SPE paper 124253.

Wang, Q., Ye, J.B., Yang, H.Y., Liu, Q., 2016. Chemical Composition and structural characteristics of oil shales and their kerogens using Fourier Transform Infrared (FTIR) spectroscopy and solid-state ^{13}C Nuclear Magnetic Resonance (NMR). Energy & Fuels 8, 6271-6280.

Warr, L.N., Ferreiro-Mählmann, R., 2015. Recommendations for Kübler Index standardization. Clay Minerals 50, 283-286.

Warr, L.N., Rice, A.H.N., 1994. Interlaboratory standardization and calibration of clay mineral crystallinity and crystallite size data. Journal Metamorphic Geology 12, 141-152.

Wei, Z., Moldowan, J.M., Dahl, J., Goldstein, T.P., Jarvie, D.M., 2006a. The catalytic effects of minerals on the formation of diamondoids from kerogen macro-molecules. Organic Geochemistry 37, 1421-1436.

Wei, Z., Moldowan, J.M., Jarvie, D.M., Hill, R., 2006b. The fate of diamondoids in coals and sedimentary rocks. Geology 34, 1013-1016.

Wei, Z., Moldowan, J.M., Zhang, S., Hill, R., Jarvie, D.M., Wang, H., Song, F., Fago, F., 2007. Diamondoid hydrocarbons as a molecular proxy for thermal maturity and oil cracking: geochemical models from hydrous pyrolysis. Organic Geochemistry 38, 227-249.

Weiss, H.M., Wilhelms, A., Mills, N., Scotchmer, J., Hall, P.B., Lind, K., Brekke, T., 2000. NIGOGA – The Norwegian industry guide to organic geochemical analyses. Edition 4.0. Published by Norsk Hydro, Statoil, Geolab Nor, SINTEF Petroleum research and the Norwegian petroleum directorate.

Wenger, L.M., Davis, C.L., Isaksen, G.H., 2002. Multiple controls on petroleum biodegradation and impact on oil quality. SPE reservoir evaluation and engineering 5, pp. 375-83.

Wilkins, R.W.T., 1999. The problem of inconsistency between thermal maturity indicators used for petroleum exploration in Australian basins. AGSO Journal of Australian Geology & Geophysics 17, 67-76.

Wygrala B.P., 1989. Integrated study of an oil field in the southern Po basin, northern Italy, PhD thesis, University of Köln, 328 pp.

Yang, S., Horsfield, B., 2016. Some predicted effects of minerals on the generation of petroleum in nature. Energy & Fuels 30, 6677-6687.

Yang, S., Schulz, H.M., Horsfield, B., Schovsbo, N.H., Noah, M., Panova, E., Heike, R., Hahne, R., 2018. On the changing petroleum generation properties of Alum shale over geological time caused by uranium irradiation. Geochimica et Cosmochimica Acta 229, 20-35.

Yang, S., Schulz, H.M., Schovsbo, N.H., Mayanna, S., 2019. The organic geochemistry of "Kolm", a unique analogue for the understanding of molecular changes after significant uranium irradiation. International Journal of Coal Geology 209, 89-93.

Yrigoyen, M.R., 2007. Reseña sobre los conocimientos y la explotación de los hidrocarburos en Argentina antes de 1907. Petrotecnia, 16-36.

Zehr, J.P., Kudela, R.M., 2009. Photosynthesis in the Open Ocean. Science 326, 945-946.

Zhao, M., Huang, C., Wang, C., Wei, G., 2006. A millennial-scale U37K′ sea-surface temperature record from the South China Sea (8°N) over the last 150 kyr: Monsoon and sea-level influence. Palaeogeography, Palaeclimatology, Palaeoecology 236, 39-55.

Zhibing, W., Moldowan, J.M., Peters, K.E., Wang, Y., Xiang, W., 2007. The abundance and distribution of diamondoids in biodegraded oils from the San Joaquin Valley: Implications for biodegradation of diamondoids in petroleum reservoirs. Organic Geochemistry 38, 1910-1926.

Zhu, X., Cai, J., Liu, W., Lu, W., 2016. Occurrence of stable and mobile organic matter in the clay-sized fraction of shale: Significance for petroleum geology and carbon cycle. International Journal of Coal Geology 160-161, 1-10.

Ziegs, V., Horsfield, B., Skeie, J.E., Rinna, J., 2017. Petroleum retention in the Mandal Formation. Central Graben, Norway. Marine and Petroleum Geology 83, 195-214.

Zong, R., Wang, Z., Jiang, T., Gong, Y., 2016. Late Devonian radiolarian-bearing siliceous rocks from the Karamay ophiolitic mélange in western Junggar: Implications for the evolution of the Paleo-Asian Ocean. Palaeogeography, Palaeoclimatology, Palaeoecology 448, 266-278.

Zumberge, J.E., 1987. Prediction of source rock characteristics based on terpane biomarkers in crude oils: a multivariate statistical approach. Geochimica et Cosmochimica Acta 51, 1625-1637.

10. Appendix

Table A 1. Sample's location and description.

Type of sample	Short ID	Description	Coordinates	Altitude m.a.s.l	Location
Rock Samples	1	dark calcareous shale	-25.15852, -65.66519	Not provided	Metán-Alemanía
	2	dark calcareous shale	-22.90827, -65.57711	Not provided	Tres Cruces
	3	dark calcareous shale	-22.90827, -65.57712	Not provided	Tres Cruces
	4	pale grey calcareous shale	-25.300300, -65.351667	1066	Metán-Alemanía
	5	dark calcareous shale	-25.292350, -65.352917	1066	Metán-Alemanía
	6	pale grey calcareous shale	-25.283733, -65.359900	1069	Metán-Alemanía
	7	pale grey shale	-25.283733, -65.359900	1070	Metán-Alemanía
	8	stromatolite	-25.283733, -65.359900	1071	Metán-Alemanía
	9	green shale	-25.283717, -65.359900	1069	Metán-Alemanía
	10	calcareous shale	-25.300117, -65.294850	974	Metán-Alemanía
	11	laminated calcareous shale	-25.300117, -65.294850	974	Metán-Alemanía
	12	dark well laminated calcareous shale	-25.180817, -65.181317	839	Metán-Alemanía
	13	grey shale	-25.180817, -65.181317	840	Metán-Alemanía
	14	pale grey shale/siltstone	-25.180817, -65.181317	841	Metán-Alemanía
	15	black shale	-25.184267, -65.776583	2204	Metán-Alemanía
	16	siltstone/very fine sandstone	-25.179317, -65.816433	2662	Metán-Alemanía
	17	dark grey shale/siltstone	-25.179317, -65.816433	2663	Metán-Alemanía
	18	stromatolite	-25.166867, -65.844050	2906	Metán-Alemanía
	19	pale grey siltstone	-25.326933, -65.892717	3148	Metán-Alemanía
	20	siltstone	-25.116283, -66.017217	3086	Metán-Alemanía
	21	siltstone	-25.116233, -66.017117	3095	Metán-Alemanía
	22	highly calcareous shale	-23.778483, -66.034867	3431	Tres Cruces
	23	laminated pale grey shale	-23.701483, -65.687867	3863	Tres Cruces
	24	calcareous shale	-23.701533, -65.688083	3866	Tres Cruces
	25	pale grey calcareous shale	-23.701400, -65.687817	3871	Tres Cruces
	26	grey-black shale	-23.701400, -65.687767	3872	Tres Cruces
	27	grey -greenish calcareous shale	-23.701467, -65.687700	3873	Tres Cruces
	28	dark grey highly calcareous shale	-23.701400, -65.687733	3875	Tres Cruces
	29	dark laminated calcareous shale	-23.701400, -65.687667	3877	Tres Cruces
	30	well laminated calcareous black shale	-23.701383, -65.687700	3878	Tres Cruces
	31	pale grey calcareous shale	-23.701417, -65.687533	3880	Tres Cruces
	32	pale grey calcareous shale	-23.701483, -65.687500	3880	Tres Cruces
	33	dark grey calcareous shale	-23.701550, -65.687433	3881	Tres Cruces
	34	grey calcareous shale	-23.701633, -65.687300	3881	Tres Cruces
	35	well laminated calcareous dark grey shale	-23.701783, -65.687050	3886	Tres Cruces
	36	limestone	-23.222033, -65.592233	3525	Tres Cruces
	37	calcareous siltstone	-23.221917, -65.592067	3602	Tres Cruces
	38	stromatolite	-23.222467, -65.592700	3613	Tres Cruces
	39	pale grey highly calcareous shale	-22.995700, -65.624933	3830	Tres Cruces
	40	dark grey highly calcareous shale	-22.995717, -65.624683	3829	Tres Cruces
	41	dark grey calcareous shale	-22.995733, -65.624600	3827	Tres Cruces
	42	highly calcareous black shale	-22.916367, -65.605267	3687	Tres Cruces
	43	dark grey calcareous shale	-22.916633, -65.605217	3697	Tres Cruces
	44	siltstone/shale	-22.916717, -65.605200	3698	Tres Cruces
	45	calcareous shale	-22.916483, -65.605050	3703	Tres Cruces
	46	stromatolite	-22.916750, -65.605117	3706	Tres Cruces
	47	green shale	no GPS signal	no GPS signal	Metán-Alemanía
	48	pale grey calcareous shale	no GPS signal	no GPS signal	Metán-Alemanía
	49	shale	no GPS signal	no GPS signal	Metán-Alemanía
	50	dark grey shale	no GPS signal	no GPS signal	Metán-Alemanía
	51	black shale	no GPS signal	no GPS signal	Metán-Alemanía
	52	pisolite	no GPS signal	no GPS signal	Metán-Alemanía

Table A 2. Bulk mineral composition for Yacoraite Fm. X-ray diffraction (XRD).

Short ID	Quartz	Calcite	Dolomite	Ankerite	Pyrite	Gypsum	Albite	Microcline	Muscovite	Kaolinite	Analcime
	%										
4	18	6	NI	NI	NI	NI	41	NI	35	NI	NI
7	17	7	NI	NI	7	NI	24	16	29	NI	NI
8	8	88	NI	1	NI	NI	2	NI	NI	NI	NI
10	5	66	4	NI	6	1	10	3	5	NI	NI
11	9	41	6	NI	NI	4	17	12	12	NI	NI
15	14	NI	NI	NI	NI	NI	24	20	41	NI	NI
23	30	31	NI	2	3	NI	18	NI	13	NI	3
28	8	71	NI	1	4	NI	5	NI	9	NI	1
29	16	62	NI	2	4	NI	8	NI	5	NI	4
30	21	57	NI	NI	8	NI	NI	NI	6	NI	8
33	35	42	NI	4	4	NI	8	NI	6	NI	2
34	29	18	NI	2	9	NI	11	11	10	7	3
35	42	18	NI	7	4	NI	8	NI	21	NI	NI
37	20	61	NI	NI	NI	NI	14	NI	5	NI	NI
39	19	53	NI	8	2	5	6	NI	5	NI	2
40	10	76	NI	2	6	NI	6	NI	NI	NI	NI
41	8	71	NI	NI	7	NI	4	3	4	NI	3
42	4	95	NI	1	NI	NI	NI	NI	NI	NI	NI
44	35	45	NI	12	2	NI	NI	NI	6	NI	NI
45	50	21	NI	2	5	NI	3	10	9	1	NI
46	14	68	14	NI	4	NI	NI	NI	NI	NI	NI
47	27	1	NI	NI	2	8	16	15	31	NI	NI
48	16	7	NI	36	NI	5	14	NI	19	NI	4
50	27	1	NI	3	NI	7	18	8	26	NI	9
51	52	NI	NI	NI	NI	NI	17	18	13	NI	NI
52	9	80	4	NI	NI	NI	5	NI	2	NI	NI
53	40	15	NI	NI	5	NI	15	14	11	NI	NI

NI: Not identified

Table A 3. Clay mineral composition for Yacoraite Fm. Fractions < 2 microns. X-ray diffraction (XRD).

Sample	Sub-basin	Lithology	Smectite	Chlorite	Illite/mica	Kaolinite
			%			
8	MA_E	St	90.5	0.2	9.2	NI
11	MA_E	Sh	NI	11.5	88.5	NI
23	TC_S	Sh	50.4	9.5	40.1	NI
28	TC_S	Sh	90.1	NI	9.9	NI
29	TC_S	Sh	70.1	NI	28.4	1.5
30	TC_S	Sh	9.1	3.5	87.4	NI
33	TC_S	Sh	86.9	NI	13.1	NI
34	TC_S	Sh	79.8	NI	20.2	NI
35	TC_S	Sh	79.1	NI	19.3	1.6
37	TC_N	Sh	47.8	NI	52.2	NI
39	TC_N	Sh	54.5	NI	45.5	NI
40	TC_N	Sh	89.2	NI	10.8	NI
42	TC_N	Sh	NI	NI	100	NI
44	TC_N	Sh	NI	NI	75.6	24.4
45	TC_N	Sh	NI	NI	89.3	10.7
46	TC_N	St	NI	NI	74.2	25.8
47	MA_W	Sh	62.4	NI	37.6	NI
48	MA_W	Sh	NI	3	97	NI
50	MA_W	Sh	44.7	NI	55.3	NI
51	MA_W	Sh	NI	NI	100	NI

(TC) Tres Cruces, (MA) Metán-Alemanía sub-basins. The sectors where samples were collected are north, south (N, S) and east and west (E, W). Sh: shales; St: stromatolites. NI: Not identified.

Table A 4. Elemental chemical composition for Yacoraite Fm. in Tres Cruces and Metán-Alemanía sub-basins. X-ray fluorescence. (XRF).

Short ID	Major elements, %										ppm																	
	MgO	Al_2O_3	SiO_2	P_2O_5	SO_3	K_2O	CaO	TiO_2	MnO	Fe_2O_3	Cr	Ni	Cu	Zn	As	Rb	Sr	Y	Zr	Nb	Mo	Cd	Ba	Ce	W	Pb	Th	U
1	29.33	4.32	35.89	NM	1.09	0.53	27.24	0.17	0.02	0.61	127	2585	171	51	NM	25	3023	NM	108	NM	9	NM	1511	254	NM	14	NM	NM
2	3.04	23.00	56.71	0.08	1.63	2.70	6.48	0.37	0.10	5.75	21	26	32	56	NM	109	400	18	84	6	8	NM	NM	493	26	8	10	NM
3	0.60	17.36	68.62	0.49	2.27	1.89	3.13	0.80	0.04	3.99	54	45	164	697	567	101	521	8	123	2	119	NM	4514	1042	126	36	NM	69
4	4.47	26.49	60.12	0.19	0.51	3.24	1.37	0.49	0.05	2.97	NM	16	NM	22	NM	47	41	3	NM	NM	24	NM	NM	638	NM	8	121	2
5	1.14	28.93	61.11	0.15	0.65	3.09	1.10	0.57	0.05	2.97	NM	26	NM	19	NM	15	NM	8	NM	NM	30	1306	NM	745	NM	9	114	NM
6	3.76	21.78	61.04	0.29	0.48	3.59	2.30	0.61	0.06	5.91	13	25	82	76	16	189	305	26	164	10	8	NM	NM	803	17	11	NM	5
7	2.74	27.16	60.13	0.15	0.62	3.53	1.93	0.47	0.04	3.04	NM	27	NM	NM	NM	19	34	NM	NM	NM	31	1009	NM	610	NM	NM	161	NM
8	7.82	8.91	24.40	NM	1.56	0.17	55.56	0.17	0.16	0.91	NM	5	23	73	NM	9	1047	9	228	NM	3	NM	1535	213	33	12	NM	NM
9	4.90	27.55	58.78	0.15	0.60	3.11	1.03	0.50	0.05	3.15	NM	25	NM	NM	NM	41	NM	2	NM	5	26	1080	NM	662	NM	NM	120	NM
10	7.09	NM	31.38	0.27	3.44	0.98	54.92	0.18	0.06	1.47	NM	NM	16	19	3	33	1757	2	64	3	16	NM	NM	243	38	11	35	NM
11	9.32	12.87	37.47	NM	5.37	1.85	30.34	0.30	0.04	1.70	NM	NM	18	730	NM	60	5701	NM	198	NM	87	NM	32	402	161	1	7	NM
12	1.72	21.98	61.33	0.42	0.46	3.13	4.09	0.67	0.07	5.88	58	35	25	65	NM	134	198	28	147	17	9	NM	852	869	16	NM	NM	NM
13	2.39	20.45	64.34	0.32	0.50	2.86	2.14	0.63	0.04	6.17	42	32	63	51	40	121	110	23	203	9	10	NM	NM	816	11	7	NM	NM
14	3.04	21.35	62.55	0.25	0.49	2.98	3.29	0.58	0.05	5.21	54	20	39	53	10	129	211	23	150	12	13	NM	583	756	3	NM	8	NM
15	0.23	33.46	56.24	0.10	0.59	4.17	0.88	0.50	0.04	3.55	NM	NM	NM	32	NM	NM	31	NM	NM	6	46	809	296	657	159	NM	222	15
16	0.08	21.49	63.69	0.21	0.45	4.28	3.62	0.54	0.07	5.11	281	1666	382	234	NM	220	194	34	216	23	14	NM	388	793	NM	70	17	5
17	2.98	20.49	61.47	0.14	1.35	5.78	3.21	0.50	0.04	3.90	NM	21	27	40	14	113	267	27	169	10	28	NM	NM	656	25	15	NM	NM
18	22.73	5.15	30.50	NM	1.84	0.52	37.58	0.17	0.03	0.58	46	NM	13	NM	23	29	8211	NM	246	NM	NM	NM	NM	222	34	35	39	NM
19	6.12	19.69	63.22	0.16	0.48	3.57	1.36	0.53	0.04	4.58	40	12	28	58	2	133	132	20	172	7	11	NM	989	700	8	1	NM	9
20	2.02	23.49	62.96	0.17	0.57	3.68	2.38	0.62	0.05	3.88	NM	10	31	54	80	305	301	20	163	11	20	NM	NM	805	18	7	8	6
21	1.66	22.81	63.11	0.25	0.43	3.82	1.47	0.67	0.05	5.58	53	23	39	91	31	202	82	23	145	13	5	NM	NM	883	17	6	7	NM
22	3.96	7.15	15.48	0.02	1.38	NM	70.96	0.04	0.11	0.64	NM	9	42	2	NM	16	2483	NM	79	NM	19	NM	NM	NM	44	18	42	NM
23	3.81	19.86	58.56	0.05	2.69	2.25	8.34	0.43	0.05	3.79	10	22	64	81	9	89	704	8	124	8	42	NM	NM	568	34	10	NM	7
24	3.98	21.41	60.99	0.25	0.60	2.57	4.42	0.56	0.07	5.00	NM	26	32	81	8	111	234	24	190	9	6	NM	NM	734	33	NM	6	NM
25	11.11	18.02	52.73	0.21	2.76	1.85	8.39	0.44	0.07	4.20	36	26	31	61	12	70	608	14	112	4	35	NM	735	573	NM	4	4	NM
26	1.06	23.02	63.70	0.20	0.72	3.12	2.54	0.45	0.04	5.01	5	20	39	128	15	133	172	20	92	12	6	NM	NM	599	34	3	10	NM

NM: not measured

Table A 4. Continuation. Elemental chemical composition for Yacoraite Fm. in Tres Cruces and Metán-Alemanía sub-basins. X-ray fluorescence. (XRF).

Short ID	Major elements, %										ppm																	
	MgO	Al_2O_3	SiO_2	P_2O_5	SO_3	K_2O	CaO	TiO_2	MnO	Fe_2O_3	Cr	Ni	Cu	Zn	As	Rb	Sr	Y	Zr	Nb	Mo	Cd	Ba	Ce	W	Pb	Th	U
27	0.93	23.00	62.11	0.11	1.55	2.66	4.19	0.45	0.06	4.77	29	34	25	59	53	265	469	19	105	2	5	NM	NM	595	24	1	7	NM
28	3.28	13.75	35.00	0.23	4.14	0.67	41.25	0.16	0.05	1.34	50	4	39	4	NM	26	926	4	68	NM	11	NM	NM	205	31	14	10	NM
29	0.91	14.58	38.67	0.04	4.48	0.70	38.79	0.20	0.05	1.41	NM	NM	46	10	NM	25	1297	2	80	NM	17	NM	NM	263	36	NM	NM	NM
30	0.32	19.63	49.93	0.10	6.65	1.66	18.41	0.34	0.05	2.41	363	2329	464	97	99	105	826	15	122	6	41	NM	NM	486	NM	42	23	20
31	2.35	22.64	62.41	0.20	0.77	2.73	4.22	0.41	0.04	4.13	NM	24	16	50	13	125	256	18	87	7	14	NM	NM	537	22	3	5	NM
32	1.89	21.91	61.09	0.12	0.81	2.96	5.15	0.42	0.05	5.48	NM	24	14	54	NM	127	296	23	93	7	11	NM	NM	544	22	18	NM	NM
33	2.81	18.52	57.61	NM	3.11	1.84	13.60	0.32	0.03	1.74	NM	10	31	21	7	103	2675	3	NM	NM	72	NM	876	422	19	10	3	NM
34	3.34	21.64	58.33	0.02	4.64	2.72	5.38	0.27	0.06	3.48	NM	20	29	91	66	62	338	7	113	NM	51	NM	NM	364	20	25	4	3
35	2.41	19.56	58.75	0.05	4.27	3.04	8.48	0.42	0.05	2.62	29	111	118	338	208	148	585	9	189	34	864	NM	NM	550	71	46	NM	300
36	3.95	14.19	32.94	0.04	1.21	0.64	44.35	0.20	0.04	1.42	483	3877	336	147	430	62	2787	10	150	NM	30	NM	1330	277	NM	147	84	NM
37	2.25	NM	70.43	NM	0.84	2.33	20.85	0.40	0.05	2.72	6	22	57	23	NM	85	467	10	91	NM	5	NM	NM	526	27	15	NM	NM
38	14.61	6.18	11.52	NM	1.19	NM	64.88	0.05	0.07	1.13	NM	NM	25	96	NM	15	3159	NM	101	NM	32	NM	NM	64	49	NM	3	NM
39	1.85	16.28	44.08	0.05	5.43	1.39	28.05	0.32	0.06	2.29	33	11	23	16	76	49	1114	4	95	NM	28	NM	NM	418	30	25	1	5
40	NM	13.77	39.92	0.13	6.68	0.73	36.63	0.18	0.07	1.71	19	1	28	3	NM	27	1364	5	71	NM	19	NM	NM	244	39	NM	NM	1
41	NM	9.35	34.31	0.01	3.18	0.26	50.70	0.15	0.05	1.11	82	4181	382	104	NM	53	2681	NM	101	NM	3	NM	743	218	NM	101	56	NM
42	8.90	5.48	9.80	NM	3.93	NM	69.74	0.26	0.07	1.03	42	NM	13	NM	NM	7	2367	NM	82	NM	64	NM	4844	320	46	NM	15	NM
43	NM	24.71	62.33	0.18	1.30	3.61	1.59	0.50	0.05	5.58	44	26	34	66	NM	178	370	22	102	5	6	NM	NM	648	13	20	NM	NM
44	3.72	16.43	51.27	NM	3.71	1.35	20.92	0.22	0.03	1.65	343	2385	257	NM	28	67	2929	NM	172	NM	38	NM	313	312	NM	53	NM	NM
45	2.05	15.23	59.57	0.34	6.39	1.62	10.89	0.33	0.04	2.66	471	1859	196	466	204	136	4488	17	322	NM	63	NM	NM	486	NM	66	NM	NM
46	17.00	NM	36.55	NM	3.95	1.17	37.36	0.24	0.10	3.40	13	7	23	35	45	20	1565	16	144	NM	19	NM	NM	321	36	7	4	NM
47	2.62	22.37	58.54	0.33	4.34	3.33	2.11	0.66	0.08	5.45	19	34	52	112	22	191	139	20	121	13	39	NM	NM	858	12	9	NM	21
48	13.86	17.37	44.59	0.10	2.27	1.94	13.95	0.33	0.17	4.86	448	2037	364	129	139	248	924	5	95	NM	15	NM	598	495	NM	104	NM	16
49	1.85	23.20	62.95	0.48	0.43	3.83	1.40	0.63	0.05	4.52	497	2030	537	300	36	469	249	116	493	59	NM	NM	701	928	76	149	33	15
50	3.15	21.68	57.92	0.17	4.01	2.76	4.34	0.54	0.09	4.90	448	1776	NM	286	39	205	546	33	216	18	10	NM	NM	790	NM	NM	NM	NM
51	0.19	22.70	65.26	0.26	0.84	4.35	1.33	0.52	0.04	3.46	1581	20	85	62	524	2490	102	NM	185	223	69	NM	428	694	32	210	12	3806
52	4.34	7.03	23.22	NM	3.36	NM	59.13	0.29	0.08	1.12	70	4966	403	205	530	31	3682	NM	125	NM	24	NM	3667	428	NM	141	NM	NM

NM: not measured

Table A 5. Elemental chemical composition for Yacoraite Fm. in Tres Cruces and Metán-Alemanía sub-basins. Inductively coupled plasma mass spectrometry. (ICP-MS).

Short ID	Li	Cd	Tl	Pb	Bi	Th	U	Be	Sc	Cr	Co	Ni	Cu	Zn	Ga	Rb	Sr	Nb	Mo	Sb	Cs	V	As
	ppm																						
47	117	0.44	5.9	18	0.64	8.5	6.9	3.3	17	71	17	42	55	109	23	264	172	20	54	1.1	20	120	26
48	31	0.19	0.97	17	0.19	5.5	10	1.2	7.2	28	7.2	17	23	47	8.9	80	718	7.6	16	1.6	6.0	65	16
49	71	0.02	1.5	13	0.37	13	16	3.3	15	74	12	26	67	74	23	280	138	19	1.4	0.58	17	131	3.9
50	64	0.32	3.1	34	0.52	12	13	2.3	13	54	15	36	35	79	20	180	453	17	15	2.5	15	92	35
51	74	0.32	7.3	39	0.36	8.4	4440	4.1	10	74	21	29	83	70	21	259	141	14	8.5	1.0	13	23519	41

Table A 6. Rock-Eval parameters for Yacoraite Fm. in Tres Cruces and Metán-Alemanía sub-basins

Sample	Sub-basin	Lithology	TOC (%)	TS (%)	S1		S2		S3		Tmax, °C		HI		OI		PI	Total Oil	Oil Quality	S2 in K	S2 in Bit	Total oil/kerogen
			BE	BE	BE	AE	BE	AE	BE	AE	BE	AE	BE	AE	BE	AE	BE	S1+S2-S2x	S1/(S1+S2-S2x)	S2x/S2	(1-S2x/S2)	(S2 in kerogen)
1	MA_W	St	0.24	NS	0.03	NR	0.73	NR	0.03	NR	443	NR	308	NC	13	NC	0.04	NC	NC	NC	NC	NC
2	TC_N	Sh	0.3	NS	0.02	NR	0.39	NR	0.03	NR	436	NR	130	NC	10	NC	0.05	NC	NC	NC	NC	NC
3	TC_N	Sh	6.88	NS	0.39	NR	41.1	NR	0.27	NR	427	NR	597	NC	4	NC	0.01	NC	NC	NC	NC	NC
4	MA_E	Sh	NM	NS	NR	0.03	0.01	0.03	0.01	0.02	NM	NR	NM	NC	NC	NC	NC	-0.02	NC	NC	NC	NC
5	MA_E	Sh	0.1	NS	NR	0.02	0.02	0.02	0.02	0.02	NM	NR	NM	NC	NC	NC	NC	NC	NC	NC	NC	NC
6	MA_E	Sh	NM	0.72	NR	0.02	0.01	0.02	0.02	0.02	NM	NR	NM	NC	NC	NC	NC	-0.01	NC	NC	NC	NC
7	MA_E	Sh	0.01	NS	NR	0.02	0.01	0.04	0.02	0.02	NM	NR	NM	NC	NC	NC	NC	-0.03	NC	NC	NC	NC
8	MA_E	St	0.03	NS	NR	0.01	0.05	0.06	0.03	0.03	446	451	108	183	108	92	NC	-0.02	NC	NC	NC	NC
9	MA_E	Sh	NM	NS	NR	0.02	NR	0.03	0.02	0.03	NM	NR	NM	NC	NC	NC	NC	-0.03	NC	NC	NC	NC
10	MA_E	Sh	0.42	0.37	0.05	0.03	2.34	1.86	0.09	0.11	440	443	558	554	21	33	0.02	0.53	0.09	0.79	0.21	0.28
11	MA_E	Sh	0.31	0.84	0.06	0.03	1.71	1.36	0.18	0.15	437	439	552	418	58	46	0.03	0.41	0.15	0.80	0.20	0.30
12	MA_E	Sh	NM	NS	NR	0.02	NR	0.01	0.03	0.02	NM	NR	NM	NC	NC	NC	NC	-0.01	NC	NC	NC	NC
13	MA_E	Sh	NM	NS	NR	0.01	0.01	0.02	0.02	0.02	NM	NR	NM	NC	NC	NC	NC	-0.01	NC	NC	NC	NC
14	MA_W	Sh	NM	NS	0.01	0.03	0.01	0.02	0.03	0.03	NM	NR	NM	NC	NC	NC	NC	NC	NC	NC	NC	NC
15	MA_W	Sh	NM	NS	NR	0.02	0.02	0.03	0.02	0.01	NM	NR	NM	NC	NC	NC	NC	-0.01	NC	NC	NC	NC
16	MA_W	Sh	NM	NS	0.01	0.03	0.02	0.02	0.02	0.02	NM	NR	NM	NC	NC	NC	NC	0.01	1.00	NC	NC	NC
17	MA_W	Sh	NM	NS	NR	0.02	0.01	0.03	0.02	0.03	NM	NR	NM	NC	NC	NC	NC	-0.02	NC	NC	NC	NC
18	MA_W	St	0.09	0.37	0.04	0.06	0.52	0.48	0.1	0.11	445	445	597	320	115	73	0.07	0.08	0.50	0.92	0.08	0.17
19	MA_W	Sh	0.01	NS	NR	0.03	NR	0.01	0.02	0.02	NM	NR	NM	NC	NC	NC	NC	NC	NC	NC	NC	NC
20	MA_W	Sh	NM	NS	NR	0.02	0.02	0.03	0.03	0.04	NM	NR	NM	NC	NC	NC	NC	NC	NC	NC	NC	NC
21	MA_W	Sh	0.04	NS	NR	0.02	0.01	0.02	0.02	0.03	NM	NR	NM	NC	NC	NC	NC	NC	NC	NC	NC	NC
22	TC_S	Sh	NM	NS	NR	0.02	0.01	0.02	0.02	0.02	NM	NR	NM	NC	NC	NC	NC	NC	NC	NC	NC	NC
23	TC_S	Sh	2.27	1	0.13	0.07	10.9	10.5	0.02	0.04	435	437	482	465	1	2	NC	0.60	0.22	0.96	0.04	0.06
24	TC_S	Sh	NM	NS	NR	0.02	NR	0.02	0.02	0.02	NM	NR	NM	NC	NC	NC	NC	NC	NC	NC	NC	NC
25	TC_S	Sh	0.19	NS	0.02	0.03	0.18	0.17	0.03	0.03	423	426	93	86	15	15	0.1	0.03	0.67	0.94	0.06	0.18
26	TC_S	Sh	0.17	NS	NR	0.03	0.11	0.12	0.03	0.03	435	437	64	72	17	18	NC	-0.01	NC	1.09	NC	NC
27	TC_S	Sh	0.22	NS	0.04	0.03	0.17	0.14	0.03	0.02	428	432	79	62	14	9	0.19	0.07	0.57	0.82	0.18	0.50
28	TC_S	Sh	0.44	NS	0.05	0.03	1.71	1.75	0.04	0.04	438	438	384	407	9	9	0.03	0.01	5.00	1.02	NC	NC
29	TC_S	Sh	1.05	0.77	0.13	0.03	6.3	5.6	0.03	0.05	436	438	600	544	3	5	0.02	0.83	0.16	0.89	0.11	0.15
30	TC_S	Sh	3.97	1.8	0.96	0.18	40.3	39.2	0.35	0.05	425	429	1015	802	9	1	0.02	2.04	0.47	0.97	0.03	0.05
31	TC_S	Sh	0.2	NS	0.01	0.03	0.2	0.21	0.02	0.03	436	437	99	96	10	14	NC	NC	NC	NC	NC	NC
32	TC_S	Sh	0.06	NS	NR	0.02	0.05	0.07	0.02	0.02	428	429	88	97	35	28	NC	NC	NC	NC	NC	NC
33	TC_S	Sh	1.4	0.88	0.27	0.08	7.81	7.28	0.04	0.04	433	436	558	552	3	3	0.03	0.80	0.34	0.93	0.07	0.11
34	TC_S	Sh	0.69	NS	0.08	0.06	2.3	2.17	0.02	0.03	431	432	334	333	3	5	0.03	0.21	0.38	0.94	0.06	0.10
35	TC_S	Sh	3.97	1.15	0.13	0.07	20.2	20.2	0.03	0.04	424	423	509	532	1	1	0.01	0.19	0.68	1.00	0.00	0.01
36	TC_N	Sh	0.07	NS	NR	0.02	0.05	0.05	0.03	0.03	446	446	71	45	43	27	NC	NC	NC	NC	NC	NC
37	TC_N	Sh	0.56	NS	0.15	0.03	1.32	0.77	0.04	0.06	442	445	235	156	7	12	0.1	0.70	0.21	0.58	0.42	0.91
38	TC_N	St	NM	NS	0.02	0.01	0.02	0.01	0.03	0.02	NM	NR	NM	NC	NC	NC	NC	0.03	0.67	0.50	0.50	3.00
39	TC_N	Sh	0.93	1.04	0.14	0.03	4.08	3.06	0.03	0.04	434	435	438	369	3	5	0.03	1.16	0.12	0.75	0.25	0.38
40	TC_N	Sh	0.89	1.13	0.08	0.02	4.85	4.51	0.04	0.04	429	426	547	535	5	5	0.02	0.42	0.19	0.93	0.07	0.09
41	TC_N	Sh	0.26	NS	0.04	0.02	1.1	0.91	0.03	0.02	441	440	415	379	11	8	0.04	0.23	0.17	0.83	0.17	0.25
42	TC_N	Sh	0.12	NS	0.23	NR	0.35	0.09	0.02	0.02	429	435	287	142	16	32	0.4	0.49	0.47	0.26	0.74	5.44
43	TC_N	Sh	0.12	NS	NR	0.02	0.08	0.07	0.03	0.04	436	438	67	56	25	32	NC	0.01	NC	0.88	0.13	0.14
44	TC_N	Sh	0.76	0.78	0.35	0.03	3.54	2.51	0.03	0.03	437	438	466	380	4	5	0.09	1.38	0.25	0.71	0.29	0.55
45	TC_N	Sh	0.23	NS	0.34	0.02	0.63	0.31	0.02	0.03	428	430	279	221	9	21	0.35	0.66	0.52	0.49	0.51	2.13
46	TC_N	St	0.1	NS	0.1	0.01	0.32	0.13	0.03	0.03	428	427	336	213	32	49	0.24	0.29	0.34	0.41	0.59	2.23
47	MA_W	Sh	3.36	1.35	0.06	0.05	8.95	7.94	0.08	0.08	424	426	266	238	2	2	0.01	1.07	0.06	0.89	0.11	0.13
48	MA_W	Sh	0.34	0.4	0.02	0.02	0.7	0.63	0.03	0.04	433	434	206	183	9	12	NC	0.09	0.22	0.90	0.10	0.14
49	MA_W	Sh	0.02	NS	NR	0.01	0.02	0.02	0.02	0.03	NM	NR	NM	NC	NC	NC	NC	NC	NC	1.00	NC	NC
50	MA_W	Sh	0.28	NS	0.02	0.02	0.19	0.15	0.05	0.05	426	422	68	56	18	19	0.1	0.06	0.33	0.79	0.21	0.40
51	MA_W	Sh	1.35	0.09	0.01	0.01	0.15	0.14	0.12	0.13	458	458	11	10	9	10	NC	0.02	0.50	0.93	0.07	0.14
52	MA_W	Pis	0.1	NS	0.1	0.01	0.21	0.13	0.03	0.02	439	442	213	217	30	33	0.32	0.18	0.56	0.62	0.38	1.38
53	TC_N	Tar	15.5	0.51	43.4	0.11	83.4	5.87	0.23	2.92	433	431	538	237	1	118	0.34	120.93	0.36	0.07	0.93	20.60

(TC) Tres Cruces, (MA) Metán-Alemanía sub-basins. The sectors where samples were collected are north, south (N, S) and east and west (E, W). BE: Rock-Eval parameter measured in whole-rock before solvent extraction. AE: Parameters measured after solvent extraction. TS: Total sulphur; S1 and S2: mg HC/g rock; S3: mg CO_2/g rock: HI: mg HC/g TOC; OI: mg CO_2/TOC. Lithology. Sh: shales; St: stromatolites; Pis: Pisolite. NR: not reported because of the high inaccuracy due to low values. NS: sample not selected for analysis. NM: not measured. NC: not calculated.

Table A 7. Biomarkers concentrations and ratios in rock extracts from Yacoraite Fm. (Tres Cruces and Metán-Alemanía sub-basins), produced oils (Lomas de Olmedo sub-basin) and oil seep samples (Tres Cruces and Lomas de Olmedo sub-basins).

Type of sample		Short ID	n-alkanes and isoprenoids													Tricyclic Terpanes				Hopanes																	
			Pr	Ph	n-C_{17}	n-C_{18}	C^{13}Pr	C^{13}Ph	Pr/ n-C_{17}	Ph/ C_{18}	n-alk/ (Pr+Ph)	Pr/Ph	DBT	P	DBT/P	C_{25}(R+S)	C_{26}(R)	C_{26}(S)	C_{26}/C_{25}	αβC_{30}	αβC_{31}R	αβC_{31}S	αβC_{32}R	αβC_{32}S	αβC_{33}R	αβC_{33}S	αβC_{34}R	αβC_{34}S	αβC_{35}R	αβC_{35}S	αβC_{31}R/ αβC_{30}	αβC_{31}22/ (22S+22R)	αβC_{32}22S/ (22S+22R)	Gamm.	GI
			mg/g oil				‰						mg/g oil			mg/g oil				mg/g oil																	
Source rock extracts		11	0.3	1.0	0.5	0.9	-29	-29	0.59	1.08	0.23	0.29	1.6	58.2	0.03	6	4.0	3.5	1.2	88	35	30	25	25	15	17	8	6	25	20	0.40	0.51	0.49	53.2	3.78
		18	0.1	0.2	NI	0.1	NI	NI	NC	2.46	0.28	0.39	NI	0.4	0.00	NI	NI	NI	NC	17	12	8	9	7	8	9	9	5	NI	NI	0.71	0.42	0.45	10.4	3.82
		23	1.6	2.0	0.6	0.6	-29	-30	2.42	3.20	0.47	0.88	NI	5.9	0.00	2	1.6	1.3	1.6	147	30	21	15	10	6	NI	4	NI	6	NI	0.20	0.36	0.40	63.0	3.00
		28	0.4	0.4	0.5	0.5	-27	-28	0.65	0.72	0.50	0.99	1.5	5.7	0.26	2	0.8	0.8	1.0	108	22	18	22	14	9	9	10	5	12	7	0.21	0.40	0.37	101.2	4.84
		29	0.1	0.1	0.1	0.1	-28	-29	0.98	0.76	0.57	1.32	NI	2.7	0.00	1	0.7	0.8	1.0	32	8	5	10	5	5	4	4	2	4	3	0.24	0.38	0.36	22.1	4.06
		30	0.3	0.9	0.2	0.2	-29	-31	1.44	3.98	0.27	0.36	3.6	5.7	0.58	2	1.6	1.7	1.3	112	20	15	17	10	13	7	10	5	15	8	0.18	0.40	0.36	67.5	3.77
		33	0.3	0.7	0.3	0.3	-31	-31	1.07	2.23	0.37	0.59	NI	3.2	0.00	1	0.8	0.7	1.5	47	19	15	10	5	3	3	3	2	3	2	0.41	0.40	0.34	26.9	3.65
		34	0.3	0.3	0.1	0.1	-24	-24	4.89	3.24	0.51	1.05	NI	3.0	0.00	NI	NI	NI	NC	16	5	2	2	1	NI	NI	NI	NI	NI	NI	0.32	0.33	0.40	4.7	2.23
		35	0.2	0.2	0.4	0.4	-25	-25	0.43	0.41	0.54	1.17	27.4	195.3	0.14	NI	NI	NI	NC	NI	2	2	NI	NI	NI	NI	NI	NI	NI	NI	NC	0.51	NC	NI	NC
		37	0.1	0.2	0.2	0.5	NI	NI	0.58	0.31	0.40	0.67	NI	0.3	0.00	4	2.4	2.2	1.2	97	23	40	26	33	18	21	12	15	12	13	0.24	0.62	0.62	88.9	4.79
		39	0.6	1.6	0.3	0.4	-29	-29	1.80	3.93	0.27	0.37	1.0	2.9	0.35	3	1.7	1.6	1.2	96	23	15	19	12	14	9	15	9	12	4	0.24	0.43	0.39	117.9	5.51
		40	0.7	0.7	0.4	0.4	-23	-25	1.66	1.67	0.49	0.98	1.3	9.7	0.14	NI	NI	NI	NC	49	16	10	16	11	8	6	7	5	8	5	0.33	0.43	0.43	22.0	3.11
		41	3.9	7.0	5.2	9.8	-29	-29	0.75	0.71	0.37	0.58	0.8	2.8	0.27	15	13	15	2	1417	318	331	254	181	117	107	75	25	29	23	0.22	0.48	0.43	NI	NC
		42	1.3	1.5	2.3	2.6	-25	-26	0.58	0.57	0.49	0.98	NI	1.0	0.00	3	3	3	2	40	11	10	11	15	6	7	6	6	5	6	0.28	0.52	0.56	37.3	4.82
		44	0.8	0.9	0.4	0.6	-26	-28	2.11	1.55	0.49	0.95	NI	0.6	0.00	4	4	3	2	148	43	52	26	26	16	15	13	12	11	10	0.29	0.53	0.52	71.2	3.25
		45	1.6	2.2	3.0	3.3	-27	-28	0.55	0.67	0.45	0.81	NI	0.5	0.00	4	2	3	1	72	20	26	12	14	8	7	5	6	4	5	0.28	0.48	0.51	59.6	4.54
		46	1.3	1.5	1.3	1.7	-25	-26	1.00	0.90	0.48	0.92	NI	0.5	0.00	3	2	3	2	83	24	25	17	22	10	12	7	8	7	7	0.29	0.51	0.56	39.1	3.21
		47	0.4	0.4	0.2	0.2	NI	NI	1.52	2.50	0.45	0.81	NI	1.4	0.00	NI	NI	NI	NC	18	10	NI	6	NI	NI	NI	NI	NI	NI	NI	0.59	NC	NC	14.3	4.49
		48	1.2	1.9	0.4	0.7	-24	-24	3.04	2.57	0.41	0.68	0.0	0.2	0.20	NI	NI	NI	NC	79	33	6	10	NI	5	NI	NI	NI	NI	NI	0.42	0.17	NC	23.6	2.31
		51	1.4	1.8	1.9	4.1	NI	-31	0.75	0.43	0.44	0.77	0.2	18.2	0.01	NI	NI	NI	NC	NI	NI	NI	NI	NI	NI	NI	NI	NI	NI	NI	NC	NC	NC	NI	NC
		52	2.0	2.1	5.0	5.1	-27	-28	0.40	0.41	0.51	1.02	0.4	4.0	0.10	3	2	2	2	42	12	18	13	20	6	7	5	6	5	6	0.28	0.56	0.57	45.4	5.20
Produced oils	Caimancito-21	1	0.9	0.6	1.4	1.5	-33	-32	0.66	0.40	0.61	1.59	1.3	31.1	0.04	12	13	13	2	69	16	27	21	25	19	15	8	10	18	18	0.23	0.57	0.59	31	3.07
	Caimancito-23	2	5.9	4.1	12.4	11.4	-27	-26	0.48	0.36	0.57	1.32	2.4	104.8	0.02	1	1	NI	1	NI	NI	NI	NI	NI	NI	NI	NI	NI	NI	NI	NC	NC	NC	NI	NC
	Caimancito-30	3	0.7	0.4	1.4	1.0	-26	-25	0.46	0.36	0.67	2.02	2.2	80.1	0.03	NI	NI	NI	NC	1	NI	NI	NI	NI	NI	NI	NI	NI	NI	NI	NC	NC	NC	2	5.95
	Well-10	4	2.1	1.9	8.2	9.0	-26	-26	0.26	0.21	0.53	1.15	1.8	42.4	0.04	NI	NI	NI	NC	11	4	5	3	4	2	3	NI	NI	NI	NI	0.39	0.51	0.63	5	3.26
	Well- 18	5	5.9	4.0	19.8	16.4	-26	-26	0.30	0.24	0.56	1.26	1.6	39.0	0.04	NI	NI	NI	NC	2	NI	NI	NI	NI	NI	NI	NI	NI	NI	NI	NC	NC	NC	NI	NC
	Well-11	6	1.3	0.4	10.5	8.3	-29	NI	0.12	0.05	0.71	2.41	NI	49.0	0.00	NI	NI	NI	NC	NI	NI	NI	NI	NI	NI	NI	NI	NI	NI	NI	NC	NC	NC	NI	NC
	Chirete x100-1	7	6.7	4.1	24.0	21.1	-26	-26	0.28	0.19	0.58	1.39	5.3	55.5	0.10	NI	NI	NI	NC	5	1	2	NI	2	NI	NI	NI	NI	NI	NI	0.30	0.53	1.00	NI	NC
	Río Pescado	8	1.0	0.6	13.2	11.9	-27	NI	0.07	0.05	0.66	1.91	3.4	132.5	0.03	NI	NI	NI	NC	NI	NI	NI	NI	NI	NI	NI	NI	NI	NI	NI	NC	NC	NC	NI	NC
Oil seeps	BN_M-O	a	NI	NI	NI	NI	NI	NI	NC	NC	NC	NC	0.8	3.3	0.00	13	9.1	8.6	1	68	21	33	25	33	17	20	11	14	11	14	0.31	0.56	0.57	99	5.91
	BN_M-O	b	NI	NI	NI	NI	NI	NI	NC	NC	NC	NC	0.4	0.8	0.49	14	9.1	9.4	1	59	18	28	28	40	15	17	11	14	9	12	0.30	0.57	0.56	103	6.34
	LB_W-O	c	0.4	0.3	0.2	0.0	NI	NI	1.55	44.98	0.55	1.22	2.1	1.5	1.41	6	4.7	4.9	2	37	8	14	9	15	11	11	5	6	NI	NI	0.22	0.58	0.56	28	4.36
	LB_M-O	d	NI	NI	NI	NI	NI	NI	NC	NC	NC	NC	0.2	1.0	0.19	NI	NI	NI	NC	14	NI	NI	NI	NI	NI	NI	NI	NI	NI	NI	NC	NC	NC	NI	NC
	LB_M-O	e	NI	NI	NI	NI	NI	NI	NC	NC	NC	NC	0.9	2.2	0.43	NI	NI	NI	NC	16	NI	NI	NI	NI	NI	NI	NI	NI	NI	NI	NC	NC	NC	NI	NC
	Fresh oil	f	NI	NI	0.0	0.0	NI	NI	NC	NC	NC	NC	NI	NI	NC	5	4.3	3.9	2	NI	NI	NI	NI	NI	NI	NI	NI	NI	NI	NI	NC	NC	NC	36	10.00
	M-O	Tar	NI	NI	NI	NI	NI	NI	NC	NC	NC	NC	NI	0.2	0.00	1	0.4	0.5	1	4	1	2	1	1	1	1	1	1	1	1	0.27	0.57	0.53	5	5.39

DBT: Dibenzothiophene; P: Phenanthrene; Gamm. Gammacerane; GI: Gammacerane Index =10 x gammacerane/ (gammacerane + C_{30}αβ-hopane). NI: not identified. NC: Not calculated.

Table A 8. Biomarkers concentrations and ratios in rock extracts from Yacoraite Fm. (Tres Cruces and Metán-Alemanía sub-basins.), produced oils (Lomas de Olmedo sub-basin and oil seep samples (Tres Cruces and Lomas de Olmedo sub-basins).

Type of sample		Short ID	Steranes GC-MS										Steranes GC-MRM-MS			Adamantanes						Diamantanes					
			C_{27}ααα R	C_{28}ααα R	C_{29}ααα R	C_{29}ααα S	C_{28}αββ S	C_{29}αββ R	C_{29}αββ S	C_{29}ββ/(ββ+αα)	C_{29}20S/(20S+20R)	C_{28}/C_{29} αββ 20S	Stig.	C_{27} D/(D+R)	C_{29}/C_{27} R. Ster.	1-MA	2-MA	1+2-MA	1-EA	2-EA	EAI	3-MD	4-MD	3+4-MD	3,4-DMD	4,9-DMD	DMDI-1
			%			mg/g oil				%			mg/g oil			mg/g oil					%	mg/g oil					%
Source rock extracts		11	NC	53	47	NI	NI	48.4	NI	23	NC	NC	NM	NM	NM	NI	NI	NC	NI	NI	NC	NI	NI	NC	NI	NI	NC
		18	NC	70	30	NI	NI	3.1	NI	39	NC	NC	NM	NM	NM	NI	NI	NC	NI	NI	NC	NI	NI	NC	NI	NI	NC
		23	NC	48	52	NI	NI	34.3	NI	20	NC	NC	NM	NM	NM	NI	NI	NC	NI	NI	NC	NI	NI	NC	NI	NI	NC
		28	NC	41	59	NI	NI	6.7	NI	19	NC	NC	NM	NM	NM	NI	NI	NC	NI	NI	NC	0.3	0.7	0.9	0.4	0.3	53
		29	NC	41	59	NI	NI	4.1	NI	18	NC	NC	NM	NM	NM	NI	NI	NC	NI	NI	NC	NI	NI	NC	NI	NI	NC
		30	38	23	38	NI	NI	39.9	NI	24	NC	NC	NM	NM	NM	NI	NI	NC	NI	NI	NC	NI	0.1	NC	0.1	0.0	74
		33	40	27	33	NI	NI	8.9	NI	22	NC	NC	NM	NM	NM	NI	NI	NC	NI	NI	NC	0.0	0.1	0.1	0.1	0.0	66
		34	77	16	8	NI	NI	3.3	NI	34	NC	NC	NM	NM	NM	NI	NI	NC	NI	NI	NC	NI	NI	NC	NI	NI	NC
		35	68	NC	32	NI	NI	NI	NI	NC	NC	NC	NM	NM	NM	NI	NI	NC	NI	NI	NC	0.5	1.6	2.1	0.8	0.3	72
		37	43	29	28	NI	NI	4.6	NI	31	NC	NC	NM	NM	NM	NI	NI	NC	NI	NI	NC	NI	NI	NC	NI	NI	NC
		39	35	38	28	18	NI	46.6	NI	18	9	NC	NM	NM	NM	NI	NI	NC	NI	NI	NC	0.1	0.2	0.3	0.1	NI	100
		40	49	23	28	NI	NI	7.8	NI	27	NC	NC	NM	NM	NM	NI	NI	NC	NI	NI	NC	0.2	0.5	0.7	0.3	0.2	60
		41	28	25	47	77	NI	219.7	NI	20	8	NC	NM	NM	NM	NI	NI	NC	NI	NI	NC	1.0	1.2	2.2	NI	NI	NC
		42	40	31	29	6	7	6.9	4	41	37	1.7	NM	NM	NM	NI	NI	NC	NI	NI	NC	0.2	0.4	0.6	0.3	0.1	75
		44	55	24	21	9	NI	12.7	6	30	26	NC	NM	NM	NM	NI	NI	NC	NI	NI	NC	0.1	0.3	0.4	0.3	0.1	78
		45	42	39	19	11	NI	16.6	6	29	24	NC	NM	NM	NM	NI	NI	NC	NI	NI	NC	NI	0.1	NC	NI	NI	NC
		46	72	16	12	6	NI	8.5	5	47	38	NC	NM	NM	NM	NI	NI	NC	NI	NI	NC	NI	0.1	0.1	NI	NI	NC
		47	45	21	34	NI	NI	4.3	NI	27	NC	NC	NM	NM	NM	NI	NI	NC	NI	NI	NC	NI	NI	NC	NI	NI	NC
		48	74	15	12	NI	NI	9.0	NI	34	NC	NC	NM	NM	NM	NI	NI	NC	NI	NI	NC	NI	NI	NC	NI	NI	NC
		51	NC	NC	NC	NI	NI	NI	NI	NC	NC	NC	NM	NM	NM	NI	NI	NC	NI	NI	NC	NI	NI	NC	NI	NI	NC
		52	40	32	27	7	NI	6.6	4	38	39	NC	NM	NM	NM	NI	NI	NC	NI	NI	NC	0.6	1.1	1.7	0.6	0.3	68
Produced oils	Caimancito-21	1	33	41	26	9	13	13.0	10	60	54	1.4	152.0	0.2	1.7	0.1	0.2	0.3	0.2	0.3	61	0.7	0.8	1.5	0.6	0.4	63
	Caimancito-23	2	70	30	NC	4	7	5.3	5	74	59	1.5	137.6	0.5	1.1	8.7	4.3	13.0	2.8	3.3	54	0.8	1.1	1.9	0.8	0.4	66
	Caimancito-30	3	68	32	NC	4	5	6.2	4	73	56	1.3	152.4	0.5	1.0	9.3	3.9	13.1	2.6	2.4	48	0.6	0.9	1.5	0.8	0.3	75
	Well-10	4	67	33	NC	3	5	5.4	4	78	52	1.2	245.6	0.6	1.5	3.7	2.2	5.9	1.6	1.6	51	0.8	0.8	1.6	0.9	0.3	75
	Well- 18	5	100	NC	NC	1	NI	0.6	1	76	56	NC	23.5	0.6	0.9	20.1	8.4	28.5	4.9	5.3	52	0.9	1.1	2.0	1.0	0.5	68
	Well-11	6	NC	NC	NC	NI	NI	NI	NI	NC	NC	NC	NM	1.0	NC	65.1	25.9	91.0	15.3	19.1	55	3.0	4.0	6.9	2.8	1.4	67
	Chirete x100-1	7	NC	NC	NC	NI	NI	NI	NI	NC	NC	NC	NI	0.5	0.0	4.7	2.9	7.6	2.3	3.9	63	1.2	1.5	2.8	1.3	0.5	71
	Río Pescado	8	NC	NC	NC	NI	NI	NI	NI	NC	NC	NC	NI	NM	NM	34.8	19.3	54.1	9.1	15.5	63	2.7	2.2	4.9	2.2	0.9	72
Oil seeps	BN_M-O	a	50	50	NC	13	14	12.9	11	68	64	1.3	NM	0.6	1.0	NI	NI	NC	NI	NI	NC	1.3	1.7	3.0	1.1	NI	100
	BN_M-O	b	60	40	NC	9	12	8.7	7	64	65	1.7	NM	0.6	1.0	NI	NI	NC	NI	NI	NC	1.5	1.2	2.7	NI	NI	NC
	LB_W-O	c	60	40	NC	16	22	26.5	17	73	60	1.3	NM	0.5	1.5	NI	NI	NC	NI	NI	NC	1.1	0.7	1.8	0.9	NI	100
	LB_M-O	d	100	NC	NC	7	NI	10.4	9	75	64	NC	NM	0.5	2.2	NI	NI	NC	NI	NI	NC	NI	NI	NC	NI	NI	NC
	LB_M-O	e	55	45	NC	6	5	8.9	5	70	62	1.0	NM	0.6	1.7	NI	NI	NC	NI	NI	NC	NI	NI	NC	NI	NI	NC
	Fresh oil	f	NC	NC	NC	4	4	NI	NI	NC	NC	NC	NM	NM	NM	NI	NI	NC	NI	NI	NC	NI	NI	NC	NI	NI	NC
	M-O	Tar	36	26	38	1	1	0.5	0	47	49	1.4	NM	NM	NI	NI	NI	NC	NI	NI	NC	0.0	0.0	0.1	0.0	0.0	59

Stig.: Stigmastane; C_{27} D/(D + R) R. Ster.: C_{27} diasteranes/(diasteranes + regular steranes); C_{29}/C_{27} R. Ster.: Regular steranes; 1MA: 1-Methyl Adamandane; 2MA: 2-Methyl Adamandane; EAI: 2EA/(2EA+1EA); 3MD: 3-Dimethyl Diamantane; 4MD: 4-Dimethyl Diamantane; DMDI-1: 3,4 DMD/(3,4 DMD + 4,9 DMD). NI: not identified. NC: Not calculated. NM: Not measured.

Table A 9. Bulk kinetic parameters

Sample No.	3	23	29	30	33	35	39	40	Tar	44	47
A (1/s)	1.38E+14	7.35E+13	1.76E+12	4.69E+12	4.53E+12	2.79E+13	7.23E+13	1.24E+13	1.19E+14	2.89E+13	1.88E+13
E(kcal/mol)											
42					0.02						
43					0.07						
44			0.43	0.42	0.5						
45			0.92	1.62							
46		0.12	3.02	4.08	3.23						0.63
47	0.22	0.15		9.25	2.56						
48	0.4		61.01		6.9		0.01				2.73
49			16.62	61.85	26.93						3.42
50		3.27	18	8.19	37.51			69.91	69.91		21.61
51		1.03		13.56	15.62	68.82		11.31	11.31		
52				0.99	6.67	6.25		15.91	15.91	91.47	21.19
53	40.54	53.12				19.83	82.37	2.87	2.87	4.03	8.93
54	18.14	21.53		0.03			0.18			4.49	2.57
55	23.28	15.67				3.49	17.44				2.86
56	4.89	1.53				1.35					0.39
57	7.37	3.58				0.26					
58	0.35										
59	3.3										
60											
61	0.88										
62	0.63										